Investigating the nuclear structure of the neutron-rich odd-mass Fe isotopes, in the beta-decay of their parent - Mn

Deyan RADULOV

Examination Committee:
Prof. Dr. N. Severijns, chair
Prof. Dr. M. Huyse, supervisor
Prof. Dr. P. Van Duppen, co-supervisor
Prof. Dr. G. Neyens
Prof. Dr. Ch. Waelkens
Prof. Dr. R. Raabe
Prof. Dr. L. M. Fraile
(Universidad Complutense de Madrid)

Dissertation presented in partial fulfillment of the requirements for the degree of Doctor in Sciences

June 2014

D/2014/10.705/27
ISBN 978-90-8649-718-8

"The best that most of us can hope to achieve in physics is simply to misunderstand at a deeper level."

– Wolfgang Pauli

Acknowledgements

Writing a thesis is difficult... And because it is so, many people are directly or indirectly involved in this process. Writing a thank you note to appreciate them, can sometimes surpass this effort and I think anyone would agree. However, hoping not to leave out someone unmentioned, I would like to a say big "thank you" to all the great people below...

I would like to thank my promoters – Mark and Piet – for giving me the opportunity for a research work, that spans outside of a Master thesis' topic in terms of experience and depth of understanding and knowledge. They have been guiding me in the heavy work of analyzing and interpreting the data by sharing their enormous experience with me.

I am grateful to all of my jury members Prof. Dr. Mark Huyse, Prof. Dr. Piet van Duppen, Prof. Dr. Riccardo Raabe, Prof. Dr. Gerda Neyens, Prof. Dr. Nathal Severijns, Prof. Dr. Christoffel Waelkens and Dr. Luis M. Fraile for all their comments, remarks and enlightening discussion during the preliminary defense.

All of my colleagues in the institute for nuclear and radiation physics at Celestijnenlaan 200D, 2418 (yes, I mean everyone in the building), were also a big part of this process, so thank you for your emotional, scientific, language and administrative support when it was truly needed.

I extend my sincere thanks and appreciation to everyone who has helped me with the interpretation of the vast amount of experimental data and especially to one person, whose sharp mind and profound understanding for nuclear physics has always amazed me – W. B. Walters.

Finally, I would like to express my gratitude towards my family and friends for their support throughout the hard times in this doctorate. **You know who you are ◡̈ !**

And of course, many thanks to my “älskling” **Mikaela**, for giving me all her love and helping me with everything.

So, **Thank you!, Köszönöm!, Hvala!, Grazie!, Ďakujem!, Bedankt!, och Tack så mycket!!!**

Deyan

Abstract (English)

For many years the shell structure of the nucleus, originally proposed by Mayer and Haxel, predicting certain energy gaps at specific proton and/or neutron numbers, has been consistent with the experimental findings at or near the line of stability. These nuclei exhibit a sequence of magic numbers – 2, 8, 20, 28, 50, 82, which is different from the one calculated using only a Harmonic Oscillator potential: 2, 8, 20, 40, 70... The strong spin-orbit term, added to the latter potential by Mayer and Haxel, is a necessary requirement for a successful description of these quantum systems, which lowers the energy orbitals with higher spins directly affecting the $l = 4$ ($1g_{9/2}$) orbit by reducing the gap at $N = 40$ and creating the $N = 50$ one. With the development of more exotic radioactive beams, however, it has been observed that for nuclei away from the stability line the traditional shell gaps have weakened, while new energy gaps have emerged instead. It has been further realized that the residual nucleon-nucleon interaction can lead to significant shifts in the single-particle energies, such that phenomena like the appearance of new shell gaps can be explained. Thus, understanding how shell structure in nuclei develops is a major goal in nuclear physics research.

The region around proton number $Z = 28$ and neutron number $N = 40$ is interesting owing to the experimental evidences, that the neutron-rich iron (Fe) and chromium (Cr) isotones exhibit increasingly collective behaviour ($N > 34$), rather than the semi-magic one expected if the $N = 40$ gap were to be robust. While the spherical $^{68}_{28}\mathrm{Ni}_{40}$ isotope shows features of a doubly-closed nucleus – high 2^+_1 excitation energy and low $B(E2; 2^+_1 \rightarrow 0^+)$ value – the nature of the high excitation energy of the 2^+_1 state could be explained as due to the presence of the opposite-parity $\nu 1g_{9/2}$ orbital across the $N = 40$ energy gap and the negative-parity pf shell. The latter orbital is necessary in order to form a 2^+ state, as the neutrons in the $p_{1/2}$ orbital of the full pf shell cannot.
Furthermore, the development of collectivity as Z decreases from 28, is seen as a result of enhanced quadrupole collectivity when promoting neutron pairs across $N = 40$. Stated another way, by removing protons from the $1f_{7/2}$ orbital, the

attractive central and tensor terms of the monopole proton-neutron interaction between the proton-holes in the $f_{7/2}$ orbital and the neutrons in the $1g_{9/2}$ and the $2d_{5/2}$ orbitals brings the neutron single-particle states down in energy. At the same time the repulsive tensor interaction between the proton-holes in the $f_{7/2}$ orbital and the neutrons in the $1f_{5/2}$ orbital pushes the latter up, further reducing the $N = 40$ closure.The quadrupole collectivity is then enhanced as a result of the presence of the $\Delta j = 2$ orbitals ($1g$ and $2d$), close to the pf shell, making it energetically more favorable to excite pairs of neutrons. The shape-driving, unique-parity $\nu 1g_{9/2}$ orbital is also facilitating spin isomerism in the region of the odd-A iron isotopes.

This thesis presents the experimentally deduced information on excited states, gamma-transitions and beta-decay branches in the consecutive decays of the odd-A $^{61-67}$Mn, $^{63-67}$Fe and $^{63-67}$Co. The radioactive source of manganese isotopes were produced in a proton-induced fission reaction experiment at ISOLDE, CERN. After selective laser ionization, acceleration and mass separation the ions of interest were implanted on a movable tape station, surrounded by several types of detectors.

The gamma- and beta-particles in the decays were detected with two triple HPGe MINIBALL detectors (three single crystals mounted in one cryostat) and three ΔE plastic scintillators in close geometry, respectively, and recorded on an event-by-event basis using digital electronics.
The analysis of the decay data reveals a wealth of new information. New excited and isomeric states have been given tentative spin and parity assignments, while the half-lives of the isomeric levels and the ground states of the mother - manganese - could be determined in many cases for the first time or with a greater than the previously measured precision.

The energy of the isomeric positive-parity states in iron can now be traced up to ^{67}Fe, completing the systematic of the metastable states in those isotopes, including a newly discovered ms-isomeric state in ^{63}Fe. The available information for the cobalt and nickel nuclei is also again greatly enhanced with respect to the 'a priori' existing data with the addition of new excited states and thus gamma-transitions.In the decay of ^{65}Fe the experimental statistics allowed for the assignment of a gamma-transition connecting the previously constructed two separate decay schemes.

A pair of states in each investigated odd-mass iron isotope, have been observed to have a strong direct beta-decay branch. The states are fed much stronger than all other observed levels, concentrating together more than half of the beta-decay strength. The pair of states, with an energy separation of about 650

keV, has been observed to move up in excitation energy with the addition of neutrons: from the ground state and the 629-keV excited state in ^{61}Fe to the 942- and the 1570-keV state in the heaviest investigated ^{67}Fe isotope. Finding these same states in each one of the odd-mass iron isotopes indicates that the spin and parity and possibly the configuration of the ground state of the beta-decaying manganese mother isotope remains the same throughout the isotopic chain, up to $A = 67$.

Abstract (Nederlands)

Voor vele jaren is het schillenmodel van de kern, voorgesteld door Mayer and Haxel, consistent geweest met experimentele bevindingen in kernen dichtbij of op de stabiliteitslijn voor energiekloven bij bepaalde proton- en/of neutron-getallen. Deze kernen vertonen een opeenvolging van magische getallen - 2, 8, 20, 28, 50, 82 - die verschillend is van degene berekend via de harmonische oscillator potentiaal: 2, 8, 20, 40, 70, enz. De sterke spin-baan interactie, toegevoegd aan deze laatsgenoemde potentiaal door Mayer en Haxel, is noodzakelijk voor een succesvolle beschrijving van deze quantumsystemen. Deze correctie verlaagt de energie van hoge-spin orbitalen, zoals het $l = 4$ ($1g_{9/2}$) orbitaal, wat ervoor zorgt dat de energiekloof bij $N = 40$ wordt verkleind en er een nieuwe onstaat bij $N = 50$.

De ontwikkeling van meer exotische radioactieve bundels heeft echter aangetoond dat voor kernen ver weg van de stabiliteitslijn de traditionele schilsluitingen verzwakt worden, terwijl nieuwe schilsluitingen ontstaan. Verder heeft men ontdekt dat de overgebleven nucleon-nucleon interactie voor significante verschuivingen kan zorgen in de één-deeltjes energieën, zodat nieuwe fenomenen zoals het ontstaan van nieuwe schilsluitingen uitgelegd kunnen worden. Dus, het begrijpen van de schillenstructuur in kernen is een van de belangrijkste doelen in kernfysisch onderzoek.

De regio rond protongetal $Z = 28$ en neutrongetal $N = 40$ is interessant doordat experimenten hebben aangetoond dat de neturonrijke ijzer (Fe) en chroom (Cr) isotonen een toenemende trend van collectief gedrag vertonen, in plaats van de semi-magiciteit die men zou vermoeden als de $N = 40$ schilsluiting robuust zou zijn. Hoewel de sferische $^{68}_{28}\mathrm{Ni}_{40}$ kern kenmerken vertoont van een dubbel-gesloten kern – hoge excitatie-energie van de 2^+_1 toestand en een lage $B(E2, 2 \rightarrow 0)$ waarde – kon de aard van deze hoge excitatie-energie verklaard worden door de aanwezigheid van een $\nu 1g_{9/2}$ orbitaal met tegengestelde pariteit gelegen boven de $N = 40$ schilsuiting en de pf schil met negatieve pariteit. Het laatsgenoemde orbitaal is noodzakelijk om een 2^+ toestand te vormen, doordat

dit onmogelijk is met de neutronen in het $p_{1/2}$ orbitaal van de volledige pf schil.

Bovendien wordt de ontwikkeling van collectiviteit met afnemende Z vanaf $Z = 28$ geïnterpreteerd als het resultaat van toegenomen quadrupool–collectiviteit doordat neutronparen geëxciteerd worden over $N = 40$. Met andere woorden, door de attractieve centrale en tensor termen van de monopole proton-neutron interactie tussen de proton-gaten in het $f_{7/2}$ orbitaal en de neutronen in de $1g_{9/2}$ en de $2d_{5/2}$ orbitalen worden de neutron één-deeltjes toestanden verlaagd in energie wanneer protonen verwijderd worden van het $1f_{7/2}$ orbitaal. Terzelfdertijd duwt de repulsieve tensorinteractie tussen de proton-gaten in het $f_{7/2}$ orbitaal en de neutronen in het $1f_{5/2}$ orbitaal deze laatste naar hogere energie, waarbij dus de energiekloof bij $N = 40$ verder gereduceerd wordt. De quadrupool–collectiviteit neemt dan toe door de aanwezigheid van $\Delta j = 2$ orbitalen ($1g$ en $2d$), dichtbij de pf schil, wat het energetisch gunstiger maakt om neutron-paren te exciteren. De vorm-gedreven $\nu 1g_{9/2}$ orbitaal met unieke pariteit maakt ook spin-isomerisme mogelijk in de regio van ijzer- isotopen met oneven A.

Deze thesis stelt de experimenteel bepaalde informatie voor van de geëxciteerde toestanden voor, met name gamma- overgangen en beta- overgangswaarschijnlijkheden in de opeenvolgende vervallen van de oneven $^{61-67}$Mn, $^{63-67}$Fe en $^{63-67}$Co. De radioactieve bron van mangaan-isotopen werden geproduceerd in ISOLDE, CERN door middel van proton-geïnduceerde fissie. Na selectieve laserionisatie, versnelling en massa-separatie worden de desbetreffene ionen geïmplanteerd op een beweegbare tape, die omgeven is door verschillende soorten detectoren.

De gamma en beta-deeltjes in de vervallen worden respectievelijk gedetecteerd met twee drievoudige HPGe MINIBALL detectoren (drie enkele kristallen gemonteerd in één cryostaat) en drie ΔE plastic scintillatie-detectoren in een compacte opstelling, en elk afzonderlijk verwerkt door digitale elektronica. De analyse van de vervaldata onthullen een rijkdom aan nieuwe informatie. Nieuwe aangeslagen en isomere toestanden hebben een tentatieve spin en pariteit toegewezen gekregen. Daarenboven konden de halfwaardetijden van deze isomere toestanden en van de grondtoestanden van de moederkernen (mangaan) in vele gevallen voor de eerste keer bepaald worden of met een grotere precisie dan de voorgaande metingen.

De energie van de isomere toestanden met positieve pariteit in ijzer zijn nu bepaald tot ^{67}Fe, wat de systematiek van de metastabiele toestanden van deze isotopen vervolledigt, inclusief een nieuwe isomere toestand ontdekt in ^{63}Fe met een halveringstijd in de orde van milliseconden. De beschikbare informatie

voor de kobalt en nikkel kernen is ook zeer hard toegenomen ten opzichte van de hiervoor beschikbare data met de toevoeging van nieuwe aangeslagen toestanden en de daarbij horende gamma-overgangen. In het verval van ^{65}Fe kon een gamma-overgang worden toegewezen die twee reeds gekende vervalschema's met elkaar verbindt.

Het is gebleken dat een paar van toestanden in elke onderzochte ijzer-isotoop met oneven massa een sterke directe beta-voeding bezitten. Deze toestanden worden veel harder gevoed dan alle andere gevonden toestanden, en zijn samen goed voor meer dan de helft van de beta-vervalsterkte. Dit paar van toestanden, met een energieverschil van om en bij 650 keV, krijgt een hogere excitatie-energie naarmate meer neutronen worden toegevoegd, gaande van de grondtoestand en de 629 keV aangeslagen toestand in ^{61}Fe tot de 942 en 1570 keV aangeslagen toestand in de zwaarste onderzochte kern ^{67}Fe. Dezelfde toestanden vinden in elk van deze ijzer- isotopes met oneven massa wijst erop dat de spin en pariteit, en mogelijk de configuratie, van de grondtoestand van de beta-vervallende moederkern mangaan hetzelfde blijft doorheen de isotopenketting tot en met $A = 67$.

Contents

Contents **1**

1 The atomic nucleus **3**
1.1 Nuclear stability 3
1.2 Theoretical description 6
1.3 Radioactive decay 11
1.3.1 Beta-decay 11
1.3.2 Gamma-decay 15

2 Motivation for research **19**
2.1 Nuclear structure research around $N = 40$ 19
2.2 The neutron-rich iron region 23
2.2.1 Even-even nuclei 23
2.2.2 Even-odd nuclei 26

3 Experimental set-up **29**

4 Results for the decay chain of $A = 61$ **37**
4.1 Previous experimental information on ^{61}Fe 37
4.2 Results for ^{61}Mn decay 41

5 Results for the decay chain of $A = 63$ **55**
5.1 Previous experimental information on ^{63}Fe 55
5.2 Results for ^{63}Mn decay 58
5.3 Previous experimental information on ^{63}Co 74
5.4 Results for ^{63}Fe decay 77
5.5 Previous experimental information on ^{63}Ni 84
5.6 Results for ^{63}Co decay 85

6 Results for the decay chain of $A = 65$ **89**
6.1 Previous experimental information on ^{65}Fe 89
6.2 Results for ^{65}Mn decay 92
6.3 Previous experimental information on ^{65}Co 109
6.4 Results for ^{65}Fe decay 111
6.5 Previous experimental information on ^{65}Ni 122
6.6 Results for ^{65}Co decay 123

7 Results for the decay chain of $A = 67$ **127**
7.1 Previous experimental information on ^{67}Fe 127
7.2 Results for ^{67}Mn decay 128
7.3 Decay scheme 135
7.4 Previous experimental information on ^{67}Co 154
7.5 Results for ^{67}Fe decay 156
7.6 Previous experimental information on ^{67}Ni 161
7.7 Results for ^{67}Co decay 163

8 Discussion on the nuclear structure of the neutron-rich iron isotopes **167**
8.1 The negative parity states 167
8.2 The positive parity states 173

9 Conclusion and outlook **179**

A Appendix **181**

Bibliography **199**

Chapter 1

The atomic nucleus

The nucleus is a complex quantum-mechanical system, governed by the strong, weak, and electromagnetic forces, which act between its constituents – protons and neutrons – called nucleons. The charged protons in the nucleus interact with each other via the electromagnetic force, while the transformation between the nucleonic states ($p \rightarrow n$ and vice-versa) is governed by the weak interaction. There is clearly another, rather pronounced interaction, that binds all nucleons into one system. It is the strong interaction that is responsible for the fact, that nuclei exist at all, since otherwise the repulsion of the positively charged protons would not allow the existence of any atomic nucleus with more than one proton. It is short-ranged and acts on distances of approximately 3 – 4 fm ($1\ \text{fm} = 1 \cdot 10^{-15}$ m); predominantly attractive, it becomes repulsive at distances of less than about 1 fm.

1.1 Nuclear stability

An unbound neutron is unstable against beta-decay, with a half-life of 614(1) s [NND13b]. However, when both types of nucleons are combined together, they can form a rich variety of nuclear systems. Theoretically predicted there are around 7000 such systems, out of which 254 nuclei are labeled as stable [Erl12]. The number of protons (Z) in the nucleus characterizes each element in the Periodic Table of elements, while the number of neutrons (N) can be different for each element and defines the isotopes of a certain element. If all isotopes are placed in a $2D$-diagram (Z, N) one can obtain the so-called chart of the nuclides, also known as the Segré Chart (see Fig 1.1). Not all combinations of protons and neutrons lead to a configuration that is stable with respect to a spontaneous transformation. This transformation is referred to as radioactivity

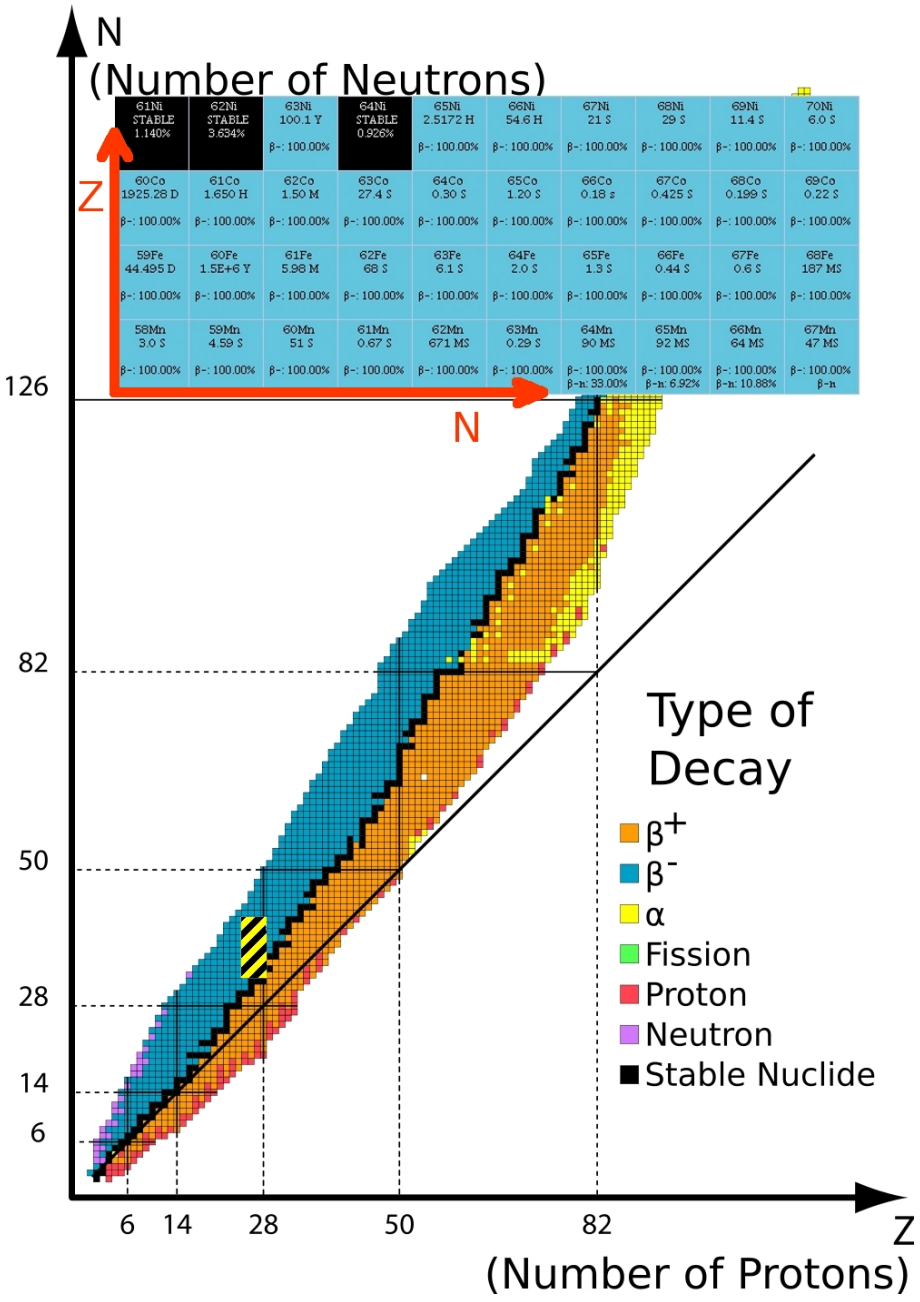

Figure 1.1: Chart of nuclides (Segré Chart): The abscissa indicates the number of protons (Z), while the ordinate axis shows the number of neutrons (N). Colour code denote types of instability (decay modes) and the black squares represent the known stable isotopes. The patterned area in the figure has been cut out and shown as an inset with reversed axes in **red**. That part of the chart represents the region of interest in this work.

or radioactive decay and was discovered in the end of the XIX century by Becquerel.
The colors in Fig 1.1 denote the type of transformation the isotopes undergo. Conventionally, the blue color stands for β^--decay, red – β^+-/EC-decay (abbreviated from Electron Capture, discussed further on), yellow denotes α-decay, while green is for spontaneous fission. There also exist other types of exotic decays, such as one or two proton emission in the proton-rich part of the Segré Chart.

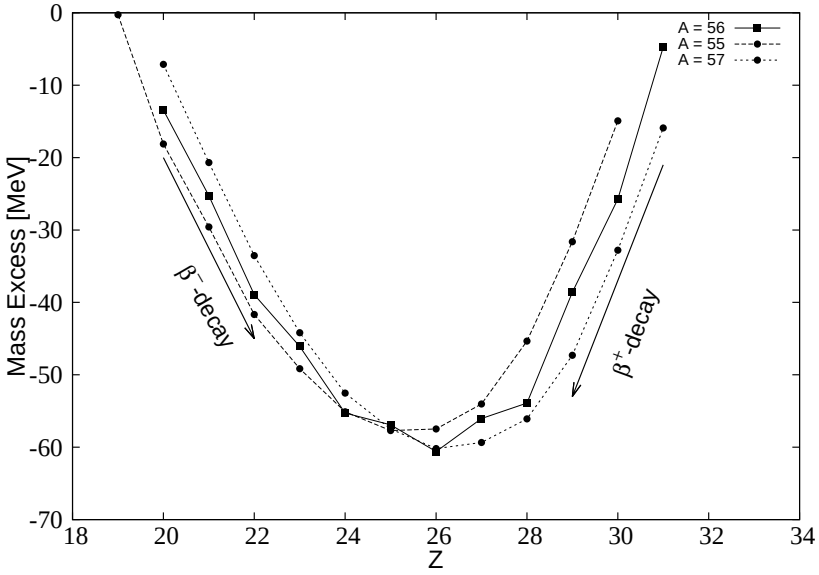

Figure 1.2: Mass parabolas for $A = 55, 56$, and 57.

There are isotopes of an element for which the ratio between the protons and the neutrons is such, that a local energy minimum is achieved (indicated by the black squares in Fig 1.1). These isotopes are the stable ones in nature and are situated along the so-called "valley of stability". The term "valley" itself can be visualized when Fig 1.1 is plotted in three dimensions. If the third axis is chosen to be the Mass Excess – the difference between the experimentally measured mass of an isotope and its atomic mass number – the isotopes form a

valley, in the bottom of which are the most stable nuclei for a given mass. A 2-D slice of the three-dimensional valley is presented in Fig 1.2 for $A = 55$, 56 and 57.

The strong interaction between the nucleons inside the nucleus of the atom is at present not completely known. This combined with the limitations of the many-body theory results in the fact that there is not a complete theory that describes any given nucleus.

Extensive, systematic experimental data available for the stable isotopes made it clear that nuclei having specific Z and/or N (**2, 8, 20, 28, 50, 82, 126** – known as the "magic numbers") are particularly favored in terms of stability [Gre96]. Certain properties of the nuclei possessing these magic numbers (large binding energies, large energies for separation of a nucleon, etc. [Kra87]) have lead physicists to assume the existence of a shell structure of the nucleus, in analogy to the electron shell structure of the atom.

1.2 Theoretical description

A theoretical model that can describe nuclei with the specific "magic" proton and/or neutron numbers, close to the stability line, was developed by [May49, Hax49]. Known as the shell model, it is based on the notion of a nuclear potential or a mean field, generated by and in which all nucleons are moving. The mathematical problem of describing the energy states in the nucleus can be dealt with by solving Schrödinger's equation of the many-body system by subtracting an empirically prescribed central potential from the Hamiltonian of the nucleus:

$$H = \underbrace{\sum_{i=1}^{A}\{T_i + U(\vec{r_i})\}}_{\mathrm{H}_0} + \underbrace{\{\sum_{i}^{A}\sum_{k>i}^{A} V_{ik}(\vec{r_i} - \vec{r_k}) - U(\vec{r_i})\}}_{\mathrm{H}_{res}}.$$

T_i in the equation is the kinetic energy of each nucleon, V_{ik} is the nucleon-nucleon interaction, i.e. the potential energy of the nucleons due to the interaction between them and $U(\vec{r_i})$ is the prescribed central potential. It is important the central potential ($U(\vec{r_i})$ be chosen such, that the second part of the equation (H_{res}) is negligible and can be treated as a perturbation. The latter term is what is referred to as the residual interaction, which as the name suggests, is the difference between the effect of the two body interaction (V_{ik}) and the central potential ($U(\vec{r_i})$). Provided that the residual term is small and applying perturbation theory, it is then possible to solve the first part (H_0) of the

Hamiltonian, which describes the motion of each nucleon.

The central, spherically symmetric, nuclear potential that manages to correctly reproduce the observed magic numbers can be written as:

$$U(\vec{r}) = \underbrace{m\omega^2\vec{r}^{\,2}/2}_{\text{Harmonic Oscillator term}} + \underbrace{D\vec{l}\cdot\vec{l}}_{\text{angular momentum term}} - \underbrace{C\vec{l}\cdot\vec{s}}_{\text{spin-orbit term}}, \quad (1.1)$$

where $\vec{l}$ and $\vec{s}$ are the orbital angular momentum and the intrinsic spin, while D and C are coupling constants. The single-particle energy spectra deduced using this potential can be seen in Fig 1.3.

Both the protons and the neutrons sequentially fill the energy levels for a given N and l until the number of particles in a given level reaches its maximum. It follows from Pauli principle, that an energy state can accommodate a maximum of $2j$+1 particles [Cas90], with $j = l + s$ being the total single-particle angular momentum. Essential for the shell model is the spin-orbit coupling term that is responsible for the splitting of the orbitals with the same l value, lowering the $j = l + 1/2$ energy level and raising the $j = l - 1/2$ level. Only with the addition of the latter in the central potential, the single-particle energy orbits arrange in such a way that the energy gaps, indicated in Fig 1.3 with a red dot, separate shells with a maximum number of particles (given in squares) equal to the magic numbers observed in nature. The energy gaps also define the different shell closures in the framework of the model

In such a way the $1g_{9/2}$ orbital is lowered due to the spin-orbit splitting and forms a unique parity orbital in the N=3 harmonic oscillator shell. Moreover, it creates a new gap at proton or neutron number 50 between the $1g_{7/2}$ - $1g_{9/2}$ doublet partners. The same mechanism applies for the $1f_{5/2}$ - $1f_{7/2}$ doublet in the shell below $N = 50$, creating the $N = 28$ gap. In this thesis work we shall concentrate our study on isotopes with $Z < 28$ and N between 28 and 40.

An important implication of the re-arrangement of the energy levels is that each major shell, starting from grouping of levels between the gaps of 28 and 50, contains a majority of levels of one parity ($\pi = (-1)^l$), called normal-parity, and one level of the opposite parity, called a unique-parity orbit [Cas90]. Since the energy separation of the unique-parity orbital from the multiplet from which it originates is large, it is characterized by pure single-particle(hole) configurations and it forms an ideal testing ground for various nuclear models [Cas90].

When a nucleus contains both as many neutrons and protons to complete a full shell, corresponding to any of the magic numbers, it is called a double-magic

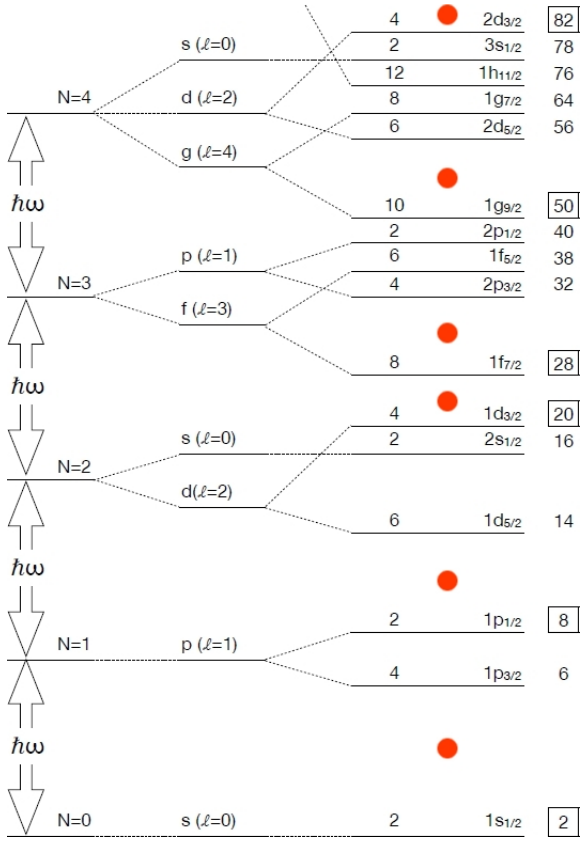

Figure 1.3: Nucleonic energy levels: using the bare Harmonic Oscillator (H.O.) potential ($\propto \vec{r}^{\,2}$; left); the H.O. plus an angular momentum term ($\propto \vec{l}\cdot\vec{l}$; center); the latter two terms with the addition of a spin-orbit term ($\propto \vec{l}\cdot\vec{s}$; right). Note that only after the addition of the last term in the central potential, the energy gaps indicated with a (red) dot correspond to the experimental magic numbers (shown in squares at the rightmost side). The figure is adapted from [Mou12].

nucleus in the framework of this model.

The single-particle shell model is successful in accounting for the spins and parities of the ground states of nearly all odd-mass nuclei, in close proximity to the shell closures.

An example for a shortcoming of the shell model, however, is the wrong

assignment of ground state spin of the odd-A $^{55}_{25}Mn_{30}$ isotope [May49]. In a simple shell model perspective the spin and parity of the isotope would be $7/2^-$, determined by the odd proton in the $f_{7/2}$ orbital. Nevertheless, experimental data indicate that the spin and parity of the ground states of $^{55}_{25}Mn_{30}$ is $5/2^-$ [NND13b] and only $^{53}_{25}Mn_{28}$ has the predicted ground-state's spin and parity (see Fig 4.9 further on).

For nuclei located away from the stability line, for example in the mass regions between 150 and 190 and $A > 230$, the shell model fails to reproduce the observed rotational bands, interpreted as "collective effects" [Hey99]. It is assumed that with the addition of more nucleons to a doubly magic nucleus the energy of the nucleon-nucleon interaction builds up and eventually makes the nucleus deviate from its spherical shape that is retained near the shell closures.

Since the spherically-symmetric central potential applied in the shell model was not sufficient to describe these nuclei, new models to describe deformed nuclei were developed.

An example for such a model is the Nilsson model [Nil55]. Generalizing on the shell model, it provides a good description of the single-particle nucleon motion in an axially symmetric (non spherical) mean field potential. Since the spherical symmetry is no longer retained, the single-particle energies in this potential will depend on the spatial orientation of their orbits with respect to the symmetry axis of the nucleus [Cas90]. The latter orientation can be specified by the projection (Ω) of the total single-particle angular momentum on the symmetry axis of the nucleus.

The $(2j+1)$-fold degeneracy of particles having the same energy in the spherically symmetric mean field will be lifted according to their Ω-projection taking values from $-j$ to $+j$. The splitting of the energy levels in the non-spherically-symmetric potential depends on the magnitude of the component of the total angular momentum along the symmetry axis of the core.

These single-particle energy splittings can be seen in Fig 1.4, where the so-called Nilsson diagram for the protons and neutrons around shell closure numbers 20, 28 and 50 is presented. Each line in the latter figure, represents a Nilsson state which is downwards or upwards sloping, with a magnitude depending on the angle of the orbit with respect to the bulk of the core and the mixing between the different configurations.

The single-particle orbitals with the most overlap with the deformed core are energetically favoured. For prolate deformations ($\varepsilon_2 > 0$) the orbitals with the

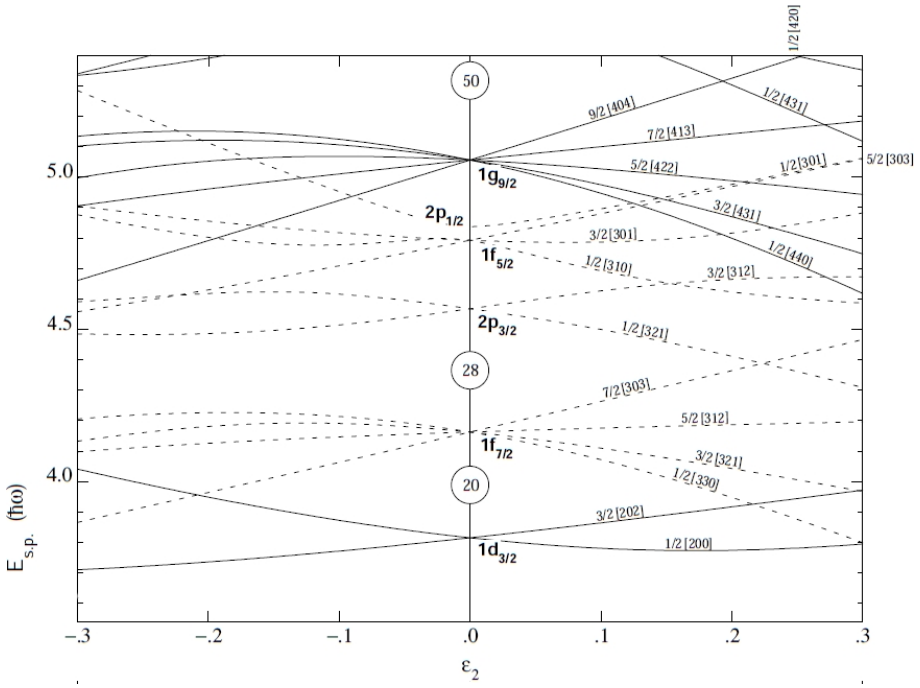

Figure 1.4: Nilsson energy diagram for protons and neutrons in the region of the magic numbers 20, 28 and 50 (adapted from [Fir96]); ε_2 is the quadrupole-deformation parameter in Nilsson's model [Cas90], which relates to the macroscopic deformation parameter (β) as: $\beta = \sqrt{\pi/5}\sum_i 4\varepsilon_2^i/3^i$ [Fir96]. Note that for $\varepsilon_2 = 0$ one gets back the shell model ordering.

smallest possible Ω projection will interact the most with the core and thus will be more tightly bound. The situation is exactly opposite for oblate deformations ($\varepsilon_2 < 0$) [Kra87].
The main success of the deformed shell model is the correct explanation of ground state spins and parities of a large number of odd-A nuclei in heavy mass region.

The spherical shell model, serves as a basis for extended calculations. Using a conveniently selected "inert" core (a double magic nucleus) and a "valence space" outside the core, occupied by extra particles/holes, computations can be performed. The introduction of the inert core is indeed necessary, because the calculations including all available nucleons are unfeasible. By selecting the inert core only residual interaction, responsible for any change or shift in the

single-particle energies needs to be determined [Cas90].

The residual interaction itself can be decomposed in monopole, dipole, quadrupole, etc. terms [Cas90]. Specifically, the monopole part of the residual interaction is to a large extent responsible for the modification of the single-particle energies in the valence space [Cas90, Sor08]. The monopole term itself can subsequently be separated into central, spn-orbit and tensor parts. The latter has been pointed out recently [Ots05] to have an attractive and a repulsive effect, when acting upon orbitals with opposite and parallel spin-orbit couplings, respectively. In some cases the strength of this term can overcome the effect of the other two, thus being the most important one [Sor08].

Shell-model calculations include information on the wave functions of the states, whose composition can indicate a possible mixing of single-particle configurations, induced by the residual interaction. The calculations also provide information about the single-particle energies, transition rates, and spin and parities of all calculated energy states.

1.3 Radioactive decay

One of the main goals of contemporary nuclear-structure research is to improve on the current knowledge of the nucleus by obtaining experimental information on nuclei far from the stability line. The extracted information can then be compared to results from theoretical calculations, in order to improve the reliability of the nuclear model-based extrapolations towards unknown regions in the nuclear chart and to obtain fundamental knowledge of the strong interaction.

While a broad spectrum of experimental techniques to obtain information on the nuclear structure exist, here we will concentrate on the β- and γ-decay spectroscopy – the subject of this thesis.

1.3.1 β-decay

β-decay involves the weak interaction mechanism and is a process of converting a neutron/proton into a proton/neutron, while keeping the mass number (A) of the nucleus the same. Nuclear β-decay is the common name for three processes: β^+–decay, β^-–decay and electron capture (EC), which can be expressed using

the following equations:

$$\begin{aligned}
\beta^+ \quad &: {}^A Z \rightarrow {}^A(Z-1) + e^+ + \nu_e \\
EC \quad &: {}^A Z + e^- \rightarrow {}^A(Z-1) + \nu_e \\
\beta^- \quad &: {}^A Z \rightarrow {}^A(Z+1) + e^- + \bar{\nu_e}.
\end{aligned}$$

On the left side of the equations, Z is the number of protons and A the mass number of the nucleus that is undergoing transformation, while $e^{\pm}$ and ν are the beta-particle and the neutrino, respectively, involved in the decay process.

The available energy for each decay (also known as the Q_β value) can be calculated using the difference in mass (= energy/c^2) between the initial and final states involved in the process:

$$\begin{aligned}
Q(\beta^+) &= (M(A,Z) - M(A,Z-1) - (2m_e))c^2 \\
Q(EC) &= (M(A,Z) - M(A,Z-1))c^2 \\
Q(\beta^-) &= (M(A,Z) - M(A,Z+1))c^2.
\end{aligned}$$

The very small mass of the neutrino, involved in all three processes, has been neglected in the latter equation, where M denotes the neutral atomic mass [Kra87].
If the Q_β value between the initial and final states is positive, the decay is energetically possible and will proceed.

β-delayed neutron emission

This process occurs at the neutron-rich side of the chart of nuclides away from the valley of stability. It takes place, only if the Q_β value is larger than the neutron separation energy (S_n) in the daughter product. The latter is the required amount of energy to remove the last bound neutron in the nucleus.

$$S_n = (M(A-1,Z) - M(A,Z) + m_n)c^2. \tag{1.2}$$

When a β-decay process with a sufficiently large Q_β value proceeds, it is possible that excited states in the daughter nucleus, that are located above the neutron separation energy are populated. There is a probability that a neutron can then be emitted from that excited state, resulting in the population of a nucleus with $N-2$ neutrons and $Z+1$ protons with respect to the beta-decaying mother. Experimental probabilities for β-delayed neutron emission were extracted and are part of the results, discussed in this work.

Transition probabilities in β-decay

The transition rate in the beta-decay can be expressed as [Kra87]:

$$\lambda = \frac{2\pi}{\hbar}|M_{fi}|^2\rho(E_f). \tag{1.3}$$

The latter equation is known as Fermi's Golden Rule [Kra87].
The transition rate (λ) is proportional to the square of the matrix element of the transition between the two states. Thus, the more alike the initial and final states are, the larger the transition rate will be. The last term in the former equation, $\rho(E_f) = dn/dE_f$, is the density of final states, i.e. the number of final states (dn) in the energy interval dE_f, where the final energy E_f is the summed energy of the beta-particle and the neutrino [Kra87]. Therefore, the transition rate will again be higher if there are many final states available for the decay.

Using Fermi's Golden Rule and equation (9.28) in [Kra87], the density of final states can be expressed as:

$$\rho(E_f) = \left(\frac{g^2 m_e^5 c^4}{4\pi^4\hbar^6}\right)\int_0^{p_{e(max)}} F(Z', p_e)\frac{p_e^2}{(m_e c)^2}\frac{(Q-T_e)^2}{(m_e c^2)^2}\frac{dp_e}{m_e c}. \tag{1.4}$$

In the equation above g is the β-decay constant giving the strength of the weak interaction, m_e is the rest mass of the β-particle (electron/positron), and the integral on the right side is between 0 and the maximum momentum of the β-particle. The integral in the equation has been made dimensionless by adding the constants within it [Kra87], whilst F – the Fermi function – accounts for the interaction of the emitted charged particle with the nucleus through the Coulomb force. The momentum distribution of the emitted β-particle ($p_e^2(Q-T_e)^2$) is a statistical factor, derived from the number of final states accessible by the emitted beta particle. Q is the available energy for the decay and T_e is the kinetic energy of the beta particle.

The integral in equation (1.4) is known as the "Fermi-integral" (commonly labeled as $f(Z',p_e)$) and has been tabulated for Z' (the daughter nucleus) and p_e [Kra87]. Using the relation: $\lambda = \ln(2)/\mathrm{t}_{1/2}$, a largely used quantity can be derived. Its common name is comparative half-life and can be expressed as:

$$ft_{1/2} = \ln(2) \times \left(\frac{2\pi^3\hbar^7}{g^2 m_e^5 c^4}\frac{1}{|M_{fi}|^2}\right) = \ln(2) \times \left(\frac{CONST.}{|M_{fi}|^2}\right). \tag{1.5}$$

This quantity presents a way to compare the β-decay probabilities in different nuclei, as the difference in $ft_{1/2}$ values must originate from the differences in

the matrix element [Kra87].

Because the half-lives of the excited/ground states can span over several magnitudes (a typical half-life of a ground state can span from 10^{-3} s to 10^{+16} yr), it is customary to use the $\log_{10}$ value of the comparative half-life, commonly known as $\log ft$ value (with the half-life given in seconds). This allows for direct comparison of the β-decay rates in different nuclei.

Compilations of nuclear decay information can be used to estimate $\log ft$ values for a given β-decay, but a purely empirical equation for the computation of the $\log f$ value in the β^--decay (in the other β-decay processes the empirical formula differs a bit) is given by [Fri81]:

$$log f_{\beta^-} = 4.0 \cdot logE + 0.78 + 0.02 \cdot Z' - 0.005 \cdot (Z' - 1) \cdot logE, \qquad (1.6)$$

where E (= Q - T_e) is the energy of the excited state in the daughter nucleus, that is being populated in the decay and Z' is the atomic number of the daughter nucleus.

Angular momentum conservation leads to a set of selection rules for the beta-decay process.
If the orbital angular momentum transfer between the initial and the final state is zero only the intrinsic spins of the electron and anti-neutrino (or positron and neutrino) need to be considered. If the spins of the two particles are anti-parallel ($s_{total} = 0$; $\Delta\pi = (-1)^L = 0$ - no change in parity), the total change in nuclear spin, ΔJ, between initial and final states is 0 and the beta decay is termed Fermi decay (often called "superallowed" transition). However, if the electron and the anti-neutrino are emitted with their spins aligned ($S_{total} = 1$; $\Delta\pi = (-1)^L = 0$ - no change in parity), the process is called Gamow-Teller decay (ΔJ = 0, 1, but not $0^+ \rightarrow 0^+$). This type of transition between states is known as allowed decay.

Transitions for which the orbital momentum transfer is different than zero ($l \neq 0$) are termed "forbidden" and they occur with less probability compared to the allowed ones. Each value of $l \neq 0$, is classified as an order of forbiddenness – first-, second-, third-forbidden decay, etc.

The selection rules for allowed and forbidden beta decays are summarized in Table 1.1.

Decay type	ΔJ (L+S)	$\Delta\pi$	logft
Super-allowed (Fermi)	0 ($0^+ \rightarrow 0^+$)	no	2.9 – 3.7
Allowed (Gammow-Teller)	0,1	no	4.4 – 6
First-forbidden	0,1,2	yes	6 – 10
Second-forbidden	1,2,3	no	10 – 13
Third-forbidden	2,3,4	yes	> 15

Table 1.1: Ranges of logft values for different degrees of forbidden transitions [Hey99]

1.3.2 γ-decay

γ-decay is the spontaneous transition from an excited state in the nucleus towards a less excited state or the ground state of the same nucleus. It involves the electromagnetic interaction. The energies of the emitted rays are typically in the range of 10 keV to 10 MeV.

The angular momentum taken away by the photon L (= I_i - I_f) determines the multipolarity of the emitted photon: $L = 1$ transitions are termed dipole, $L = 2$ are quadrupole, etc. The change in parity, $\Delta\pi$, between the initial and final states determines the electric (E) or magnetic (M) character of the transition. Therefore, the selection rules for gamma-decay can be written as:

$$|I_i - I_f| \leq |L| \leq |I_i + I_f|$$

$$\Delta\pi = 0 \text{ (no)}: \quad L = \text{even (electric)}, L = \text{odd (magnetic)}$$

$$\Delta\pi = 1 \text{ (yes)}: \quad L = \text{even (magnetic)}, L = \text{odd (electric)},$$

where $I_{i,f}$ are the initial and final spin of the levels involved, respectively.

In order to judge whether a transition between an initial and a final state is relatively weak or strong, one often determines reduced transition probabilities, where the energy factor has been removed. They are expressed in single-particle or Weisskopf units [Kra87]. In the framework of the shell model, the reduced transition probabilities can be written as [Mar82]:

$$B_{s.p.}(EL)\downarrow = (\frac{3}{3+L})^2 R^{2L} \frac{1}{4\pi b^L} \quad [\mathrm{e}^2 b^L] \tag{1.7}$$

$$B_{s.p.}(ML)\downarrow = (\frac{3}{3+L})^3 R^{2L-2} \frac{10}{\pi b^{L-1}} \quad [\mu_N^2 b^{L-1}], \tag{1.8}$$

where $b = 10^{-24}$ cm^2, $e^2 = 1.440{\cdot}10^{-10}$ keVcm, $\mu_N^2 = 1.5922{\cdot}10^{-38}$ keVcm^3 and $R = 1.2{\cdot}10^{-13}A^{1/3}$cm. Equations (1.7) and (1.8) are known as Weisskopf single-particle estimates for electric and magnetic transitions, respectively. The Weisskopf estimates of the reduced transition probabilities can be converted into so-called Weisskopf estimates of the half life of a certain gamma transition.

The experimentally obtained half-lives of excited states ($\propto 1/\mathrm{B}(\sigma L)$) can be compared to the estimates in Weisskopf units (W.u.):

$$B(\sigma L)[W.u.] = \frac{B(\sigma L)_{exp}}{B(\sigma L)_{s.p.}} = \frac{T^{s.p.}_{1/2}(\sigma L)}{T_{1/2}(\sigma L)_{exp}}, \tag{1.9}$$

which can give an indication of the nature of the transition in the frame work of the model [Kra87].

Table 1.2 lists the single-particle estimates for the transition half-lives of different electric and magnetic multipoles, using Weisskopf's formulas for the reduced transition probability [Fir96]. From Table 1.2 it is clear that electric transitions

Electric	$T^{s.p.}_{1/2}$ (s)	Magnetic	$T^{s.p.}_{1/2}$ (s)
$E1$	$6.76 \cdot 10^{-6}/(E_\gamma^3 A^{2/3})$	$M1$	$2.20 \cdot 10^{-5}/(E_\gamma^3)$
$E2$	$9.52 \cdot 10^{6}/(E_\gamma^5 A^{4/3})$	$M2$	$3.10 \cdot 10^{7}/(E_\gamma^5 A^{2/3})$
$E3$	$2.04 \cdot 10^{19}/(E_\gamma^7 A^{2})$	$M3$	$6.66 \cdot 10^{19}/(E_\gamma^7 A^{4/3})$
$E4$	$6.50 \cdot 10^{31}/(E_\gamma^9 A^{8/3})$	$M4$	$2.12 \cdot 10^{32}/(E_\gamma^9 A^{2})$

Table 1.2: Formulas for single-particle transition half-life, corrected for internal conversion [Fir96]. The energy is in units of keV.

are faster than the magnetic ones of the same order and that the transition of order $L + 1$ are much less probable than transitions of order L. For a given transition between two states, it is possible that several multipole radiations can be emitted (for example $E2/M1$ or $E1/M2$ transitions are possible).

γ-transitions between two 0^+ states are forbidden due to conservation of angular momentum (the gamma-ray always carries away $L > 0$ angular momentum). Apart from gamma decay, the transition between two states can occur via electron conversion. In this process, an inner-shell atomic electron gets emitted instead of a photon. The electromagnetic field of the nucleus interacts with one of the atomic electrons close to it, resulting in the transfer of the excitation energy to that electron and its ejection. The energy of the emitted electron equals the difference in energy between the two states, minus the atomic binding energy of that electron. The total decay rate constant (λ_t) of a given transition

between an initial and a final state is then equal to the γ-decay rate, combined with the sum of all possible electron conversion transitions:

$$\lambda_t = \lambda_\gamma + \sum_i \lambda_e = \lambda_\gamma(1 + \alpha_i), \tag{1.10}$$

where α_i is the internal conversion coefficient for i^{th} electron shell (typically K, L and M). The magnitude of the internal conversion coefficient depends on the type, the energy and the multipolarity of the transition, as well as on the atomic number of the nucleus. The conversion coefficients can be calculated using e.g. the following website [BrI13]. As gamma decay between two 0^+ states can not occur this transition happens only via electron conversion.

Isomers

Isomers are long lived excited states in the nucleus. Contrary to other excited states with a typical half-life in the pico- or nano-second range, the isomeric half-lives are much larger – ranging from nanoseconds to many years [Wal99]. The isomeric states can de-excite via γ- or particle emission (β or α), depending on the quantum numbers and the energy difference of the initial and final states. The origins of existence of these states give also their classification as shape-, spin- or K-isomers [Wal99].

Isomers resulting from a large difference in the spin of the state under consideration and the states below are a common type of isomers found in nuclei. In order to de-excite and match the spin difference of the two connected states the nucleus must emit a photon with a high multipolarity (L) and thus much less probability. Such excited states can have long half-lives. Most of the spin isomers discovered and discussed in this work decay by photon emission or electron conversion. However, there can be such isomers that decay via particle emission (see Section 7.4 for an example). Spin isomers and more specifically the isomers in the odd-A iron isotopes, are studied in the present work. Their existence is predominantly due to the spin difference between the positive-parity $g_{9/2}$ and the negative-parity $pf_{5/2}$ orbitals around $N = 40$.

Chapter 2

Motivation for research

2.1 Nuclear structure research around $N = 40$

For many years the shell structure of the nucleus, originally proposed by Mayer [May49] and Haxel [Hax49], predicting certain energy gaps at specific nucleon numbers, has been consistent with experimental findings at or near the valley of stability.

The strong spin-orbit interaction term, added to the central nuclear potential by Mayer and Haxel, is a necessary requirement to successfully describe these quantum systems by lowering the energy of the orbitals with high angular momentum (l+1/2). This directly affects, for example, the $l = 4$ ($1g_{9/2}$) orbital by reducing the energy gap at $N = 40$ and creating the $N = 50$ one.

With the development of more exotic radioactive beams, however, it has been observed that the strength of the traditional shell closures have weakened, while new energy gaps have emerged instead. It has been further realized that the proton-neutron interaction can lead to significant shifts in the single-particle energies, such that phenomena like the appearance of new shell gaps can be explained [Ots01]. Thus, understanding how shell structure in nuclei develops is a major goal in nuclear physics, where magic numbers can exist for both of their constituents.

Systematic studies of nuclei in the vicinity of closed proton and/or neutron shells, such as $Z = 28$ and $N = 40$, provide an important testing ground for theory and search for collective phenomena. The $N = 40$ energy gap in the shell model, originates from the bare harmonic oscillator (H.O.) potential and is a relic, washed out by the strong spin-orbit interaction. It is formed

between the degenerate states with principle quantum numbers N = 3 and N = 4.

Strong proton-neutron residual interaction is known to be present between the neutrons in the $\nu f_{5/2}$ and the proton-holes in the $\pi f_{7/2}$ orbitals and the neutrons in the $\nu g_{9/2}$ orbitals and the holes in the latter proton orbital [Ots05]. Quantifying the effects of these interactions is one of the important goals of experimental studies, including this one.

The $\nu g_{9/2}$ orbital has a high spin and a unique parity in the pf shell between $N = 20$ and 50, facilitating the formation of isomers. The region around $N = 40$, subject of this study, is moreover an ideal testing ground for the effective nucleon-nucleon interactions used in large-scale shell-model calculations today [Len10].

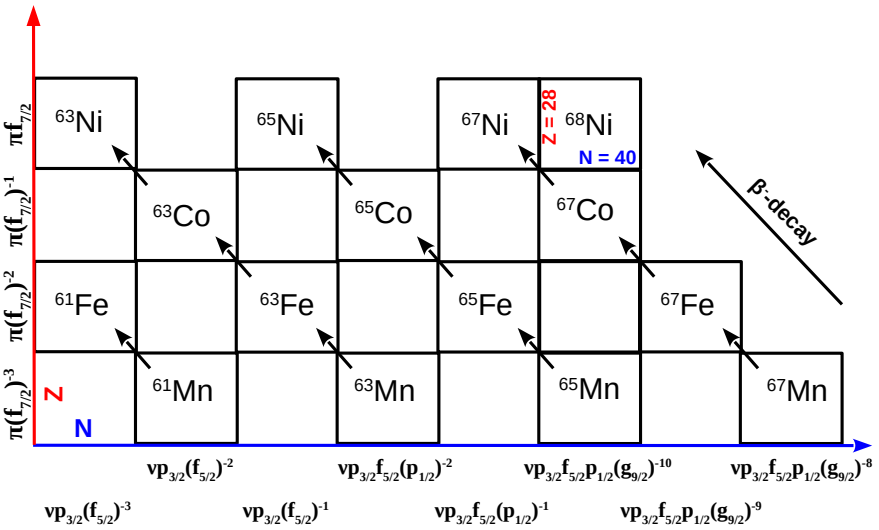

Figure 2.1: Selected part of the chart of the nuclides in the neutron-rich region around $Z = 28$ and $N = 40$ and expected configurations for the protons and the neutrons, respectively, from a simple shell model perspective. Note, that the for the sake of simplicity the $\nu d_{5/2}$ orbital is not indicated, but it may have an important role in the configurations. The arrows connecting the boxes indicate the decays presented in the next chapters.

A doubly-magic character of ^{68}Ni nucleus was inferred in [Ber82, Lom83], where it was suggested that the first excited state in this isotope has a (0^+) spin and parity and the calculations performed in the latter references concluded that the ^{68}Ni isotope "constitutes a good signature of shell closure".

Another experimental evidence supporting this claim was made by Broda et al. [Bro95], by observing the isotope's 2_1^+ excited state at an excitation energy of 2.033 MeV, considerably higher than its neighbouring nuclei. The large 2_1^+ energy and the small $B(E2)$ value for ^{68}Ni [Sor02] were interpreted as the sign for a sub-shell closure at $N = 40$. In fact, the extracted $B(E2)$ is comparable to the $B(E2)$ values for the double-magic nuclei $_8O_8$ and $_{20}Ca_{20}$ [Sor02]. However, the difference in the separation energy of two neutrons (ΔS_{2n} = $S_{2n}(N)$ - $S_{2n}(N+2)$) in the vicinity of $N = 40$, which is another good test for determining the magic character of the nuclei, does not show a strong evidence for a shell closure [Oro00]. This can be inspected in Fig 2.2, where a considerable peak in the energy difference at $N = 40$ is expected.

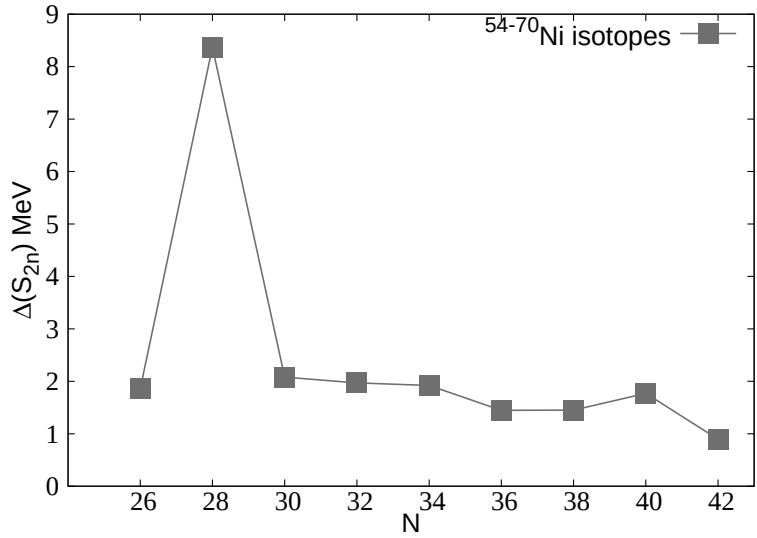

Figure 2.2: Difference between the two neutron separation energy (S_{2n}) in the nickel isotopic chain [NND13b].

The high excitation energy and low $B(E2)$ value for ^{68}Ni could be explained by the fact, that the opposite-parity $\nu g_{9/2}$ orbital lies across the negative-parity pf shell and the $N = 40$ energy gap, and that the neutrons in the full $p_{1/2}$ shell cannot form a 2^+ excited state.

^{68}Ni is an interesting nucleus also owing to its number of excited 0^+ states. The isotope has two identified low-lying excited 0^+ states, which may be an indication for a shape coexistence [Shi12]. New state-of-the-art Monte Carlo Shell Model calculations predict a ground state of a spherical shape, 0^+_2 ($\sim$ 1.8 MeV) of an oblate (β = -0.2) form and an excited 0^+_3 ($\sim$ 2.5 MeV) state with a prolate ($\beta = 0.4$) deformation (see Fig.3 in [Tsu13]). The later work also infers, that 2^+_1 and 0^+_2, as well as 2^+_2 and 0^+_3, respectively, have similar shapes. These two statements have been recently confirmed in shell-model calculations with four different interactions in an investigation of the low-lying low-spin structure of ^{68}Ni [Rec13]. The latter reference also suggests a new experimental value for the 0^+_2 excited state in this isotope – 1603.5(3) keV.

Both of the latter excited $0^+_{2,3}$ states could possibly be due to neutron excitations across the $N = 40$ sub-shell gap with a wave-function admixture of $2p - 2h$ (and to some extent $> 4p - 4h$ for the 0^+_2 state) excitations to the $g_{9/2}$ orbital, coupled to $J^\pi = 0^+$ [Rec13].

Even though the $Z = 28$ gap is a major shell closure, one could expect a 0^+ excited state at low energy with a π(2p-2h) nature, due to the strong pairing correlations and the proton-neutron residual interaction [Pau10]. A prediction for such a state was given at an energy of 2202 keV [Pau10], as a result of the sum of the energies of the identified π(1p-2h) and π(2p-1h) excited levels in ^{67}Co and ^{69}Cu, respectively. Remarkably, an excited isomeric state with an identical energy and a proposed 0^+ spin and parity was reported in [Dij12a], 168 keV above the 2^+_1 state with a half-life of 216(66) ns. Soon after that however, a multi-nucleon transfer reaction experiment, using ^{70}Zn beam impinging on different targets, could not confirm the existence of such a state as no transition of 168 keV was found in (delayed) coincidence with the 2033 keV ground-state transition [Chi12].

The decay data in the current experiment allows for the determination of the precise energy of the excited 0^+_2 state. It is found to be 1605 keV [Fla13], in perfect agreement with the work of [Rec13]. Its half-life could be deduced as well and confirms the value of 270(5) ns [NND13b]. Furthermore, the intensity of the $E0$ transitions that could connect the different 0^+ states have been given upper limits. The lack of clear observation of such hint to a different nuclear structure for the three 0^+ states. New γ transitions have also been established

between some of the other excited and the 0^+ states, inferring tentative (2^+) spin and parity assignments for the former [Fla13].

Interesting to note is that the 0_2^+ states in ^{68}Ni and its counterpart ^{90}Zr ($Z = 40$, $N = 50$) are similar in energy (around 1.8 MeV) and electric monopole strength [Pau10]. The measured $\rho^2(E0)$ for the zirconium isotope could be reproduced by a model that allows for strong $\pi 2p_{1/2}$ and $\pi 1g_{9/2}$ configuration mixing – an evidence for a mixture between the 0_1^+ ground and the 0_2^+ excited state [Pau10]. Although the similarity in the monopole strength is not understood, as the configurations of the 0_2^+ states in $^{68}_{28}\mathrm{Ni}_{40}$ and $^{90}_{40}\mathrm{Zr}_{50}$ come from excitations of a pair of neutrons and protons, respectively, the similarity in energy of the excited states in nickel and zirconium suggests comparable single-particle configurations [Pau10].

2.2 The neutron-rich iron region

2.2.1 Even-even nuclei

The region around the magic $Z = 28$ and semi-magic $N = 40$ numbers is interesting also owing to the experimental evidences, suggesting that with the removal of protons from the $f_{7/2}$ orbital the neutron-rich iron and chromium isotopes have been observed to exhibit increasingly collective behaviour, rather than the semi-magic one expected if the $N = 40$ gap were to be robust. By removing protons from the $1f_{7/2}$ orbital the attractive proton-neutron tensor interaction between the proton-holes and the neutrons in the $1g_{9/2}$ and the $2d_{5/2}$ orbitals comes into play by bringing down the neutron single-particle energies. At the same time the repulsive tensor interaction between the proton-holes and the neutrons in the $1f_{5/2}$ orbital pushes the latter orbital up, further reducing the $N = 40$ sub-shell closure [Ots05]. In other words, the development of collectivity, south from $Z = 28$, is understood as a result of the narrowing of the sub-shell gap, while the enhancement of quadrupole collectivity is due to the increased probability for promoting of neutron pairs across it.

The $\mathrm{E}(2_1^+)$ systematic of the even-even $_{24}$Cr, $_{26}$Fe and $_{28}$Ni isotopes are presented in Fig 2.3. When approaching the $N = 40$ neutron number the chains of iron and chromium isotopes show a rather different behavior, compared to the nickel isotopes. Starting at $N = 36$ and $N = 32$ in iron and chromium, respectively, they both exhibit a drop in the excitation energy of their 2_1^+ states, when quite the opposite is seen for the nickel chain. This decrease in energy is interpreted as an onset of deformation for the two chains. The deformation seems stronger in the chromiums, where the $\mathrm{E}(2^+)$ decreases slightly steeper, compared to the one for iron [Rot11]. The experimental curves also indicate, that the deformation

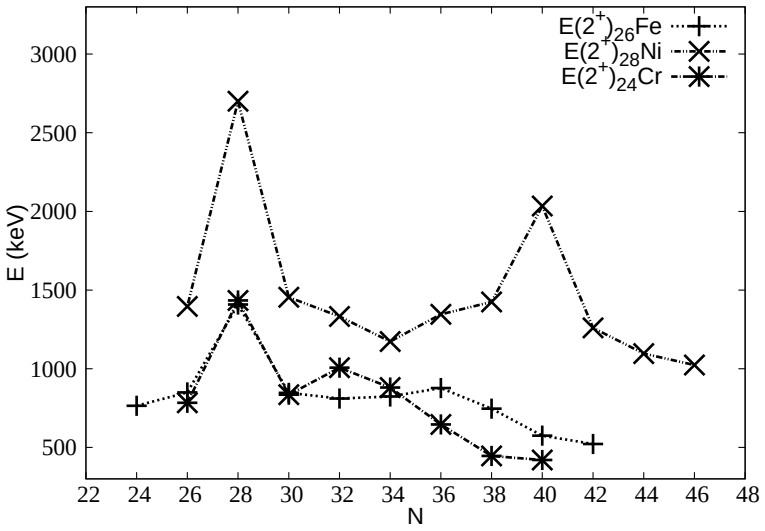

Figure 2.3: Systematic of the first 2^+ excited state in the even-even chromium, iron and nickel isotopes in the vicinity of $N = 28$ & $N = 40$ [NND13b].

and collectivity increases with the increase of N [Gad10, Sor03b].

In the case of the chromium chain, this can be explained by the fact that the $\nu f_{7/2}$ shell is half filled, corresponding to a maximum number of valence protons, therefore an increased probability for excitation of neutron pairs across the already reduced energy gap at $N = 40$.

A collective behaviour for the same neutron-rich isotopic chains can be also inferred by looking into the systematic of the reduced transition probabilities ($B(E2; 2^+ \rightarrow 0^+)$), shown in Fig 2.4 [Rot11]. In the case of the isotopic chain of iron, the $B(E2)$ values are roughly stable from $N = 32$ to $N = 36$. The addition of one more pair of neutrons to $^{62}Fe_{36}$ induces a rapid increase of the $B(E2)$ value in ^{66}Fe (344(33) e^2fm^4 [Rot11]), marking the onset of collectivity.

New experimental results in [Cra13] indicate that ^{68}Fe has the largest measured $B(E2)$ value (355(43) e^2fm^4) in the neutron-rich iron isotopes. Calculations in

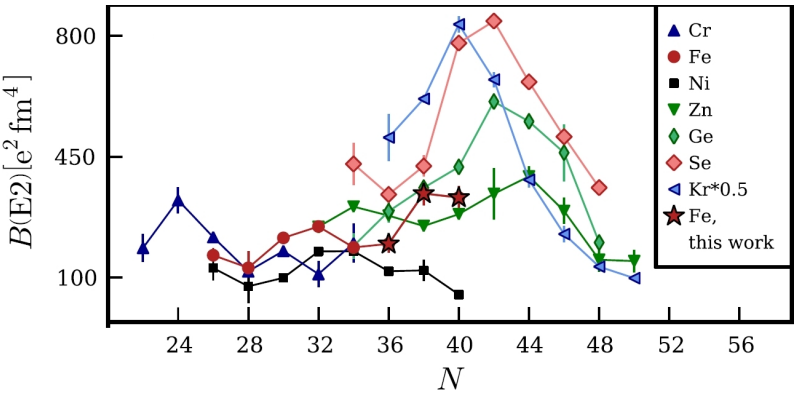

Figure 2.4: Systematics of the $B(E2)$ values in several isotopic chains around $N = 40$ from [Rot11].

the latter reference conclude that ^{62,64}Cr are well deformed with a quadrupole deformation parameter of $\beta = 0.3$ [Cra13].

Contradictory to the previous statements, authors like [Car13], suggest that the ground states of the neutron-rich $^{62-68}$Fe possess a rather dominant spherical configuration. Furthermore, the ratio of the excitation energies between the 4_1^+ and the 2_1^+ states in this isotopic chain is only around 2.4, way below a ratio of 3.3 expected for a good rotor [Hot06]. In contrast to the iron isotopes, however, the ground states of the $^{60-64}$Cr isotopes are associated with a deformed shape in [Car13].

To better understand the onset of collectivity in the neuron-rich iron and chromium chains, large-scale shell-model calculations were performed in [Sor03b, Lju10] using different valence spaces. Only the valence space including the full $fp + 1g_{9/2}2d_{5/2}$ configuration was able to reproduce the low experimental E(2_1^+) excitation energies measured for ^{60,62}Cr [Gad10] and ^{64,66}Fe [Rot11, Cra13]. This demonstrates the major role played by the $2d_{5/2}$ neutron orbital in triggering collectivity in these nuclei.

These conclusions can also be derived from the shell-model calculations performed by Lenzi et al. [Len10], using the LNPS interaction, developed especially for this region. The calculated Effective Single Particle Energies for the valence orbitals at $N = 40$ are shown in Fig 2.5. The figure shows, that with the removal of protons the energy gap between the $1f_{5/2}$ and $1g_{9/2}$ neutron orbitals decreases, making it easier to promote pairs across.

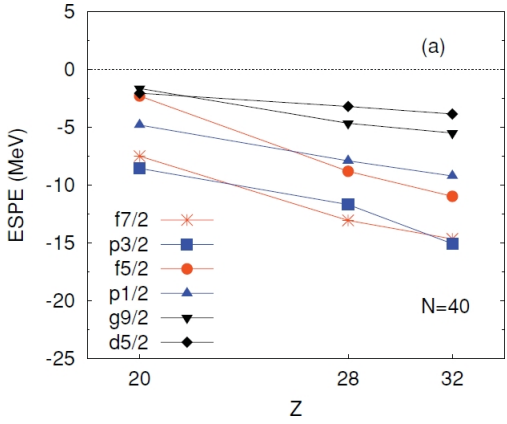

Figure 2.5: Calculated Effective Single-Particle Energies (ESPE) as a function of the proton number Z at $N = 40$ using the $fp + gd$ model space [Len10].

2.2.2 Even-odd nuclei

Such an intriguing picture exists as well for the odd-A isotopes near the $N = 40$ sub-shell and the $Z = 28$ shell-closure.

The excitation energy and the $B(E2)$ values for the first two excited states ($(1/2^-)$ and $(5/2^-)$, respectively) in the heavy ^{69,71,73}Cu isotopes have been measured [Ste08]. The determined excitation energies have been observed to decrease when N increases beyond 40. At the same time the reduced transition probability ($B(E2)$) between the $(5/2^-)$ excited and the $(3/2^-)$ ground state decreases by a factor of three between $N = 38$ and $N = 40$. The $B(E2)$ values between the $1/2^-$ excited state and the ground state, however, increase by a factor of three between $N = 40$ and $N = 42$ and continue to increase further on [Ste08]. These measurements lead to the interpretation that the $5/2^-$ and $1/2^-$ states in the copper isotopes are of single-particle and collective characters, respectively.

A pair of $7/2^-$ excited states have been identified in each of these nuclei as well. The second $7/2^-$ state follows the evolution of excitation energy and the $B(E2)$ values of the 2_1^+ excited state in the neighboring even-even nickel nuclei. Therefore, the former has been interpreted as a single $\pi p_{3/2}$ particle coupled to the 2^+ excitation energy of the nickel core. It may be stated then that different structures coexist in the odd-A copper isotopes – single particle and collective ones. The increase in collectivity in the copper nuclei around $N = 40$ appears

to follow the increase of the occupation of the $\nu g_{9/2}$ orbital. Thus, the gap between the $\pi f_{7/2}$ and the $\pi f_{5/2}$ proton orbitals across the $Z = 28$ shell is observed to rapidly decrease with the addition of neutron pairs in the $g_{9/2}$ orbit [Fra98].
At $N = 46$, the energy gap is so small, that two orbitals are reversed – the ground state becomes the $5/2^-$ spin and parity state in ^{75}Cu [Fla09]. The lowering of the $1/2^-$ state, on the other hand, gives rise to proton intruder isomeric states and also indicates possible shape coexistence in ^{75}Cu [Fla09].

In analogy to the copper isotopes, the isotopes of cobalt ($Z = 27$) are observed to have such characteristics, namely, coexistence of different types of states. Recent experimental results have shown, that the systematic of the energy of the $9/2^-$ state in the odd-A cobalt isotopes and that of the excited 2_1^+ in nickel are much similar beyond $N = 28$ [Pau08a]. The excited $9/2^-$ state is therefore interpreted as a proton hole in the $\pi f_{7/2}$, coupled to the 2_1^+ state of the spherical nickel core. However, a deformed proton-intruder configuration, i.e. a particle excitation across the $Z = 28$ shell closure, was suggested for an excited state only 492 keV above the ground state in ^{67}Co$_{40}$ [Pau08a].

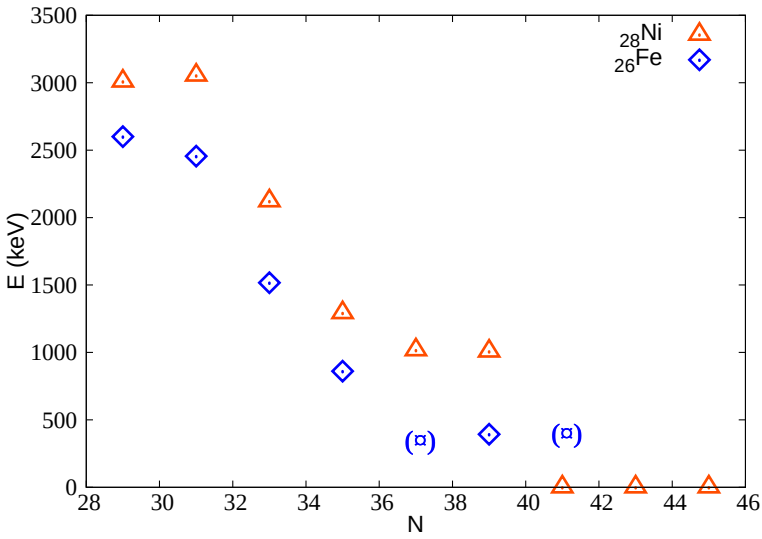

Figure 2.6: Energy systematics of the positive-parity isomeric state in the neutron-rich iron and nickel isotopes [NND13b].

At $Z = 26$, an isomeric state in the odd iron isotopes has been discovered. It is interpreted as an excitation of a neutron in an orbital based on the $\nu 1g_{9/2}$. The systematic trend and the expected lowering of the energy of the isomeric state with filling of the pf-shell, can be seen in Fig 2.6 for the nickel and iron isotopic chains. As the Fermi level rises in the two chains with the addition of each neutron pair, the energy gap between the pf and g orbitals decreases. In the nickel isotopes, after $N = 39$ the positive-parity $g_{9/2}$-state becomes the ground state, expected from a simple shell-model perspective. The excitation energy of the isomeric state in the odd-A iron isotopes, however, levels off at around 400 keV for $N \geq 35$. Prior the analysis of these data, both experimental energies in the figure, substituted by symbols, were not known, although certain experimental considerations constrained the excitation energy at $N = 37$ to no more than 350 keV [Pau09b] and to about 400 keV at $N = 41$ [Dau11].

The scarce experimental information and incomplete systematic on the odd-A iron isotopes, consisting mostly of a couple of excited states with almost no spin and parity information, do not allow for a proper comparison to shell-model calculations. In order to further investigate the nuclear structure of the odd-A iron isotopes, as well as of their even-even neighbours, a dedicated experimental β-decay campaign took place at ISOLDE, CERN.

Chapter 3

Experimental set-up

In a measuring campaign at ISOLDE, CERN, radioactive $^{58,60-68}$Mn nuclei, were produced in a proton-induced fission reaction experiment, where 1.4-GeV protons impinged upon a UC_x target (45 g/cm^2). The reaction products were selectively ionized by the RILIS laser ion source using a three-step ionization scheme [Fed12, RIL13a]. The radioactive nuclei were accelerated over a 60-kV

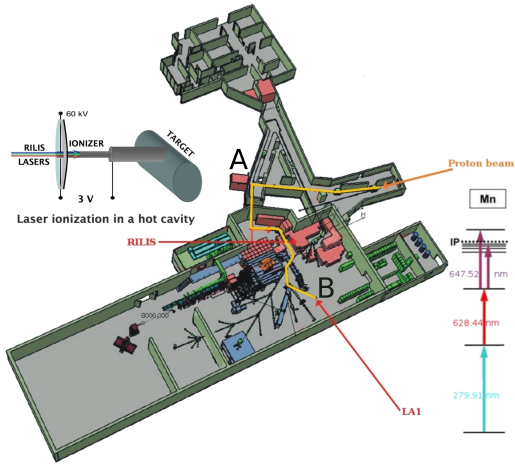

Figure 3.1: The ISOLDE experimental hall (top view): The yellow line follows the path of isotope production (point "A") and transfer of the radioactive beam to the detection system (point "B"). In-sets: target place, where the laser ionization takes place and the used ionization scheme of manganese.

potential difference and mass separated on the basis of their A/Q ratio, through the High-Resolution Separator (HRS) [Rii10] (Fig 3.1). The manganese beam was implanted on an aluminized mylar tape, inside a movable tape station [Pau08b] surrounded by three plastic ΔE β-detectors and two MINIBALL γ-detector clusters [Ebe01, War13] in close geometry, as schematically shown in Fig 3.2. Lead-brass-copper shielding was used to cover the germanium

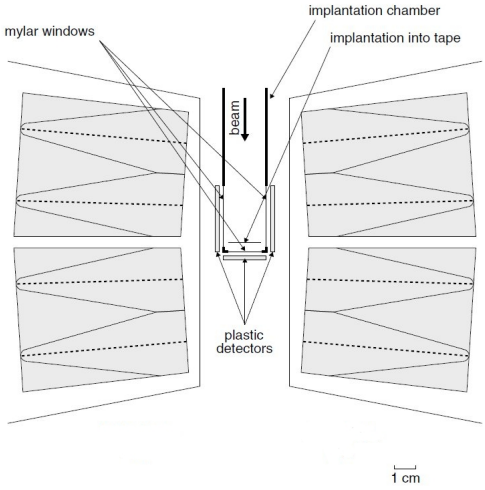

Figure 3.2: Schematic representation of the experimental set-up (top view) from [Pau08b].

detectors in order to decrease the natural gamma- and X-ray background from the surrounding walls, as well as the background produced by the on-line sources, that are moved away by the tape station.

A polyethylene-borax shielding was built around the entire set-up to minimize the effect of neutron-induced gamma radiation at the detection station. The two shielding methods brought the background count rate of the germanium detectors down to around 50 Hz for all six cores when the production target was irradiated with protons.

The germanium detectors were energy and efficiency calibrated, after the experiment, using intensity calibrated ^{60}Co, ^{133}Ba, ^{241}Am and ^{152}Eu gamma sources. The sources, with known activities, were placed at the implantation site on the aluminized tape. During the final stage of the experiment, the radioactive isotope ^{82}Rb was implanted on the mylar tape, with the purpose of

obtaining relative γ-efficiency for high-energy gamma transitions. The deduced relative efficiencies for several transitions were scaled and used as data points in order to determine the efficiency curve up to high excitation energy (see Fig 3.3).

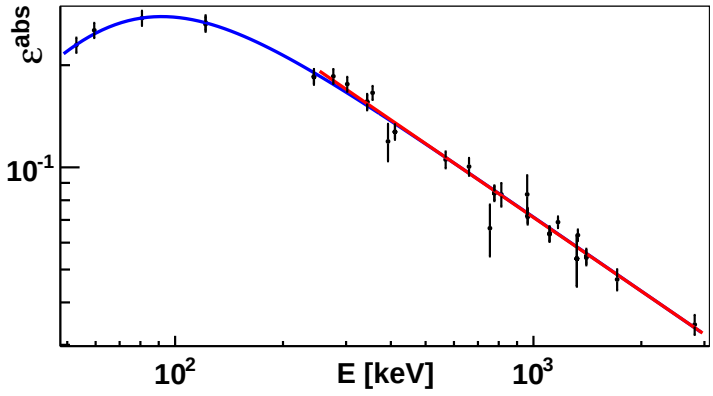

Figure 3.3: Deduced γ-efficiency curve from the calibration sources and the scaled gamma efficiency from the decay of ^{82}Rb. The red curve is used for energies $\geq$ 250 keV, while the blue one defines the photo-peak efficiency in the region below 250 keV.

A full GEANT4 simulation was performed in order to correct the intensities of the gamma transitions from ^{60}Co and ^{152}Eu calibrations sources, in order to account for summing effects in the close-geometry experiment [Ven10]. The photo-peak γ-efficiency for all six germanium detectors we obtain for an energy of 1332 keV is 5.8(1)%.

The experimental data was recorded on an event-by-event basis using digital electronics, with no hardware trigger applied. The trigger-less recording provides the flexibility for off-line software sorting of the data, allowing for setting gates outside the prompt time windows and the search for isomeric states. The digitally obtained, prompt coincidence time window for β-γ coincidences is from 0 to 600 ns, while the prompt window for γ-γ coincidences is from -700 to +700 ns. The large prompt windows are due to digitization, see Figures A.1 and A.2, respectively.

The analysis of the decay data was performed, using the software ROOT [Bru97]. The data were structured in singles, β-gated and γ-gated trees, where the gated trees require gamma-events, that are coincident with either a β-event from any of the three scintillator detectors (for the β-gated) or a gamma-ray in any core of the MINIBALL detectors (for the γ-gated).

The beta detection efficiency (ε_β) can be determined for each experimental decay set of nuclei with the same mass number. It is defined as the ratio between the number of counts in γ_i, in the beta-gated, prompt, gamma-spectrum to the number of counts in γ_i in the singles' gamma-spectrum. Previous experiments indicate that the expectation value for ε_β is around 50%, for beta-decay Q values higher than 5 MeV [Pau08b] as shown in Fig 3.4. The LISOL decay station coupled to MINIBALL detectors was already successfully used to study the decay of the neutron-rich cobalt isotopes, that will be discussed in later chapters and the reader is referred to [Iva07] for a complete description of the set-up.

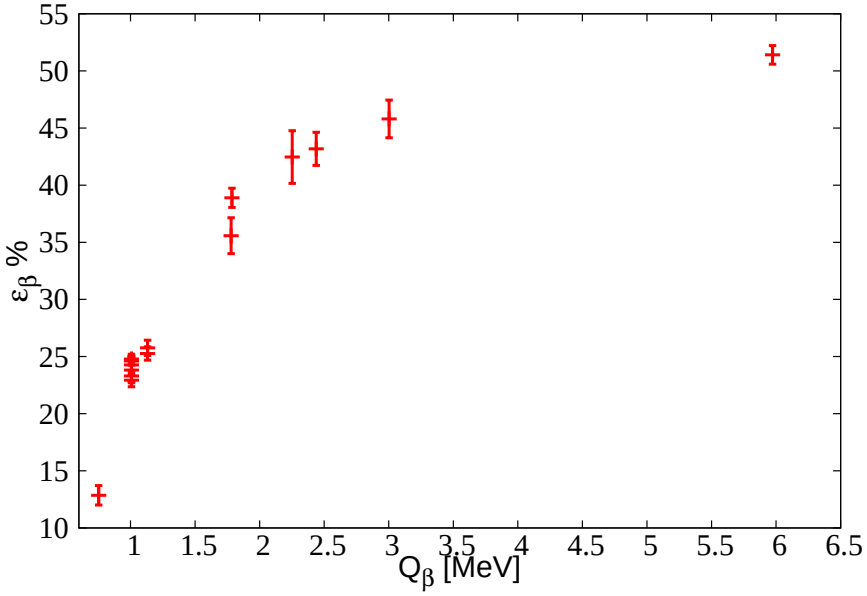

Figure 3.4: Combined beta efficiency of the three ΔE plastic scintillator detectors as a function of Q_β endpoint energy [Pau13].

During the analysis of the data, it was observed, that the experimentally deduced

value for the beta efficiency was not always around 50% as expected, but rather fluctuating between 34% and 52%, depending on which decay set was analyzed. It was established, that the efficiency of the middle detector (see Fig 3.2), though not affected by different Q_β values, is affected by the count rate in it. This experimental observation is presented in Fig 3.5, where for each count rate (or

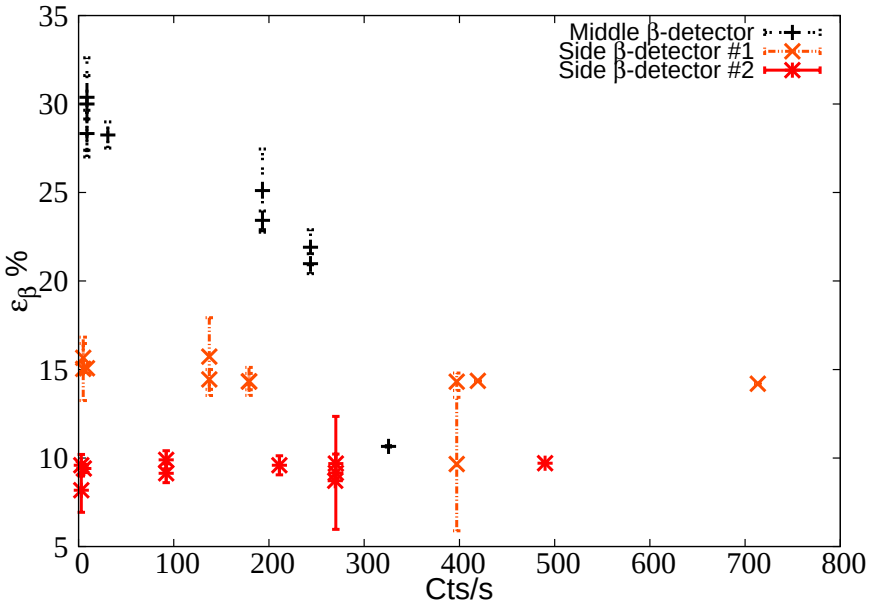

Figure 3.5: Beta efficiency with respect to the count rate in each scintillator detector, for different masses and Q_β values.

mass) in the same colour, the different points, correspond to different decays in the mass chain (different Q_β values). Because of this dependence with respect to the change in the count rate, a weighted average value, is obtained for the sum of the two side detectors in each decay set and used as a beta efficiency for the further analysis.

The acquisition of the decay data was based on the CERN super cycle structure. A super cycle (SC) contained from 37 to 49 proton pulses (PP) with a certain sequence, distributed with a difference of 1.2 s between each of them. The

proton pulses with respect to the SC signal for each odd mass can be viewed in figures: A.3, A.7, A.10 and A.14 in the Appendix. After each PP a delay time was introduced, before the separator beam gate was opened, to let the radioactive beam implant on the tape. The delay time was introduced to suppress the implantation of the isobaric contaminant gallium, which is surface ionized and released very fast. The manganese ions are released slower, but the production rate is so high, that only a small implantation time is needed in order to not overload the detectors. Details regarding the experimental settings in each decay set is given in Table 3.1

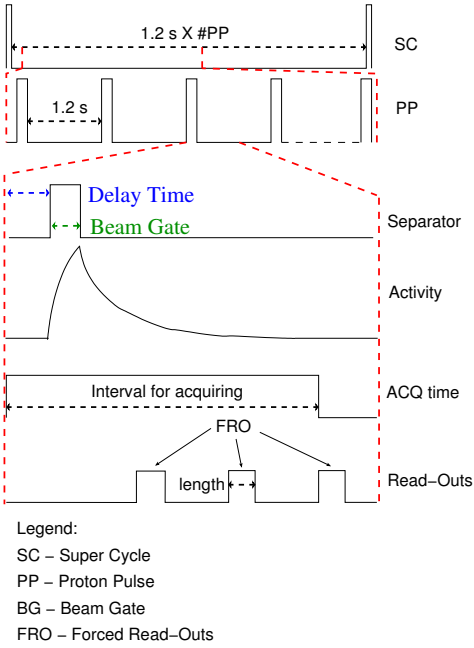

Figure 3.6: Schematic structure of the CERN proton super cycle and decay data taking.

For certain data files, due to the high yields of manganese [RIL13b], controlled forced read-outs of the digital buffers were used, in order to allow for a proper fit of the half-life of manganese, by requesting the read-outs before the buffer was filled and at precise times during the acquisition time. An overview of the measuring cycle is given in Fig 3.6, while the experimental details per each mass are summarized in Table 3.1. Before a new SC starts, the tape is moved

A	LON (s)	LOFF (s)	D (ms)	I (ms)	FRO	ACQ (s)	Ions/s
61	1531	170	10	5	YES	1	2600
63	7014	1174	10	10	YES/NO	1	1000
65	22421	4685	1	100	YES	2.2	300
67	32180	6896	0	100	NO	2.2	10

Table 3.1: Experimental details in each of the decay data sets: Implanted mass (A), Laser-on time (LON), Laser-off time (LOFF), Delay (D) before implantation, Implantation (I) time, whether Forced-Read-Out was present (see text and Figure 3.6), ACQuisition time and calculated yield of manganese ions per second, using the number of counts in the area of the strongest transitions in each decay, accounted for the absolute branching as deduced from the constructed decay schemes of manganese and including the calculated P_n branch.

and a new implantation-decay cycle begins.

Laser ionization provides a clean and efficient method for selecting radioactive isotopes of interest [Fed12]. In combination with a proper implantation-decay time structure and high-resolution mass separation source purity of almost 100% can be achieved. This enables the possibility to follow the decay of the respective daughters and draw conclusions on the completeness of the decay schemes, addressing missed gamma-ray intensity and direct ground-state feeding. In the following chapters, the present knowledge of the odd-mass ^{61}(Fe), ^{63}(Fe, Co, Ni), ^{65}(Fe, Co, Ni) and ^{67}(Fe, Co, Ni) isotopes is presented, followed by the results for the neutron-rich manganese beta-decay chains obtained in this study.

Chapter 4

Results for the decay chain of $A = 61$

4.1 Previous experimental information on ^{61}Fe

Although the nucleus ^{61}Fe is close to the stability line, the information on its level scheme is quite limited. A beta-decay experiment of ^{61}Mn identified three excited states with energies 207, 391 and 629 keV [Run85]. The decay scheme was built on the basis of energy sum-relations and the time behavior of the intensity of the observed transitions. The ground state of ^{61}Mn was assigned $(5/2^-)$ [Run85] and a recent value of its half-life was reported to be $T_{1/2} = 0.62(1)$ s [Han99]. The beta-delayed neutron branching was determined to be 0.6(1)% of all ^{61}Mn decays [Han00].

The direct ground-state beta feeding of ^{61}Mn to ^{61}Fe was calculated, using time analysis of beta and gamma intensities from the decays of ^{61}Mn, its daughter, and granddaughter, and amounts to 74% [Run85]. The obtained logft value of 4.4 for the ground state points to an allowed Gamow-Teller transition from $\nu f_{5/2}$ to $\pi f_{7/2}$ and restricts the spin and parity to $(3/2^-, 5/2^-)$, based on the determined low logft value [Run85]. The most recent half-life value of the ground state of ^{61}Fe is reported to be 5.98(6) min [Bro75], consistent with previous measurements. The excited state at 629 keV was previously identified as 620(20) keV [Cos77] in a ^{64}Ni(α,^{7}Be) reaction.

A new level with an isomeric character was identified in two reaction studies [Bro98, For94]. Its energy was reported to be 862 keV and the measured half-life – $T_{1/2} = 0.22$ μs. The existence of such a state, with a half-life of $T_{1/2} = 0.25(1)$

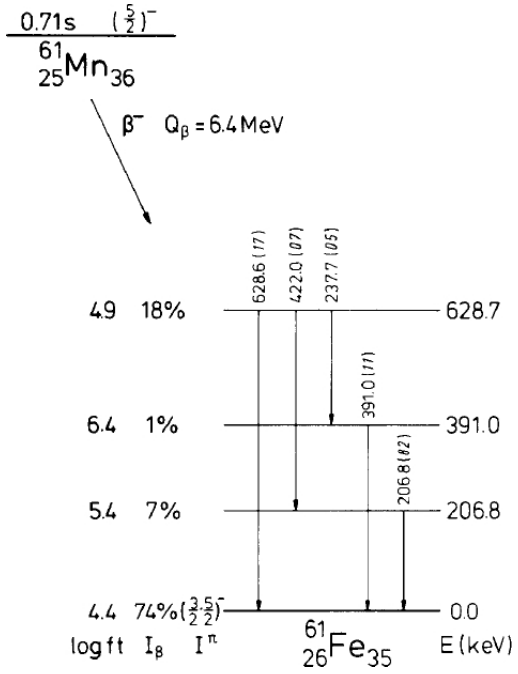

Figure 4.1: Decay scheme of ^{61}Mn deduced by Runte et al. [Run85]. The Q_β value in the plot is different from the one found in literature (7.2 MeV [NND13b])

μs [Grz98], was confirmed in a later fragmentation experiment, using an ^{86}Kr beam on a ^{nat}Ni target. It was proposed that its spin and parity are $(9/2^+)$, originating from the excitation of a neutron to the $g_{9/2}$ shell-model orbital. The state was found to decay to the previously observed excited state at 207 keV, with a transition of 654 keV. Because of its half-life, the transition was assigned an $(M2)$ multipolarity [Grz98]. The $9/2^+$ spin and parity have been confirmed together with the multipolarities of the cascade transitions in two fragmentation experiments, aiming at measuring the magnetic and quadrupole moment of that state [Mat04, Ver07], respectively. In both cases, ^{61}Fe was produced at GANIL in a reaction of ^{64}Ni on a ^{9}Be target. The extracted gyromagnetic factor in the former work [Mat04] is -0.229(2), consistent with shell-model calculations for a $9/2^+$ spin and parity.

The half-life of the isomeric state was determined with a better precision: 239(5) ns [Mat04]. The spectroscopic quadrupole moment was determined to be $|Q_s| =$

41(6)$e$fm^2 [Ver07]. A perturbed angular distribution function analysis [Ver07] concluded that the 207-keV transition has a $M1$ multipolarity, while the 654-keV one has $M2$. Prolate deformation was suggested for the isomeric state and possible excited states on top of it, analogous to experimental data for ^{57,59}Fe [Nat78, War77].

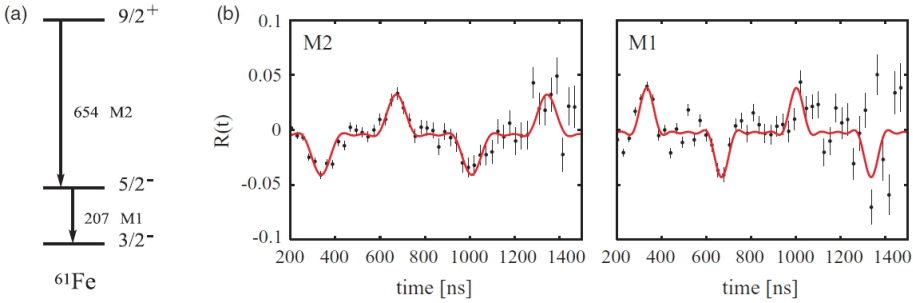

Figure 4.2: The 654-207-keV cascade in ^{61}Fe (a) and the theoretical fit of the angular correlation function (b), for each transition – M2 for 654 and M1 for 207 keV [Ver07].

The reduced transition probability, $B(E2)$, for the 207-keV line was determined in a Coulomb-excitation experiment to be 17(7) W.u. [Wal09].

The yrast and near yrast structure of ^{61}Fe was revealed in two experiments [Lun07, Hot08], using ^{64}Ni beams on ^{238}U targets at LNL, Legnaro and ANL, Argonne, respectively. In the first case, four transitions were observed. A transition of 752 keV, coincident with the 207 keV, defined an excited state at 960 keV, while two other transitions, a 788 keV and a 1341 keV, were found to be coincident with each other, but not with the former two gamma rays.
It was proposed that the latter two defined yrast states above the known isomeric state and were interpreted as a coupling of the 2^+ and 4^+ states in ^{60}Fe with a $g_{9/2}$ neutron, which gives rise to states with spins and parities of $13/2^+$ and $17/2^+$, respectively [Lun07]. It was noted that the observation of such a decoupled band, on top of the $9/2^+$ level, is consistent with a prolate deformation of β_2=0.24, suggested for the isomeric state on the basis of the measured quadrupole moment and of mean-field calculations in [Ver07].

In the second experiment, [Hot08], new excited states were populated, while an angular-correlation analysis firmly set the multipolarities of many transitions, including the 655-207-keV cascade. The yrast states at 1650 and 2993 keV, built

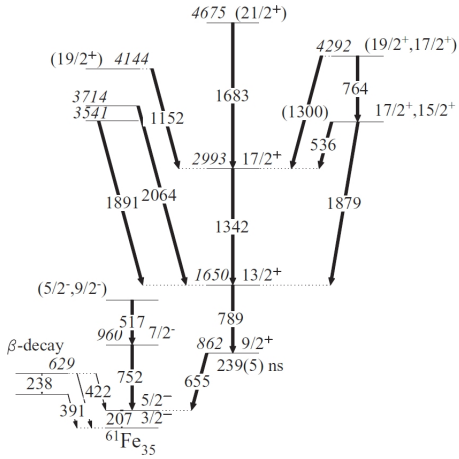

Figure 4.3: Excited states, populated in the work of Hoteling et al. [Hot08]. The states at 629 and 391 keV were not populated in that experiment. Spins and parities without brackets are firmly defined by angular correlation analysis.

on top of the 862-keV level and decaying by the observed coincident transitions 789 and 1342 keV, have been assigned as $13/2^+$ and $17/2^+$ on the basis of angular correlations.

4.2 Results for ^{61}Mn decay

Experimental Details

Decay data corresponding to a total measuring time of 1531 s with the lasers set on resonance for manganese ionization and 170 s without lasers (Laser-off) were recorded. The dead time of the acquisition system was determined with the aid of a pulser in a channel of the digital ADC, set to a frequency of 100 Hz. Laser ionization provides a clean and efficient method for selecting radioactive isotopes of interest. In combination with a proper implantation-decay time

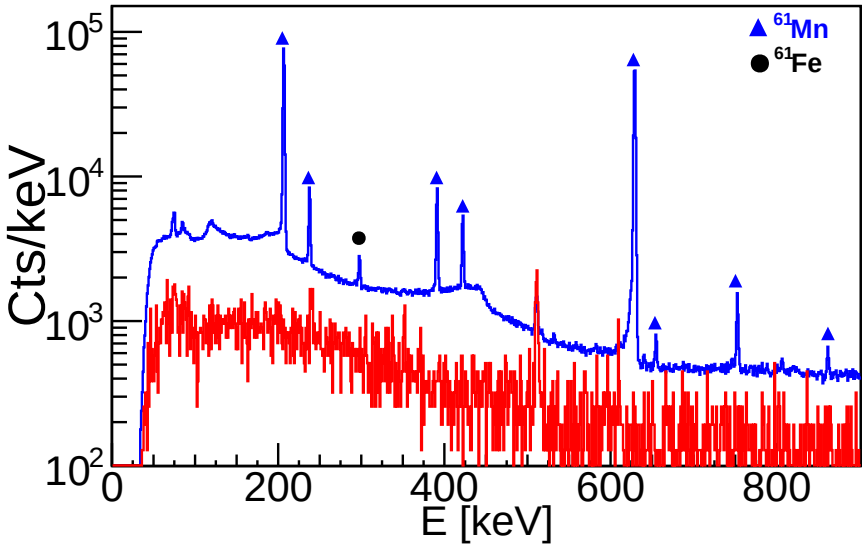

Figure 4.4: Selected part of the singles γ-spectrum when the separator was set to mass 61. Lasers-on (in blue) is compared to a Laser-off spectrum (red – scaled for visual comparison ($\sim$ 8 times)) in the same experimental conditions. Triangles indicate ^{61}Mn lines, while the circle indicates a line following ^{61}Fe decay.

structure and high-resolution mass separation, source purity of almost 100% can be achieved, as in the case of ^{61}Mn. This enables the possibility to follow the decay of the respective daughters and draw conclusions on the completeness of the decay schemes, addressing missed gamma-ray intensity and direct ground-state feeding.

A representative picture of the quality of the data in singles is shown in Fig 4.4, where all of the visible transitions were identified as following the decay of ^{61}Mn and its daughter (the very low background conditions in the experiment can be appreciated in the laser-off singles spectrum, drawn in red).

Half-life Determination

The structure of the data taking allowed for the determination of the half-life of ^{61}Mn, as well as for the identification of new transitions in ^{61}Fe following the decay of ^{61}Mn, through their decay behavior. The intensities of the strongest gamma transitions following ^{61}Mn decay, in different time periods with respect to the PP signal (Fig 4.5), were fitted with an exponential decay function. The

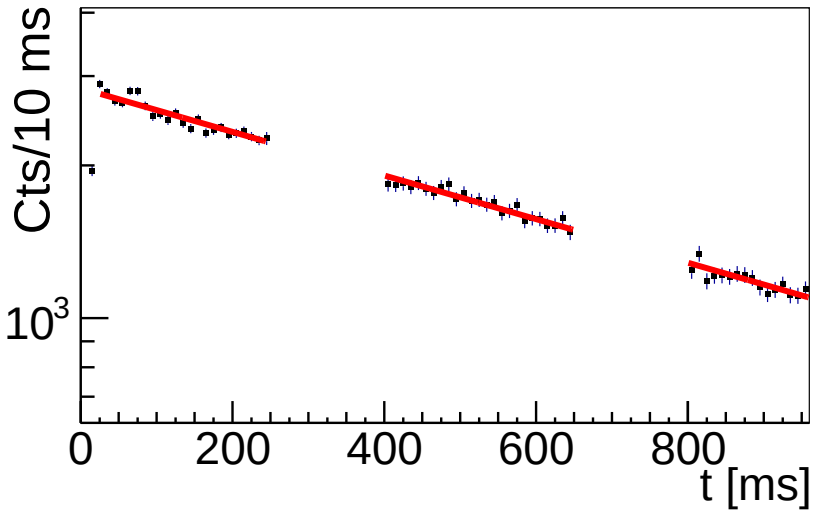

Figure 4.5: Exponential decay fit on the time behavior of the 629-keV transition. Each data point contains the integrated number of counts in the peak area for the selected time interval with respect to the ISOLDE proton pulse signal. Points inside the time intervals 0-20 ms (implantation of the radioactive ions), 250-400 ms (forced read-out) and 650-800 ms (forced read-out), are omitted from the fit.

data point for each time slice corresponds to the number of counts in the peak area of the investigated gamma transition following manganese decay, deduced from a Gaussian fit including a constant background. The fits yield a weighted average value of $T_{1/2} = 0.708(8)$ s for the half-life of ^{61}Mn, consistent with the

value adopted by NNDC – $T_{1/2} = 0.67(4)$ s [NND13b].

Note, the uncertainty on the half-life value is only statistical and that a possible constant background contribution to the points in the decay histogram, which would bring the half-life value down, is not taken into account by the exponential fit, since it is difficult to be estimated from the experimental data.

Decay scheme

In order to build the decay scheme of ^{61}Mn, gamma-gamma coincidence gates were placed on the lines identified, through their half-life, as belonging to ^{61}Mn decay. The intensities of the weak transitions, not observed in singles, but observed in coincidence with a strong transition in ^{61}Fe, were calculated using the coincidence data. Example coincidence spectra, gated on the three strongest

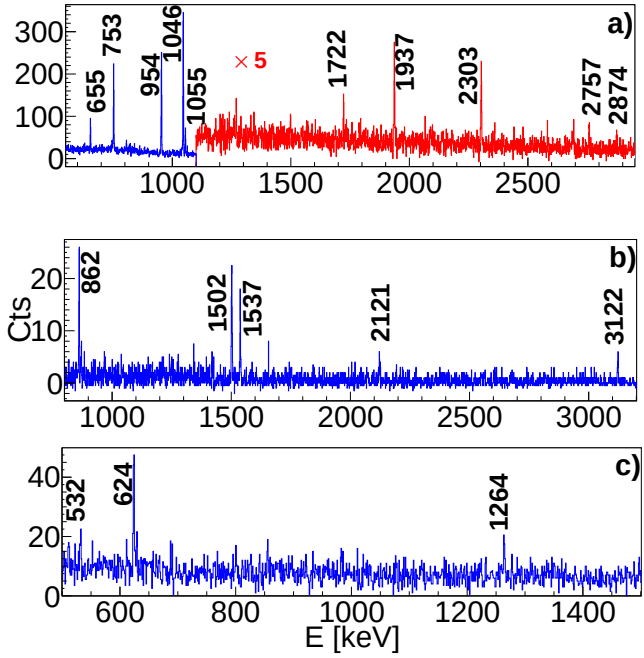

Figure 4.6: Prompt gamma-gamma-coincidence spectrum, gated on (a) the 207-keV, (b) the 391-keV, and (c) the 629-keV transitions. The energies of the strongest coincident transitions are indicated in keV.

transitions in the decay, are presented in Fig 4.6. The analysis of the decay

data revealed 48 gamma transitions, distributed over 20 excited states in ^{61}Fe.

The isomeric $9/2^+$ level at 862 keV was observed in this decay study, evidenced by the observation of the 655-207-keV cascade in beta-triggered delayed-gamma coincidence. A combination of two spectra with different time gates is shown in Fig 4.7. A subtraction remnant of the strongest transition in ^{61}Fe is visible next to the 655-keV transition.

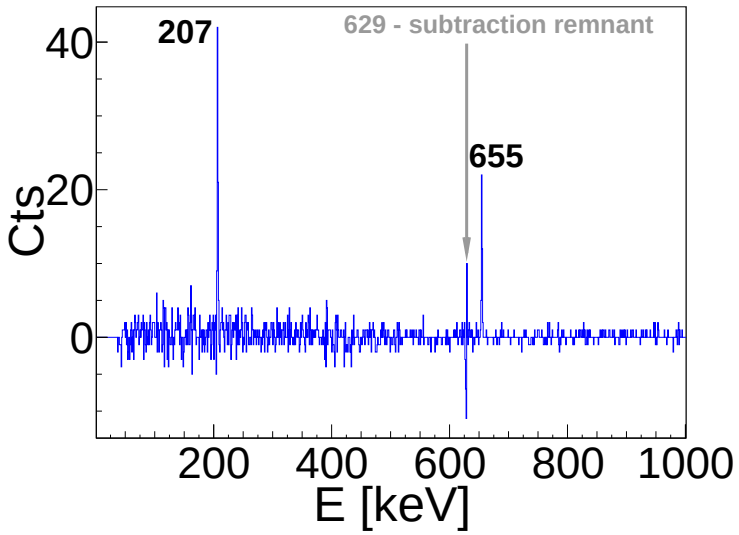

Figure 4.7: The decay of the 239(5)-ns, $9/2^+$ isomer. Selected part of the beta-triggered delayed-gamma spectrum with conditions: gamma-rays in 700 – 1420 ns time interval with respect to a beta-event (outside the prompt window); a spectrum in the time interval 2500 – 3220 ns (randoms) was subtracted.

The identified gamma transitions that belong to ^{61}Mn decay, their relative intensities and coincidence relationships can be inspected in Table 4.1.

Table 4.1: Gamma transitions and their relative intensities, following the decay of ^{61}Mn, identified in this study together with gamma transitions observed in coincidence. The asterisk, "$*$", indicates that the transition was not seen in the singles' spectrum, but its intensity was calculated using the coincidence data.

E_γ (keV)	Relative I_γ%	Observed coincidence transitions (keV)
201.6(5)*	0.24(4)	753
206.8(1)	54(2)	422, 655, 753, 807, 954, 1046, 1055, 1185, 1270, 1498, 1722, 1937, 2090, 2303, 2757, 2874
237.8(1)	4.61(6)	391
391.2(1)	7.37(9)	238, 862, 1502, 1538, 2120, 3122
422.2(1)	4.55(8)	207
517.9(5)*	0.12(4)	753
531.5(3)	0.15(4)	629
624.0(5)*	0.77(8)	629
629.0(1)	100	532, 624, 1264
640.5(3)	0.18(5)	1046, 1253
654.7(1)	0.56(6)	207
752.6(1)	1.89(6)	202, 207, 518, 1185, 2090
806.6(3)	0.21(5)	207
861.5(1)	0.49(5)	391
954.1(1)	2.88(9)	207
959.4(2)	0.43(12)	2090
982.4(5)*	0.22(8)	1161
1013.0(1)	1.30(7)	1131, 1498
1046.0(1)	4.49(9)	207, 641
1055.3(1)	1.05(7)	207
1130.6(1)	0.65(7)	1013
1161.0(1)	6.15(11)	982, 1351
1184.6(5)*	0.23(7)	207, 753
1239.7(1)	0.53(8)	1270
1252.9(1)	3.66(10)	641, 1259
1258.5(5)*	0.26(12)	1253
1262.7(1)	0.54(15)	—
1263.7(5)*	0.63(10)	629

1270.4(1)	0.71(15)	207, 1240, 1572
1350.8(5)*	0.31(10)	1161
1498.3(5)*	0.25(4)	207
1498.3(5)*	0.18(7)	1013
1501.7(1)*	0.76(9)	391
1537.7(1)	0.36(6)	391
1571.9(3)	0.24(7)	1270
1722.1(2)	0.29(6)	207
1893.9(3)	0.57(14)	—
1928.9(2)	0.86(12)	—
1936.8(1)	0.90(11)	207
2089.6(5)*	0.35(10)	207, 753, 959
2120.3(5)*	0.25(6)	391
2143.7(1)	5.54(14)	—
2303.5(1)	1.18(9)	207
2510.5(1)	2.86(12)	—
2757.4(5)*	0.37(7)	207
2873.7(3)	0.26(9)	207
3079.2(3)	0.34(10)	—
3122.1(4)	0.32(9)	391
1690.2(5)$^\diamond$	0.19(6)	
1738.5(5)$^\diamond$	0.15(6)	
1846.7(5)$^\diamond$	0.16(5)	
3146.1(10)$^\diamond$	0.26(10)	

Table 4.2: Table.4.1 continued. The diamond, "$\diamond$", indicates unplaced transitions. For absolute intensity, multiply by 0.363(7) ($= \frac{100 - \text{direct feeding of g.s.}}{\sum I(\gamma+EC) \text{ to g.s.}}$).

β-delayed neutron branch

An upper limit for the beta-delayed neutron branching of ^{61}Mn to the first-excited state in ^{60}Fe was determined using the upper limit of the number of counts in the area of the 824-keV ($2^+ \rightarrow 0^+$) transition in ^{60}Fe, as this line was not observed in singles. From this, the limit for the direct beta-delayed neutron feeding to this excited state is deduced to be $P_n \leq 0.2\%$. The total beta-delayed neutron branch could not be determined due to the long half-life of ^{60}Fe ($T_{1/2}$ = 1.5×10^6 y [NND13b]).

Hannawald [Han00] reported a total P_n value of 0.6(1)%. In view of the narrow window between the Q_β value of 7.18 MeV [Wan12] and the neutron separation energy (S_n) of 5.58 MeV [NND13b], the two values could be consistent. Hence, a value of P_n = 0.6(1)% is used further on.

Direct beta-decay or missed gamma transitions, feeding the ground state of ^{61}Fe

Making use of the high purity of the produced ^{61}Mn sources it is possible to connect the intensities of all placed gamma transitions in the mother decay to the intensities of the placed gamma transitions in the daughter decay.
For certain cases in this region of the nuclear chart, the decay chains can be quite complicated, due to the short half-lives and also the beta-delayed neutron decay channel can be important.

The intensity balance is a strong test for judging the completeness of the obtained decay schemes and for determining the amount of direct beta feeding towards the ground state or the amount of missed ground-state gamma rays. Before a complete intensity balance can be made, and thus the absolute branching ratios deduced, it is convenient to define a new coefficient α for each beta-decaying state in the decay chain, following the decay of the manganese parent. It is the ratio between the efficiency-corrected number of counts of the strongest ground-state gamma transition feeding the beta-decaying state of the daughter nucleus, relative to the sum of the efficiency-corrected number of counts of all identified ground-state transitions in the daughter nucleus. As stated earlier, α is used only for convenience to determine the total number of gammas decaying towards the ground state in each decay and can be substituted with the total number of counts in all identified ground-state transitions in the corresponding decay. The intensity of the ground-state transitions used for comparison is corrected for electron-conversion coefficient where needed. In the case of the beta decay of ^{61}Mn, the strongest transition is the 629-keV line and the calculated coefficient is α_{Mn} = 55(1)%. Two methods were used to calculate the (beta and/or missed

gamma) ground-state feeding in ^{61}Fe.

Method.1 Using the full acquisition cycle and the information from the beta detectors:

In this first method, the decay information from the whole acquisition cycle in this study is used, thus including the decay of ^{61}Fe in addition to the decay of ^{61}Mn.
No direct beta feeding from the $(3/2^-, 5/2^-)$ ground state of ^{61}Fe [Run85] to the $7/2^-$ ground state of ^{61}Co has previously been observed [Ehr67]. Using the normalization factor adopted in the NNDC evaluation to obtain the absolute intensity per 100 decays (0.436 ± 0.045 [NND13b, Bha99]), the α_{Fe} value for the 1027-keV ($3/2^- \rightarrow 7/2^-$, I$\gamma = 98(5)$ [Bro75]) ground-state transition, becomes 43(5)%.
A simplified scheme of the $A = 61$ decay chain can be seen in Fig 4.8. The beta-delayed neutron branch of ^{61}Mn is adopted to be 0.6(1)% and

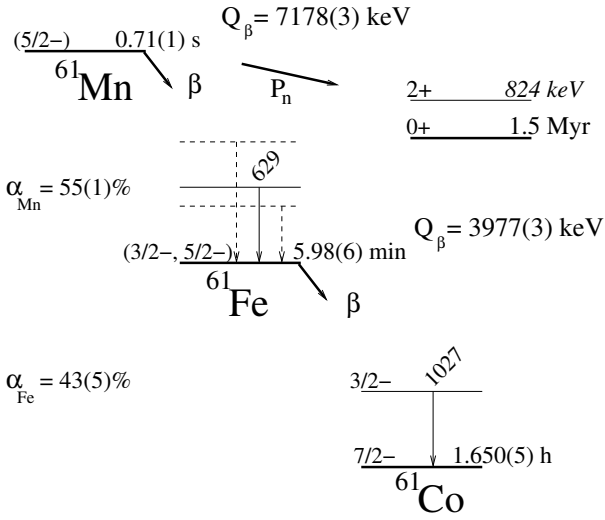

Figure 4.8: Schematic representation of the $A = 61$ decay chain. All data but the half-life of ^{61}Mn and the calculated α_{Mn} are from [Bha99], while the Q_β values are taken from [Wan12].

is ignored in the calculation.
The apparent number of ^{61}Mn and ^{61}Fe decays, based on gamma detection, is calculated using the efficiency-corrected number of counts of the 629-

and 1027-keV transitions in singles, respectively, and the α_{Mn} and α_{Fe} coefficients.
Using the experimental beta efficiency of the ΔE plastic scintillators [ε_β = 23.8(2)%], the total number of manganese plus iron decays, based on beta radiation, can also be extracted (= $N_\beta^{total}/\varepsilon_\beta$, where N_β^{total} is the number of beta-triggers in the whole acquisition cycle, corrected for the time-normalized number of beta counts in the laser off file(s)). The feeding of the ^{61}Fe ground state, due to missed gamma rays or direct beta feeding, is then deduced out of the comparison of the number of ^{61}Mn and ^{61}Fe decays from beta- and gamma-rays. This results in a value of **33(1)%**.

Method.2 Single event data in different times, with respect to the proton pulse impact:

In the second method, only information of the first proton pulse in the super cycle is taken into account, in order to minimize the amount of ^{61}Fe decays. The beta-delayed neutron branch of ^{61}Mn is once again ignored for the calculation.
A gamma spectrum with time constraints in the first proton pulse is created (see Fig A.3). Due to the long half-life of the ground state of ^{61}Fe with respect to the acquisition time of 1 s, no transition following its decay is observed. This means, that the intensity of the 629-keV line and the α_{Mn} factor can be used to calculate the apparent number of ^{61}Mn gamma decays and again be compared to the number of decays extracted from the beta counts in the same time constraint. The obtained value for the missed feeding is **32(1)%**.

The agreement between the results obtained using the two methods shows that the relevant information on the decay chain of $A = 61$ (constructed decay scheme of ^{61}Mn and published decay scheme of ^{61}Fe) is consistent. The adopted value of 33(1)% is given in the decay scheme as the direct beta feeding to the ground state of ^{61}Fe, although one should realize that this is only an upper limit due to missed ground-state gamma transitions.

The direct beta-decay feeding of each excited level is calculated from the intensities of its feeding and de-exciting transitions and can be seen in Table 4.3. Important to note here is the fact that the calculated beta-feeding listed in the latter table should be considered as upper limits, owing to the high Q_β value for that decay, even though several lines with energies above 2.5 MeV are observed, with relative intensities below 0.5% (see Table 4.1). The complete ^{61}Mn decay scheme is presented in Fig 4.10, where the excited levels marked in red were observed in other experiments [Run85, Grz98, Hot08]. All gamma rays observed in this study as belonging to the decay of ^{61}Mn are given in Table

E (keV)	I_β (%)	logft	$T_{1/2}$	J^π
GS	33(1)	5.02(3)	5.98(6) min [Bro75]	$3/2^-$
206.8	12.6(8)	5.38(3)		$5/2^-$
391.2	< 0.28	> 7.3		$(1/2^-)$
629.0	39.0(6)	4.77(1)		$(3/2^-)$
861.5	< 0.22	> 7.1	239(5) ns [Mat04]	$9/2^+$
959.5	0.49(7)	6.6(1)		$7/2^-$
1013.0	< 0.30	> 7.0		$(1/2^-)$
1160.9	3.23(9)	5.68(1)		$(5/2^-)$
1252.8	3.25(9)	5.64(1)		$(3/2^-)$
1262.3	0.57(6)	6.40(5)		
1477.2	< 0.17	> 7.3		$(9/2^-)$
1705.1(5)	< 0.11	> 7.1		
1893.0	0.78(7)	6.04(4)		
1928.9	0.55(5)	6.18(4)		
2143.6	2.7(1)	5.40(2)		
2510.6	1.8(1)	5.43(2)		
2716.8	0.19(3)	6.32(7)		
2963.9(4)	0.13(2)	6.37(7)		
3049.1(2)	0.21(5)	6.12(11)		
3080.2(3)	0.22(5)	6.09(10)		
3513.3(4)	0.12(3)	6.14(11)		

Table 4.3: Identified levels, their calculated beta-feeding intensities and logft values in the decay of ^{61}Mn. The uncertainty on the level energy is better or equal to 0.1 keV, if not specified. Half-lives of the excited states are given, where information is available.

4.1, together with the gamma rays in coincidence.

Following the presentation of preliminary results of this study at the ARIS-2011 conference, Waite et al. [Wai] reexamined the same deep-inelastic-scattering (DIS) data set used in [Hot08] in the study of high-spin positive-parity levels that populate the $9/2^+$ level in ^{61}Fe. A general characteristic of DIS reactions is the population of yrast and near-yrast states; as the 207-keV, $(5/2^-) \rightarrow (3/2^-, 5/2^-)$ transition is yrast, double gates were systematically set on all transitions identified in this decay study as populating the level. Extensive high-spin structure was observed above the 1477-keV level and one additional transition was observed populating the 1161-keV level. This will further be used to narrow down the spin assignments.

The ^{61}Mn decay scheme.

Expected shell-model configurations for neutrons and protons, in this region, primarily involve the $\nu(p_{3/2}, f_{5/2}, p_{1/2}, g_{9/2})$ and $\pi(f_{7/2})$ orbitals, respectively. Having an even number of neutrons and with three proton holes in the $\pi f_{7/2}$ orbital, one would expect a $7/2^-$ ground state for the odd-A manganese isotopes. The experimental information shows that this is not the case. In fact, the only isotope to exhibit such a spin and parity of its ground state is the neutron closed-shell nucleus $^{53}Mn_{28}$ [NND13b] (see Fig 4.9).

One of the first attempts to describe the observed spins and parities of the ground states of the manganese isotopes was done in [Com71], in a model using a deformed representation of a single particle in the Nilsson orbitals coupled to a rotor. It was shown that this model describes significantly well the isotopes of ^{55,56}Mn. The ground state was calculated to be $5/2^-$ and a deformation of $\beta \sim 0.27$ was assigned to it. These experimental observations have been addressed also in the work of Paar [Paa73], where a model that describes the excited states in a nucleus with three particles or holes outside a single-closed shell has been discussed. The calculated nuclei are represented as a three-hole cluster, coupled to the low-frequency quadrupole vibration of ^{58}Ni. The agreement in the description of the isotopes of ^{51,53,55}Mn was improved.

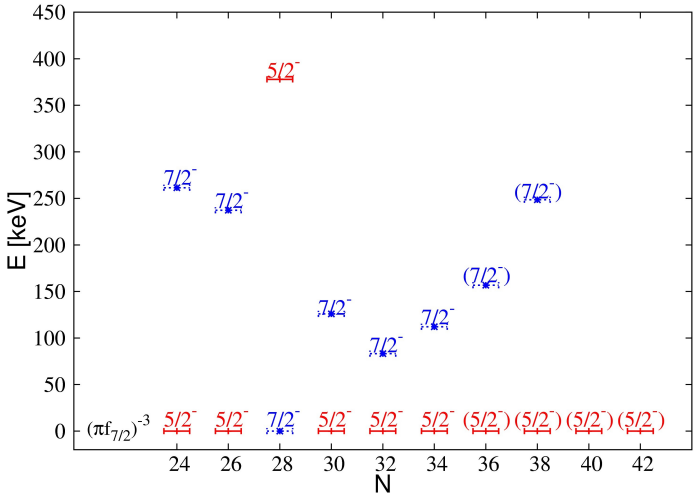

Figure 4.9: Systematics of the ground state and first excited state in odd-A $^{49-67}Mn_{24-42}$ isotopes [NND13b, NND13a].

The trend of $5/2^-$ spin-parity for the ground state and $7/2^-$ for the first-excited state is very well reproduced by recent shell-model (GXPF1A) calculations [Cha10], where excellent agreement for the odd-mass $^{51-55}$Mn isotopes is obtained.
For the further spin and parity discussion, it is interesting to compare the obtained decay scheme of ^{61}Mn and the levels in ^{61}Fe with the information on the $A = 59$ decay chain.

The beta decay of ^{59}Mn has been investigated in [Oin01]. Allowed beta transitions from the $5/2^-$ ^{59}Mn ground state were observed to the ground state of ^{59}Fe and three low-lying excited states at 473, 571, and 726 keV. In a neutron-transfer experiment, ^{58}Fe(d,$p\gamma$)^{59}Fe [McL72], different states in ^{59}Fe were populated. Using the experimental cross-section distributions and DWBA calculations, the spin and parity assignments for most of them could be firmly fixed. Two states below 1 MeV were strongly populated, indicating their single-particle character – the ground state and the 473-keV level. This strong population was confirmed in a later (d,p) study [Tay80].
Combining the beta-decay work [Oin01], the transfer works [McL72] and [Tay80], an (n,γ) work [Ven80], and a fusion-evaporation study [Dea07], leads to a number of firm spin and parity assignments of excited levels in ^{59}Fe, presented in Fig 8.1.

The situation concerning the spin and parity of the ground state of ^{61}Mn is not yet fully settled, as till now no direct measurement has been reported. Therefore, we keep the tentative $(5/2^-)$ assignment for its ground state. As the beta-decaying level of ^{61}Mn has such a spin and parity, direct, allowed and forbidden decays are possible to levels with spins 3/2, 5/2, and 7/2 in ^{61}Fe.

Seven strong beta transitions with logft values below 5.7 are observed to the ground state, 207-, 629-, 1161-, 1253-, 2144- and 2511-keV levels, supporting firm negative-parity assignment for these levels (Table 4.3). Comparing the measured logft values with the published values for ^{59}Mn, a striking analogy between the two decay chains is apparent and a number of spin assignments can be inferred, supported by the preliminary analysis of the DIS data [Wai].

The similarity in direct ground-state feeding and the feeding to the 207-keV level, together with the decay pattern of the $9/2^+$ isomer (an $M2$ – $M1/E2$ cascade with no cross-over) fixes firmly the spin and parity of ^{61}Fe's ground state to $3/2^-$ and of the 207-keV state to $5/2^-$, confirming the results from the experiments noted in the introduction.

A tentative $(3/2^-)$ assignment is proposed for the 629-keV level, analogous to the 726-keV state in ^{59}Fe (Fig 8.1), based on the observed beta-decay feeding.

A $(1/2^-)$ tentative assignment can be made for the 391-keV level in analogy to the 287-keV level in ^{59}Fe. The absence of strong beta-decay feeding and absence of feeding to that state in the DIS reaction supports such a spin and parity assignment for the 391-keV level. In particular, the lighter odd-mass $^{55-59}$Fe nuclei exhibit a $1/2^-$ level below 500 keV, hence the 391-keV level is the only candidate for such a state in this energy range in ^{61}Fe. Based on the latter conclusion for a $(1/2^-)$ spin and parity, all of the high-energy levels that decay into the 391-keV level, would be limited to spin and parity of $\leq 5/2^-$.

The spin and parity of the excited state at 959 keV was determined to be $7/2^-$ following the angular-correlation analysis in [Hot08].

The absence of any feeding in the DIS data suggests spins below 7/2 for the levels at 1013, 1253 and 1262 keV. The lowest of these can also be tentatively assigned as $(1/2^-)$ on the basis of the determined $\log ft$ of > 7, see Table 4.3, while the strong beta branches for the levels at 1161 and 1253 keV rule out a $1/2^-$ assignment. Again, based on the analogy with levels in ^{59}Fe, where the second $5/2^-$ level is below the third $3/2^-$, the 1253-keV state can be tentatively assigned as $(3/2^-)$ and the one at 1161 keV as $(5/2^-)$ spin and parity.

In [Hot08], a 517-keV transition was found to be coincident with the 752-207-keV cascade de-exciting the level at 959 keV, defining an excited state at 1477 keV (Fig 4.10). A $(5/2^-, 9/2^-)$ assignment is proposed based on the angular-correlation measurement in [Hot08]. Information in the current decay work – the high $\log ft$ value and the lack of a transition to the ground state, can narrowed this down to $(9/2^-)$. The observations in [Wai], combined with the gamma-decay branching and the absence of strong beta decay towards that state as well as to the 862-keV state, are consistent with the proposed $(9/2^-)$ and the established $9/2^+$ spin and parity assignments, respectively. Due to the experimental conditions, though, it is not clear if the $9/2^+$ level at 862 keV is directly fed or through gamma decay from higher-lying levels.

The 1705-keV level in the beta decay of ^{61}Mn is fed with a $\log ft$ of > 7.1 (Table 4.3). Its comparison with the values for the tentative $(1/2^-)$ at 391 keV and the $(9/2^-)$ at 1477 keV supports either of the spin and parity assignments for the former.

The beta feeding towards the state at 2144 keV suggests an allowed transition, thus spins and parities ranging from $(3/2^-)$ to $(7/2^-)$. Since no transition to the $7/2^-$ state at 959 is observed, a tentative $(3/2^-, 5/2^-)$ assignment is adopted in Fig 4.10.

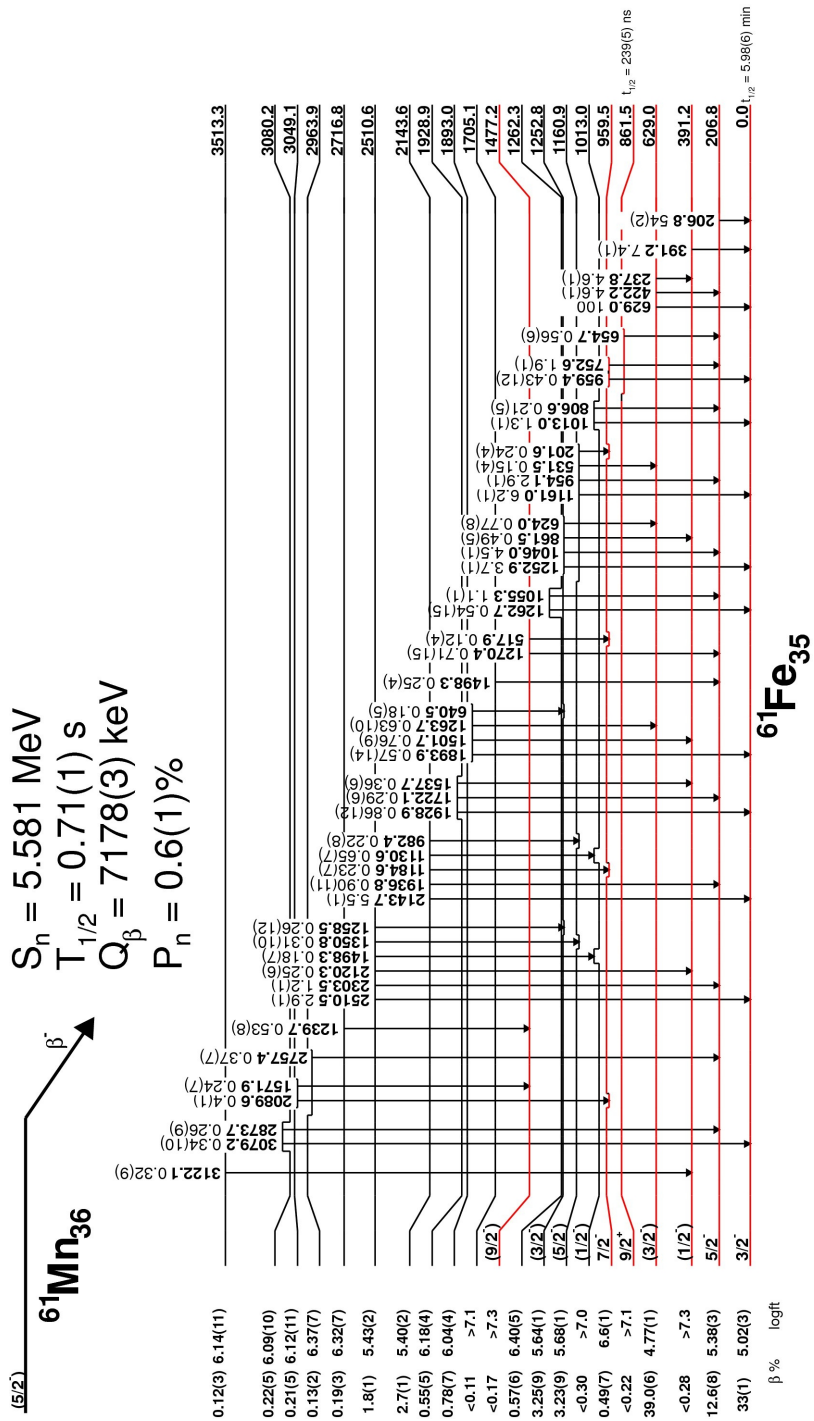

Figure 4.10: Decay scheme of ^{61}Mn, deduced from the present data. See Sec.4.2 for discussion on the levels with assigned spins and parities. The Q_β value is from [Wan12], P_n has been measured in [Han00], while the S_n and the half-lives of the ground and isomeric 862-keV states of ^{61}Fe are from [Bha99].

Chapter 5

Results for the decay chain of $A = 63$

5.1 Previous experimental information on ^{63}Fe

The ground-state of ^{63}Mn has a half-life of $T_{1/2} = 275(4)$ ms [Han99] and is assigned as $(5/2^-)$ spin and parity based on the systematics of the lighter odd-A isotopes (Section 4.2, Fig 4.9). Its β-delayed neutron branch was deduced in the PhD work of Hannawald [Han00] and was found to be 30.5(5)%.

A number of β-decay experiments have observed the first excited state in ^{63}Fe at the energy of 356(1) keV [Bos85, Sor99]. In his thesis, Gaudefroy observed gamma transitions in ^{63}Fe [Gau05], following the subsequent β-decay of ^{63}Mn, as daughter of ^{63}Cr, produced in a fragmentation reaction in GANIL. The identified transitions, were placed in a decay scheme, where excited states with energies 356, 451, 626 and 1132 keV (see Fig 5.21 in [Gau05]) were identified on the basis of sum relations. Low $\log ft$ values were deduced for the excited states of 357 and 1132 keV, of 5.0 and 4.7, respectively, corresponding to 31% and 32% of direct β-decay population. The rest of the decay intensity was assumed to go directly to the ground state of iron, which resulted in a $\log ft$ value of 4.9.

Another β-decay experiment was performed by Mach et al. [Mac09]. The decay scheme of ^{63}Mn was extended up to $\sim$ 1.5 MeV and is presented in Fig 5.1, where transitions and excited states, observed by Gaudefroy are indicated with a bullet. An ($M1$) character was assumed for the 93- and the 357-keV transitions, on the basis of the deduced half-lives for the first two excited states of 110 and 780 ps, respectively, for the 357 and 451 keV. The attempt, by Mach et al., to

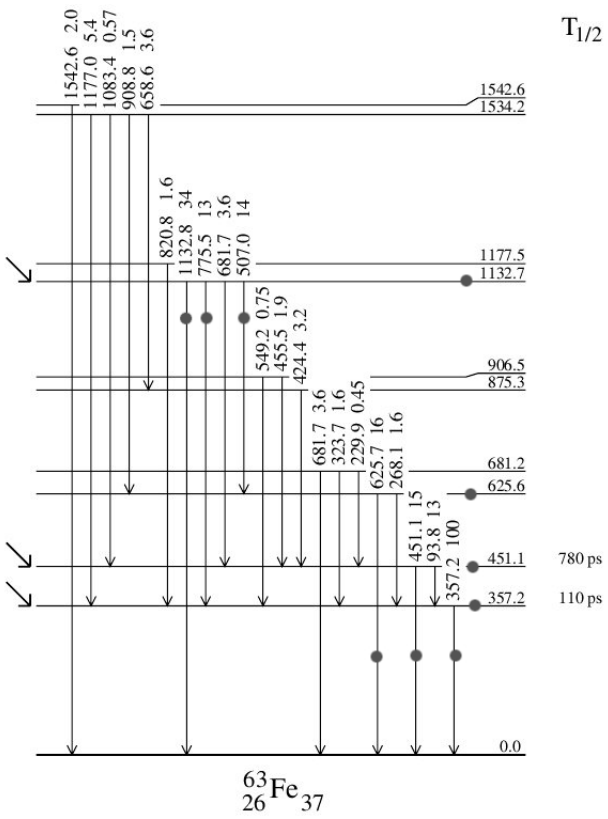

Figure 5.1: Decay scheme of ^{63}Mn, deduced in [Mac09]. Excited states and transitions, observed in [Gau05] are indicated with a bullet. The arrows on the left side point to levels with calculated $\log ft$ of ~ 5.

establish absolute gamma-ray intensities in ^{63}Fe, by normalizing to its decay was unsuccessful, as the sum of the intensities from the decay of ^{63}Mn exceeded the maximum amount of 100% by a factor of five, those in the decay of iron [Mac09]. This was not the case, if normalization was done using the absolute intensities of ^{63}Co decay from [Run85], where the sums matched within error bars. It became clear, that the previously reported, absolute intensities for the decay of ^{63}Fe in [Run85], are incorrect. Furthermore, the beta-decay analysis of ^{63}Mn suggested, that the ground-state to ground-state direct beta-decay branch is very weak or close to zero. It was implied, that the previous assignment of $(5/2^-)$ spin and parity for the ground-state of ^{63}Fe [Run85], based on the observed strong

decay branch towards the $7/2^-$, ^{63}Co ground state, is questionable. It was proposed, that the first three states in ^{63}Fe have J^π of $(1/2^-)$, $(3/2^-)$ and $(5/2^-)$, respectively, on the basis of the weak beta-decay towards the ground state and the assumed $(M1)$ characters for the 94- and the 357-keV transitions.

A recent beta-decay study, aiming at measuring the half-lives of excited level in the neutron-rich iron isotopes, showed preliminary results for the observed experimental half-lives of the first two excited state in ^{63}Fe [Ola11]. The deduced values seemed in a good in agreement with Fig 5.1 and are respectively, $T_{1/2}$(364 keV) = 100(30) ps and $T_{1/2}$(451 keV) = 950(80) ps.

A multi-nucleon transfer reaction experiment [Lun07], populated two excited states in ^{63}Fe, which decay via two coincident transitions – 819 and 1404 keV. The latter were not in coincidence with the observed 356-keV line and were proposed to feed a $(9/2^+)$ isomeric state, similar to the neighbouring 61Fe (see Section 4.1). The supposed $\nu g_{9/2}$ excited state, was not observed in the work of Grzywacz et al. [Grz98], where a search for isomeric levels, around $N = 40$, was performed.

The ground state of the ^{63}Fe isotope has a half-life of $T_{1/2} = 6.1(6)$ s [Run85].

5.2 Results for ^{63}Mn decay

Experimental Details

The data set, recorded when the HRS magnets were on mass 63, consists of 9 files with a total laser-on recorded time of 7014 s, with respect to 1174 s for laser-off. During this measurement the ISOLDE target station received 33 consecutive proton pulses, starting from proton pulse number 3 (see Fig A.7). Part of the data files were taken without forced read-out (FRO; see Chapter 3), while another part was recorded with. The delay of the beam gate was set for 10 ms, followed by a 10 ms implantation period. The decay data was recorded for 1 s after each proton pulse (PP), while the forced read-outs, when present, were starting at 500 ms after the PP for a duration of 170 ms.
Fig 5.2 shows a γ-singles, laser-on spectrum, compared to a laser-off one in the same experimental conditions.

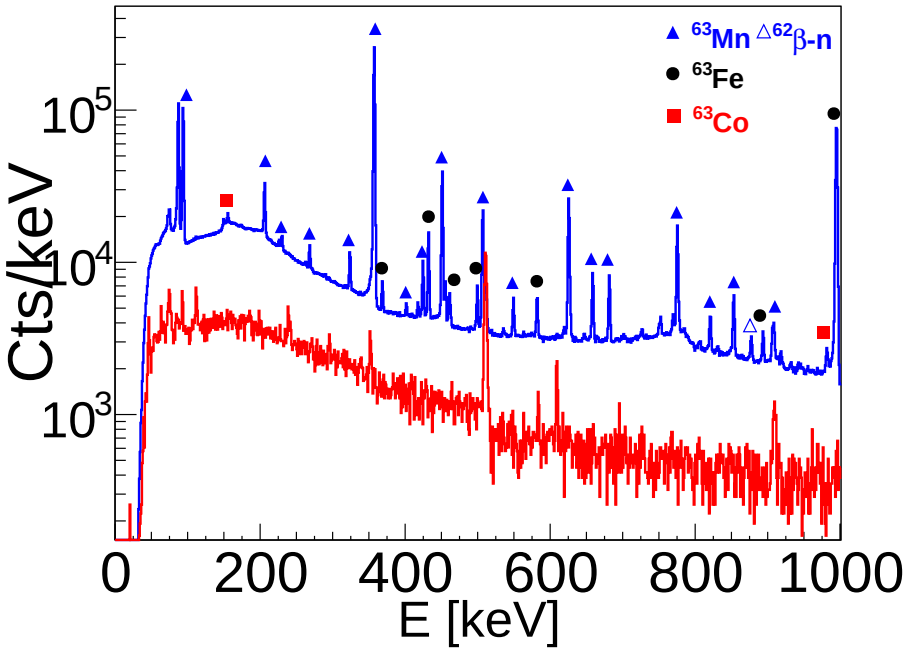

Figure 5.2: (Color online) Singles' γ-spectrum for $A = 63$: laser-on, compared to laser-off (scaled for visual comparison). Some of the strongest transitions following the decay of ^{63}Mn and its daughter and grand-daughter, as well as observed transitions in the β-delayed neutron branch are indicated.

Half-life Determination

The half-life of ^{63}Mn was experimentally deduced to be $T_{1/2} = 283(2)$ ms, using the implantation-decay curves for multiple transitions identified as ^{63}Mn lines in the singles data, for both data subsets. It is found to be in agreement, within 2σ, with the previously determined value of $T_{1/2} = 275(4)$ ms [Han99]. Sample implantation-decay spectra, for ^{63}Mn, can be seen in Fig 5.3, where an exponential decay function is fit on the data points for the subsets of data with and without FRO. Note, the uncertainty on the half-life value is only statistical

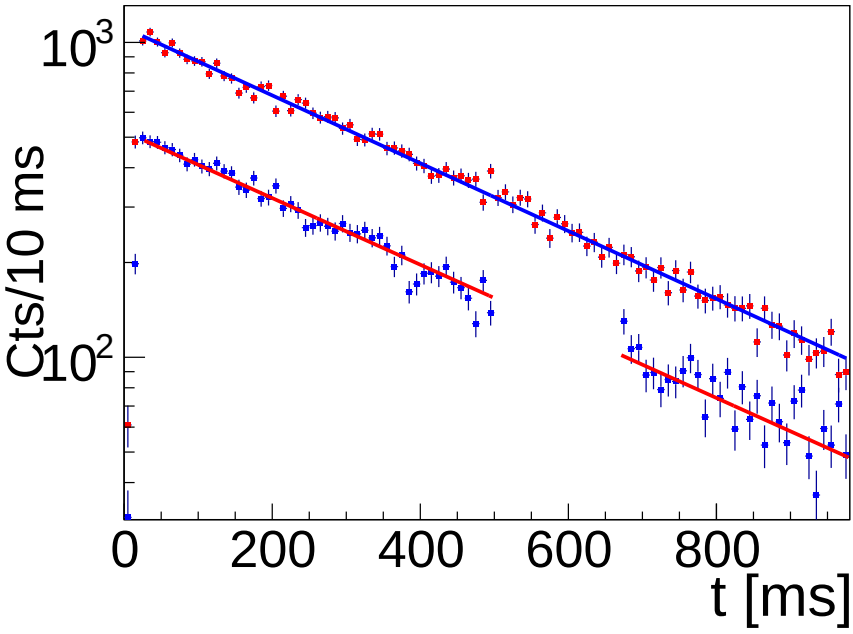

Figure 5.3: Implantation-decay behaviour of an 1132-keV transition, following the decay of ^{63}Mn, with respect to the PP signal, for both data subsets, yielding half-life values of 285(6) ms and 280(4) ms, for the fits without FRO and with FRO, respectively. Each point in the histogram correspond to the number of counts in the area of the investigated transition, deduced by a fit of a Gaussian plus a constant background function.

and that a possible constant background contribution to the points in the decay histogram, which would bring the half-life value down, is not taken into account

by the exponential fit, since it is difficult to be estimated from the experimental data.

Decay Scheme

The decay scheme of ^{63}Mn was built, using the information, obtained via the implantation-decay behaviour of the transitions in singles and γ-γ-coincidence gates. A γ-spectrum, gated by the strongest transition (357 keV) identified in this decay can be seen in Fig 5.4.

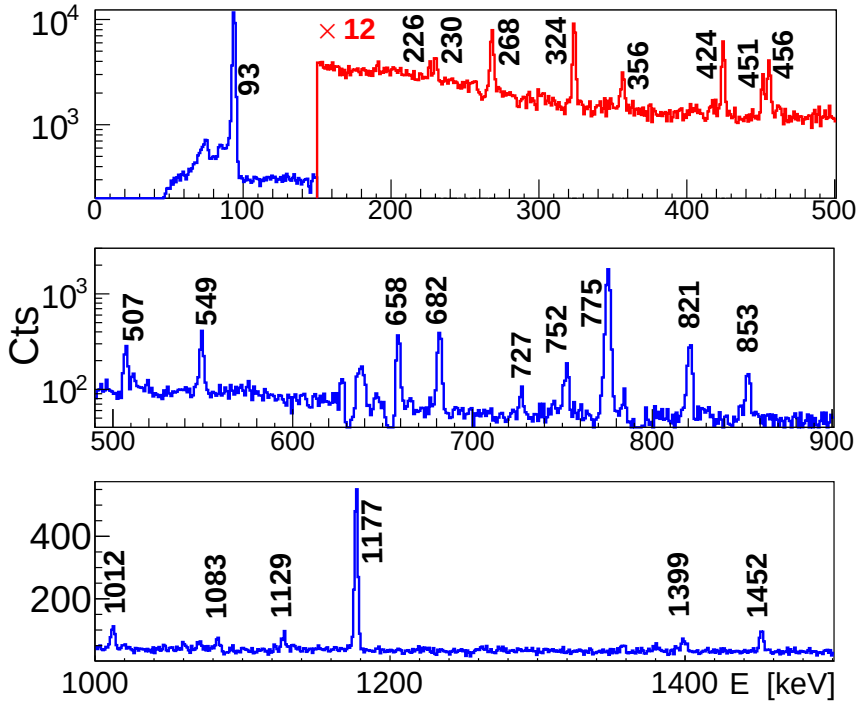

Figure 5.4: Prompt γ-γ coincidence gate, set on $E = 357 \pm 2$ keV. The strongest coincident transitions are labelled.

None of the two coincident transitions (819 and 1404 keV), found by Lunardi et al. [Lun07], were observed in this decay, suggesting that they probably de-excite states with spins larger than 9/2. Such states would not be directly fed in the decay of a $(5/2^-)$ manganese ground state. All identified transitions, belonging to the decay of ^{63}Mn, together with their relative intensities and observed coincidences can be inspected in Table 5.1.

Table 5.1: Gamma transitions and relative intensities, identified as following the decay of ^{63}Mn. For absolute intensities per 100 decays, multiply by 0.538(12).

E_γ (keV)	Rel. Int. (%)	Observed coincidence transitions (keV)
24.3(1)	8(1)	not observed
93.2(1)	18(1)	256, 230, 357, 425, 456, 628, 658, 682, 727, 853, 918, 1060, 1083, 1129, 1358, 1605, 1736, 1880, 3114
206.0(1)	4.96(6)	451, 853
225.8(1)	0.38(4)	93, 357, 456
229.6(1)	0.80(4)	93, 357, 451, 456, 853
268.3(1)	1.17(4)	357, 507, 907
323.8(1)	1.88(5)	357, 451, 853
356.1(1)	0.38(8)	727, 821
357.3(1)	100.0	93, 226, 230, 268, 324, 356, 425 ,456, 507, 519, 549, 658, 659, 727, 752, 775, 821, 853, 918, 1012, 1083, 1129 ,1177, 1399, 1452, 1677, 1880, 2236, 2475
401.6(1)	0.37(3)	451, 507, 775, 1133
424.8(1)	0.77(12)	658, 752
424.6(1)	1.8(1)	93, 357, 451, 635
451.2(1)	1.6(1)/15.7(1)	206, 230, 324, 356, 402, 451, 230, 425, 451, 455, 628, 658, 727, 918, 1060, 1083, 1129, 1358, 1605, 1736, 1880, 3114
455.5(1)	1.6(1)	93, 226, 357, 451, 628, 849, 1129
507.1(1)	10.1(2)	268, 357, 402, 626
518.5(4)	0.22(2)	357, 659
549.4(1)	1.3(1)	357, 628, 1129
625.5(1)	15.5(1)	507, 909, 1409, 2206, 2704
627.8(1)	0.81(10)	93, 451, 456, 549, 907
634.8(1)	0.08(2)	425
658.5(1)	1.1(2)	425, 451, 519
658.4(1)	2.5(2)	93, 357, 425, 451, 1222
681.5(1)	3.6(1)	93, 357, 451
726.5(1)	0.37(6)	93, 356, 357, 451
751.8(1)	1.1(1)	357, 425, 1222
775.4(1)	10.8(1)	357, 402
820.8(1)	1.7(6)	356, 357
848.7(1)	0.15(4)	456, 549
853.2(1)	3.2(1)	93, 206, 230, 324, 357, 451
877.3(1)	**0.92(5)**	–, IN ^{62}FE

906.7(1)	0.49(12)	628, 1129
908.6(4)	1.5(1)	268, 626
918.0(1)	0.34(5)	93, 357, 451
1011.9(1)	0.42(5)	357
1060.1(1)	0.42(6)	93, 451
1082.7(1)	0.66(5)	93, 357, 451
1129.1(2)	0.51(9)	456, 549, 908
1132.6(1)	29.6(2)	402
1153.3(4)	0.14(3)	357, 821
1176.7(1)	4.7(1)	357
1221.6(5)	0.13(6)	658, 752
1357.7(1)	0.35(6)	93, 357, 451
1369.6(1)	1.7(2)	—
1399.0(1)	0.49(6)	357
1409.4(3)	0.19(3)	626
1451.8(1)	0.84(5)	357
1533.9(1)	0.36(7)	—
1604.6(3)	0.18(6)	93, 357, 451
1677.0(1)	0.30(4)	357
1735.6(2)	0.31(5)	93, 357, 451
1808.9(1)	0.99(7)	—
1856.0(1)	0.71(6)	— (placed on the basis of energy difference)
1879.7(2)	0.37(6)	93, 357, 451
2206.3(2)	0.31(6)	268, 626
2235.9(4)	0.21(5)	357
2474.7(1)	0.48(5)	357
2703.6(3)	0.20(7)	626
3328.8(9)	0.17(5)	—
3113.8(4)	0.24(5)	93, 357, 451
1183.4(5)	0.37(3)	—
2483.3(5)	0.23(10)	—
2774.8(5)	0.58(8)	—
3059.5(5)	0.23(5)	—
3656.9(5)	0.28(8)	—
3695.2(5)	0.14(4)	—

Table 5.2: Table 5.1 continued. Gamma transitions below the horizontal line are observed in the clean ^{63}Mn decay spectrum, but not placed in the decay scheme.

β-delayed neutron branch

Only the $2^+ \rightarrow 0^+$ (877 keV [NND13b]) ground-state transition in ^{62}Fe was observed in this decay set, with an intensity of 0.9(1)%, relative to the 357 keV transition in ^{63}Fe. The gamma-gamma coincidence gate set on the 877-keV line showed no evidence of population of the 4^+ state in ^{62}Fe in the beta-delayed neutron process. In order to calculate the total β-delayed branching, a transition following the decay of the 68(2) s [NND13b] ground-state of ^{62}Fe is necessary. The strongest line in that decay is a 506-keV transition, with an absolute gamma intensity of 83(3)% [Pau13]. Because a transition with an energy of 507 keV exists in the decay of ^{63}Mn (see Table 5.1), certain considerations were taken into account to calculate correctly the P_n branching ratio.

A clean manganese-decay gamma-spectrum was produced (see e.g. Section 5.2, Method.3), where the intensity ratio of the 507-keV line (here only originating from the ^{63}Mn decay) relative to another strong ^{63}Mn decay line (1132-keV line) was deduced. This ratio was used to calculated the amount of 506-keV counts, following ^{62}Fe decay, in the singles' full statistics γ-spectrum. The amount of counts, correlated with the latter decay, was calculated to be $N = 5600(600)$ cts, compared to the total amount in the 507(2)-keV area of $N_t = 46000(300)$ cts. Using the deduced number of counts in the 506-keV line, the branching ratio and the half-life correction factors for manganese and ^{62}Fe decay of 1.09(1) and 6.85(1), respectively, the total number of ^{62}Co nuclei was deduced.
The half-life correction factors in the comparison are needed, because of the ISOLDE super cycle structure and the finite decay acquisition time. The total number of ^{62}Co nuclei was the accordingly distributed towards the observed excited state and the ground state of ^{62}Fe.
The result per 100 decays is summarized in Table 5.3, while the deduced P_n branch amounts to 3.3(6)% of all manganese decays, much lower than the previous value of 30.5% [Han00].

Table 5.3: Table of P_n distribution in the β-decay of ^{63}Mn, normalized to 100%.

E + S_n (keV)	E (keV)	P_n %	J^π [NND13b]
4176	GS	85(23)	0^+
5593	877.3	15(3)	2^+

Indications for an isomeric state

While plotting the implantation-decay behaviour of some of the strongest transitions, a noticeable difference was found. The difference is seen in the very beginning of each decay histogram, where there seems to be some delay in the expected decay point of the corresponding transition. Such a difference was only observed for the 357-, 451- and 94-keV transitions and was not present elsewhere. The apparent difference is shown in Fig 5.5, where the decay behaviour of the 1132-keV transition is plotted (in blue), in comparison to the same of the 94-keV transition (in red). These three lines are placed at the bottom of the level scheme of ^{63}Fe.

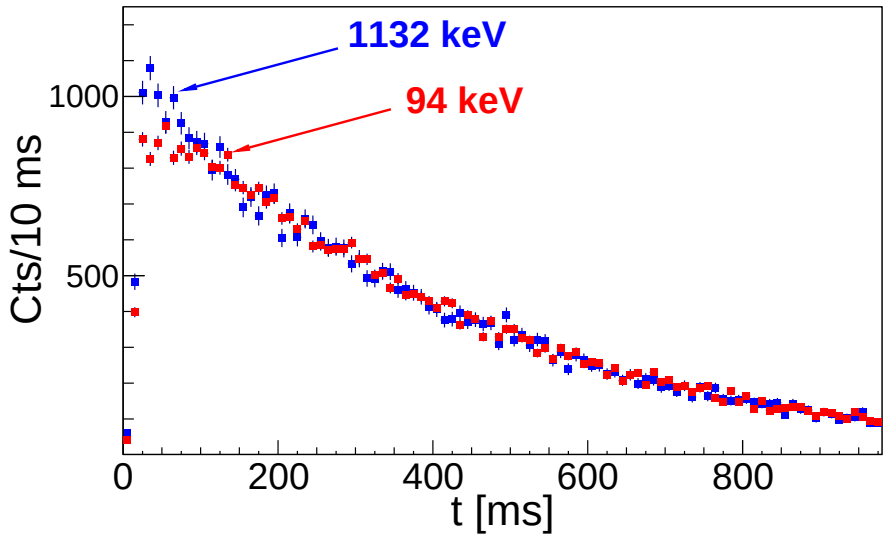

Figure 5.5: Comparison between the implantation-decay behaviour curves of the 1132- and 94-keV transitions, with respect to the PP signal. For the sake of clarity, the intensity of the 94-keV transitions is scaled down to match the 1132-keV line in the region between 200 – 300 ms.

It can be concluded, that part of the feeding of the three transitions, passes an isomeric state. Since this behaviour was noticed for the aforementioned transitions only and the 357 and 451 keV are the first two excited states in ^{63}Fe, the isomeric state would have to lie above the 451-keV excited level; the 94 keV

is placed between the 451- and 357-keV level.

Furthermore, in the β-gated, prompt gamma-spectrum, the relative intensities of these three lines, compared to the other lines in the decay of ^{63}Mn, is lower. This effect appears as a decrease in the β-efficiency of the three lines as 20.5(4)% for the 94- and the 451-keV transitions and 26.2(2)% for the 357-keV line, with respect to an average value of $\varepsilon_\beta = 27.4(3)\%$. The averaged value here, includes data from multiple gamma lines in ^{63}Mn, ^{63}Fe and ^{63}Co decay. This observation further indicates, that part of the intensity of those transitions comes delayed with respect to a beta event.

To deduce the half-life of the isomeric level in ^{63}Fe, a combination of a pure exponential decay and a growing-in decay function was fit on the decay part of each of the transitions de-exciting the 451-keV level:

$$F(t) = M(t) \times a + D(t) \times (1 - a)\,,$$

where $M(t)$ is the pure exponential decay function for ^{63}Mn with the determined half-life of 283(2) ms and $D(t)$ a combination of a pure isomeric decay (with an unknown $T_{1/2}$) function with a growing in ($T_{1/2} = 283(2)$ ms) function. The parameter a, can be understood as the fraction of pure exponential decay of the mother ($M(t)$). Thus, if no isomeric decay was present, a would be 100%. For the fit on the data points of 94- and 451-keV transitions, free parameters were the half-life of the isomeric state and the parameter a. The results of the fit for the subset of experimental data without forced read-outs, are shown in Fig 5.6. Notice, that the fit starts only at 20 ms after the proton pulse when the separator beam is switched off. The amount of ^{63}Fe isomer already produced during the implantation is taken into account by the function $D(t)$.

The isomeric half-lives extracted from this fit are 34(8) and 29(8) ms for the 94 and 451 keV, respectively, while the values for the parameter a, were determined to be 0.77(5) and 0.70(8), respectively. Adding the deduced half-lives from the data subset with a forced read-out, results in a weighted mean value for a of 0.75(4) and a weighted average value for the isomeric half-life of 30(5) ms. Since the relative intensity of the 94 keV transition is 18(1)% (I_γ^{94}; see Table 5.1), it would mean that 4(1)% ($= I_\gamma^{94} \times$(1-a)) of the feeding of the 357-keV line comes as a delayed intensity. The experimental fit of the 357-keV implantation-decay behaviour with a half-life of ^{63}Mn fixed to 283(2) ms and an isomeric half-life fixed to 30(5) ms, yields a 93(1)% for the parameter a, which is within 2σ of the expected 96(1)% (100% - 4(1)%).

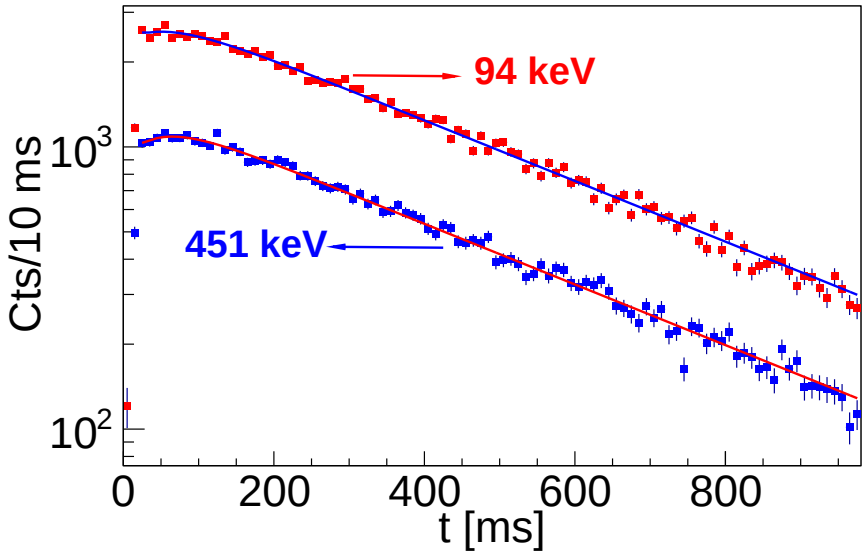

Figure 5.6: Implantation-decay histograms for the 94- (red points) and 451-keV (blue points) transitions, with respect to the PP signal, fitted with a fraction of a pure mother function (a) and fraction of daughter function (1-a). The shown histograms are from the data subset where no forced read-out was used.

Placement of the isomer in ^{63}Fe

It is already clear, that the newly found isomeric state should lie above the 451-keV excited state. While building the decay scheme of ^{63}Mn, a transition of 206 keV was found in the single-events spectrum, as well as the beta-gated prompt spectrum. The transition's decay behaviour indicated, that it belongs to ^{63}Mn decay and its relative intensity was determined to be 5.0(1)%.

The beta-efficiency, deduced for this transition is 27.7(17)%, which implies that no part of its intensity passes through the newly discovered isomer. In the prompt γ-coincident spectrum, gated by the 206-keV line, only a 451-keV and an 853-keV line was observed (see Table 5.1). The lack of prompt coincidence with the 357-keV line indicates, that the 451-keV line is not the line de-exciting the 451-keV level as then through the 93-keV also the 357-keV should have been observed. The former is a weaker part of a doublet structure with energy of 451 keV (1.5% versus 15.7%). The 853-kev line is further coincident with the 93-, 230-, 324-, 357- and 451-keV lines.

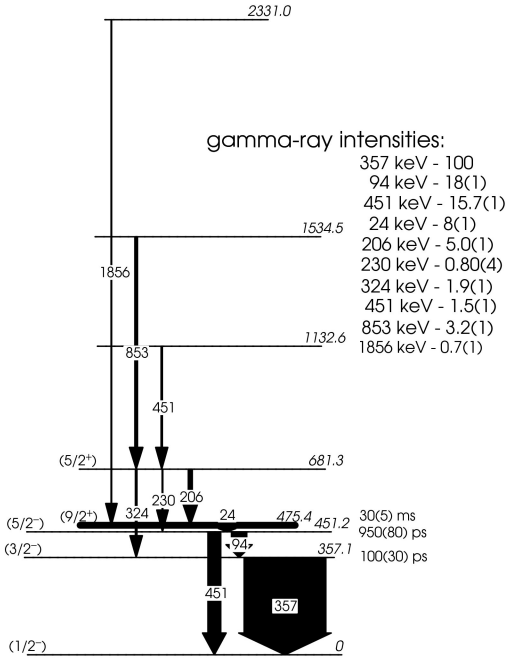

Figure 5.7: Partial level scheme of ^{63}Fe. The width of the transitions corresponds to their relative intensity (see description aside). The pico-second half-lives in the figure are from [Ola11], although one should use the values in [Mac09] also in Table 5.4.

All of this leads to new levels at 681, 1133 and 1535 keV, which are further confirmed when the full level scheme of ^{63}Fe is constructed. As both the 853-keV and weaker doublet of the 451-keV lines de-excite the nucleus to a state with an energy of 681 keV, the 206-keV line must de-excite the latter level, which ends up at a level at 475 keV. This must be the 30(5) ms level, the candidate for the expected $9/2^+$ isomer in ^{63}Fe, which remained unobserved in the work of Grzywacz [Grz98]. The isomeric transition of 24 keV towards the 451-keV level remains unobserved (below our electron and gamma energy threshold).

Following these considerations, one can draw a partial level scheme of ^{63}Fe, seen in Fig 5.7, including the isomeric state in question. Note, that the relative intensity of the transitions is given and not all the transitions de-exciting a particular level are plotted, but only the essential ones for this discussion. The

transition with an energy of 1856 keV was found in the clean ^{63}Mn decay spectrum and was placed in the decay scheme on the basis of energy differences.

The relative intensity of the unobserved 24-keV line, was calculated using the deduced isomeric contribution for the two lines, de-exciting the 451-keV level. Since the weighted mean of the fits gives a value for (1-a) of 24(3)%, it means that based on the determined relative intensities of the 94- and the 451-keV transitions, 8(1)% are needed to produce such an isomeric decay. The total intensity of the lines placed feeding the isomeric state is 5.7(1)%, indicating that one or several transitions with a summed intensity of 3(1)% are still unaccounted for in the decay scheme.

Direct beta-decay or missed gamma transitions, feeding the ground state of ^{63}Fe

The direct beta-branching towards each excited state in ^{63}Fe was calculated, using the identified feeding and de-exciting transitions for each corresponding level.
The calculation for the direct ground-state feeding or missed gamma intensity, from ^{63}Mn to ^{63}Fe, was done using different methods, based on the fact, that the radioactive beam composition is purely ^{63}Mn:

Method.1 Using the known decay scheme of ^{63}Co:

In a β-decay experiment, Runte et al. [Run85], deduced the decay scheme of the $7/2^-$ ground-state of ^{63}Co, where 93(5)% of the decay intensity was found to directly feed an excited state in ^{63}Ni at 87 keV, and none of the feeding was found to go towards the ground-state ($J^\pi = 1/2^-$ [Erj01]).

Using the number of counts of the 982-keV line in the decay of ^{63}Co, its absolute intensity (2.11(8)% [Run85]) and the calculated half-life correction factors due to the implantation-decay periods in the ISOLDE super cycle (1.09(1) and 5.53(2) for manganese and cobalt, respectively), the number of ^{63}Co decays can be deduced. This number can be compared to the number of ^{63}Mn, decaying through all observed ground-state transitions, deduced from the constructed decay scheme in Fig 5.8. This number can be deduced by using the efficiency-corrected number of counts in the strongest transition in the decay of ^{63}Mn and applying cycle and gamma-branching ($\alpha^{357}_{Mn} = 0.610(3)$, see Chapter 4.2 for details on the coefficient) correction factors. The observed difference between the number of manganese decays and the number of ^{63}Co decays is **12(16)%**.

Method.2 β-gated spectra with a time constraint, with respect to the ISOLDE super cycle:

By using only the first proton pulse, where ^{63}Mn is implanted for each super cycle, the amount of the granddaughter (^{63}Co, $T_{1/2}$ = 27.4(5) s [Erj01]) can be neglected and the number of beta radiation is only coming from manganese and iron. Taking advantage of the digital electronics, one can draw a β-triggered, prompt (0-600 ns), gamma spectrum in the time period of the first ISOLDE proton pulse (see Fig A.7). The number of beta-rays (N_β) can be obtained from the singles' β-spectrum in the same time period. Based on the published half-life of ^{63}Fe, $T_{1/2} = 6.1(6)$ s [Run85], the percentage of betas, related only to that decay is calculated to be 6.3(6)% ($N^{\%}_{Fe}$).

Using the newly obtained information on the P_n branch in the decay of ^{63}Mn and $N^{\%}_{Fe}$, the number of obtained betas N_β, corrected for the latter contributions, is compared to the number of ^{63}Mn gamma decays, deduced from the constructed decay scheme. The calculated difference between these two numbers is **7(21)%**. The large uncertainty here, as well as in the previous method, is due to the subtraction of big numbers.

Method.3 Single event data in different times, with respect to the proton pulse impact:

Another way to disentangle the β- and γ-spectra and the different decay contributions is to only use the first PP and the seventh PP in the super cycle, that are sent to the ISOLDE target. Further enhancing the purity of the singles' gamma-spectra is to only use the 0 – 290 ms of the first PP and the 700 – 980 ms of the seventh PP, focusing respectively on ^{63}Mn and ^{63}Fe decay. The 7^{th} PP (see Fig A.7) was chosen in order to minimize the effect of cobalt decay in the constructed spectra. One can combine the two gamma spectra, in order to produce a clean ^{63}Mn and a clean ^{63}Fe decay spectrum. The appropriate scaling coefficients are deduced by using the number of counts in the strongest manganese and iron decay lines in both spectra.

The same coefficients can be used to split up the number of β-counts in the 0-290 ms of the first PP and the 700-980 ms of the seventh PP in a pure manganese part and a pure iron part.
A number of manganese decays (N^{Mn}_{γ}) is deduced from the number of counts in the area of the 357-keV line, in the clean gamma spectrum and its gamma branching (α^{357}_{Mn}). This number is compared to the ε_β-corrected

number of pure manganese betas via

$$\frac{N_{\beta}^{Mn} - N_{\gamma}^{Mn}}{N_{\beta}^{Mn}},$$

which gives a difference of **11(3)%**.

A weighted average value of 11(2)% is then deduced, while the value of $< 13\%$ is adopted in Table 5.4 for the direct beta-feeding towards the ground-state of ^{63}Fe. This is, though, only an upper limit and can be due to missed gamma intensity in the decay of ^{63}Mn.

Table 5.4: Excited levels and direct β-feeding in the decay of ^{63}Mn.

E (keV)	I_β %	logft	J^π	$T_{1/2}$
GS	< 13	> 5.4	$(1/2^-)$	6.1 s [Run85]
357.3(1)	30(1)	4.98(2)	$(3/2^-)$	???(30) ps [Mac09]
451.0(1)	7(1)	5.59(7)	$(5/2^-)$	???(80) ps [Mac09]
475.1(2)	< 2	> 6.5	$(9/2^+)$	30(5) ms
625.5(1)	1.8(2)	6.13(4)		
681.1(1)	1.5(1)	6.19(2)	$(5/2^+)$	
875.8(1)	0.43(13)	6.69(13)	$(7/2^-)$	
906.7(1)	0.8(1)	6.42(7)		
1109.4(1)	1.4(1)	6.11(5)		
1132.7(1)	29(1)	4.80(2)	$(3/2^-)$	
1178.1(1)	1.0(1)	6.25(2)		
1369.4(1)	1.3(1)	6.09(4)	$(5/2^-)$	
1511.0(1)	0.26(3)	6.74(7)		
1534.2(1)	7.3(3)	5.29(2)		
1756.3(1)	0.26(3)	6.67(5)		
1809.0(1)	1.1(1)	6.02(2)		
2034.6(1)	0.52(6)	6.29(5)		
2055.8(3)	0.09(3)	7.05(15)		
2186.8(2)	0.16(3)	6.76(6)		
2331.0(2)	0.71(6)	6.06(4)		
2593.2(4)	0.11(3)	6.79(12)		
2831.9(1)	0.42(4)	6.13(5)		
3329.1(3)	0.19(5)	6.30(10)		
3564.9(4)	0.12(3)	6.41(10)		

The ^{63}Mn decay scheme

Identification of 23 excited states with detailed feeding and de-excitation pattern is deduced for ^{63}Fe, including an isomeric one with an excitation energy and half-life of 475.1(2) keV and 30(5) ms, respectively. Further down the decay scheme, there is no strong evidence for direct ground-state feeding (^{63}Fe to ^{63}Co < 13 %, ^{63}Co to ^{63}Ni measured to be zero). The ground-state spins of ^{63}Co and ^{63}Ni have been measured to be $7/2^-$ and $1/2^-$, respectively.

The available neutron shell-model orbitals in this region, while the protons are occupying the $f_{7/2}$ shell, are the $p_{1/2}$, $p_{3/2}$, $f_{5/2}$, $g_{9/2}$ and the $d_{5/2}$. The ground state of ^{63}Mn can be tentatively assigned as $(5/2^-)$, on the basis of the lighter odd-A isotopes (see the discussion in Section 4.2).

Mach et al. [Mac09], suggested $(1/2^-)$ for the spin and parity of the ground state of ^{63}Fe. The lack of beta-feeding towards the ground state of ^{63}Fe supports this tentative assignment. The determined $T_{1/2}$ of the first two excited states in ^{63}Fe [Mac09], were recently confirmed in a new fast-timing experiment performed at ISOLDE [Ola11].
These half-lives, are consistent with $(M1)$ multipolarities for the 357- and the 93-keV, suggesting possible $(3/2^-)$ and $(5/2^-)$ spin and parity for the 357 and the 451 keV, respectively, supported by the $\log ft$ values deduced in the current experiment. The tentatively assigned J^π of the isomeric state with an energy of 475 keV is $(9/2^+)$ with a half-life of $T_{1/2} = 30(5)$ ms.
This state decays only to the $(5/2^-)$ at 451 keV via a 24-keV transition (not observed in the present experiment) and not to the ground state. The Weisskopf estimate for the half-life of a 24-keV $M2$ transition is 247 ms. Taking into account the electron conversion factor of more than 70, the expected single particle half-life becomes of the order of 3 ms, denoting a retardation factor of 10, which is within the Recommended Upper Limits for such a hindrance in this mass region, according to [End79]. No other multipolarity can explain the observed half-life. This fact, together with the lack of transitions towards the state at 357 keV and towards the ground state, further supports the tentative assignments of $(5/2^-)$, $(3/2^-)$ and $(1/2^-)$ for the excited states at 451, 357 keV and the ground state, respectively.

The excited state with an energy of 681 keV is tentatively assigned as $(5/2^+)$, due to its de-excitation pattern towards the positive-parity isomeric level via the 206-keV transition and the deduced $\log ft$ value of 6.2.

The level at 876 keV de-excites only to the first $(3/2^-)$ and $(5/2^-)$ excited states, but not towards the $(1/2^-)$ ground state, therefore a spin and parity of

$(7/2^-)$ can be tentatively assigned to it.

At higher excitation energy, the level at 1133 keV is observed to receive substantial beta-feeding and is also tentatively assigned as $(3/2^-)$ spin and parity, based on the deduced $\log ft$ value of 4.9(1).

And finally, the excited state at 1369 keV can be tentatively assigned as $(5/2^-)$ on the basis of the observed transitions towards the ground state, the 357- and the 451-keV levels and the calculated $\log ft$ value.

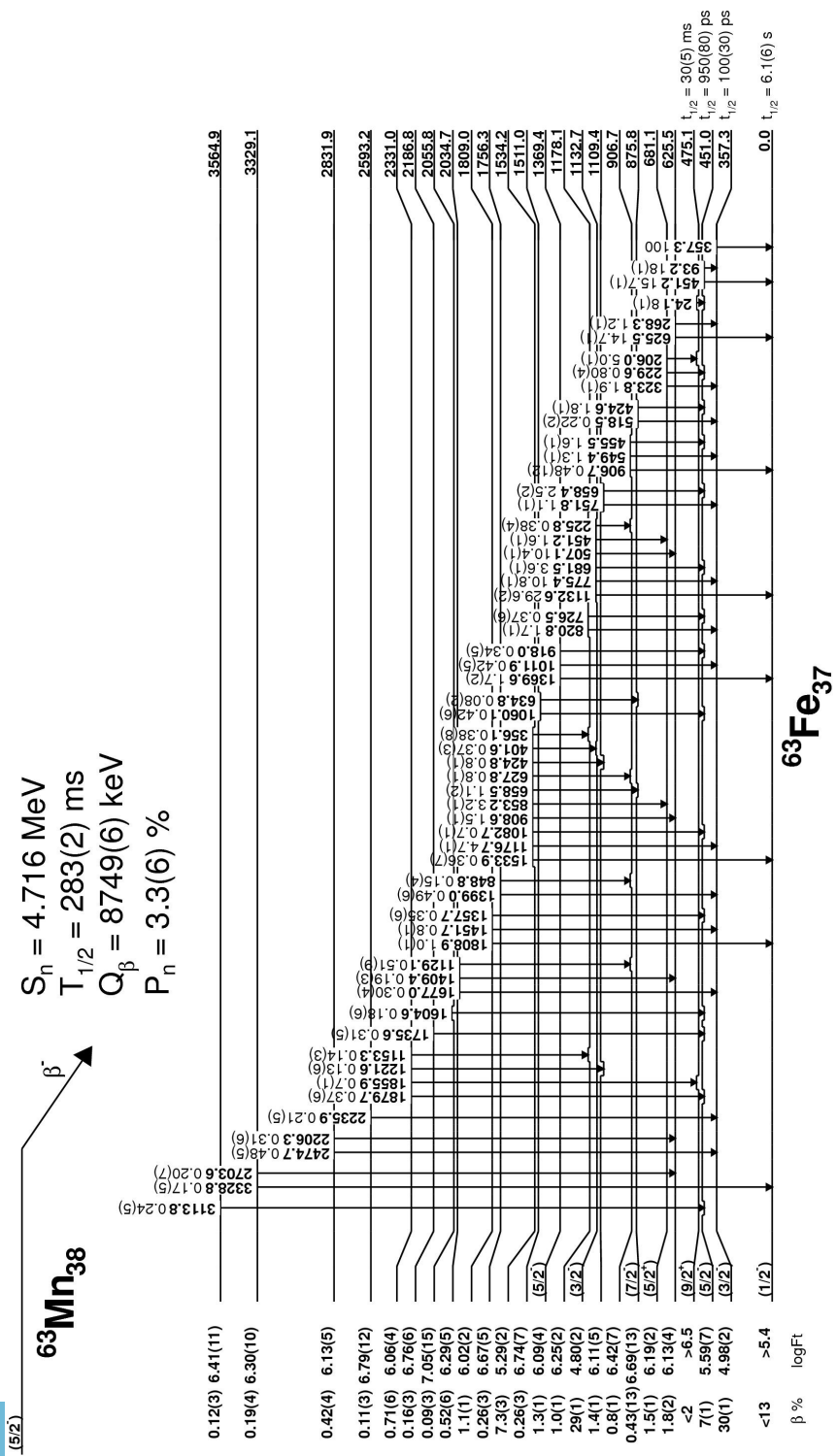

Figure 5.8: Decay scheme of ^{63}Mn, deduced in the current study.

5.3 Previous experimental information on ^{63}Co

Decay studies on ^{63}Fe were performed by Runte et al. in two consecutive experiments [Run83, Run85]. The deduced decay scheme is presented in Fig 5.9.

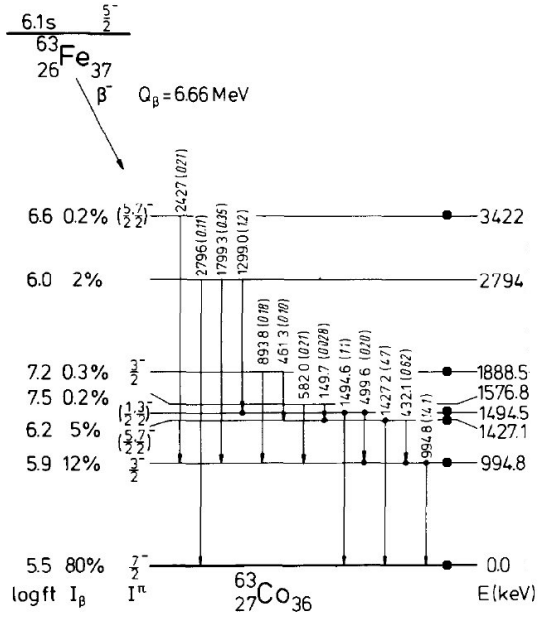

Figure 5.9: Decay scheme of ^{63}Fe, deduced by Runte et al. [Run85]. Levels, marked with a dot, were previously observed in transfer reactions [Bla66, Han79, See91, See92].

Seven excited states were identified, while 80% of the β-strength was assigned towards the ground state of cobalt. This latter assignment has been disputed in Section 5.1, where the absolute beta-decay branching ratios for the decay of ^{63}Fe in [Run85] are challenged by Mach et al. [Mac09]. The spin and parity of the excited states, seen in the decay scheme (Fig 5.9) are assigned with the assumption, that the ground state of ^{63}Fe has $(5/2^-)$ quantum numbers.

A ^{64}Ni(t, α) transfer reaction was performed by Blair et al. [Bla66], where excited states up to 3.4 MeV in ^{63}Co were populated. Following these results, a proton pick-up reaction – ^{64}Ni(d, ^{3}He)$^{63}_{27}$Co – was performed, to deduce more

information on excited states and spin and parities [See91, See92] in cobalt. The latter, combined high-resolution unpolarized deuteron reaction with low-resolution polarized deuteron reaction to deduce unambiguous spins and parities of $7/2^-$, $3/2^-$, $7/2^-$, $1/2^+$ and $7/2^-$ for the five states at energies 0, 995, 2128, 2191 and 2330 keV, respectively. Excited states at 1384, 1427 and 1494 keV with different momentum transfer values of 3, 1 and 3 respectively, object of a discussion in a previous (d, ^{3}He) reaction study [Han79], were also resolved.

In the work of Regan et al. [Reg96] excited yrast and near yrast levels, were populated using the ^{18}O(^{48}Ca, $p2n\gamma$) reaction. The resulting level scheme can be seen in Fig 5.10, where angular correlation measurements allowed for precise spin and parity assignments to some of the excited states populated in the experiment.

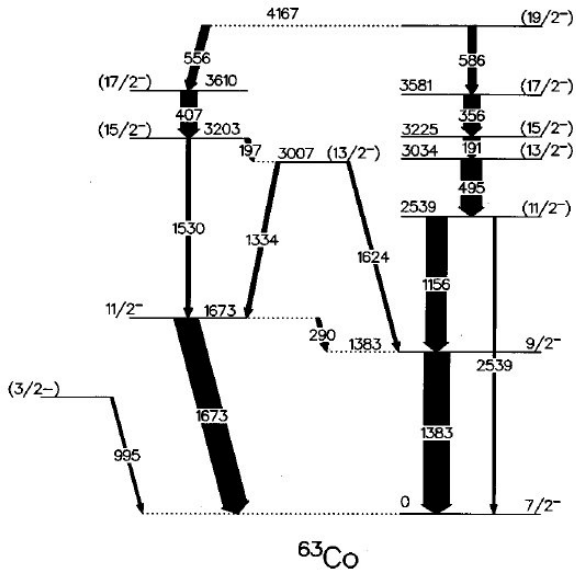

Figure 5.10: Level scheme of ^{63}Co, deduced by Regan et al. [Reg96]. Spins and parities are from angular correlation measurements performed in the same experiment.

Recent multi-nucleon transfer reaction experiments by Dijon et al. and Recchia et al. [Dij11, Rec12], have confirmed the yrast states built on top of the excited $9/2^-$ state in Fig 5.10. Interpretation, based on the coupling of the ground state and the 995-keV level to the 0^+ and the 2^+ excited state of ^{64}Ni and

^{62}Fe, respectively, is suggested by Dijon et al. [Dij11]. Experimental lifetimes of the first two excited state, the 995 keV and the 1384 keV, were measured as 15.4(8) and 0.9(4) ps, respectively, which can be linked to $B(E2)$ values for the transitions connecting the $3/2^-$ at 995 keV and the $9/2^-$ state at 1384 keV to the ground-state [Dij11]. The deduced values are 3.71(43) and 12.2(54) W.u., respectively, assuming for the latter a pure $E2$ multipolarity.

In the experiment of Recchia et al. [Rec12], the transitions de-exciting the strongest populated states – 1383 and 1674, were found to be consistent with an $(M1+E2)$ and an $(E2)$ multipolarity, respectively (Fig 5.10). An interpretation, based on coupling of the observed 1383- and 1674-keV states to the 2^+ excited state in ^{64}Ni is suggested. The large-scale shell model calculations in the former work proved satisfactory in reproducing energies and spins and parities.

It is important to state here, that the adopted spin and parity values for the 1427- and the 1495-keV levels in the NNDC [NND13b] are reversed, with respect to the experimentally determined angular distributions from Seeger et al. [See91] and should be considered as $(1/2^-, 3/2^-)$ and $(5/2^-, 7/2^-)$, respectively.

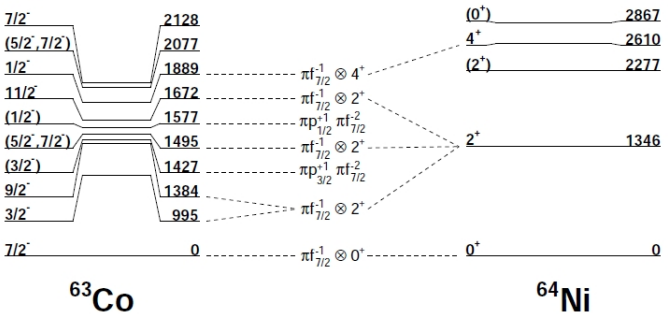

Figure 5.11: Interpretation of the low-lying energy structure of ^{63}Co on the basis of coupling to the adjacent nickel isotope (Particle-core Coupling Model [Oro00]), from [Pau09b].

A comprehensive interpretation in terms of coupling of excited states in the adjacent nickel isotone, was proposed also in the thesis work of D. Pauwels [Pau09b] (Fig 5.11), on the basis of the results in the transfer studies, where proton one-particle two-hole states are identified at 1427 and 1577 keV, based on the low population in $(d, {}^3\mathrm{He})$ reaction [See91]. The 2077-keV excited state, was assigned $(5/2^-, 7/2^-)$ by Seeger et al., based on the observed gamma decay to the ground state [See92].

5.4 Results for ^{63}Fe decay

Using the same experimental analysis techniques, as in the decay of ^{63}Mn, coincidence relationships of transitions, identified as following ^{63}Fe decay, were investigated by placing gamma-gamma gates to build a decay scheme. Compared to the previous decay information (seen in Fig 5.9), 16 new excited levels and more than 40 new gamma transition were identified as belonging to this decay, see Table 5.5.

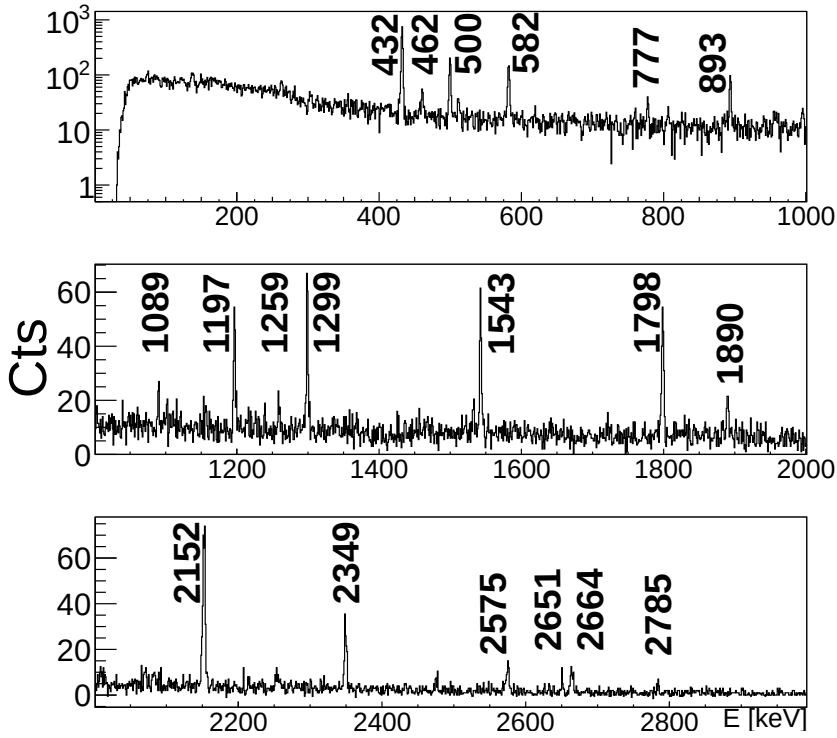

Figure 5.12: Gamma-gamma prompt coincidence gate set on the 995 keV in the decay of ^{63}Fe.

Table 5.5: Gamma transitions and relative intensities, identified as following the decay of ^{63}Fe. For absolute intensities per 100 decays, multiply by 0.663(32).

E_γ (keV)	Rel. Int (%)	Observed coincidence transitions (keV)
149.6(1)	0.51(7)	1427
256.3(2)	0.19(4)	1543
262.8(1)	0.24(7)	418, 432, 893, 956, 1427, 1458, 1890
368.4(1)	1.4(1)	930, 2425
417.5(1)	0.61(8)	949, 2376
432.2(1)	6.5(1)	461, 995, 1101, 1299, 1366, 1458, 1720
461.3(1)	1.8(1)	432, 777, 995, 997, 1259, 1427, 2152
499.6(1)	1.9(1)	930, 995, 1299
535.9(1)	0.22(5)	2611
549.4(1)	0.15(5)	1299, 1798
581.9(1)	2.1(1)	995, 1090, 2011, 2069
619.0(1)	0.23(4)	1101, 1427
645.9(1)	0.25(5)	1427
777.4(2)	0.16(3)	461, 893, 995
806.1(1)	0.35(9)	20, 32
893.2(1)	1.4(1)	777, 995, 1259
930.0(2)	0.27(6)	368, 1495
949.1(2)	0.12(4)	418, 1427
955.6(2)	0.23(4)	1197
994.9(1)	100.0	263, 432, 461, 500, 582, 777, 806, 893, 997, 1090, 1197, 1259, 1299, 1533, 1543, 1798, 1890, 2152, 2349, 2475, 2575, 2651, 2664, 2785
996.9(1)	0.29(3)	263, 995
1089.7(1)	0.32(6)	582, 995
1100.6(1)	1.1(1)	461, 619, 995, 1427
1196.6(1)	0.83(8)	995, 1197
1239.1(1)	1.5(1)	461, 1427
1258.9(1)	0.64(8)	432, 893, 995
1298.7(1)	7.5(1)	500, 1495
1365.5(2)	0.42(8)	461, 1427
1427.1(1)	32.0(2)	150, 263, 432, 619, 646, 949, 1101, 1239, 1259, 1366, 1458, 1720, 2143, 2403

1458.2(1)	1.4(1)	263, 461, 1427
1494.6(1)	8.0(1)	930, 1299, 1818
1532.6(2)	0.33(11)	995
1542.7(1)	1.5(1)	256, 995
1719.9(1)	0.69(6)	461, 1427
1798.4(1)	2.1(1)	549, 995
1818.4(2)	0.36(13)	1495
1889.9(1)	0.76(8)	263, 995
2010.9(2)	0.30(6)	150, 582
2068.7(2)	0.50(7)	582
2143.0(2)	0.43(10)	1427
2151.8(1)	4.2(1)	995
2164.4(1)	0.42(10)	1495
2349.0(1)	1.7(1)	995
2375.8(1)	0.60(8)	418
2402.7(2)	0.20(7)	1427
2424.9(1)	1.6(1)	368
2474.9(1)	0.27(6)	995
2537.3(2)	1.1(1)	—
2575.1(2)	0.49(7)	995
2611.4(1)	0.18(5)	536
2650.5(1)	0.43(10)	995
2664.0(1)	0.64(7)	995
2785.2(2)	0.32(7)	582, 995
2792.4(3)	0.20(6)	—
3146.2(8)	0.23(7)	—
1640.1(5)	0.82(11)	—

Table 5.6: Table 5.5 continued. Gamma transitions below the horizontal line are observed in the clean ^{63}Fe decay spectrum, but were not placed in the decay scheme.

The direct ground state beta feeding in the decay of ^{63}Fe could be determined via the different ways as described earlier.

Method.1 Using the known decay scheme of ^{63}Co:

The first method involves the knowledge of the decay scheme of ^{63}Co and the observed number of counts in the 995-keV transition, strongest in the decay, in singles. The half-life correction factor for ^{63}Fe decay lines is calculated to be 1.67(2). The gamma branching for the strongest transition, based on the decay scheme in this experiment, is deduced to be 0.695(3) (α_{Fe}^{995}). Correcting the number of counts of the 995-keV line for these two factors and the gamma-efficiency and comparing it to the number of calculated ^{63}Co decays, as explained in Method.1 in Sec.5.2, yields a value of **4(16)%**, or $< 20\%$ for the direct beta-decay ground state feeding or missing γ-ray intensity.

Method.2 β-gated spectra in a time constraint, with respect to the ISOLDE super cycle:

In the second method, the expected number of betas in the gamma spectrum from the first PP, correlated with the decay of iron, can be calculated merely on the basis of the determined half-life [NND13b] ($N_{Fe}^{\%}$ = 6.3(6)% of all manganese decays) and compared to the intensity of the 995-keV transition in the beta-triggered spectrum, taking into account ε_γ and α_{Fe}^{995}. This comparison leads to negative values, but **consistent with zero within the experimental uncertainties**.

Method.3 Single event data in different times, with respect to the proton pulse impact:

For the third method a clean ^{63}Fe spectrum was created using the ratio of the number of counts in the 357-keV transition in the two spectra described previously. This determined coefficient was used to deduce the number of betas, correlated only with the decay of ^{63}Fe in that time interval. The intensity of the 995-keV transition, as described above, is compared to the ε_β-corrected iron beta counts. The strongest transition in ^{63}Ni (the 87-keV line) was observed in the clean iron gamma-spectrum, thus the number of ^{63}Fe betas was corrected for the contribution of ^{63}Co decay as well. This was accounted for by subtracting the calculated value:

$$\frac{N_\gamma(87) \times \varepsilon_\beta}{\varepsilon_\gamma(87) \times I_{87}^{abs}},$$

from the number of deduced ^{63}Fe-correlated beta counts, where $N_\gamma(87)$ is the number of counts observed in the area of the 87-keV line in the clean ^{63}Fe γ-spectrum and I_{87}^{abs} is the absolute branching ratio for the 87-keV transition [Run85]. The difference between β and γ counts for ^{63}Fe is **8(11)%**, or $< 19\%$.

The weighted average of these values is determined to be **5(8)%**, or $< 13\%$, consistent with the missing intensity determined in the decay of ^{63}Mn and is adopted in the decay scheme seen in Fig 5.13, as well as in Table 5.7.

The ^{63}Fe decay scheme

An extended decay scheme of ^{63}Fe is deduced in this study, presented in Fig 5.13. The absolute beta-decay branching ratios deduced here are different from the ones obtained by Runte et al. [Run85].

Twenty five excited states were populated in the decay of ^{63}Fe, of which 16 new. The spin and parity of the ground state and the first excited state of ^{63}Co is measured to be $7/2^-$ and $3/2^-$, respectively [See91]. The $7/2^-$ ground state is not directly fed ($< 13\%$), which is consistent with the $(1/2^-)$ assignment for the spin and parity of the ^{63}Fe ground state. The strong beta-feeding towards the $3/2^-$ level at 995 keV and the $(3/2^-)$ level at 1427 keV also supports this.

The excited state at 1888 keV was tentatively assigned as $(1/2^-, 3/2^-)$ by Seeger [See91], on the basis of the deduced $l = 1$ transfer in that work. Because no ground-state transition is observed from this level, a tentative $(1/2^-)$ is preferred.

The state at 2192 keV was identified in [See91] as a $1/2^+$ spin and parity. The calculated logft of 6.8(1) and based on the $(1/2^-)$ spin and parity of the parent nucleus, supports the assignment for the ground state of iron.

Higher in energy, the level at 2376 keV has a tentative $(5/2 - 9/2)^-$ assignment, but since a linking transition to a $(3/2^-)$ excited state at 1427 keV is found, the spin and parity can be narrowed down to $(5/2^-, 7/2^-)$.

Although the level at 2793 keV has a $(5/2, 7/2)^-$ assignment [NND13b], the strong feeding and accordingly low logft makes a $(3/2^-)$ assignment more plausible. The low logft value can be used, as well, to narrow down the assignment of the excited state with an energy of 2885 keV to $(3/2^-)$ (see Table 5.7).

As the 3147-keV level has de-exciting transitions to levels with spins $1/2^+$, $1/2^-$ – $7/2^-$, this fixes the spin and parity of this level to $3/2^-$. The logft value of 5.3(1) rules out a positive-parity assignment for that level.

Table 5.7: Excited levels and direct β-feeding in the decay of ^{63}Fe. The excited states with a "*" are the new levels in the decay scheme of ^{63}Fe, deduced in this study.

E (keV)	I$_\beta$ %	logft	J_π [NND13b]	J_π
GS	< 13	> 6.6	$7/2^-$	$7/2^-$
994.9(1)	50(4)	5.2(1)	$3/2^-$	$3/2^-$
1427.1(1)	20(2)	5.4(1)	$(3/2^-)$	$(3/2^-)$
1494.5(1)	< 1.2	> 6.8	$(7/2^-, 5/2^-)$	$(7/2^-, 5/2^-)$
1576.8(1)	0.8(1)	6.7(1)	—	—
1888.4(1)	1.4(2)	6.3(1)	$(1/2, 3/2)^-$	$(1/2^-)$
2073.1(1)*	0.17(4)	7.2(2)	—	—
2191.5(1)	0.40(7)	6.7(1)	$1/2^+$	$1/2^+$
2376.0(1)	0.08(8)	7.3(3)	$(5/2, 7/2, 9/2)^-$	$(5/2, 7/2)^-$
2424.8(1)*	0.35(8)	6.7(2)	—	—
2527.7(1)*	0.79(11)	6.4(1)	—	—
2537.5(1)*	1.3(2)	6.0(1)	—	—
2611.4(1)*	< 0.07	> 7.6	—	—
2666.2(1)*	1.3(1)	6.0(1)	—	—
2793.3(1)	8.0(7)	5.1(1)	$(5/2, 7/2)^-$	$(3/2^-)$
2885.3(1)	1.4(2)	5.8(1)	$(1/2, 3/2)^-$	$(3/2^-)$
3146.7(1)*	4.4(4)	5.2(1)	—	$3/2^-$
3312.9(2)*	0.24(9)	6.3(2)	—	—
3343.6(1)*	1.5(2)	5.6(1)	—	—
3469.8(1)*	0.18(4)	6.4(2)	—	—
3570.1(1)*	0.61(9)	5.8(1)	—	—
3587.7(1)*	0.20(4)	6.2(2)	—	—
3645.5(1)*	0.61(9)	5.7(1)	—	—
3658.9(1)*	0.70(10)	5.6(1)	—	—
3829.9(1)*	0.13(5)	6.2(2)	—	—
4362.0(1)*	0.21(5)	5.6(1)	—	—

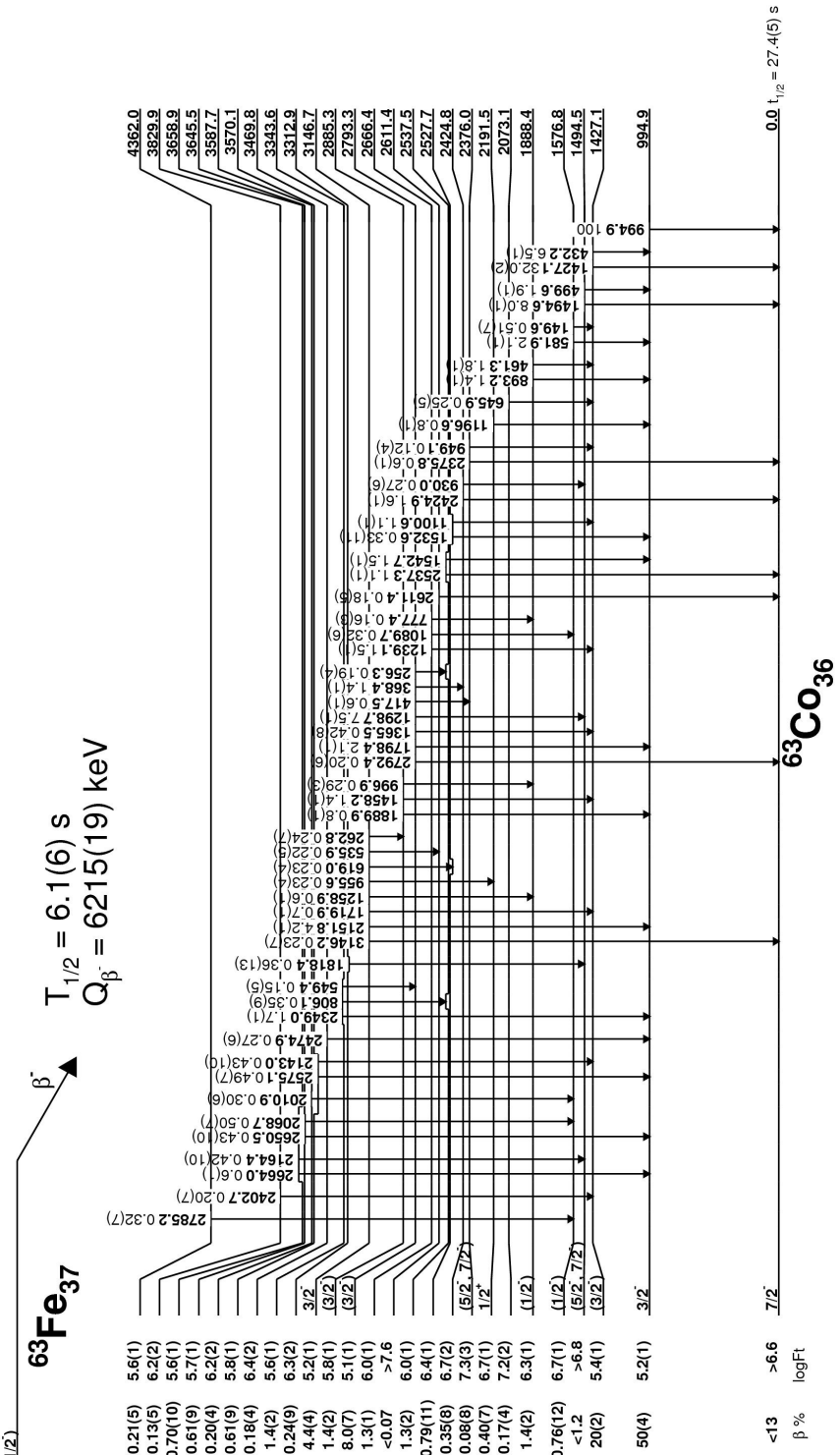

Figure 5.13: Decay scheme of ^{63}Fe, constructed using the data in the current experiment.

5.5 Previous experimental information on ^{63}Ni

A β-decay study was performed by Runte et al. [Run85], where the decay scheme of ^{63}Co was deduced (see Fig 5.14). It was found, that 92.1% of the beta-decay strength goes towards an excited level at 87 keV, assigned as $5/2^-$ spin and parity from transfer reaction studies [Dae68, Run68, Anf70]. It was also suggested, that the decay of cobalt does not feed directly the ground state of ^{63}Ni with $J^\pi = 1/2^-$, consistent with the $7/2^-$ assignment for the ground state of ^{63}Co. The excited states with energies 1452 and 2262 keV, seen in Fig

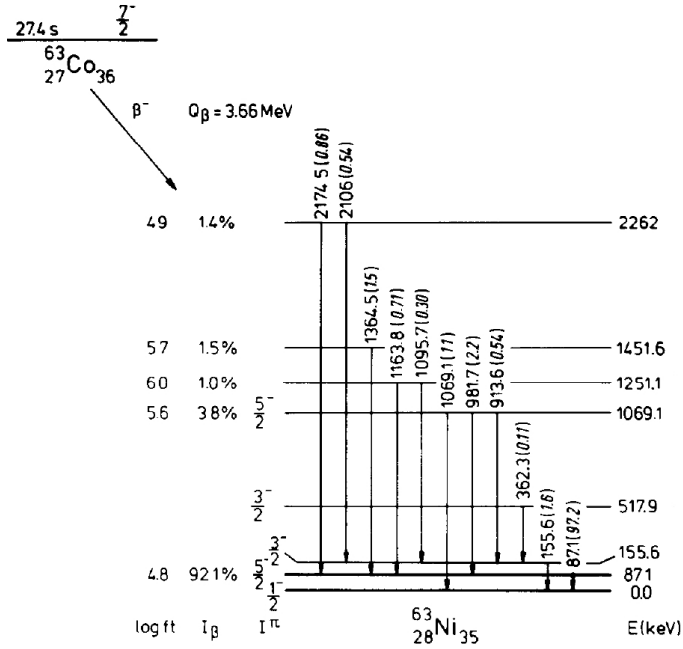

Figure 5.14: Decay scheme of ^{63}Co, presented by Runte et al. [Run85]. Indicated are absolute gamma intensities. All excited levels have been identified in transfer reactions, see e.g. [Dae68, Run68, Anf70].

5.14 have been tentatively assigned as $(5/2, 7/2, 9/2)^-$ and $(5/2, 7/2)^-$ spins and parities, respectively [Erj01].

A fusion evaporation study [War78], populated excited levels with energies 1292, 2184 and 2814 keV. The three states were suggested to be members of a strongly decoupled band, built on top of the tentative $(9/2)^+$, 1292-keV level.

5.6 Results for ^{63}Co decay

An energy spectrum with time constraints, such that the decay of ^{63}Co is enhanced, can be inspected in Fig 5.15. A selected part of the singles gamma spectrum is shown for gammas, recorded with a time stamp of the last two proton pulses only and furthermore, 600 ms after the PP signal. Only the strongest identified transition are indicated either by a symbol, or via an energy label (in keV). The strongest transition in ^{63}Co decay, the 87-keV line, can be

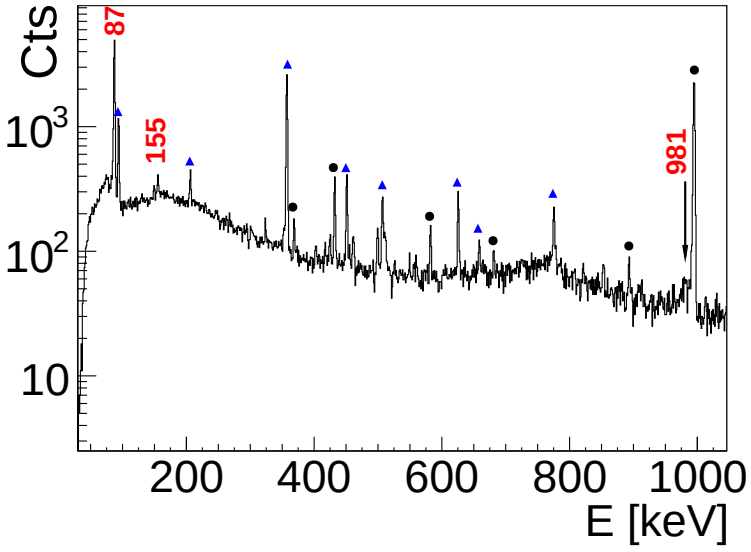

Figure 5.15: Selected part of the statistics in the singles γ-spectrum in the last two proton pulses, with a time constraint of $t_\gamma \geq 600$ ms with respect to the PP. Only the strongest transitions are indicated: a triangle and a circle for ^{63}Mn and ^{63}Fe decay lines, respectively. The energy labels in keV denote transitions in ^{63}Ni.

visually compared to the 155-keV transition with a relative intensity of 1.6(2)%, deduced from coincidence data.

The decay scheme of ^{63}Co was built on the basis of gamma-gamma coincidences and the already established decay scheme from [Run85]. The deduced scheme is in agreement with the one, established in 1985, with the only difference, that a low-intensity transition with an energy of 1743 keV was observed in coincidence

with the 155 keV line, seen in Fig 5.16. The latter coincidence defines an excited

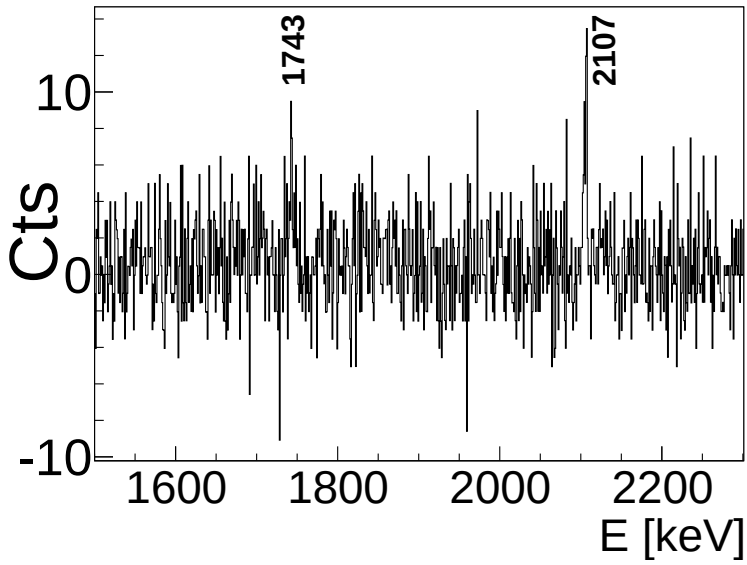

Figure 5.16: Selected part of the prompt γ-γ-coincidence gate, placed on the 155-keV line. Two coincident transitions, 1743 and 2107 keV, are indicated by their energy labels.

state at 1898 keV. A level at 1910(15) keV was populated in [Dae68, Ful65]. The latter was a ^{64}Ni(d,t) reaction study, where the assigned momentum transfer for that level was $l = 3$. In the ^{62}Ni(d,p) study by Anfinsen et al. [Anf70], an $l = (1)$ momentum was assigned to an excited state with energy of 1899(10) keV. The 1899 keV level is tentatively assigned as $(5/2^-, 7/2^-)$ [Erj01], based on the (d,t) study in [Ful65].
Table 5.8 gives information on the coincidence relationships of all observed transitions, along with their deduced relative intensities, while the direct beta-feeding towards the excited states in ^{63}Ni is presented in Table 5.9. A column containing the beta intensities, deduced in the previous decay measurement [Run85] is given for comparison. The direct feeding to the ground state of ^{63}Ni is measured to be zero in [Run85].
The deduced level scheme can be viewed in Fig 5.17.

Table 5.8: Gamma transitions and their relative intensities, identified as following ^{63}Co decay. Italic text denotes γ-γ–delayed (0.8 – 6 μs) coincidence relationship. For absolute intensity per 100 decays, multiply by 0.021(4) (electron conversion coefficient is taken into account; note that for the low-energy 86.5 keV line, the theoretically calculated [NND13b] conversion coefficient is 0.998(1)).

E_γ (keV)	Rel. Int (%)	Observed coincidence transitions (keV)
86.5(1)	2359(387)	*982, 1164, 1364, 2174*
155.3(1)	75(13)	362, 136, 914, 1096, 1743, 2107
362.0(5)	5(1)	–
913.5(2)	23(4)	155
981.6(2)	100	*87*
1069.2(3)	25(7)	—
1095.8(2)	14(3)	155
1164.2(2)	30(10)	*87*
1364.4(2)	85(19)	*87*
1742.8(2)	7(2)	155
2106.8(2)	15(3)	155
2173.7(2)	38(9)	*87*

Table 5.9: Excited levels and direct β-feeding in the decay of ^{63}Co. The calculated beta-decay intensity includes the electron-conversion coefficient of the 86.5-keV transition such that a clear comparison with the previous decay data from [Run85] (in column number 3) can be made. The assignments of spin and parity for the excited states as well as their half-lives are taken from [NND13b].

E (keV)	I_β %	$I_\beta^{[Run85]}$ %	logft	J_π	$T_{1/2}$
GS	—	—	—	$1/2^-$	101.2(15) y
86.5(1)	93(11)	93(5)	4.8(1)	$5/2^-$	1.67(3) μs
155.3(2)	0.23(17)	0.15(15)	7.4(2)	$3/2^-$	
517.3(2)	0.10(2)	0.11(2)	7.6(1)	$3/2^-$	
1068.5(2)	3.1(3)	3.71(24)	5.7(1)	$(5/2^-)$	
1250.9(2)	0.9(2)	0.99(15)	6.1(1)	—	
1450.9(2)	1.8(3)	1.43(14)	5.6(1)	$(5/2^-, 7/2^-, 9/2^-)$	
1898.1(2)	0.15(4)	—	6.3(1)	$(5/2^-, 7/2^-)$	
2261.1(2)	1.1(2)	0.53(11)	5.0(1)	$(5/2^-, 7/2^-)$	

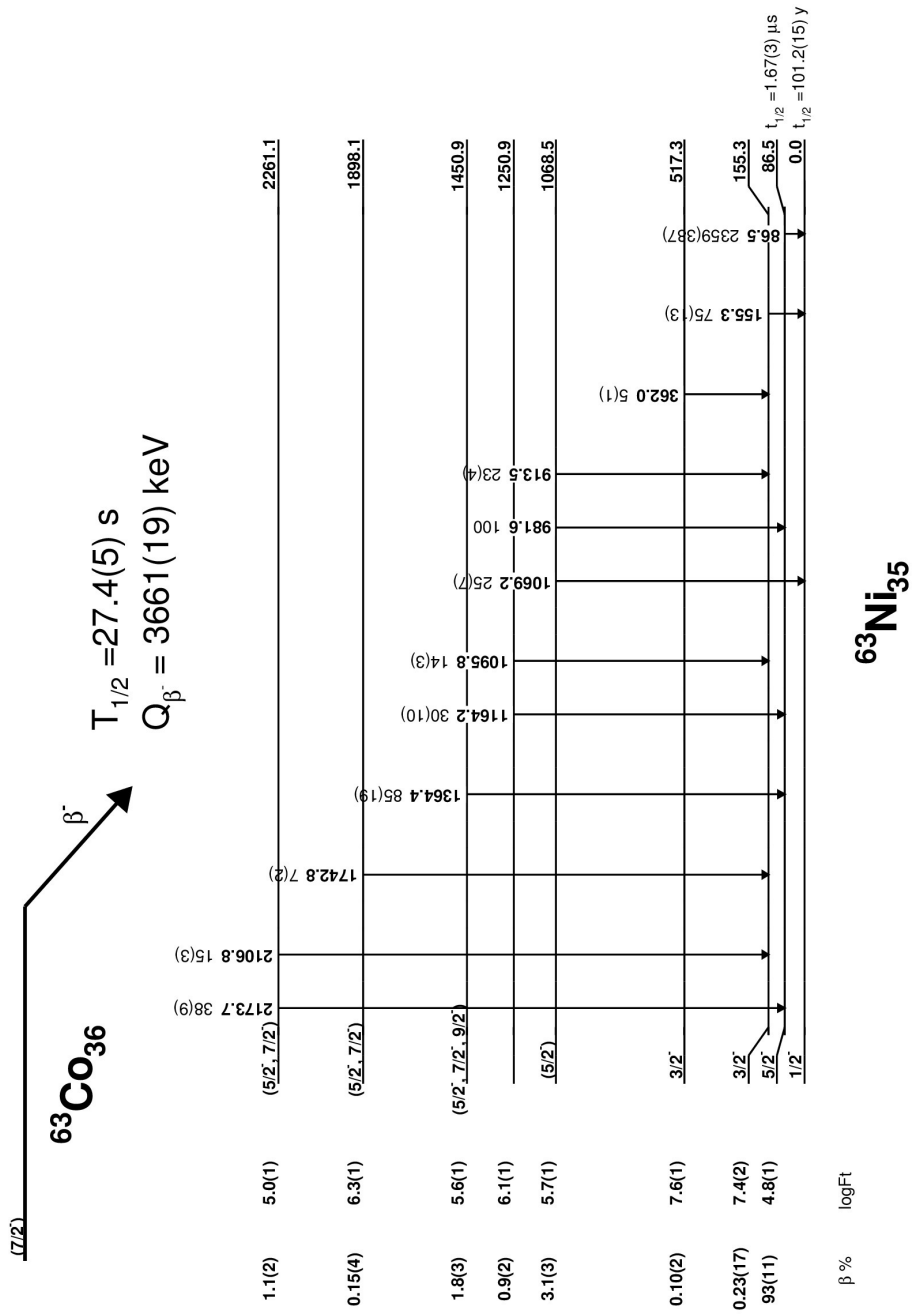

Figure 5.17: Decay scheme of ^{63}Co, constructed using the data from the current experiment.

Chapter 6

Results for the decay chain of $A = 65$

6.1 Previous experimental information on ^{65}Fe

The ground state of ^{65}Mn is tentatively assigned as $(5/2^-)$ spin and parity based on the systematics of the lighter, odd mass, manganese isotopes (Section 4.2, Fig 4.9) and has an adopted half-life of $T_{1/2} = 92(1)$ ms [Sor03a]. Its β-delayed neutron branch was determined to be $P_n = 21.0(5)\%$ [Han00].

After several experiments with sometimes contradicting and confusing results, the low-lying level structure of ^{65}Fe can be summarized as follows: two excited states at 364 and 397 keV are found, one of them with an isomeric character and a half-life of $T_{1/2} = 0.43(13)$ μs was determined by [Grz98].
At first it was thought that the metastable state is at the energy of 364 keV, but a later decay study found that this is not the case by observing an ($E1$) 33.5-keV line in coincidence with the previously observed 364 keV [Dau06], shifting the energy of the isomeric state to 397 keV. This fact was later confirmed in the thesis work of Gaudefroy [Gau05], where the half-life of the 364 keV is stated to be in the order of only a few tens of nanoseconds.

In a multi-nucleon transfer experiment at LNL, Legnaro, Lunardi et al. [Lun07] observed two gamma transitions they could assign to ^{65}Fe – a 772 and an 1118 keV. The statistics, did not allow to observe coincidences, but similarity of the energies of the transition to the ones observed for ^{61,63}Fe allowed them to place the lines in a cascade, forming a band on top of an unknown $(9/2^+)$ isomeric level [Lun07]. An interpretation of a decoupled band, built on top of a

not yet observed, positive-parity, isomeric $(9/2^+)$-state, based on shell model calculations in a truncated model space, was suggested.

The half-life of the ground state of ^{65}Fe was determined for the first time by Czajkowski et al. [Cza94] as $T_{1/2} = 450(150)$ ms, but in a dedicated experiment, Sorlin et al., deduced a new value for it – $T_{1/2} = 1.3(3)$ s [Sor99], proposing the existence of a beta-decaying isomeric state in ^{65}Fe, due to the large difference in the deduced half-lives.

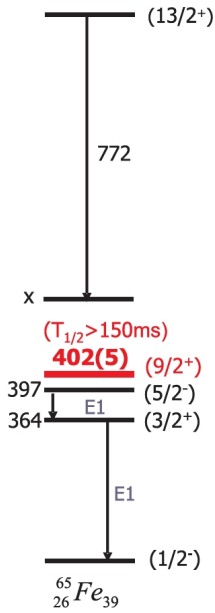

Figure 6.1: Level scheme of ^{65}Fe taken from [Blo08].

This was confirmed in a Penning trap mass measurement experiment, where Block et al. [Blo08] discovered a new isomeric state in ^{65}Fe at an excitation energy of around 402(5) keV (later on corrected to 402(10) keV [Fer10]) and a lower limit on its half-life of $T_{1/2} \geq 150$ ms. This excited level is the most probable candidate for an expected, as in the neighbouring ^{61}Fe, $(9/2^+)$ spin and parity state. It was proposed, that the J^π of the ground state of ^{65}Fe is $(1/2^-)$, in order to account for the long experimental half-life of the observed isomeric level [Blo08] (see Fig 6.1).

In a proton-induced fission reaction experiment at LISOL, Pauwels et al. [Pau09a] produced ^{65}Fe and studied its decay with the aid of laser ionization with the same experimental set-up used in the current decay study. Both the ground state and the β-decaying isomeric state were produced. The half-lives of the two beta-decaying levels were determined as $T_{1/2} = 0.81(5)$ s and $T_{1/2} = 1.12(15)$ s, for the ground state and the isomeric state, respectively.

A recent β-decay study was performed, aiming at measuring the half-lives of excited states in the neutron-rich iron isotopes [Ola11] using the fast-timing technique and $LaBr_3(Ce)$ fast scintillators. Preliminary results suggest, that the half-lives of excited states at 364 keV and a second excited level at 451 keV are $T_{1/2} = 93(3)$ ps and $T_{1/2} = 350(10)$ ps, respectively, much like the ones determined for ^{63}Fe in the same study.
Logft values were calculated for the latter excited levels as 4.6 and 5.2, respectively, and no direct feeding to the ground state of iron was observed. Proposed were spin and parity configurations of $(1/2^-)$ for the ground state and $(3/2^-)$ and $(5/2^-)$ for the two excited states, on the basis of the determined half-lives and logfts. The report from reference [Ola11] is already published [Ola13] and the final results from that study are compared with the ones deduced here in Table 6.4 further on.

6.2 Results for ^{65}Mn decay

Experimental Details

The decay set on $A = 65$ consists of a total laser-on duration of 19242 s, with respect to 4685 s for laser-off. The delay on the beam gate, after the proton pulse impact, was set for 1 ms, with a 100 ms of implantation time. The decay data was recorded for 2.2 s after each proton pulse (see Fig A.10). Two read-outs were set while acquiring – at 500 and 1100 ms after the PP, with a length of 150 ms. The quality of the obtained spectra can be inspected in Fig 6.2, where a laser-on spectrum is compared to a laser-off one, in the same experimental conditions (the laser-off part is scaled for visual comparison).

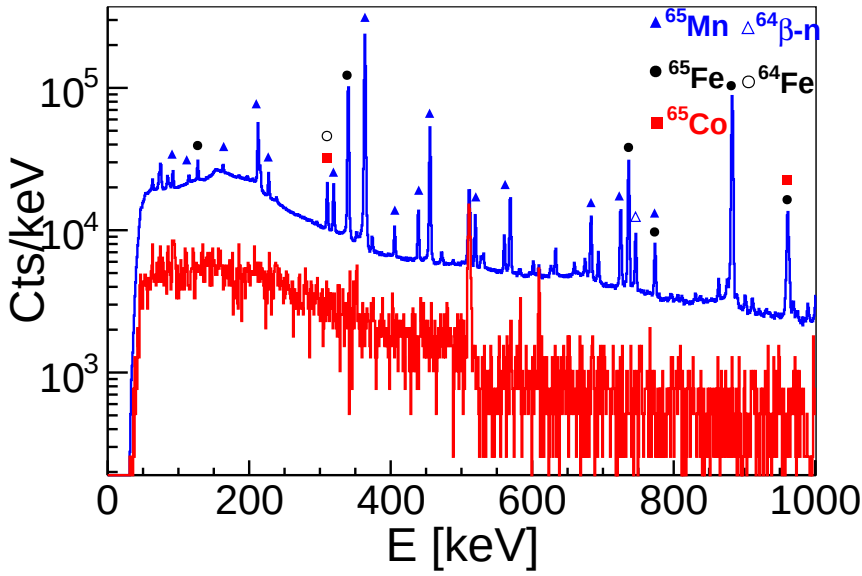

Figure 6.2: Singles gamma laser-on compared to a laser-off spectrum in the same experimental conditions. The laser-offff spectrum is scaled for visual comparison, while some of the identified transitions, belonging to a certain decay are indicated.

Half-life Determination

The half-life of ^{65}Mn could be determined using multiple transitions, identified as following its decay. An exponential decay function on a constant background was fit on the data points of the strongest lines. An example decay fit can be seen in Fig 6.3. The weighted mean value of all fits results in a half-life of $T_{1/2}$

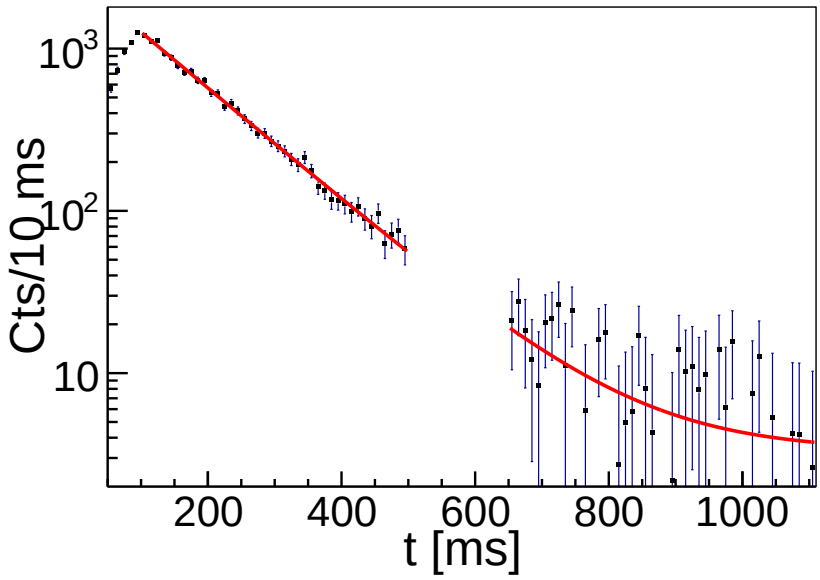

Figure 6.3: Implantation-decay curve of a 725-keV transition, identified as following ^{65}Mn decay. The performed fit does not take into account the points in the forced read-out regions (e.g. 500-650 ms). The determined half-life value from this fit is $T_{1/2} = 87(2)$ ms

= 87.9(4) ms for ^{65}Mn, found to be a bit shorter than the adopted value of 92(1) ms [Sor03a], but in very good agreement with the results from [Han99]. The recent beta-decay experiment in [Ola13] presents the value of 91.9(9) ms for the half-life of ^{65}Mn, which is also not in agreement with the one deduced here.

The half-life of the isomeric state at 397 keV (420(13) ns [Dau06], 437(55) ns [Ola13]) could also be deduced as seen in Fig 6.4. The figure shows the decay curve of the 364-keV transition, outside of the $\beta\gamma$-prompt time window. An exponential decay function on a constant background, results in a half-life of

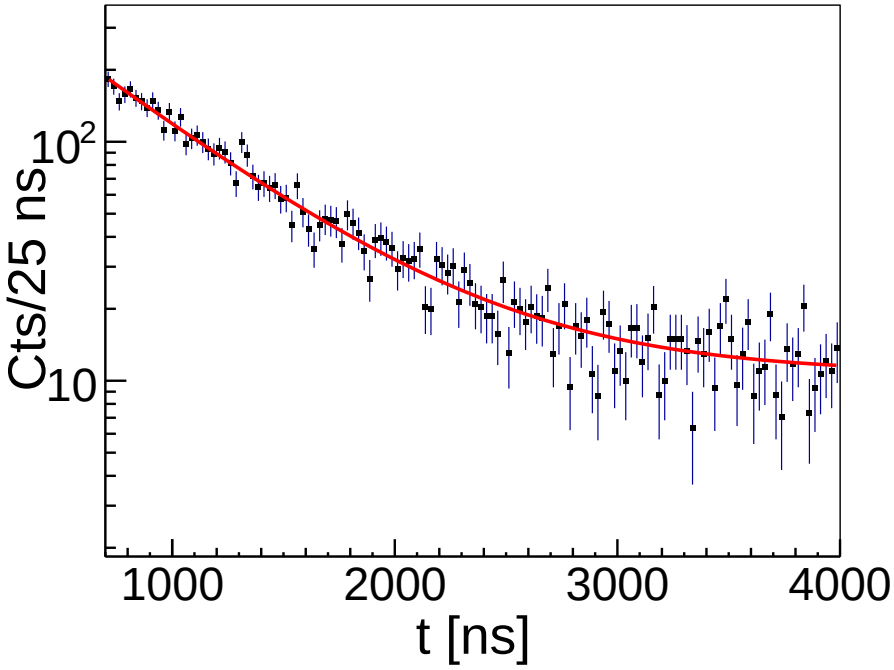

Figure 6.4: Exponential fit of the decay curve of the 364-keV line plus a constant background, outside the prompt $\beta\gamma$-window (0 – 600 ns), resulting in a half-life of $T_{1/2} = 428(11)$ ns.

$T_{1/2} = 428(11)$ ns, in a very good agreement with the previously determined values.

Decay Scheme

The decay scheme of ^{65}Mn was built, by placing prompt and delayed γ-γ-coincidence gates on the transitions, identified as belonging to manganese decay. Such a prompt gate can be seen in Fig 6.5, where the gamma lines, coincident with the 364-keV line transitions are labeled. A γ-γ coincidence gate was also placed on the 364-keV transition, outside the prompt gamma-gamma window, to allow for identification of transitions feeding the 428-ns, 397-keV isomeric level. This coincidence gate is presented in Fig 6.6, where two spectra with different time conditions are compared. The first one is the gate on the 364-keV line with the time condition on the coincident events as: $t_\gamma \in$ [-700 : -1975]

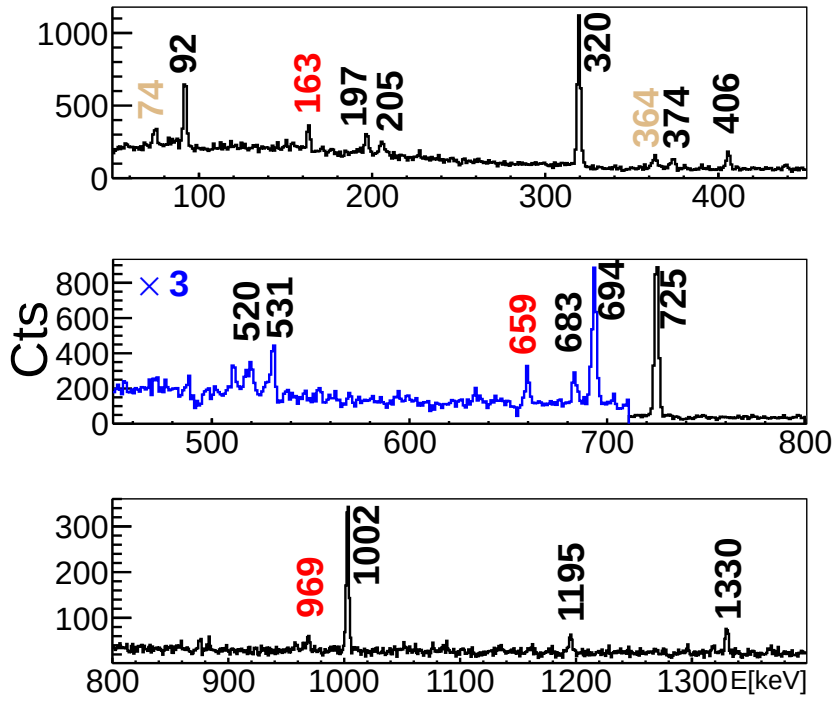

Figure 6.5: Prompt γ-γ-coincidence gate, set on the 364-keV transition, in the time interval 10 – 880 ms after the PP. Coincident transitions are labeled. Dark orange indicates background/random transitions, while red colour denotes transitions, placed feeding the 397-keV state.

ns. The latter statement denotes transitions *preceding* the 364-keV line by at least 700 ns. Indicated by their energy labels in keV are coincident lines, placed feeding the short-lived metastable state. Some of them are also observed in Fig 6.5 as a result of the large (-700 – +700 ns) prompt window. The latter spectrum is compared to a spectrum in the randoms time interval of $t_\gamma \in$ [-3000 : -4275] ns.
Delayed gamma rays with respect to a beta event, can be investigated by looking at the $\beta\gamma$-tree, once again, outside the prompt coincidence time window of 600 ns. Note, that the prompt coincidence windows in the β-γ and the γ-γ tree are different (see Figs A.1 and A.2, respectively).

Since γ-rays are always following the β-particle, only delayed transitions are

observed in Fig 6.7. In the beginning of the spectrum, at the edge of the hardware energy threshold, one can observe the 33.5(5)-keV transition, reported in [Dau06]. The centroid of the gamma-energy peak is found to be at 34.1 keV, in accordance with the previous results.

A line at 397 keV in the latter spectrum, indicated with an arrow, is observed in this decay spectrum and amounts to 1.7(3)% in relative to the delayed 364-keV area units. An estimation using the single-particle rates in Table 1.2, the retardation factor for an $E1$ transition from [End79] and a factor of 0.05 deduced for a retardation of an $M2$ transition in this mass region, based on the 655-keV line in ^{61}Fe and the unobserved 24-keV line in ^{63}Fe, shows that the expected relative branch for such an $M2$ transition is 1.2(5)% in agreement with the observed branching ratio. The 397-keV line, though, can be partially explained by the true summing of the 364-keV strong gamma-transition and the feeding ($E1$) 34-keV line in the same germanium crystal.

GEANT4 simulations including a detailed description of the experimental set-up, showed that the estimated ratio of the two transitions (the delayed 364-keV and the true-summing 397-keV lines), with the electron conversion for the 34-keV $E1$ line, taken into account, is 1.2(1)%. This means, that comparing the theoretical expectations and the simulated true summing in close geometry, one cannot be conclusive whether the 1.7(3)% experimentally observed branching ratio is due to a real, or a summed transition. Thus further on it is referred to as a tentative one.

All transitions, that belong to ^{65}Mn decay, identified through coincidence gates and implantation-decay behaviour, can be seen in Table 6.1.

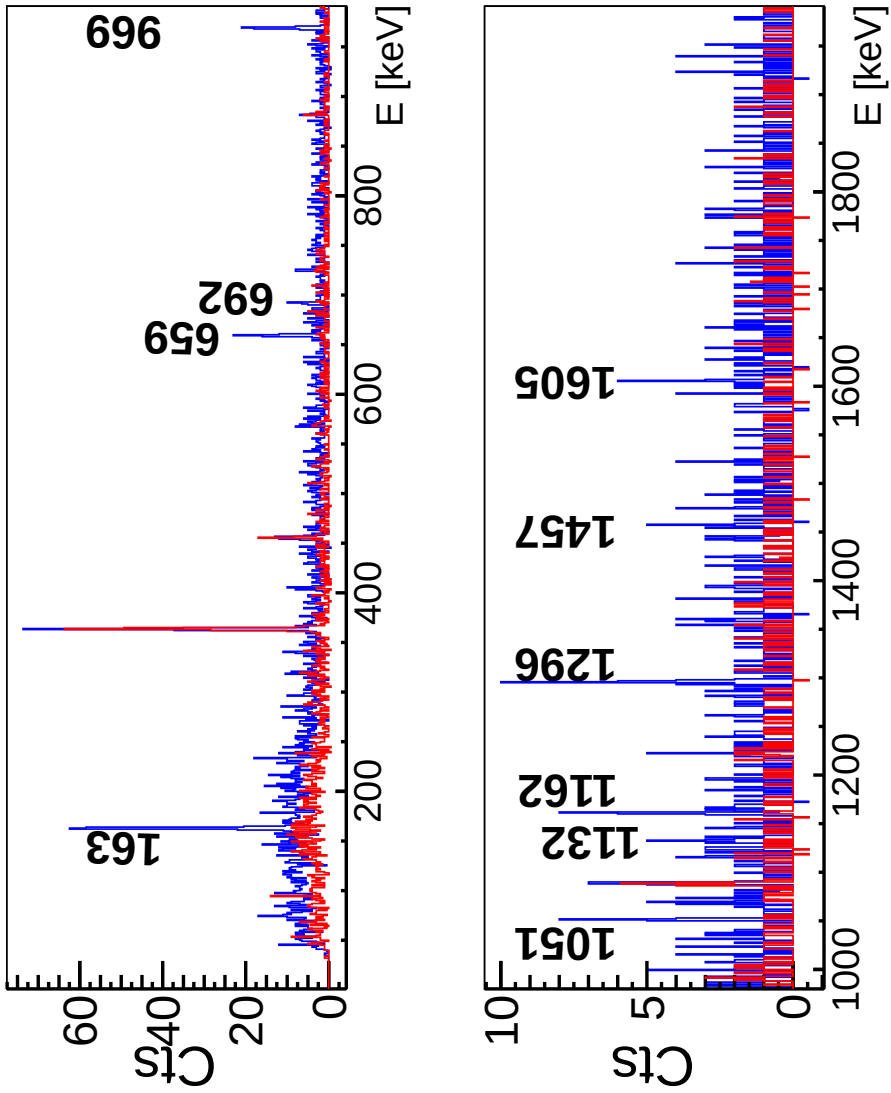

Figure 6.6: Γ_{364}–γ spectrum outside the prompt $\gamma\gamma$-window, where $\gamma_t \in$ [-700: -1975] ns. The red spectrum is drawn in the randoms interval of $\gamma_t \in$ [-3000: -4275] ns, while the transition placed feeding the 428-ns isomer are labelled by their energy in keV.

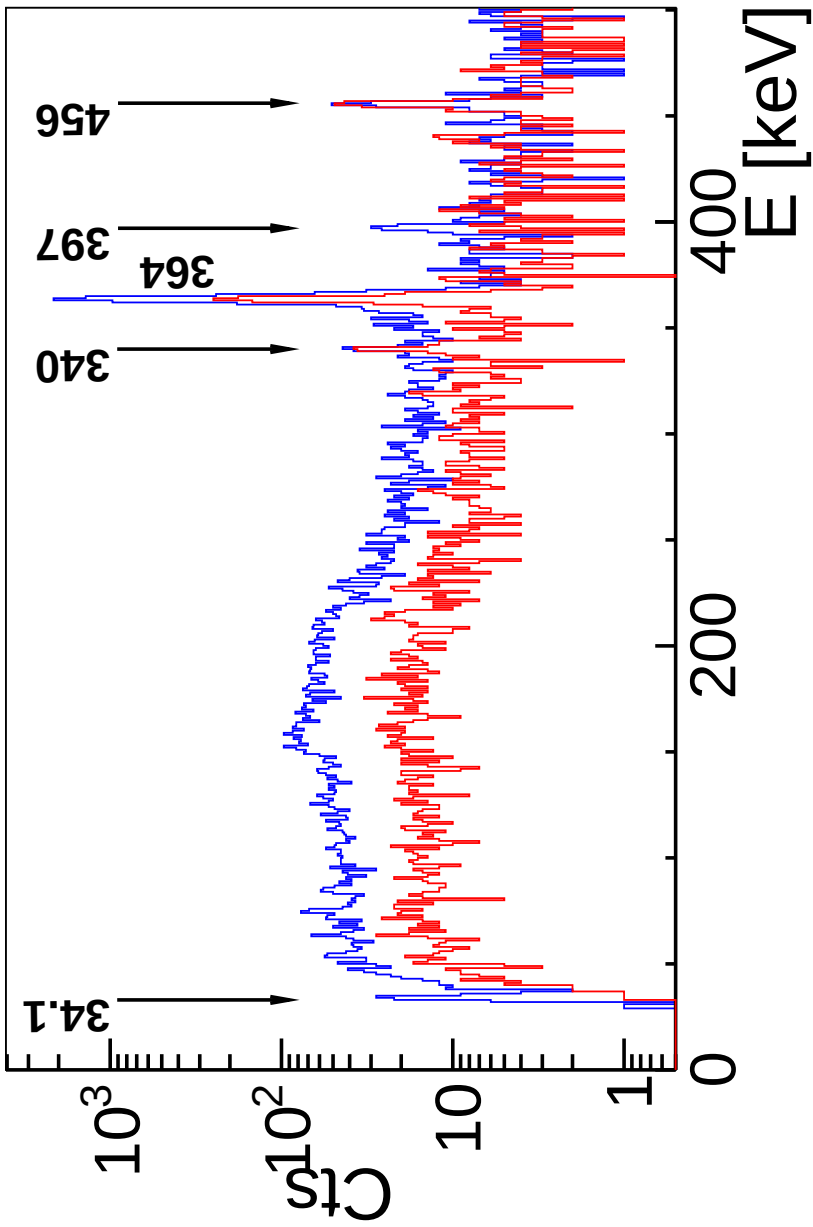

Figure 6.7: Beta-gated gamma-delayed spectrum, plotted in the $\beta\gamma$ time window (600 – 1875 ns), outside the prompt region. A spectrum in the randoms time interval 3000 – 4275 ns is plotted in red. The observed transitions are indicated by their energy label in keV. The lines with energies of 340 keV (^{65}Fe decay) and 456 keV (^{65}Mn decay) are randoms.

Table 6.1: Gamma transitions and relative intensities, identified as following ^{65}Mn decay. Italic font denotes γ-γ-delayed coincidence relationship (Fig 6.6). For absolute intensities per 100 decays, multiply by 0.522(10).

E_γ (keV)	Rel. I_γ %	Observed coincidence transitions (keV):
34.0(1)	7.9(1)	–
92.0(1)	1.0(1)	228, 364, 439
114.0(1)	0.24(4)	569
163.1(1)	0.60(9)	*364*, 528
197.3(1)	0.43(6)	364
205.2(1)	0.54(11)	364, 520, 531
215.7(1)	2.4(2)	448, 757, 763, 1123, 1392
227.6(1)	2.4(1)	364, 374, 406, 456, 683, 876
319.5(1)	4.5(1)	364, 374, 406, 683, 876, 1319
363.6(1)	100	*163, 659, 692, 969, 1051, 1132, 1162, 1296, 1457, 1605*, 92, 197, 205, 228, 320, 374, 406, 531, 683, 694, 725, 876, 969, 1003, 1195, 1319, 1330, 1368
397.5(1)	0.13(2)	–; tentative placement
374.0(1)	0.91(6)	228, 320, 364, 456, 683
405.6(1)	1.9(1)	228, 320, 364, 456, 683
439.1(1)	3.2(1)	92, 364, 456, 472, 959
447.8(5)	0.07(2)	216
455.5(1)	24.4(1)	228, 374, 406, 439, 472, 602, 633, 683, 773, 911, 959, 1002, 1103
471.8(1)	0.81(6)	92, 439, 456, 531
488.2(1)	0.19(4)	569
519.7(1)	4.1(1)	569
527.9(1)	0.89(12)	163, 561
531.0(1)	0.85(12)	364, 472
560.7(1)	2.6(1)	528, 806, 812, 2366, 2372
569.0(1)	8.5(1)	114, 488, 520, 769, 990, 1433
601.6(1)	0.75(6)	456
633.1(1)	1.9(1)	456
659.4(1)	0.50(8)	*364*
683.1(1)	4.2(1)/2.1(1)	228, 320, 374, 406, 683, 876, 1319
692.3(5)	0.17(5)	*364*
693.5(1)	1.7(1)	364
695.1(5)	**0.23(5)**	746; IN ^{64}FE
725.0(1)	8.6(1)	364
746.2(1)	**4.7(1)**	695, 1017, 1106; IN ^{64}FE
757.4(1)	0.14(3)	216
762.8(5)	0.10(4)	216
772.8(5)	0.40(5)	456
796.4(1)	0.27(5)	569
805.8(1)	0.34(7)	561
811.6(1)	0.42(11)	561

875.8(1)	0.95(6)	320, 364, 683
911.1(1)	0.55(7)	456
958.5(1)	0.57(7)	439, 456, 531
968.9(1)	0.68(16)	*364*
989.8(1)	0.76(9)	569
1001.8(3)	0.51(19)	456
1002.8(1)	4.9(2)	364
1017.1(5)	**0.52(8)**	764; IN ^{64}Fe
1050.9(5)	0.16(6)	*364*
1057.1(1)	0.64(11)	—
1088.6(1)	16.0(2)	—
1103.2(1)	1.0(1)	456
1106(1)	**0.06(3)**	746; IN ^{64}Fe
1122.9(1)	0.28(5)	216
1132.1(1)	0.14(6)	*364*
1161.5(3)	0.23(7)	*364*
1195.1(1)	0.66(9)	364
1296.1(1)	0.34(8)	*364*
1318.5(1)	0.66(9)	320, 364, 683
1330.1(1)	1.0(1)	364
1366.9(5)	0.17(13)	—
1368.3(5)	0.33(8)	364
1391.8(5)	0.15(6)	216
1432.6(2)	0.55(10)	569
1449.3(3)	0.67(8)	—
1456.7(7)	0.35(6)	*364*
1559.2(5)	0.30(11)	—
1605.2(5)	0.17(9)	*364*
1693.3(1)	0.33(12)	—
1732.4(5)	0.21(8)	—
1851.2(5)	**0.44(11)**	—; IN ^{64}Fe
2366.4(5)	0.09(5)	561
2371.9(1)	0.33(8)	561
817.2(5)	0.15(9)	—
1221.8(5)	0.10(3)	—
1234.7(5)	0.34(9)	—
1471.8(5)	0.23(5)	—
1673.7(5)	0.17(6)	—
1951.3(5)	0.21(11)	—
2302.5(5)	0.27(11)	—
2445.5(5)	0.17(10)	—
2534.4(5)	0.30(11)	—
2639.6(5)	0.31(13)	—
2839.2(5)	0.49(16)	—
3013.6(5)	0.44(12)	—
3534.3(5)	0.37(11)	—

Table 6.2: Table 6.1 continued. Transitions below the horizontal line were found in the clean ^{65}Mn decay spectrum and not in the laser-off one, but not placed in the decay scheme.

β-delayed neutron branch

Two transitions, that are known to be de-exciting levels in ^{64}Fe, were clearly observed in the singles gamma spectrum. Those are the 746 keV ($2^+ \rightarrow 0^+$ indicated in Fig 6.2 with an empty triangle) and the 1017 keV ($4^+ \rightarrow 2^+$) [Hot06]. When placing a prompt coincidence gate on the 746-keV line, two other transitions were found to be present in that spectrum – a 695- and an 1106-keV line, belonging to the β-decay of ^{64}Mn [Han00, Pau13], corresponding to excited states at 1441 and 1852 keV, respectively.

The number of ^{64}Fe decays was obtained, using the absolute branchings of the the 310- and the 1250-keV transitions [Pau13], following the decay of ^{64}Fe, in separate calculations. The half-life correction factors, from the subsequent decay of the 2.0(2) s [Run85] ground state of ^{64}Fe, was determined to be 1.31(1). Since both transitions appear to be doublets in the current decay set, special care was taken to determine what part is related only to ^{64}Fe decay. This was done through gamma-gamma coincidence relationships in the $A = 65$ decay chain.

Since it was found, that the deduced numbers of ^{64}Co nuclei via the two aforementioned transitions are in agreement within error bars, a weighted mean of the two values was taken for the final value of the number of ^{64}Fe decays. The direct β-delayed neutron feeding is then accordingly distributed over the observed excited state in ^{64}Fe and is summarized in Table 6.3. The obtained

Table 6.3: Distribution of the β-delayed neutron strength in the decay ^{65}Mn, normalized to 100%.

E + S_n (keV)	E (keV)	P_n %	J^π [NND13b]
4179	GS	74(34)	0^+
4925	746	22(6)	2^+
5622	1443	0.5(2)	$(1^+, 2^+)$
5942	1763	1.2(4)	4^+
6033	1854	2.5(9)	$(1^+, 2^+)$

value for the P_n branch is 10(3)% of all manganese decays, much lower than the previously deduced value of 21.0(5)% [Han00], while in a very good agreement with the value of 7.9(12)% from [Ola13].

Energy of the $(9/2^+)$ isomer in ^{65}Fe.

As will be discussed later on, the constructed ^{65}Fe level scheme will be used to extract the feeding to the different levels and the missed beta- or gamma-feeding to the ground-state of ^{65}Fe. Already here one can state, that the latter is receiving little or no direct β-feeding.

The first excited state identified already in previous studies, at 364 keV and receives considerable beta-feeding. These two observations are in agreement with previous spin and parity assignments of $(5/2^-)$ for the ^{65}Mn ground-state, $(1/2^-)$ for the ground-state of ^{65}Fe and $(3/2^-)$ for the 364 keV. The 110(20) ps half-life of the 364-keV transition [Ola11] is supporting the $M1/E2$ character of the line. The gamma lines in coincidence with the latter can be divided in two groups: the ones that are in prompt coincidence and are directly feeding the 364-keV level, and the ones that are in delayed coincidence and are feeding the 364-keV level through the 34-keV isomeric transition, de-exciting the 428(11)-ns level at 397 keV.

The observation of this γ-line by Daugas et al. [Dau06] and also in this work (see Fig 6.7) already limits its multipolarity to a dipole transition, as higher multipolarities lead to large conversion coefficients and thus a very small gamma intensity. A magnetic dipole character is excluded as then the possible spin-parity assignments $(1/2^-, 3/2^-$ or $5/2^-)$ would enable strong transitions to the $(1/2^-)$ ground-state from the isomeric level.

The 1.12(15) s β-decaying $(9/2^+)$ isomer is measured in a Penning trap measurement to be located at 402(10) keV [Fer10].
The long half-life of the state indicates, that its decay is mainly beta, making it hard to find any connection to the lower-lying states in ^{65}Fe. In order to fix its position more precisely a search was thus conducted to find possible feeding transitions from already known higher-lying states.

An observed 216-keV line, with ^{65}Mn decay time signature, is determined to have a relative intensity of 2.4(2)% and has no delayed (< 1 μs) coincidences with gamma-rays de-exciting the lowest levels in ^{65}Fe. It is, therefore, an excellent candidate for feeding the $(9/2^+)$ isomer. As can be seen in Table 6.1, it has prompt coincidences with a number of low-intensity gamma-lines, which were not observed in coincidence with any other strong gamma line in the decay of ^{65}Mn.

Two coincident gamma lines (757 and 763 keV) have an energy difference which matches the energy difference between the 1366- and the 1372-keV levels (see

Fig 6.8). If, indeed, these two gamma lines de-excite the respective levels, the position of the $(9/2^+)$ isomer can be fixed to 393.3(1) keV, in agreement with the mass measurement. With this new and a more precise value, the other gamma lines, coincident with the 216-keV one, can also be placed de-exciting levels determined already through other coincidence and energy relations. The latter placement of the $(9/2^+)$ isomeric state was recently confirmed by [Ola13].

The relative intensity of the 216-keV line can explain most of the intensity observed for the 393-keV level, through its beta-decay towards ^{65}Co (See Fig 6.9B). The next level observed in this decay study is at 455 keV and was previously observed by [Gau05, Ola11]. From then on, all the levels presented in Table 6.4 and Fig 6.8 are new.

Direct beta-decay or missed gamma transitions, feeding the ground state of ^{65}Fe

The direct β-feeding towards each excited state is calculated, using the identified feeding and de-exciting transitions, resulting in Table 6.4.
The direct β-feeding or missed gamma intensity towards the ground state of ^{65}Fe, can be calculated via different methods, analogous to those discussed in Section 5.2:

Method.1 Using the known decay scheme of ^{65}Co:

The decay scheme of ^{65}Co is known from the work of Pauwels et al. [Pau09a]. In that decay it was found that 97.7(8)% of the beta-decay strength goes directly to the ground state of nickel, assigned as $5/2^-$ spin and parity on the basis of several transfer reactions (see e.g. [Anf70, Fly79]).

The absolute branching for the γ-transition of 1141 keV in the decay of ^{65}Co was calculated to be 3.3(1)%. Using that branching and the intensity of the latter, the total number of ^{65}Ni nuclei was deduced and compared to the total number of ^{65}Mn decays, calculated via the sum of the intensities of all identified ground state transition. The number of gamma decays can also be deduced using only the 364-keV line and the information from the deduced decay scheme to obtain an α_{Mn}^{364} of 0.635(3). Half-life correction factors of 1.02(1) and 1.32(1) for ^{65}Mn and ^{65}Co, respectively and γ-efficiencies were taken into account to deduce a difference of **8(2)%**.

Method.2 β-gated spectra with a time constraint, with respect to the ISOLDE super cycle:

In order to minimizing the effect of ^{65}Co decay, beta-gated gamma-spectrum, in the time constraint of the first 200 ms of the first proton pulse was produced, along with a corresponding time-constrained beta-spectrum from the single events data.
The total number of betas was extracted from the latter, while a number of beta-rays, correlated with the decay of ^{65}Fe was calculated on the basis of the determined half-life of its ground state [Pau09a]. It was found, that this number should be 4.3(2)% of the observed beta counts. Accounting for the latter number, along with the 10(3)% of P_n branch, the number of ^{65}Mn decay β-counts was obtained from the beta-singles spectrum with time conditions.

The difference between the deduced number of beta-rays and the gamma decays, obtained via the 364-keV transition with an $\alpha_{Mn}^{364} = 0.635(3)$ is calculated to be **12(5)%**.

Method.3 Single event data in different times, with respect to the proton pulse impact:

Again, minimizing the contribution from ^{65}Co decay, γ– and β-spectra in the intervals 100–276 ms (100 ms is the implantation period of ^{65}Mn) and 300–476 ms after the first proton pulse are created, where the decay of manganese and iron, respectively, is enhanced.
The number of beta counts is deduced from the β-singles spectra in the same time interval and the two gamma-spectra are combined in order to produce a clean spectrum for each of the decays (see Section 5.2, Method.3). The deduced subtraction coefficient can then be used to split up the amount of beta counts, related to ^{65}Mn and 65Fe decay in the corresponding time-constrained beta-spectra.

The observed contribution from the P_n branch is accounted for and subtracted from the number of betas, correlated to manganese decay from the clean 65Mn β-spectrum. The β-counts related only to ^{65}Mn decay into excited states in ^{65}Fe are then compared to the number of manganese gamma-decays, deduced via the 364-keV transition observed in the clean ^{65}Mn gamma spectrum, using the α_{Mn}^{364} coefficient of 0.635(3)% (defined as described in Method.3 of Section 5.2). The difference between betas and gammas, calculated in this way, amounts to **11(5)%**.

A weighted average of 9(2)%, relative to all ^{65}Fe nuclei, is calculated for the missing beta- or gamma branch, feeding directly the ground state of ^{65}Fe.

Taking into account all manganese decays, thus also the P_n branch, the value deduced relative value is determined to be 7(2)%, further adopted as < 9 in the decay scheme and in Table 6.4. This upper limit is in excellent agreement with the result for the direct beta-decay branch of ^{65}Mn obtained in [Ola13]. One should not forget, that due to the high Q_β-value (see Fig 6.8), this amount is probably the result of unobserved ground-state transitions.

A comparison is made between the information deduced in this decay study and the one from [Ola13], presented Table 6.4. Despite a slight difference in some of the deduced beta-feedings and the intensity of gamma-transitions (see [Ola13] for information on the said γ-intensities), the overall agreement in the deduced excitation energies, the distribution of the beta-strength and the spin and parity assignments is excellent.

The ^{65}Mn decay scheme.

Twenty-three excited states with detailed information on their feeding and de-excitation pattern are identified in the decay of ^{65}Mn. Two excited levels, at 364 and 1089 keV, are found to receive substantial beta strength with logfts of below 5.

Based on observed γ-transitions in coincidence with a 216-keV line, following the decay of ^{65}Mn, the precise excitation energy of the long-living metastable state in ^{65}Fe could be deduced as 393.3(1) keV, in agreement with the recent Penning-trap mass measurement value of 402(10) keV [Fer10].

Experimental evidences point to the conclusion, that the ground state of ^{65}Co does not receive direct β-feeding (see Section 6.4). The very weak direct feeding towards the ground state of cobalt suggests, that the spin and parity quantum numbers for the ground state of ^{65}Fe are $(1/2^-)$, as was the case in ^{63}Fe (see Section 5.2).

In the thesis work of Dijon [Dij12b] it was suggested, that an observed transition with an energy of 721 keV in ^{63}Mn is a line connecting the $(9/2^-)$ and the $(7/2^-)$ excited states. This transition's energy is very close to the energy of the $2^+ \rightarrow 0^+$ transition in ^{64}Fe (746 keV [NND13b]). In the latter experiment by Dijon, a single gamma line was observed in ^{65}Mn with an energy of 536 keV, proposed to be a ground-state transition. Based on the similarity in energy to the ground-state transition de-exciting the 2^+ state in ^{66}Fe (574 keV), the observed line is assigned as connecting an excited $(9/2^-)$ state with the $(7/2^-)$ ground state of ^{65}Mn. Thus, the ground state of ^{65}Mn in [Dij12b] was

Table 6.4: Excited levels and direct β-feeding in the decay of ^{65}Mn. The data in columns 5, 6, 7 and the half-lives in the pico-second range are from [Ola13]. Higher-lying excited states that do appear in the latter reference but were not observed here are omitted. The half-lives of the two beta-decaying, long-living isomers are from [Pau09a].

E (keV)	I_β %	logft	J^π	E (keV)	I_β	J^π	$T_{1/2}$
GS	< 9	> 5.6	$(1/2^-)$		< 8.8	$(1/2^-)$	0.81(5) s
363.6(1)	35(1)	4.8(1)	$(3/2^-)$	363.7(1)	42(5)	$(3/2^-)$	93(3) ps
393.3(1)	0.44(22)	6.6(2)	$(9/2^+)$	393.7(2)	—	$(9/2^+)$	1.12(15) s
397.5(2)	2.3(3)	5.9(1)	$(5/2^+)$	397.6(2)	0.1(6)	$(5/2^+)$	428(11) ns
455.5(1)	7.5(4)	5.4(1)	$(5/2^-)$	455.6(1)	8.1(11)	$(5/2^-)$	350(10) ps
560.7(1)	0.67(13)	6.4(1)		561.0(2)	1.5(2)	$(3/2^\pm, 5/2^-)$	390(50) ps
569.0(1)	1.5(1)	6.1(1)		569.1(1)	0.9(4)	(1/2, 3/2)	< 12 ps
609.0(2)	0.85(12)	6.3(1)	$(7/2^+)$	609.5(3)	1.0(1)	$(7/2^+)$	
683.1(1)	2.4(1)	5.8(1)		683.3(1)	2.1(3)	$(3/2^\pm, 5/2^-)$	24(12) ps
894.6(1)	1.4(2)	6.0(1)	$(7/2^-)$	894.8(1)	1.4(2)	$(7/2^-)$	< 27 ps
1057.1(2)	2.4(1)	5.8(1)	$(5/2^-)$	1057.3(1)	2.9(2)	$(3/2^-, 5/2^-)$	< 8 ps
1088.6(1)	17.2(6)	4.9(1)	$(3/2^-)$	1088.7(1)	20.7(9)	$(3/2^-, 5/2^-)$	< 8 ps
1228.3(1)	0.20(3)	6.8(1)		1228.2(2)	0.2(1)		
1366.2(3)	5.1(2)	5.4(2)	$(5/2^-)$	1366.6(2)	6.3(3)	$(5/2^-)$	< 8 ps
1372.4(3)	0.27(6)	6.7(1)		1372.6(3)	0.3(1)		
1448.7(3)	0.43(5)	6.5(1)		1449.1(4)	0.3(1)		
1457.3(3)	0.26(10)	6.6(2)		1457.2(5)	0.5(1)		
—	—	—	—	1472.0(6)	0.1(1)		
1529.6(5)	0.07(3)	7.2(2)		1530.0(5)	0.2(1)		
1558.8(2)	2.0(1)	5.7(1)		1558.9(5)	2.4(1)		
—	—	—	—	1674.2(7)	0.1(1)		
1693.7(1)	0.86(10)	6.0(1)		1693.7(1)	1.3(1)		
1732.0(5)	0.42(6)	6.4(1)	$(5/2^-)$	1732.5(4)	1.4(1)		
1853.0(1)	0.47(5)	6.0(1)		1853.5(4)	1.2(1)		
2001.6(1)	0.78(9)	6.1(1)		2002.0(3)	0.7(1)		
2927.1(7)	0.05(3)	7.0(3)		—	—		
2932.6(2)	0.17(4)	6.4(1)		2932.6(4)	0.4(1)		

tentatively assigned as $(7/2^-)$ spin and parity.

In the present decay data no evidence for such a spin assignment of ground state was found, thus, the spin and parity of the ground state of ^{65}Mn is adopted as $(5/2^-)$. Based on the latter, the logft values determined here and the results for the half-lives of the 357- and 451-keV excited levels in [Ola13], the excited state at 364 keV can be tentatively assigned as $(3/2^-)$ and the one at 451 keV as $(5/2^-)$, in analogy to the assignments in ^{63}Fe.

The logft value calculated for an excitation energy of 397 keV, with the branching

ration from Table 6.4 supports a $(5/2^+)$ spin and parity assignment for that level.

The observation, in this study, of a 34-keV transition from that state confirms the results in [Dau06]. This low-energy transition remained unobserved in the fast-timing experiment [Ola13], due to the used energy threshold. The expected $M2$ branch from that excited state, towards the ground state was estimated to be around 1.2%, as discussed earlier. Such a line was identified in the beta-gated delayed gamma spectrum, but the complementary information from the performed GEANT4 simulations, do not allow to firmly confirm the presence of a such a cross-over transition. Thus, it is presented in the decay scheme as a tentative one. The observed low-energy gamma transition of 34 keV can be assigned as $E1$, indicating a change of parity between the latter level and the 364-keV state.

The newly deduced excitation energy of the $(9/2^+)$ state is such, that the 397-keV level does not feed it. Based on the single transition of 216 keV, feeding the $(9/2^+)$ excited state and the lack of observation of a ground-state transition, the level at 609 keV is tentatively assigned as $(7/2^+)$. It is found that the latter does not de-excite towards the $(5/2^+)$ at 397 keV, since no transition matching such an energy difference, was observed in the γ-γ-spectrum, outside our prompt window, as can be inspected in Fig 6.6, nor does it decay towards the tentatively assigned $(5/2^-)$ at an energy of 456 keV.

The level at 895 keV de-excites only to the $3/2^-$ and the $(5/2^-)$ at 456 keV, but not towards the $1/2^-$ ground state, therefore a tentative spin and parity of $(7/2^-)$ can be assigned, supported by the apparent feeding of the latter.

Based on the de-excitation patterns of the excited levels at 1057 and 1366 keV, feeding tentatively assigned $(1/2^- - 7/2^+)$ states, as well as their calculated $\log ft$ values, the spin and parity of these levels can be inferred as $(5/2^-)$. Such conclusions can be drawn for the excited state at 1089 keV, but the deduced low $\log ft$ value points to a tentative $(3/2^-)$ spin and parity.

The excited state at 1732 keV is also tentatively assigned as $(5/2^-)$, due to its de-excitation pattern towards the $(1/2^-)$ ground state and the 609-keV $(7/2^+)$ level.

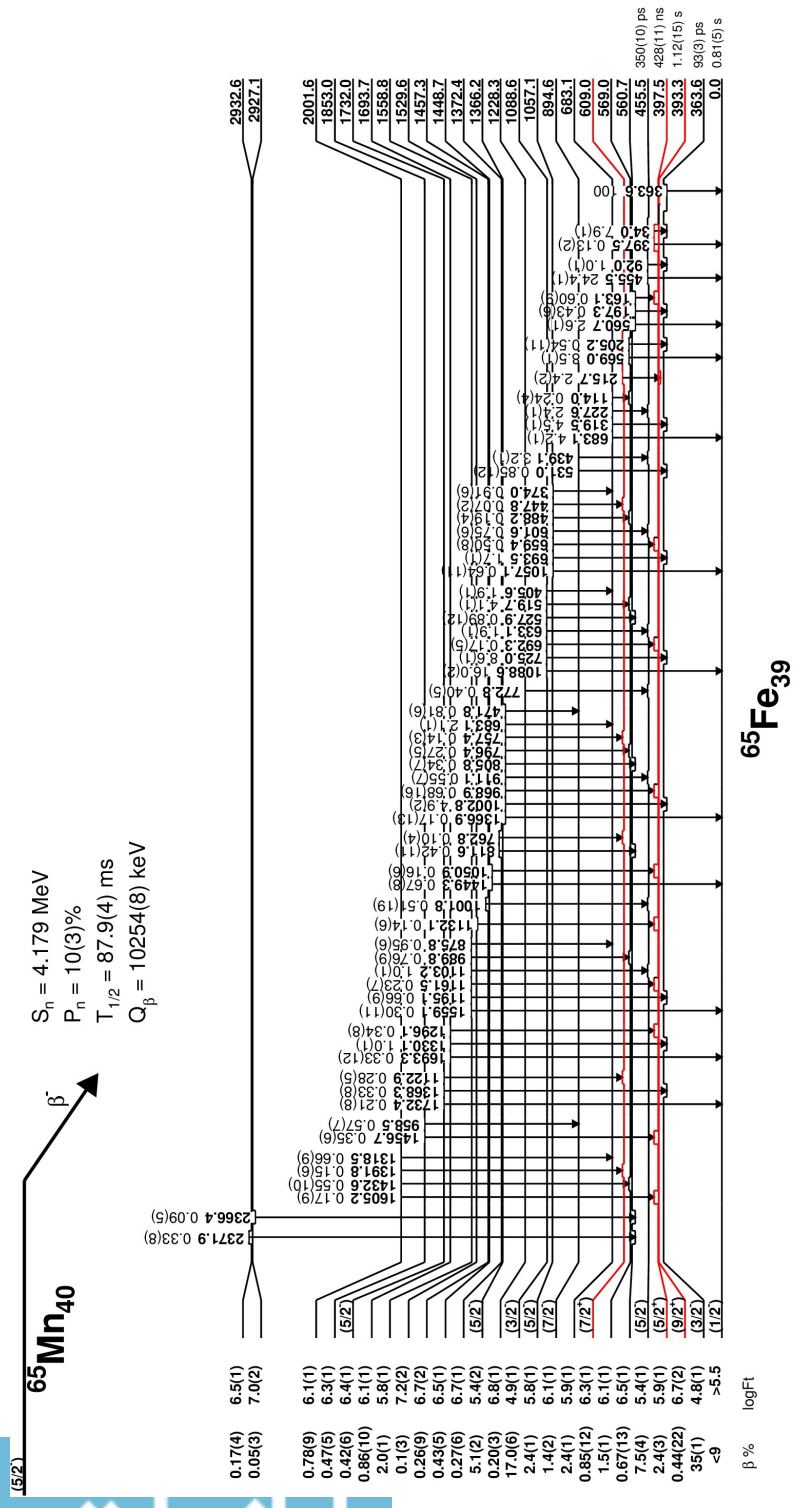

Figure 6.8: Decay scheme of ^{65}Mn, deduced in the current study. Red colour denotes tentative positive-parity states.

6.3 Previous experimental information on ^{65}Co

The experimental information on the excited states in this isotope comes mainly from β-decay studies, as no results from transfer reactions, involving ^{65}Co, are currently available.

A tentative $(7/2^-)$ spin and parity is assigned for the ground state, found to be consistent with the systematic of the lighter odd-A cobalt neighbours [Run85, Bos88]. This assignment is also based on the calculated low $\log ft$ values towards the ground state of ^{65}Ni, in a recent β-decay study [Pau09a].

Decay lines with energies 340 and 882 keV, placed in ^{65}Ni by Bosch et al. [Bos88], were unambiguously placed in ^{65}Co [Gau05, Pau09a], following the β-decay of iron. More than 50% of the beta strength, in the decay of iron, was assigned towards the ground state of ^{65}Co by Gaudefroy [Gau05].

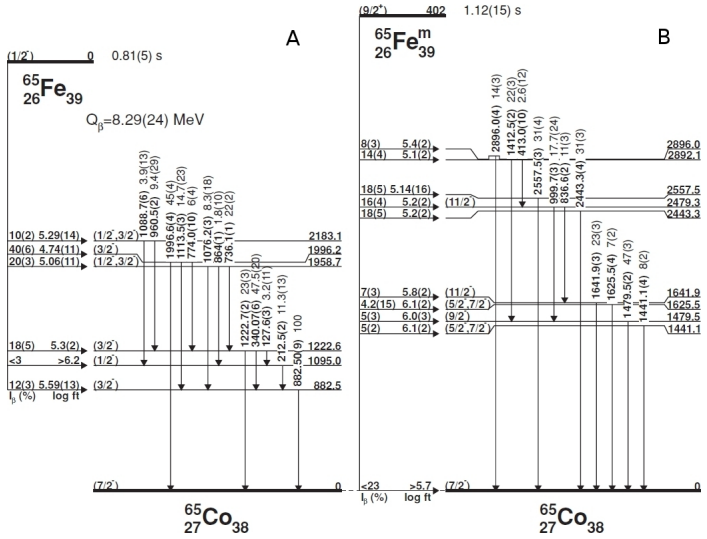

Figure 6.9: Decay schemes of ^{65,65m}Fe deduced by Pauwels et al. [Pau09a].

The decay of ^{65}Fe and its long-living isomeric state, was investigated in [Pau09a], produced in a proton-induced fission reaction on a ^{238}U target and selectively ionized by the LISOL ion-source. Two separate decay schemes were constructed, corresponding to ^{65}Fe and ^{65m}Fe decay, as no linking transition between them

was found (Fig 6.9).

The analysis of the decay data was supplemented by a deep inelastic reaction study, performed at ANL, Chicago, where with the help of triple gamma coincidences, the yrast and near-yrast level structure of ^{65}Co was revealed [Pau09a]. As in the case of ^{63}Co in Section 5.3, most of the low-lying excited states in this isotope are interpreted as a coupling of a $\pi f_{7/2}$-hole to the 2^+ excited state in the adjacent ^{66}Ni isotone (see Fig 13 in [Pau09a]).

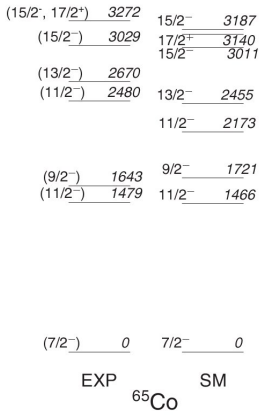

Figure 6.10: Comparison of the experimental excited states and large-scale shell model calculations by Recchia et al. [Rec12]

An upper limit of ≤ 17 ps for the half-life of the yrast 1479-keV state, was given by Dijon et al., in a multi-nucleon transfer reaction [Dij11]. The state was proposed to be with a $(9/2^-)$ spin and parity in the decay work of Pauwels et al. [Pau09a], but the recently determined R_{ASYM} ratio in the work of Recchia et al. [Rec12], suggests a $\Delta I = 2$ character for the 1479-keV transition. The observed difference in the intensity ratio of the 1479-keV and 1643-keV transitions, with respect to the corresponding transitions in ^{63,61}Co and the latter asymmetry measurement, suggest an inversion of the previous J^π assignments [Pau09a] of $9/2^-$ and $11/2^-$ for those two excited states, respectively.
Shell model calculations [Rec12] support an inversion of the J^πs of the latter levels (Fig 6.10).

6.4 Results for ^{65}Fe decay

The decay schemes of the ground state of ^{65}Fe and the ^{65m}Fe were build on the basis of the previously known results [Pau09a] and prompt gamma-gamma coincidences in the current study.

The final population of the ground and isomeric states in ^{65}Fe via the means of β-decay of ^{65}Mn and through direct production of the isotope in a proton-induced fission reaction [Pau09a] is different. Note here, that the production of ^{65}Fe with RILIS at ISOLDE is indirect and the iron, due to long release time and its half-life, does not come out of the ion source. The ratio of the

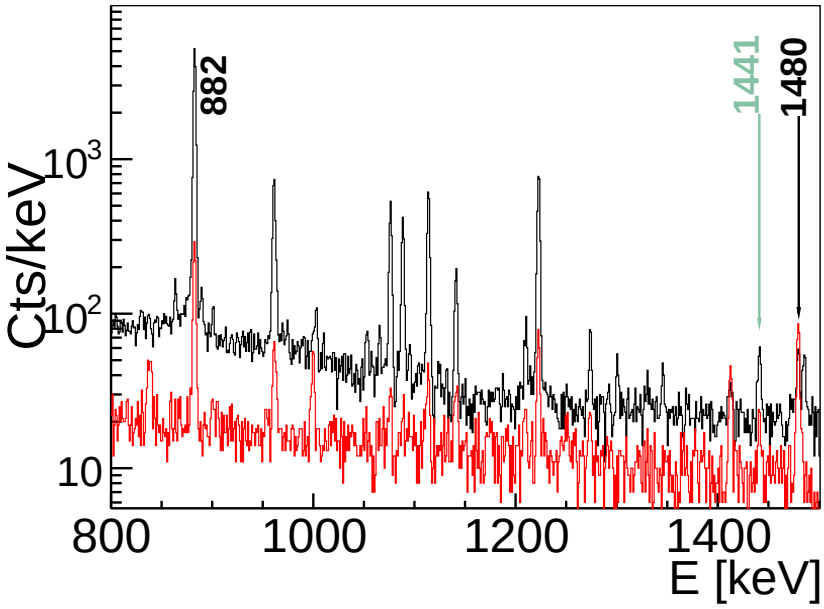

Figure 6.11: Beta-gated γ-spectra in the **(p,^{238}U)^{65}Fe** reaction [Pau09a] and the **current** β**-decay** study. The relative intensities of the labeled transitions (in black) are $\mathbf{I_\gamma(882) = 100\%, I_\gamma(1480) = 47(3)\%}$ versus $\mathbf{I_\gamma(882) = 100\%, I_\gamma(1480) = 1.0(1)\%}$. The cyan arrow points to the 1441-keV transition, yet another one with a different intensity in both experiments (see text for details).

population of the $(9/2^+)$ to the population of the $(1/2^-)$ in ^{65}Fe, deduced via the 882 and 1480 keV lines, changes from about 50% to about only 1%, for the direct production and the beta-decay experiments, respectively. This is

illustrated in Fig 6.11, where a selected part of the β-gated γ-spectra in both studies, are compared, as the same experimental set-up was used. This means, that almost everything observed in these new data is from the decay of the $(1/2^-)$-state.

Indicated in the figure are the strongest transitions in the deduced, separate decay schemes of ^{65}Fe and ^{65m}Fe [Pau09a]. Though a small population of states decaying to the $(9/2^+)$ state in the β-decay is observed, valuable information from both isomeric decays is obtained.

Another difference is seen in the intensity of the 1441-keV line, indicated with an arrow in Fig 6.11. While in the work of Pauwels et al., the ratio of the intensity between the 1480 and 1441 keV is about six [Pau09a], in the decay of ^{65}Mn the deduced ratio is of about one, meaning that the 1441-keV level is also fed by the low-spin beta-decaying state in ^{65}Fe. In its turn the latter has consequences on the final attribution of the gamma-ray intensity to one or the other isomer.

^{65m}Fe $(9/2^+)$ decay: Two new transitions coincident with lines in Fig 6.9B could be found. A transition of 743 keV showed up in the prompt gamma-gamma spectrum, gated on the 1441-keV line (Fig 6.12a), which matches the energy difference of the 2184-keV level, identified also in the previous β-decay study, and the excited state of 1441 keV.
Another gamma line of 777 keV was found to be coincident with the 1625-keV transition, shown in Fig 6.12b. This coincidence defines a new excited state at the energy of 2402 keV.

The relative gamma intensities in [Pau09a] do not match the relative gamma intensities observed here. Only a fraction of 2.3(2)%, relative to all observed iron decays proceeds, in this study, through the beta-decay of the $(9/2^+)$ state in ^{65}Fe. Furthermore, in the high-spin decay scheme, constructed from this data set, some of the observed transitions have a higher intensity than expected, if normalized to the 1480-keV. Based on the deduced decay scheme from Fig 6.9B, the amount of beta feeding in the two decays – $(9/2^+)$ and $(1/2^-)$ – could be separated.

It was found, that for the transitions observed in the in-beam level scheme (Fig.7 in [Pau09a]) of 1000, 1412, 1480 and 2558 keV, the ratio of the intensities of the latter to the intensities of the same transitions observed in this study was about 40. A factor several times higher than the ratio of the 1625-keV line in the two experiments, for example.
A weighted average value of 42(5) was deduced for the expected ratio, based on

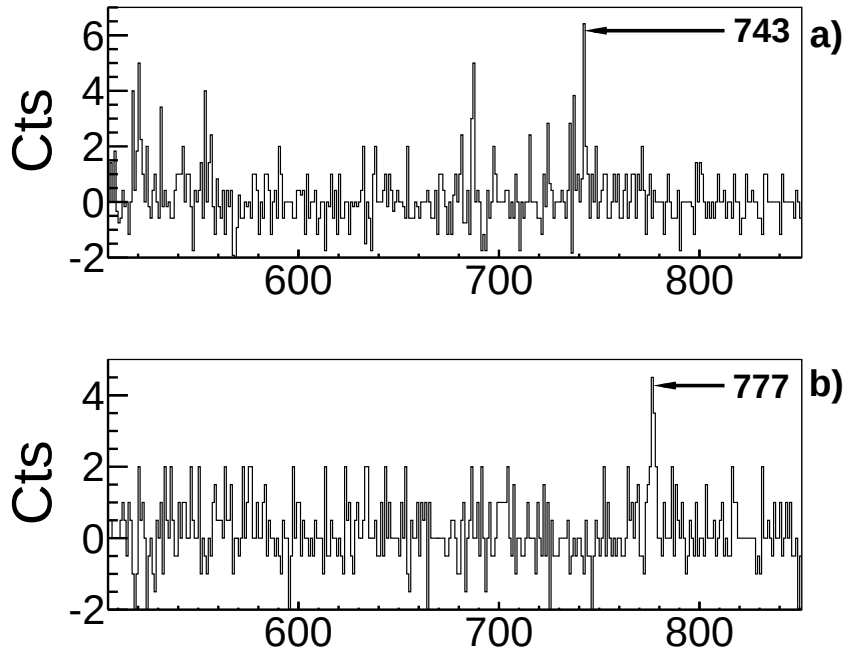

Figure 6.12: Selected part of the prompt coincidence gamma gates, set on the a) the 1441- and b) the 1625-keV transitions ($\vec{O}X$ is in keV).

the latter high-spin transitions and used to split-up the intensities of the lines which appear to be fed also by the $(1/2^-)$ decay.

^{65}Fe $(1/2^-)$ decay: A prompt γ-γ-coincidence spectrum, gated on the strongest transition in the low-spin decay of ^{65}Fe is shown in Fig 6.13, where also the coincident transitions are labeled in keV and a doublet gamma line with an energy of 1642 keV is visible.

Using the gamma-gamma-coincidence relationships (see Table 6.5) deduced in this study, excited states up to 4.4 MeV were identified in the β-decay of the ground state of ^{65}Fe.

The newly obtained decay scheme includes excited states, indicated in red in Fig 6.14, that are fed by both isomeric decays of iron. Their intensity was deduced, using the weighted average value of the ratio between the high-spin transitions

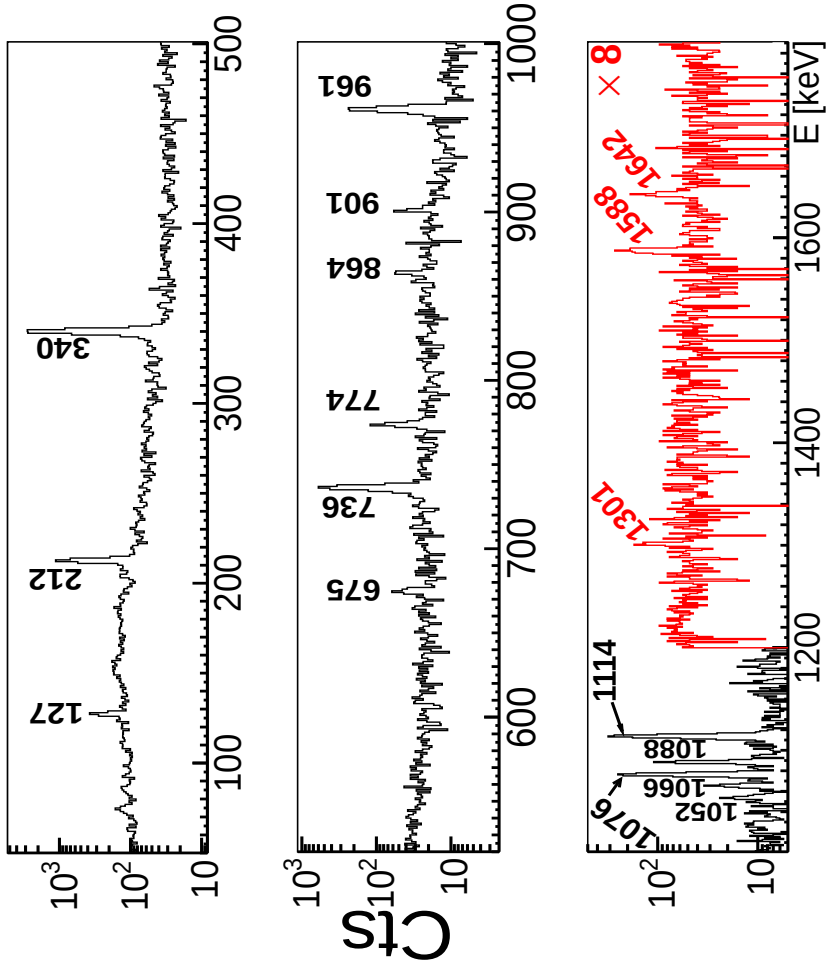

Figure 6.13: Prompt γ-γ-coincidence spectrum, gated on the 882-keV transition in ^{65}Co. Coincident lines are indicated by their energy in keV.

in [Pau09a] and the transitions with the same energy observed here, in order to determine what part of the intensity of the corresponding transitions should be assigned to the high-spin decay of ^{65}Fe.

Table 6.5: Gamma transitions with their relative intensities, identified in the decay of ^{65}Fe and ^{65m}Fe, compared to [Pau09a]. The "*" indicates the energy of the transitions whose intensity is placed in the decay of ^{65m}Fe. **Bold font** indicate the transitions whose ratios was used to split up the intensities of the mixed gammas. For absolute intensity per 100 decays, multiply by 0.590(6).

E_γ (keV)	Rel. I_γ %	Rel. I_γ % [Pau09a]	in coincidence with (keV):
127.4(1)	2.2(1)	3.2(11)	213, 736, 883
212.6(1)	12.6(5)	11.3(13)	127, 736, 864, 883, 901, 961, 1089, 1181, 2017, 2313, 3119, 3772
340.0(1)	50.7(2)	47.5(20)	736, 774, 883, 961, 1053, 1620, 2051
412.1(5)*	0.05(2)	2.6(12)	1000
439.1(1)	1.1(2)	—	675, 1558
511.0(1)	1.3(1)		736, 883, 1076
626.0(5)	0.10(2)		675, 1557
674.8(1)	1.1(1)		883
736.3(1)	25.6(2)	22(2)	127, 213, 340, 439, 883, 1223
742.7(2)	0.17(6)		1441
776.8(5)	0.13(5)		1626
773.7(1)	4.3(2)	6(4)	340, 883, 1223
837.1(1)*	0.38(18)	11(3)	1642
863.6(1)	1.2(1)	1.8(10)	213, 883
882.7(1)	100	100	127, 231, 340, 511, 675, 864, 901, 1053, 1066, 1076, 1089, 1114, 1301, 1588, 1642, 2230, 2494
900.9(1)	1.0(1)		213, 883
961.4(1)	9.3(3)	9.4(29)	127, 213, 340, 883, 1223
999.7(1)*	0.53(16)	17.7(24)	412, 1480
1053.2(1)	1.1(1)		340, 883, 1223
1065.6(1)	1.2(1)		883
1076.4(1)	11.2(1)	8.3(18)	511, 883
1088.5(1)	3.7(2)	3.9(13)	213, 883
1113.8(1)	13.9(1)	14.7(23)	883
1180.7(5)	0.14(6)		213
1222.8(1)	21.5(2)	23(3)	511, 736, 774, 961, 1053, 2051
1250.0(2)*	0.16(6)		1642
1300.8(1)	0.8(1)		883
1412.6(1)*	0.53(9)	22(3)	1480
1441.1(1)	1.0(1)		743
1441.1(1)*	0.19(6)	8(2)	743
1479.7(1)*	1.05(9)	47(3)	1000, 1413
1557.5(1)	2.3(2)		439, 626, 1851, 1874
1587.6(1)	1.8(1)		883

1619.5(1)	0.7(2)		340
1625.5(1)	0.7(1)		—
1625.6(1)*	0.17(6)	7(2)	777
1642.4(1)	1.3(3)		883
1642.4(1)*	0.53(24)	23(3)	837, 1250
1851.2(1)	0.52(13)		675, 1558
1873.6(1)	0.45(10)		675, 1558
1996.5(1)	34.2(2)	45(4)	—
2017.0(1)	0.40(9)		213, 883
2051.0(2)	0.9(1)		340, 883, 1223
2184.4(2)	0.27(10)		—
2229.7(4)	0.51(11)		883
2312.8(1)	0.25(5)		213, 883
2443.3(1)	0.40(13)		—
2443.3(1)*	0.74(15)		—
2494.5(7)	0.35(10)		883
2558.2(2)*	0.76(13)	31(4)	—
2770.8(2)	0.28(6)		213
2897.7(2)	0.65(13)		—
2897.6(2)*	0.34(11)	14(3)	—
3119.0(10)	0.31(9)		213
3220.3(10)	0.19(7)		340, 1223
3408.0(10)	0.15(8)		—
3664.0(10)	0.30(11)		340
3772.0(10)	0.11(5)		213
1787.0(3)	0.37(8)		—
1802.0(3)	0.45(9)		—
2168.5(3)	0.56(7)		—
3059.4(3)	0.36(8)		—
3093.6(3)	0.34(6)		—
3330.2(3)	0.33(7)		—

Table 6.6: Table 6.5 continued. Transitions below the horizontal line were found in the clean ^{65}Fe decay spectrum and not in the laser-off one, but not placed in the decay scheme.

Ground-state feeding of ^{65}Co

The direct ground-state feeding or the missed gamma intensity in the decay of ^{65}Fe can also be determined using the methods described for ^{65}Mn decay.

Method.1 Using the known decay scheme of ^{65}Co:

When comparing the number of gamma decays of ^{65}Fe decay and using the decay scheme of ^{65}Co by Pauwels et al. [Pau09a] to deduce the number of ^{65}Ni nuclei, as described in Method.1 Section 6.2, the apparent difference between the two number of counts was calculated to be **4(1)%**. The α_{Fe}^{883} factor, deduced from the constructed decay scheme is 0.612(3), with a cycle correction factor of 1.26(1) deduced on the basis of the determined half-life of the ground state of ^{65}Fe in [Pau09a].

Method.2 β-gated spectra with time constraint, with respect to the ISOLDE super cycle:

In Method.2 Section 6.2, the number of beta-rays related to the decay of ^{65}Fe was calculated, again, solely on the basis of the determined half-life in [Pau09a] and compared to the deduced number of gamma decays, determined using the 883-keV transition in the β-gated gamma spectrum with the time constraints described in Sec.6.2), corrected for ε_γ and the α_{Fe}^{883} coefficient. This comparison yields negative results, but **consistent with zero within the uncertainties.**

Method.3 Single event data in different times, with respect to the proton pulse impact:

In the last method we compare the number of ^{65}Fe betas, deduced with an appropriate coefficient (see Sec.5.2), from two enhanced singles gamma spectra, to the number of gamma decays, calculated using the 883-keV transition in the time-constrained, clean, ^{65}Fe decay spectrum, which leads to a percentage difference of **5(5)%**.

The weighted mean of the three methods, described above is **4(1)%**, found to be consistent with no direct ground state feeding and is presented as < 5 in Table 6.7. This value should be considered as an upper limit, due to unobserved ground-state γ-transitions.

The $A = 65$ iron decay schemes.

Twenty-six excited levels were identified in the decay of ^{65}Fe, including detailed feeding and de-excitation patterns (Table 6.7) while the scheme for ^{65m}Fe decay resulted in the previously known nine excited states (Table 6.8).

Two excited states, at 1223 and 1997 keV, in the low-spin decay scheme are found to receive beta-strength with logfts of around 5, while a number of levels, previously thought to be fed by the high-spin decay only, are presented in red in Fig 6.14, as partially fed by the ground state decay of iron. Note, that the excited states sharing feeding from both decaying levels, should have a limitation on their spins and parities. The experimental evidences suggest, that there is no direct beta-feeding towards the ground state of ^{65}Co, supporting a $(1/2^-)$ spin and parity assignment for the isomer in iron, with a half-life of 0.81(5) s.

The ground state of ^{65}Co is assigned $(7/2^-)$ on the basis of the systematics of the lighted odd-A isotopes and expectations from shell model.

In the decay study by Pauwels et al., the first excited state at 882 keV, was tentative assigned as $(3/2^-)$ spin and parity, on the basis of the deduced low logft value of 5.6(1). The new decay results, seen in Table 6.7, only show how sensitive β-decay schemes are, with respect to unobserved γ-transitions. The much higher statistics in the decay of ^{65}Fe in this case, allows to find more gamma lines, that feed the 883-keV level, thus decreasing the amount of calculated direct β-feeding to such an extent, that the newly calculated logft value of 6.2(1) is 5σ away from the previous one in Fig 6.9A. The spins and parities for the excited 883-, 1095- and 1223-keV states are adopted from [Pau09a], being consistent with the results obtained there.

The first two levels, denoted by red colour in Fig 6.14, were previously assigned as $(5/2^-, 7/2^-)$ by Pauwels et. al. It was found in the current study, that both levels are also fed in the decay of the low-spin ground state of ^{65}Fe, thus their tentative spin and parity assignment could be narrowed down to $(5/2^-)$ for both states at 1441 and 1626 keV.

The excited states at 1959, 1996 and 2183 keV have tentative $(1/2^-, 3/2^-)$, $(3/2^-)$ and $(1/2^-, 3/2^-)$, respectively, assignments [Pau09a]. On the basis of the calculated direct β-feeding in Table 6.7, and observed ground-state transitions from the higher-lying two levels, a $(3/2^-)$ spin and parity is proposed.

Table 6.7: Excited levels and direct β-feeding in the decay of ^{65}Fe. The new excited states are indicated by an "$*$".

E (keV)	I_β %	logft	J^π [NND13b]	J^π
GS	< 5	> 6.3	$(7/2^-)$	$(7/2^-)$
882.7(1)	3.0(4)	6.2(1)	$(3/2^-)$	$(3/2^-)$
1095.3(1)	1.8(4)	6.2(1)	$(1/2^-)$	$(1/2^-)$
1222.7(1)	18.3(4)	5.2(1)	$(3/2^-)$	$(3/2^-)$
1441.1(1)	0.52(7)	6.7(1)	$(5/2^-, 7/2^-)$	$(5/2^-)$
1557.5(1)*	0.85(18)	6.5(1)	—	
1625.5(1)	0.33(7)	6.5(1)	$(5/2^-, 7/2^-)$	$(7/2^-)$
1948.3(1)*	0.71(6)	6.4(1)	—	
1959.1(1)	22.2(4)	4.9(1)	$(1/2^-, 3/2^-)$	$(3/2^-)$
1996.5(1)	32.9(4)	4.7(1)	$(3/2^-)$	$(3/2^-)$
2184.0(1)	8.6(2)	5.3(1)	$(1/2^-, 3/2^-)$	$(3/2^-)$
2275.9(1)*	0.75(9)	6.3(1)	—	—
2402.3(5)*	0.08(3)	7.3(2)	—	—
2443.3(1)	0.24(8)	6.7(2)	—	—
2470.1(1)*	1.8(1)	5.8(1)	—	—
2525.0(1)*	0.56(9)	6.3(1)	—	—
2842.3(1)*	0.42(12)	6.3(1)	—	—
2897.6(2)	0.39(8)	6.3(1)	—	—
3112.3(2)*	0.55(8)	6.1(1)	—	—
3273.8(1)*	0.54(7)	6.0(1)	—	—
3377.2(5)*	0.21(6)	6.4(1)	—	—
3408.1(1)*	0.56(10)	6.3(1)	—	—
3431.3(2)*	0.27(6)	6.3(1)	—	—
3866.1(2)*	0.17(3)	6.3(1)	—	—
4214.6(5)*	0.18(5)	6.1(1)	—	—
4443.0(2)*	0.12(4)	6.2(1)	—	—
4867.0(3)*	0.24(7)	5.6(1)	—	—

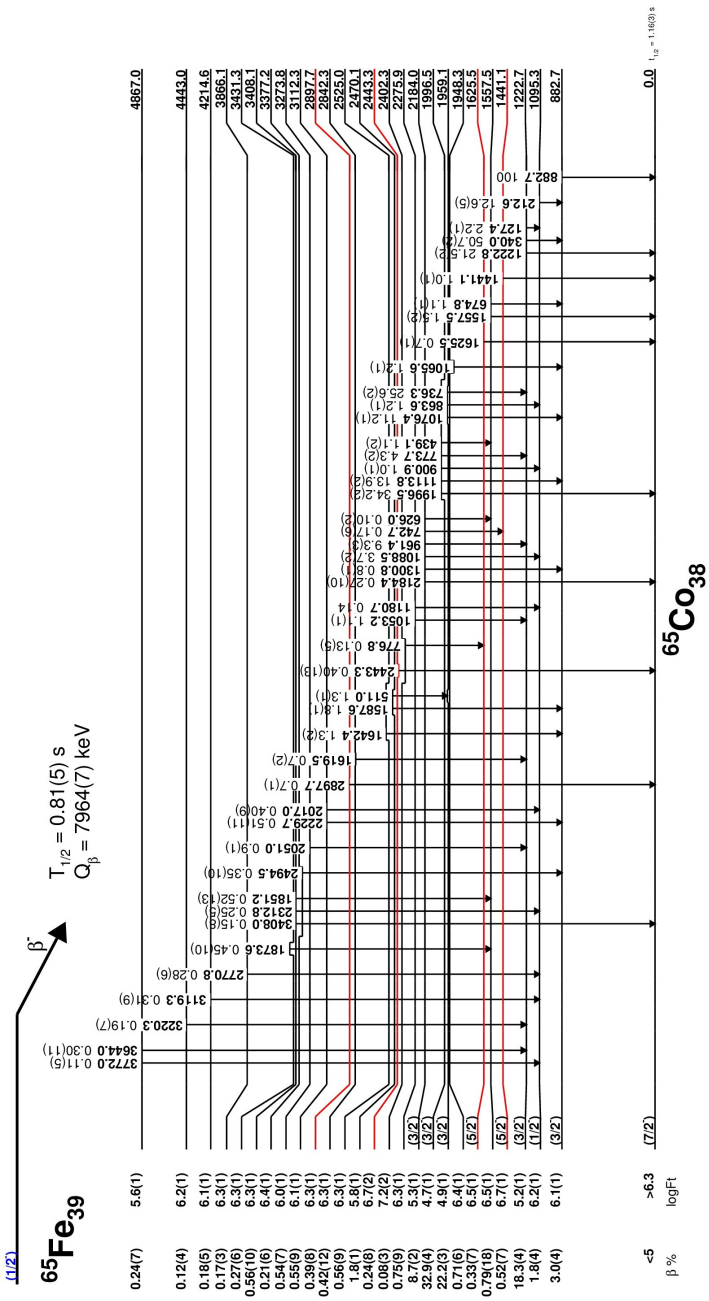

Figure 6.14: Decay scheme of ^{65}Fe, constructed using the data in the current experiment. The direct β-feeding towards the red-coloured levels is deduced from the gamma intensities left in the de-exciting transitions, after normalizing to the decay scheme of ^{65m}Fe, obtained by Pauwels et al. [Pau09a].

The separate decay scheme of ^{65m}Fe is by definition, consistent within the error bars, with the decay scheme presented in Fig 6.9B.

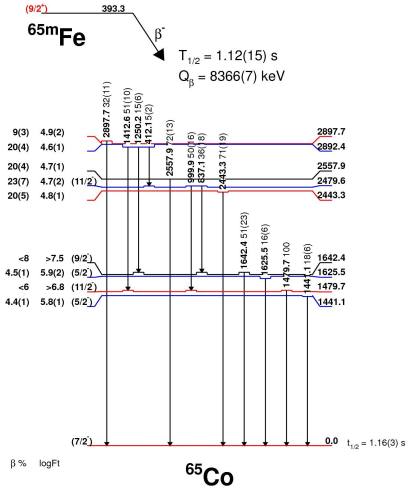

Figure 6.15: Decay scheme of ^{65m}Fe, constructed using the data in the current experiment and the decay scheme in Fig 6.9B. The blue levels are also populated in the deep in-elastic reaction in [Pau09a], while the colour red, denotes excited states that are fed by the ^{65}Fe ground-state decay as well.

Table 6.8: Excited levels and direct β-feeding in the decay of ^{65m}Fe. The spins and parities are adopted from [Pau09a], except for the 1441 and the 1626-keV states, narrowed down to $(5/2^-)$ in the preceding discussion on the ^{65}Fe decay scheme.

E (keV)	I$_\beta$ %	logft	J_π
GS	—	—	$(7/2^-)$
1441.1(1)	4(1)	5.8(1)	$(5/2^-)$
1479.7(1)	< 6	> 6.8	$(9/2^-)$
1625.6(1)	4(2)	5.9(2)	$(5/2^-)$
1642.4(1)	< 8	> 7.5	$(11/2^-)$
2443.3(1)	20(5)	4.8(1)	—
2479.4(1)	23(7)	4.7(2)	$(11/2^-)$
2558.2(2)	20(4)	4.7(1)	—
2892.3(1)	20(4)	4.6(1)	—
2897.6(2)	9(3)	4.9(2)	—

6.5 Previous experimental information on ^{65}Ni

The β-decay of ^{65}Co was investigated for the first time by Bosch et al. [Bos88] and later by Pauwels et al. [Pau09a]. Two of the excited states in the decay scheme by [Bos88] (882 and 1223 keV) have been correctly assigned as belonging to ^{65}Fe decay. The resulting level scheme from the second study is presented in Fig 6.16.

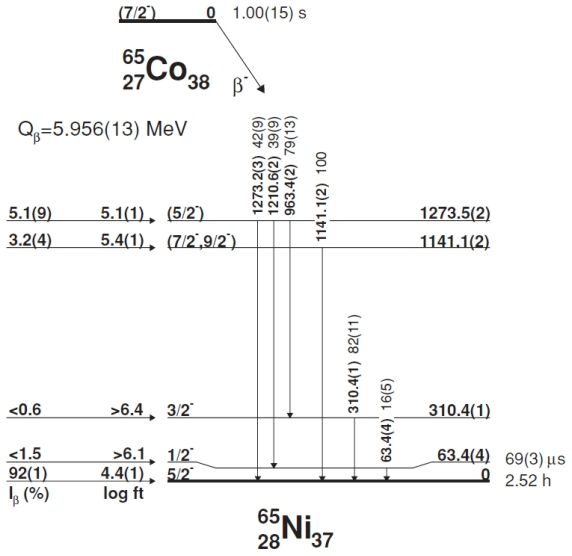

Figure 6.16: Decay scheme of ^{65}Co [Pau09a].

Another difference between the two decay studies is found to be an excited level at 692 keV in the work of Bosch et al., also observed in a number of other experiments [Bro10]. A transition of 383 keV, connecting the latter state and the 310-keV level, was observed in [Bos88]. The excited states of 1141 and 1274 keV have been tentatively assigned as $(5/2^-)$ and $(7/2^-, 9/2^-)$ spin and parity, on the basis of the deduced logft in [Pau09a].

Spins and parities of excited levels and the ground state of ^{65}Ni have been also assigned on the basis of a number of transfer reaction experiments, such as (d,p) [Lit72]; $(\vec{d},\mathrm{p})$ [Ven78]; $(\vec{t},d)$ and (α,t) [Fly79] and [Rou70], respectively. In the former reference, a $9/2^+$ state at 1013(10) keV has been confirmed.

6.6 Results for ^{65}Co decay

The decay scheme of ^{65}Co was built using the available information from previous decay studies and setting coincidence gates in this work.

Figure.6.17a) shows a beta-gated gamma-gamma coincidence spectrum, set on the 64-keV line (with a half-life of $T_{1/2} = 69(3)\mu$s [Bro10]), outside the $\beta\gamma$-prompt region. As expected, a 1210 keV transition is observed in coincidence, while a line of 629 keV is also present in the spectrum. The latter 629-keV transition was observed before, see e.g. [Paw94, Arn71], but not in any of the decay studies mentioned earlier.

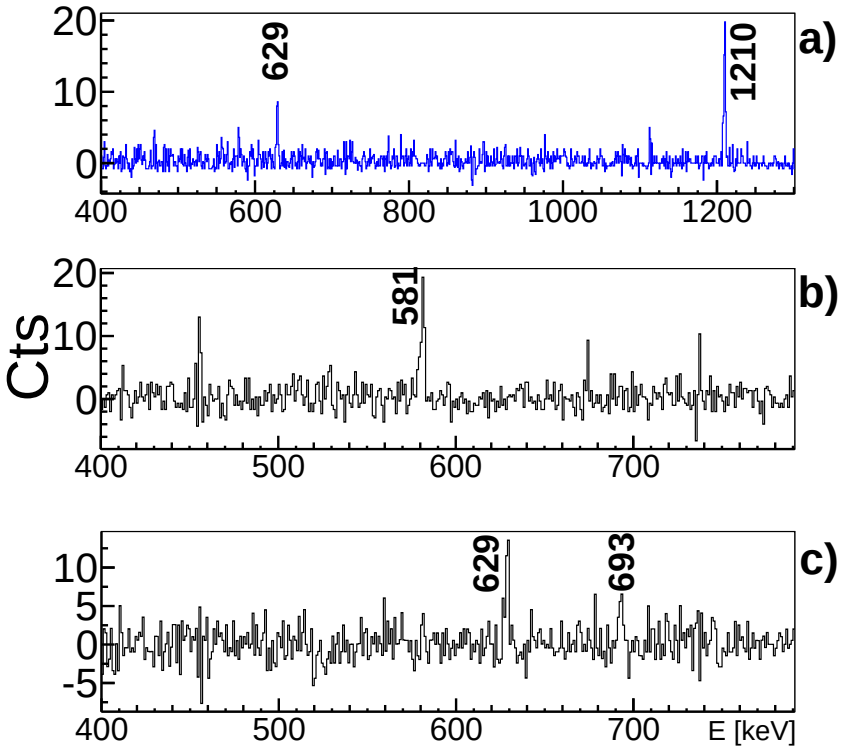

Figure 6.17: Selected part of the: a) delayed β-γ-γ-coincidence spectrum in the time interval 0.7–180μs, gated on the 64 keV transition b) prompt γ-γ-coincidence spectrum, gated on the 629 keV transition c) prompt γ-γ-coincidence spectrum, gated on the 581 keV transition.

A prompt γ-γ-coincidence gate on the 629-keV line, is seen in Fig 6.17b. A 581-keV transition, connecting the 693- and the 1274-keV states can be identified in that spectrum.
In the last panel, Fig 6.17c, the reverse gate on the 581-keV line is presented, where we find back the 629-keV transition, but also what seems to be a ground-state transition with an energy of 693 keV. It is clear from Fig 6.17c), that the intensity ratio of the 629- and 693-keV lines is about 2:1, in this data set, while the same ratio is adopted as $\sim$ 7:1 in [NND13b], following a thermal neutron capture study by [Arn71].

Noteworthy to state is that the transition of 383 keV, de-exciting the latter 693-keV level, observed by Bosch et al. [Bos88] was not observed in this decay study. The lower limit of its relative intensity was deduced on the basis of gamma-gamma coincidences as $< 0.3\%$.

These new, as well as previously observed, transitions are presented in the decay scheme in Fig 6.18. It is noteworthy to say, that due to the long half-life of ^{65}Ni, no information about its direct ground-state β-feeding could be extracted. Instead, the value for it, was set to 91.7% [Bro10] and the feeding towards the rest of the excited levels was calculated on that basis. Since a new ground-state transition was identified in this study, in a second iteration the feeding from the previously unobserved and weak 692-keV line was included, and the ground-state feeding was deduced as 91.6%.

The decay scheme of ^{65}Co is found to be in a good agreement with the results from the other β-decay studies [Bos88, Pau09a].
The coincidence relationship of the transitions, that belong to ^{65}Co decay, are given in Table 6.9, while the deduced logfts for the excited states are to be found in Table 6.10.

The assigned spin and parities of the observed states in this decay study are from [Bro10], found to be in agreement with the experimental observations in the presented decay study.

Table 6.9: Gamma transition, relative intensities and observed coincidences in the decay of ^{65}Co. Italic text denotes delayed (0.7 – 180 μs) coincidence relationship. For absolute intensities per 100 decays, multiply by 0.028(1) (with electron conversion taken into account; note that for the low-energy 63.5-keV transition, the theoretically calculated electron-conversion coefficient is 3.23(9) [NND13b]).

E_γ (keV)	Rel. I_γ %	Observed coincidence transitions (keV):
63.5(2)	18(3)	*581, 629, 1210*
310.4(4)	81(4)	831, 963
382.5	<0.3	unobserved
581.4(3)	8(2)	629, 693
629.0(5)	4.8(9)	*64*, 581
693.0(5)	2.1(6)	581
830.8(2)	10(2)	310
963.3(2)	71(3)	310
1141.1(2)	100	—
1210.4(2)	44(2)	*64*
1273.8(2)	46(2)	—

Table 6.10: Excited levels and direct β-feeding in the decay of ^{65}Co.

E (keV)	I_β %	logft	J^π [NND13b]	$T_{1/2}$
GS	91.6(31)	4.4(1)	$5/2^-$	2.5175(5) h [NND13b]
63.5(2)	< 1	> 6.7	$1/2^-$	69(3) μs [NND13b]
310.4(4)	< 0.2	> 7.1	$3/2^-$	
692.5(5)	< 0.1	> 7.3	$3/2^-$	
1141.1(2)	3.0(2)	5.5(1)	$(7/2^-, 9/2^-)$	
1273.8(2)	4.6(2)	5.3(1)	$(5/2^-)$	

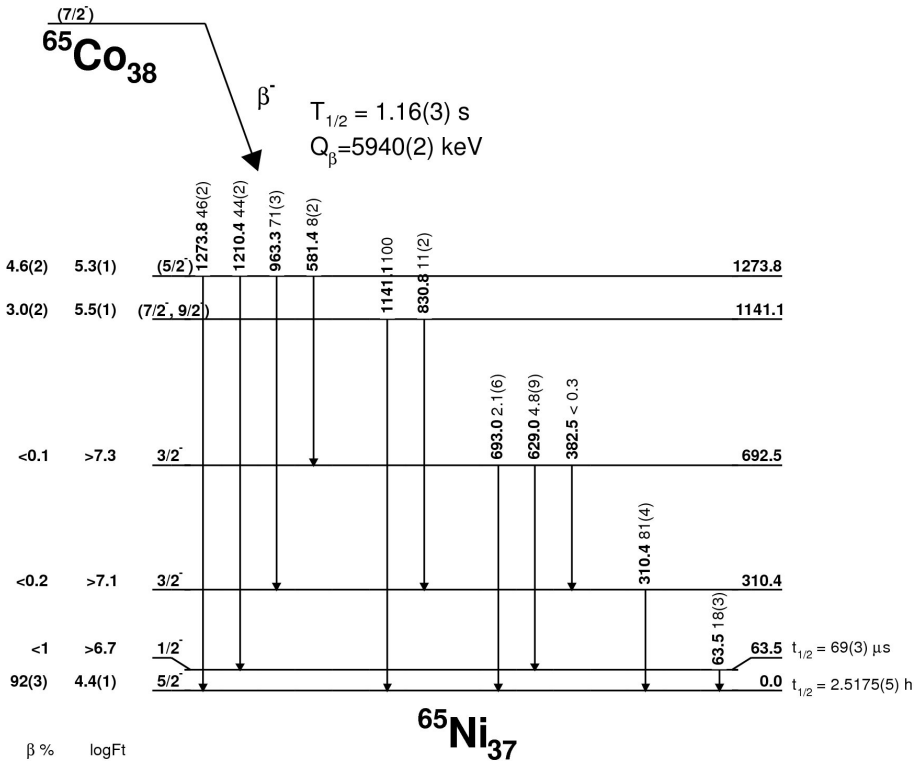

Figure 6.18: Decay scheme of ^{65}Co, constructed using the data in the current experiment.

Chapter 7

Results for the decay chain of $A = 67$

7.1 Previous experimental information on ^{67}Fe

The experimental information on ^{67}Fe prior to this experiment was very scarce and is compiled in [Jun05]. The ground state of the manganese parent is tentatively assigned as $(5/2^-)$ on the basis of the lighter odd-A systematics (Section 4.2, Fig 4.9), while its half-life was adopted as $T_{1/2} = 47(4)$ ms, deduced in a fragmentation experiment at GANIL [Sor03a].
The beta decay of ^{67}Mn was investigated in the thesis work of Gaudefroy [Gau05]. Although no decay scheme was presented, he reported on the observation of two lines, previously observed in other studies ([Grz98]: 367 keV, $T_{1/2} = 43(30)$ μs and [Saw03]: 387 keV (12(2)% of the 367-keV line), $T_{1/2} = 75(21)$ μs).
A low energy transition of 20 keV, unobserved in the latter source, was suggested to connect the two excited states [Saw03]. However, from the β-study by Gaudefroy, the two transitions were observed prompt after the β-decay, suggesting that the metastable state is yet above the 387 keV, but close enough in energy, so that the de-exciting transition(s) was not observed.
Fragmentation of ^{86}Kr beam on a ^{nat}Ta target, was used for decay spectroscopy and half-life determination after the β-decay of ^{67}Mn [Dau11]. The half-life of ^{67}Mn was deduced to be $T_{1/2} = 51(4)$ ms, in agreement with the adopted value [Jun05]. The two transitions of 367(1) and 388(1) keV were only observed in prompt coincidence with the beta-radiation and further an estimate for the P_n branch was given as 10(5)%.
The half-life of the ground state of ^{67}Fe was determined as $T_{1/2} = 416(92)$ ms, in a β-decay experiment at LISOL [Pau08a].

7.2 Results for ^{67}Mn decay

Experimental details

The experimental information on mass 67 consists of 32180 s of total measuring time for the laser-on, with respect to 6896 s for the laser-off files.

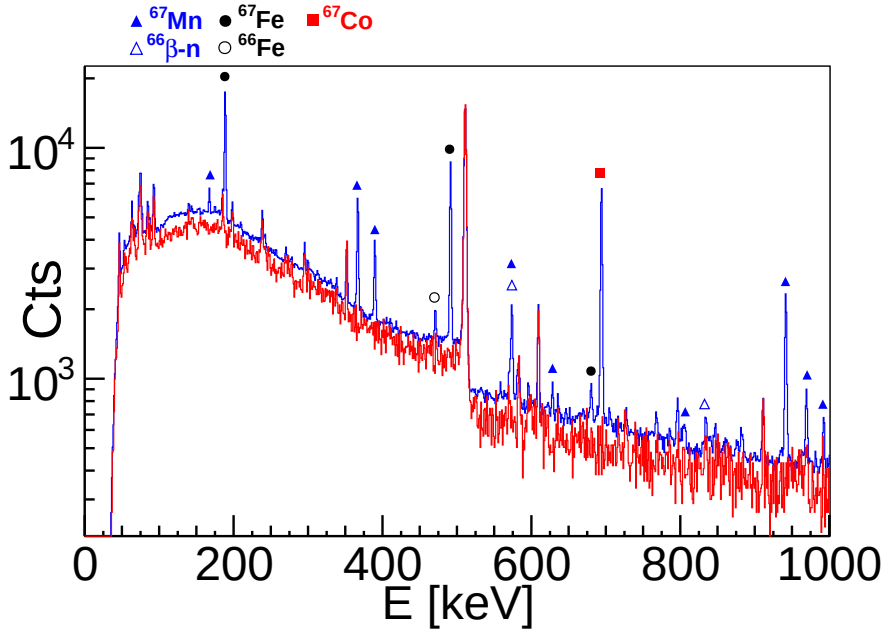

Figure 7.1: Laser-on spectrum, compared to a laser-off, in the same experimental conditions, when the mass separator is at $A = 67$ (the laser-off is scaled for visual comparison). Some of the strongest identified transitions are labeled.

The experimental set-up received every other proton pulse, from the ISOLDE super cycle, starting from pulse number 2, totaling 16 PP per super cycle. The decay data were recorded with an implantation time of 100 ms after the PP signal and an acquisition time of 2.2 s, with no forced read-out during the measurement (see Fig A.14). The quality of the data can be inspected in Fig 7.1, where a laser-on spectrum is compared to a laser-off one, in the same experimental conditions.

The laser-off spectrum is scaled for visual comparison and the transitions following the decay of ^{67}Mn are indicated with a closed triangle. Note, that in the presented spectrum, two lines identified as β-delayed neutron gamma transitions in ^{66}Fe are indicated with an open triangle and will be discussed in the dedicated section.

Half-life Determination

The half-life of ^{67}Mn was determined using the implantation-decay behaviour of multiple transitions, identified as belonging to its decay. Such a spectrum can be seen in the top panel of Fig 7.2, where the number of counts in the area of a 942-keV line is plotted with respect to the proton pulse impact with a binning of 10 ms.

The half-life extracted from this exponential decay fit amounts to $T_{1/2} = 43(2)$ ms. A combination of such results yields a weighted mean value of 44(1) ms for the half-life of ^{67}Mn, in agreement with the adopted value of 47(4) ms [Jun05].

In contrast to Daugas et al., there is evidence that also the μs-isomeric state is fed following the beta-decay of manganese, thus it was possible to extract its half-life, as shown in the bottom panel of Fig 7.2, where the decay behaviour of the transition de-exciting the 367-keV level is plotted with respect to a beta event, outside the prompt (0 – 600 ns) time interval.
The result from the exponential fit on a constant background is a half-life of 152(11) μs, a value at least twice as large as the one previously determined, which can be explained by the superior quality of data and statistic in the current experiment with respect to [Saw03].

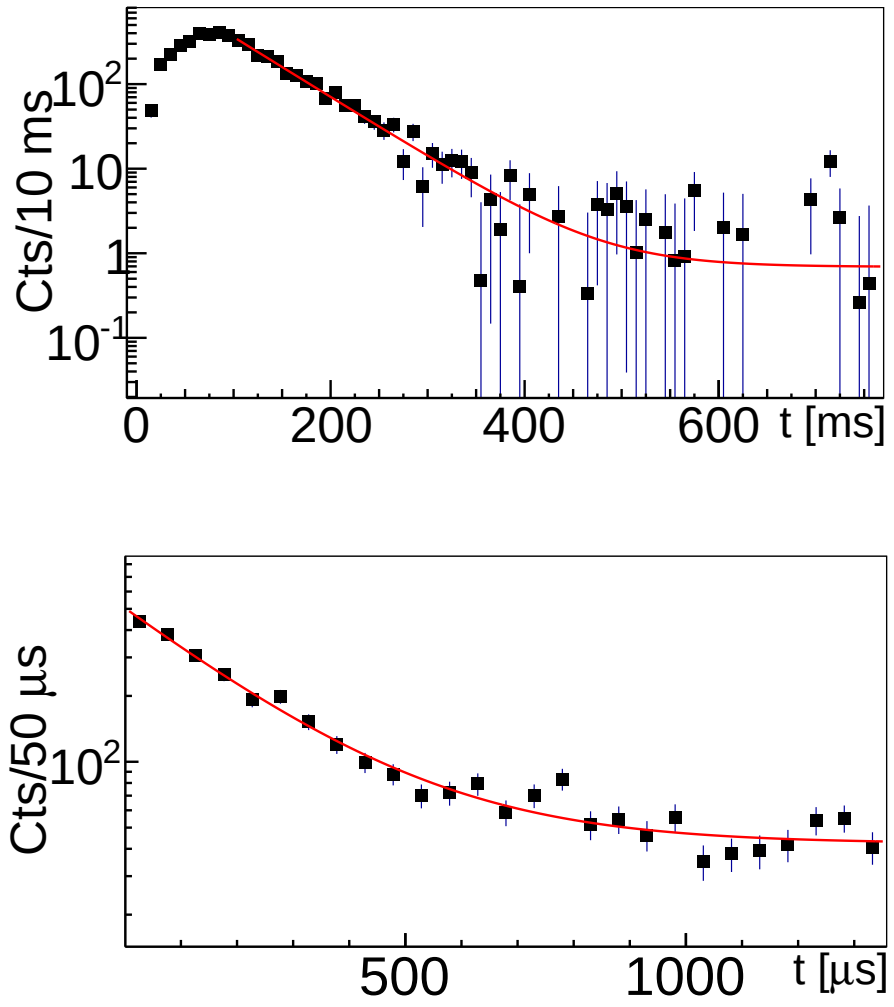

Figure 7.2: (Top) Implantation-decay behaviour of a 942-keV transition, identified as following ^{67}Mn decay. The fit of the exponential function results in a $T_{1/2} = 42(2)$ ms.
(Bottom) Selected part of the decay behaviour of the β-gated delayed (1 – 1·10^4 μs) 367-keV line, in bins of 50 μs. The half-life extracted from the fit is $T_{1/2} = 152(11)$ μs

Evidence for a doublet structure of the 390 ± 2 keV level

The fact that isomeric state is fed via the beta-decay of ^{67}Mn is clearly seen in Fig 7.3, where selected part of the singles spectrum within a time gate of 132 ms

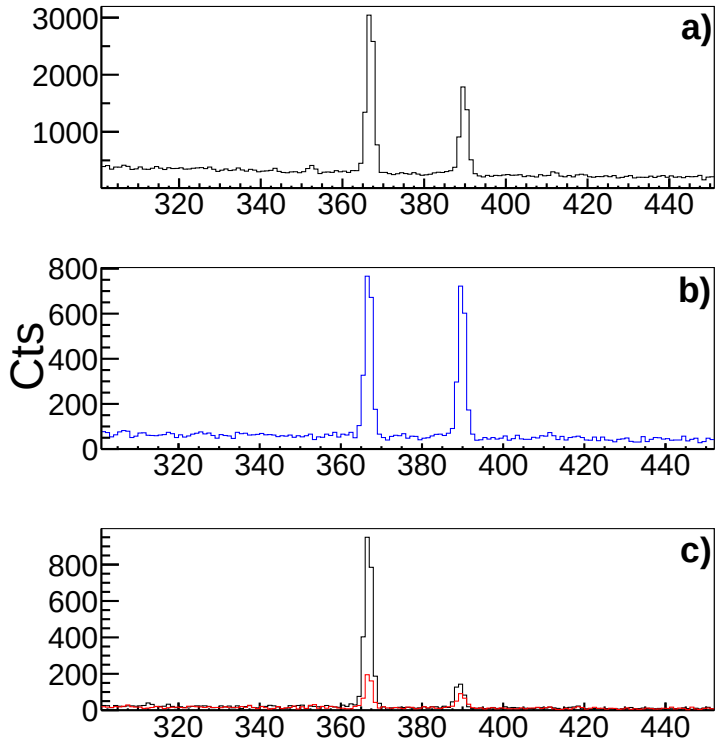

Figure 7.3: Selected part of the a): **singles' gamma spectrum** , within 132 ms after the proton pulse ($A = 67$); b): the β-gated prompt spectrum, within 132 ms after the proton pulse ($A = 67$); c): the beta-gated gamma-spectrum with a time difference in the interval of 1 – 451 μs, with respect to a beta event, compared to a gamma-spectrum in the random's (1000 – 1450 μs) time interval ($A = 67$). The intensity ratio ($I(390)/I(367)$) of the two transitions changes completely, from **0.57(1) in a)** to 0.97(4) in b).

after the PP (3 × 44 ms) is compared to the prompt and the delayed β-gated gamma spectra. The intensity ratio between the 390-keV and the 367-keV lines changes from 0.53(2) in Fig 7.3a) to 0.97(4) in Fig 7.3b), giving evidence that the spectrum in the singles contains contribution from the delayed, isomeric

decay.

The last panel in that figure presents the beta-gated delayed (1 – 451 μs) gamma-spectrum, compared to a spectrum in the randoms' time interval. It is observed, that the 367-keV transition has a delayed component, while most of the delayed intensity of the 390-keV line can be explained as a contribution from the randoms in that spectrum.
A small part of the latter, though, remains unexplained by the randoms.

The ratio of the number of counts in the area of the 390 $\pm$ 2 keV to the number of counts on the area of the 367 $\pm$ 2 keV line, when random counts are taken into account is 9(2)%, to be compared to the ratio of 12(2)% deduced by Sawicka et al. [Saw03]. Furthermore, note that the remaining extra intensity in the area of the higher-energy transition in Fig 7.3c), seems to be slightly left of the 390-keV centroid in the random spectrum.

The same conclusions, for the delayed part, can be derived from the experimental information, taken when the separator was set to $A = 68$. Note, that this decay branch selectively populates states in ^{67}Fe and is later on used to set limits on the spins and parities of the low-lying excited states in this isotope.
Interesting to note here, is that the prompt P_n feeding pattern is completely different than the case of ^{67}Mn beta-decay, observed in Fig 7.4b). It is seen, that the excited state at 390 keV receives more feeding in the beta-gated prompt spectrum of ^{68}Mn.

The spectrum in the randoms' interval (denoted in red colour in Fig 7.4c)) in the case of $A = 68$, is less dominated by the 367- and the 390-keV lines (see also singles spectrum in Fig 7.4a)). This makes the peaks around the 367 and 390 keV in the beta-gated delayed spectrum cleaner. The centroid of the latter is at 388.4(3) keV and deviates from the 389.8 keV peak in the prompt spectrum of the two figures indicating a doublet structure.

The ratio of the two transitions determined from that figure, taking the contribution from random counts in both areas, is found to be 13(3)%, again in agreement with [Saw03]. The evidence for a doublet structure can be seen more clearly by comparing directly the experimental data for both masses.

Figure 7.5 shows a selected part of the gamma singles ($A = 67$ in black), beta-gated prompt ($A = 67$ in blue), beta-gated delayed ($A = 67$ in magenta) gamma spectra and the beta-gated delayed spectrum in $A = 68$ (in red). It is observed that the centroid of the high-energy transition is shifted to the left of the centroid of the 389.8 prompt gamma-ray transition.

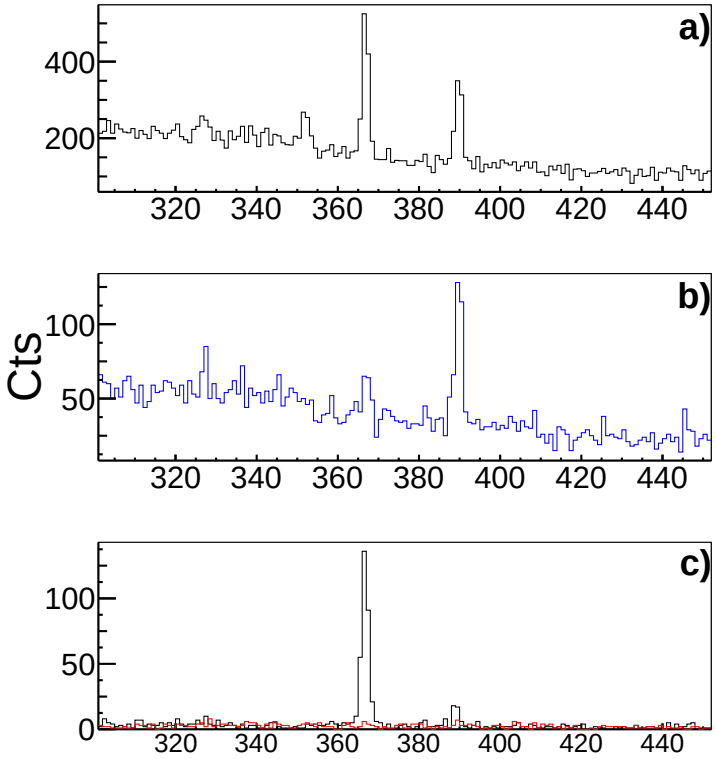

Figure 7.4: Selected part of the a): **singles' gamma spectrum** , within 220 ms after the proton pulse ($A = 68$); b): the β-gated prompt spectrum, within 220 ms after the proton pulse ($A = 68$); c): the beta-gated gamma-spectrum with a time difference in the interval of 1 – 451 μs, with respect to a beta event, compared to a gamma-spectrum in the randoms (1000 – 1450 μs) time interval.

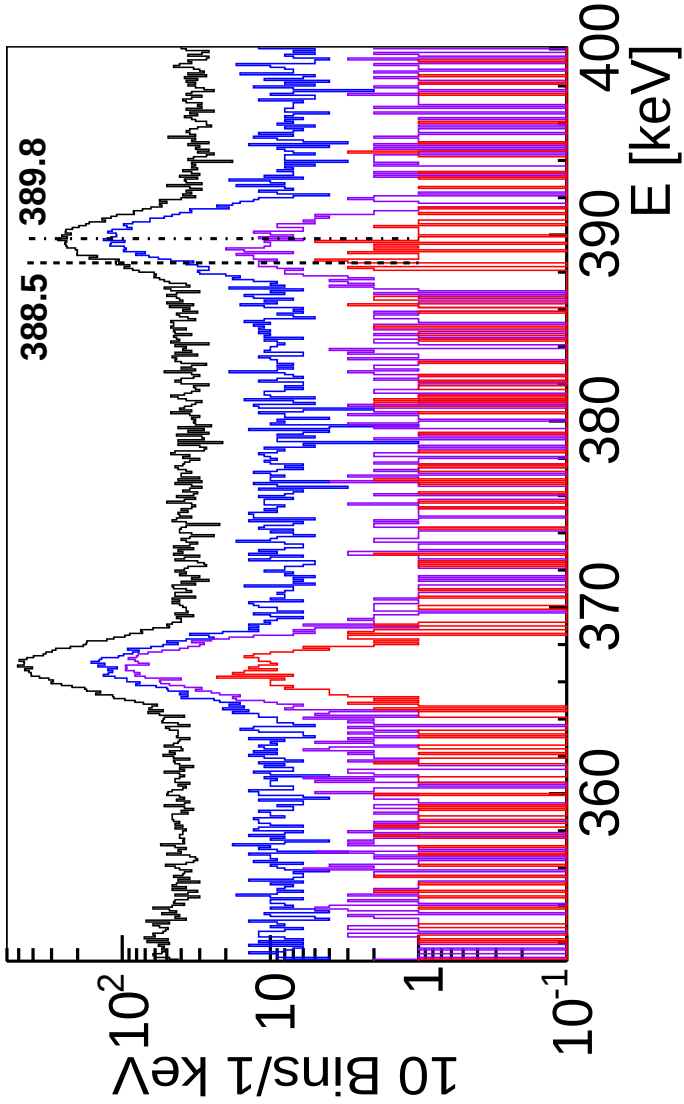

Figure 7.5: Selected part of the $A = 67$ **single gamma events**, $A = 67$ β-gated prompt (0 – 600 ns) gamma events, $A = 67$ β-gated delayed (1 – 451 μs) gamma events and the $A = 68$ β-gated delayed (1 – 451 μs) gamma events, plotted with increased binning. Further constraint for the created spectra is the $\gamma_t \leq 5\times{}^{A}\mathrm{Mn}(\mathrm{T}_{1/2})$ with respect to PP_t, where ${}^{67}\mathrm{Mn}(\mathrm{T}_{1/2}) = 44(1)$ ms and ${}^{68}\mathrm{Mn}(\mathrm{T}_{1/2}) = 34(1)$ ms [Pau13]. The indicated value of 388.5 is the result of a weighted average, see text.

7.3 Decay scheme

The decay scheme of ^{67}Mn was built by placing gamma-gamma-coincidence gates on transitions identified as following manganese decay, via their half-life behaviour. In order to build up the level scheme of ^{67}Fe use is made firstly of the γ rays in prompt coincidence with the 367-keV and the 390-keV lines. The corresponding spectra are presented in Fig 7.6, where the transitions, coincident with the two lines, are labeled by their energy in keV. This analysis leads to

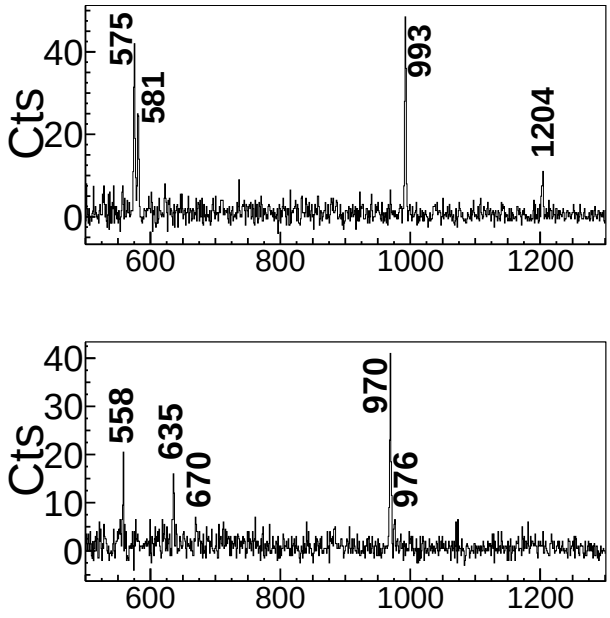

Figure 7.6: Selected part of the prompt γ-γ-coincidence gate, set on the 367-keV (top) and the 390-keV (bottom) lines. Coincident transitions are identified by their label in keV.

the establishment of 12 levels between 941 and 3054 keV. These levels and the connecting transitions are presented in Fig 7.7 in black colour.

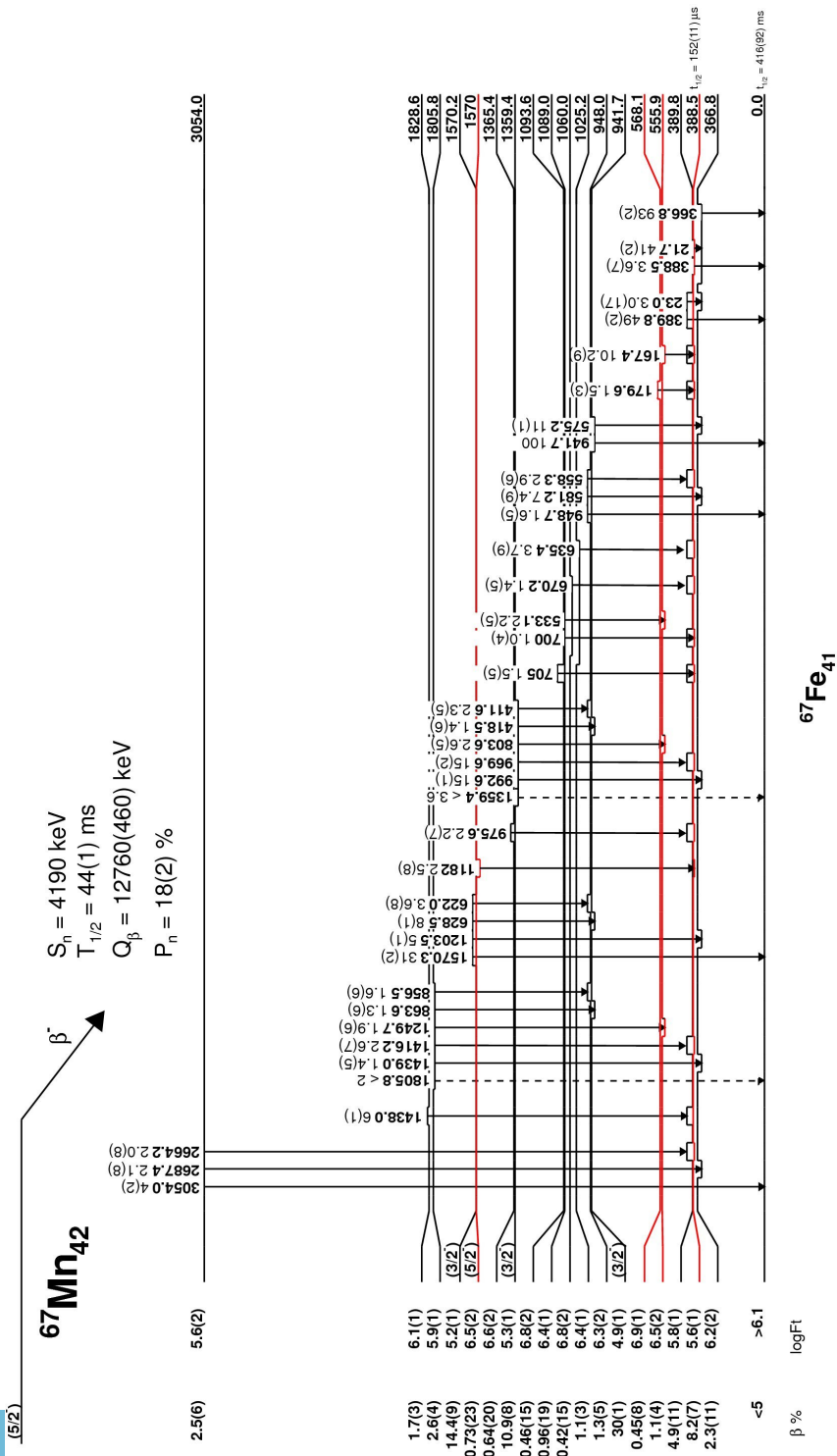

Figure 7.7: Decay scheme of ^{67}Mn, constructed using the data in this data set.

Secondly, in order to identify gamma rays feeding the isomer, a delayed gamma-gamma coincidence gate is placed, 1 to 451 μs before the 367-keV line (Fig 7.8). The position of the 152-μs isomer and levels built upon it are deduced from γ

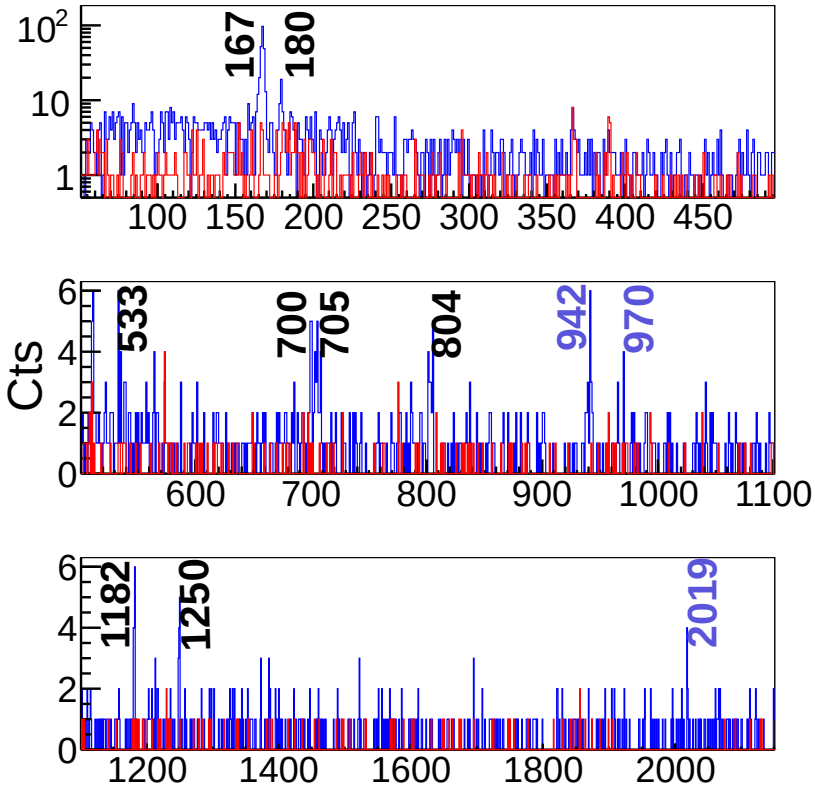

Figure 7.8: Gamma–367 gamma-gated delayed (-1 – -451 μs) coincidence spectrum, compared to the gamma-gamma gate on the same energy but in the randoms (-750 – -1200 μs) time interval, within 5 $\times$ $T_{1/2}$ of ^{67}Mn.

rays in coincidence with the delayed 367-keV transition and prompt coincidences amongst those lines. Noteworthy to state is that the 390 $\pm$ 2 keV transition, also appears to be coincident with the 167-keV line (strongest coincident line in Fig 7.8) in the corresponding beta-gated delayed spectrum, based on the observed 8(3) counts in the area of the 167-keV transition, compared to the 3(2) counts in the same area but in the randoms time interval, which further supports the doublet structure of the 390-keV line. These results lead to the conclusion, that

the isomeric level must be a doublet of the 390-keV, promptly-fed, excited state.

Some of the lines observed in Fig 7.8 (see also Table 7.1) are in a prompt coincidence with the 167-keV line, but the two lines around 700 keV and the 1182-keV one are not and are placed feeding directly the isomeric state. The latter placement defines a doublet excited state at 1570(1) keV in the decay scheme. Transitions indicated with a purple colour (except the strong prompt doublets of the 942- and the 970-keV lines), are not included in the decay scheme, as not enough evidence was found for their placement. Nevertheless, one can observe that the isomeric state receives feeding from gamma transitions at high energy and the further deduced $\log ft$ value should be considered as a lower limit.

Combining all the information, deduced from prompt and delayed gates, as well as from the implantation-decay behaviour of the transitions, results in Table 7.1, containing all identified ^{67}Mn-decay transitions. It is noteworthy to say here, that upper limits of the intensities of the ground-state transitions de-exciting the 1806 keV and the 1359 keV states were determined, based on the statistical analysis in [Hel83] and correspond to a one sigma confidence level, while the intensity of the transition with an energy of 948 keV was determined using the background-subtracted number of counts in that area.

Table 7.1: Gamma transitions and relative intensities, identified as following ^{67}Mn decay. Italic text denotes β-γ-γ-delayed (1 – 450 μs) coincidence relationship. The energies of the 21.7-, 23.0-, 388.5-, 948.0, 1182- and 1359.4-keV transitions were determined on the basis of energy difference between excited states. For absolute intensities, multiply by 0.289(10).

E_γ (keV)	Rel. I_γ %	Observed coincidence transitions (keV):
21.7(2)	41(2)	—
23.0(1)	< 5	—
167.4(1)	10.1(9)	533, 804, 1250, *367, 388.5*
179.6(2)	1.5(3)	*367*
366.8(1)	93(2)	*167, 180, 533, 700, 705, 804, 1182, 1250*, 575, 581, 622, 857, 993, 1203, 1439, 2687
388.5(2)	3.6(7)	*167*
389.8(1)	49(2)	558, 635, 670, 969, 975, 1416, 1439, 2664
411.6(5)	2.3(5)	367, 390, 558, 581
418.5(5)	1.4(6)	575, 942
533.1(5)	2.2(5)	167
558.3(1)	2.9(6)	389, 412
573.7(5)	**34(2)**	834; IN ^{66}FE
575.2(1)	11(1)	367, 418
581.2(1)	7.4(9)	367, 412, 622
622.0(3)	3.6(8)	581
628.5(3)	8(1)	575, 942
635.4(3)	3.7(9)	390
670.2(8)	1.4(5)	390
700(1)	1.0(4)	*367*
705(1)	1.5(5)	*367*
803.6(3)	2.6(5)	167, *367*
834.0(5)	**10.0(5)**	574; IN ^{66}FE
856.5(5)	1.6(6)	367, 390, 558, 581
863.6(5)	1.3(6)	575, 942
941.7(1)	100	418, 628, 864
948.7(1)	1.6(5)	—
969.6(1)	15(2)	390
975.6(4)	2.2(7)	390
992.6(1)	15(1)	367
1182(1)	2.5(8)	*367*
1203.5(3)	5(1)	367
1249.7(5)	1.9(6)	167
1359.4(1)	< 3.6	—
1416.2(3)	2.6(7)	390
1438.0(3)	6(1)	390
1439.0(5)	1.4(6)	367
1570.3(1)	31(2)	—
1805.8(1)	< 2	—
2664.2(5)	2.0(8)	390
2687.4(6)	2.2(8)	367
3054.0(4)	4.2(16)	—

Placement of the 152-μs isomer in ^{67}Fe.

The doublet structure of the 390-keV line points to the existence of two levels around 390 keV, of which the lower one is associated with the 152 μs half-life. The question arises if this level is the isomeric one or if an unobserved transition feeds this state. Assuming the former and using the gamma coincidences with the 167-keV line, known to be feeding the isomer, two gamma lines are found which fit in the level scheme deduced from the prompt coincidences with the 367- and 390-keV transitions (black levels in Fig 7.9).

Those are the 803.6 and the 1249.7 keV transitions, both coincident with the 167.4-keV line and defining two cascades de-exciting the respectful states:
$E^* = 1359.4 \Rightarrow 803.6 \rightarrow 167.4 = 388.4(3)$ keV
$E^* = 1805.8 \Rightarrow 1249.7 \rightarrow 167.4 = 388.7(3)$ keV

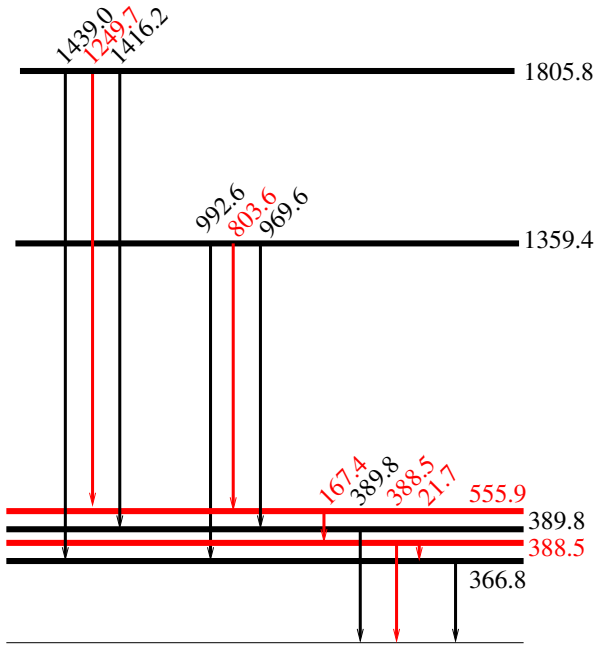

Figure 7.9: Partial level scheme of ^{67}Fe. The energy of the excited states is not drawn to scale. The combination of the de-exciting lines of 1250 and 167 keV, and 804 and 167 keV from 1.8 and 1.3 MeV states, respectively, leads to the same excited state.

Note, that the energy of each excited states, presented in the calculation, were determined using at least two decay paths, e.g. 1439 keV + 367 keV and 1416 keV + 390 keV, where the energy of the gamma transitions was also deduced using the fits in different (singles, beta-gated, gamma-gamma coincidence, etc.) spectra.

The obtained values are in excellent agreement with the value of 388.4(3) for the gamma line in Fig 7.4c). A weighted mean value is of 388.5(2) keV is determined using the results from the two cascades and the centroid of the higher-energy transition in the latter figure.

The 388.5 keV state then decays through a 21.7-keV line towards the 367-keV level and with a 388.5 keV to the ground state with a respective intensity of 41(2)% and 3.6(7)%, relative to the 942-keV line, deduced from the beta-delayed gamma data (see Fig 7.3c)).

An upper limit of $< 5\%$ (3.0(17)%) was deduced for a transition of 23.0 keV, that could connect the prompt 390- and the 367-keV states. This was done using the prompt gamma-gamma coincidence gate, set on the strong 970-keV line feeding the 390-keV level (see Table 7.1). The number of counts in the 367 $\pm$ 2 keV area in the latter gamma-gated spectrum, relative to the 390-keV line was found to be 6(3)%.

β-delayed neutron branch

Observed transitions in ^{66}Fe are indicated in Fig 7.1 with an open blue triangle, while the line following the ^{66}Fe decay (471 keV: $1^+ \rightarrow (7^-)$ [Pau13]) – by an open black circle. In that figure, the $2^+ \rightarrow 0^+$ in ^{66}Fe is indicated as a doublet with a line coincident with the 367-keV transition, following ^{67}Mn decay (see Fig 7.6). Actually, the 573 $\pm$ 2 keV is a triplet in this data set, since a 571-keV line is also in a prompt coincidence with the 190 keV in the decay of ^{67}Fe (see Section 7.5).
Having that in mind, extra attention was taken when determining the β-delayed neutron branch in the decay of ^{67}Mn. Analogous to the case of ^{65}Fe, the expected number of counts in the singles spectrum for transitions with energies 575 (in ^{67}Mn decay) and 571 keV (in ^{67}Fe decay), was calculated on the basis of coincidence relationships with the 367- and 190-keV lines, respectively.

Placing prompt-coincidence gates on the 573-keV line ($I^{rel}_{triplet} = 51(2)\%$) reveals only one transition in coincidence in ^{66}Fe, which can be seen in Fig 7.1 – the

834-keV $4^+ \rightarrow 2^+$ transition.

Table 7.2: Distribution of the β-delayed neutron strength in the decay ^{67}Mn, normalized to 100%.

E + S_n (keV)	E (keV)	P_n %	J^π
4190	GS	45(12)	0^+
4764	573	39(5)	2^+
5598	1408	16(2)	4^+

The 471-keV line, following ^{66}Fe decay, was used to calculate the number of ^{66}Co nuclei, in order to determine the P_n branching ratio in ^{67}Mn decay. Using half-life correction factors of 1.02(1) for the ^{66}Fe decay line and the absolute branching of the latter, $I^{abs}(471) = 23(1)\%$ [Pau13], the amount of ^{66}Co nuclei was deduced and used to distribute accordingly the direct feeding towards the observed excited levels in ^{66}Fe, resulting in Table 7.2. The half-life correction factor for gamma transitions in ^{67}Fe is 1.00, as all manganese decays ($T_{1/2} =$ 44(1) ms) are observed during the acquisition time of 2.2 s.
The total amount of the beta-delayed neutron branch is calculated to be 18(2)% out of all ^{67}Mn decays.

Direct beta-decay or missed gamma transitions, feeding the ground state of ^{67}Fe

The beta-feeding to all identified excited states in ^{67}Fe was calculated using the feeding and de-exciting transitions. The direct β-feeding or missed gamma intensity towards the ground state of ^{67}Fe, as in the case of ^{61,63,65}Fe, can be calculated via the different methods mentioned earlier, based on the purity of the implanted radioactive source:

Method.1 Using the known decay scheme of ^{67}Co:
The decay of ^{67}Co was investigated in the work of Weissman et al. [Wei99], where a logft of 4.7 was measured for the excited state at 694 keV in ^{67}Ni. No direct beta-feeding was assigned to the tentative $(1/2^-)$ ground state. The absolute branching of the transition de-exciting the 694 keV level was determined to be 92(4)% in that work. Taking into account the cycle correction factor, calculated for ^{67}Co lines as 1.07(3) and the determined absolute branching ratio, the number of ^{67}Ni nuclei can be calculated and compared to the number of ^{67}Mn gamma decays, determined with the sum of all identified ground state transitions. The deduced difference is found to be **negative, but consistent with zero within the uncertainty**.

Method.2 β-gated spectra with a time constraint, with respect to the ISOLDE super cycle:

In the data set using the first 200 ms of the first proton pulse, only events from the decay of ^{67}Mn and ^{67}Fe should be present. The number of betas, corresponding to that time constraint, was extracted from the beta-singles spectrum. Using the half-life of ^{67}Fe [Pau08a], 13.8(8)% of the total amount of betas was calculated to belong to the decay of ^{67}Fe. As the beta-delayed neutron branch is important in this case the percentage of beta particles, related to ^{66}Fe decay was also calculated and was determined to be 11.2(9)%, again on the basis of the half-life of the isotope. Using the new information on the beta-delayed neutron branch and the calculated percentage of ^{67}Fe-decay and ^{66}Fe-decay correlated betas, a number of beta-rays, related only to the decay of ^{67}Mn was deduced from the total number of observed beta particles. This number is then compared to the gamma decays, deduced from the 942-keV transition in the beta-gated gamma spectrum and using the α_{Mn}^{942} of 0.36(1). The calculated in this way difference is, as in the case of Method.1, **negative, but consistent with zero within the uncertainty**.

Method.3 Single event data in different times, with respect to the proton pulse impact:

Another way to deduce the missing intensity is to use the singles' γ- and β-spectra in first proton pulse. Again, to obtain cleanest possible conditions, the spectra are created in the time intervals of 10 – 160 ms and 161 – 561 ms, after the first proton pulse impact, where the decays of manganese and iron, respectively, are enhanced and the contribution from cobalt decay is negligible. Clean decay spectra are created by combining the two γ-spectra in the way explained in Section 5.2 or 6.2. The deduced number of beta-particles, related to manganese decay, obtained with a proper coefficient and accounted for the beta-delayed neutron emission branch, is compared to the number of ^{67}Mn decays deduced via gammas, resulting in a difference of **10(13)%**.

A consistency check can be performed, using the constructed decay schemes for $A = 67$ and the beta-delayed neutron branch (information on $A = 66$ decay chain taken from [Pau13]). Taking the full statistics in singles, the total number of betas is extracted and compared to the total gamma intensity, deduced from the number of counts in the strongest transition in each decay, up to ^{67}Ni, using the α_{decay}^{γ} coefficients, as defined in Section 4.2.

The deduced difference between betas and gammas amounts to 14(3)%. This difference can be distributed in all of the decays and can be due to missed gamma-ray intensity via Pandemonium effect, or in the unlikely case the latter

number can be contained in one decay only. If the former is true, only about one third of the missed intensity should be attributed to the decay of ^{67}Mn. This is consistent with the value of <5%, resulting from Method.1 (Table 7.4), adopted for the missed intensity.

Spin and parity assignments

Seventeen excited states were identified in this decay study (see Table 7.4), with detailed feeding and de-excitation patterns, including the previously observed isomeric state at low excitation energy.
The experimental half-life of the metastable state in this work, was determined to be $T_{1/2} = 152(11)$ μs, a value twice as large as the previously determined one by Sawicka et al. [Saw03].
Its precise energy was also determined to be 388.5(2) keV (see Sec. 7.3). Two excited states, at 942 and 1570 keV, are fed fast with logfts of around 5.

The ground state of the β-decaying mother is tentatively assigned as $(5/2^-)$, on the basis of the lighter odd-A systematics in Fig 4.9. The ground state of ^{67}Fe is proposed to be $(1/2^-)$ by Block et al. [Blo08] and Daugas et al. [Dau11], supported by experimental evidences here, that the $(7/2^-)$ ground state of ^{67}Co does not receive direct beta-feeding and that most of the beta-fed levels in cobalt have spins $(1/2^-)$ or $(3/2^-)$ (see Section 7.5).

It was also concluded, that there is very little or no evidence, that the ground state of ^{67}Fe receives direct β-feeding in the decay of manganese. Based on the results coming from this study and the limitations by the obtained statistics, spin and parity of $(3/2^-)$ cannot be completely excluded for the ground state of iron.

Complementary information on the excited states in ^{67}Fe was obtained also via the analysis of the P_n branch of the (4^+) ground state of ^{68}Mn [Pau13]. Coincident, prompt and delayed, gamma gates were set on the observed 367-, 390-, 167-, 180-, and 670-keV transitions to identify states in ^{67}Fe, which are populated in that process.

Only two transitions were observed in coincidence with the 390-keV line in that decay set. A clear 670-keV line also appears in the beta-gated prompt gamma-spectrum, while a less clear 635-keV line was identified in the gate of the 390-keV. No prompt coincident transitions were observed in any of the other gates set on the above-mentioned lines, while the delayed coincidences only confirmed the results presented in Fig 7.8, although with much less statistics.

The results from the deduced 26% beta-delayed neutron emission branch can be seen in Table 7.3. Two gamma transitions, the 190 and the 492 keV, following ^{67}Fe decay, were used to calculate the number of ^{67}Co nuclei taking into account the calculated half-life correction factors.

Table 7.3: Distribution of the β-delayed neutron strength in the decay ^{68}Mn.

E + S_n (keV)	E (keV)	P_n %
5507	GS	18(5)
5874	367	9(4)
5895	388.5	18(6)
5897	390	15(5)
6063	556	15(4)
6073	568	9(2)
6532	1025	5(2)
6567	1060	11(3)

Based on the logft values in Table 7.3 and the tentative (4^+) assignment for the ground state of ^{68}Mn [Pau13], it can be inferred that the excited states receiving more than 10% of feeding in the P_n branch of $A = 68$, have spins $I \geq 3/2$, although one should also consider the possibility of unobserved gamma transitions feeding the states as well.

The half-life of the 388.5-keV isomeric level implies, that the low-energy transition feeding the 367-keV state has an $L = 2$ multipolarity rather than $L = 1$, based on a comparison to Weisskopf, single-particle, estimates. The partial half-life of that transition is about 165 μs, and is consistent with an $E2$ transition with a hindrance factor of 3.5 or an enhanced $M2$ by a factor of 20. As no enhanced $M2$ transitions are expected in this mass region [End79], the transition connecting the isomer and the excited state at 367 keV must then be an $E2$, consistent with experimental findings around $N = 40$ and $Z > 28$ [NND13b].

Starting from ^{61}Fe it is possible to "scale" the observed $M2$ transitions in the heavier odd-A iron isotopes on the basis of the single-particle estimations in Table 1.2.
The deduced half-life for the 655-keV transition in the former is 239(5) ns [Mat04]. The experimental data in this set suggest that a single 24-keV $M2$ transition is de-exciting the $(9/2^+)$ state at 475 keV in ^{63}Fe with a half-life of 30(5) ms. The ratio of the energies of the two lines is about 27 which put the power of 5, for quadrupole transitions and corrected for electron conversion for the low-energy one, gives an estimated half-life of 46 ms. It is worth to mention

here, that virtually the same result, 45 ms, is achieved when comparing the 398-keV $M2$ in the isotonic $N = 37$, ^{69}Ge, where the half-life of the excited state with an energy of 398 keV is deduced to be 2.8 μs [NND13b].

If we compare the $M2$ of 655 keV to the 397-keV $M2$ branch in ^{65}Fe, provided that it is a true cross-over transition and does not come from the summing of the ($E1$) and ($M1$) transitions, the estimated half-life is of the order of 2.9 μs, while the partial half-life of the latter is 26 μs, or a factor of 9 retarded.

Such a calculation is consistent also for the $M2$ transition ($9/2^+ \rightarrow 5/2^-$) with a half-life of 13.3 μs [Grz98] in ^{67}Ni. The estimated in this case half-life on the basis of the 655-keV transition is 10 μs.

If the 388.5-keV line in ^{67}Fe were to be an $M2$ transition, the expected half-life calculated in this way is 3.3 μs, while the partial half-life of the latter is determined to be 1.9 ms, that means a much more retarded transition, compared to the previous cases. This is an indication, that the multipolarity of the 388.5 keV transition might not be an $M2$ and supports a different nuclear structure picture in this iron isotope.

The partial half-life of about 2 ms for the 388.5-keV transitions yields unphysical results for multipolarities less than 3. A two times enhanced $E3$ transition is possible according to the Recommended Upper Limits (RUL) [End79]. An $M3$ transition would be 95 times enhanced and has not been observed in this mass region. The $E2$ character of the 21.7-keV line implies, that the 366.8 and 388.5 keV levels have the same parity, while the $E3$ character of the 388.5-keV transitions fixes an opposite parity for the ground state. This fixes an $E1$ multipolarity for the 366.8-keV transition. The prompt character of the 389.8 keV line ($T_{1/2} < 200$ ns) allows $E1$, $M1$ and $E2$ multipolarities. Although limited by statistics, in the gamma spectrum gated by transitions feeding the 389.8 keV level a non-negligible peak is observed at 367 keV. This is an evidence for a 23-keV transition connecting the two states, with an intensity of 6(3)%, relative to the 389.8 keV intensity and a limited multipolarity of $E1$ or $M1$.

On the basis of comparison of the two transitions feeding the isomeric state to the transition in the lighter odd-A neighbours, tentative multipolarities can also be assigned. The intensity of the 180-keV line, 1.5(3)% (Table 7.1), is consistent with the intensity of the 2.4(2)%, 216-keV line ($(7/2^+) \rightarrow 9/2^+$) in ^{65}Fe (see Table 6.1). Such conclusions can be drawn also for the multipolarity of the 167-keV line, from a comparison to the $(5/2^+) \rightarrow (9/2^+)$, 206-keV line in ^{63}Fe, thus an $L = 2$ transition.

We have now firmly fixed the multipolarities of the 21.7-, 366.8- and the 388.5-keV transition to $E2$, $E1$ and $E3$, respectively, and can infer tentative multipolarities for the 167.4- and the 179.6-keV lines as $(E2)$ and $(M1)$. The former assignment leaves several possibilities for the spin and parities of the excited states at low-energy in ^{67}Fe, presented in Fig 7.10.

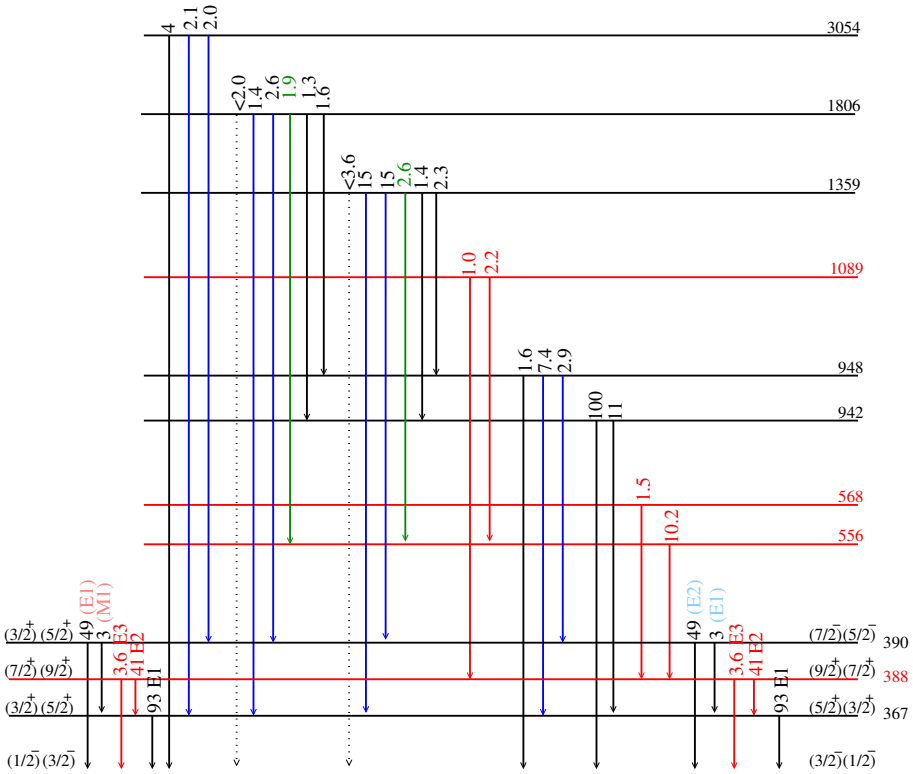

Figure 7.10: Partial level scheme of ^{67}Fe, showing the two proposed scenarios for the first four states (see text). The relative intensity of the transitions is indicated on top of each arrow.

The Weisskopf analysis of the 388.5-keV line, which suggests an $L = 3$ transition, and the limitations of $I \leq 3/2$ for the ground state of iron force the spin and parity of the metastable state to be either $(7/2^+)$ or $(9/2^+)$, consistent with the deduced P_n feeding from $A = 68$ data set and also with the assumptions in the previous studies [Dau11]. Table 7.4 suggests a non-zero direct beta-decay branch towards the isomeric state, but due to the high Q_β value, the extracted

$\log ft$ should be considered as an upper limit.

If the isomeric level were to be a $(7/2^+)$, then the ground state would become a $(1/2^-)$ spin and parity, connected via the $E3$ transition. This leaves the excited state at 367 keV to be with a $(3/2^+)$ quantum numbers.

Assuming a spin and parity of $(9/2^+)$ for the isomeric state would then make the first excited level a $(5/2^+)$ and the ground-state a $(3/2^-)$, based on the $E2$ and $E3$ multipolarity of the 21.7-keV and 388.5-keV lines. A $(5/2^+)$ assignment for the excited state at 367 keV is also consistent based on a comparison of determined direct feeding of 2.3% to the feeding of 2.4% deduced for the $5/2^+$ state in ^{65}Fe.
For both of these cases, the multipolarities of the transitions de-exciting the prompt 390-keV excited state are consistent with $(E1)$ and $(M1)$, as shown in the left hand-side of Fig 7.10 in pink. Depending on the spin and parity of the ground state and thus the metastable level, the excited state at 390 keV becomes either $(3/2^+)$ or $(5/2^+)$. This means that the excited levels at 390 and 367 keV could both have the same spin and parity.

The $L = 1$ assignment of the 23- and the 390-keV lines is in agreement with the performed analysis, using Weisskopf single-particle estimates and conversion electron coefficients in the way that, if the 390-keV were to be an $(E1)$ and the 23 keV were to be an $(M1)$ transition, comparing the observed branching ratio of the two lines, the 390-keV is 130 times more retarded than the $(M1)$ of 23 keV, which is consistent within the RUL in the corresponding mass region [End79]. The ratio of the retardation factors of the two types of transitions is about 100, in favour of the magnetic type, in the mass region of $45 \leq A \leq 90$ [End79], which is also what is observed here. The opposite situation, where the $E1$ is faster than the $M1$ is rather improbable and contradicting the systematics in [End79].

Another possibility for the multipolarities of the 390- and 23-keV lines, again in agreement with both of the proposed spin and parities of the isomeric and the 367 keV state is $(E2)$ and $(E1)$, respectively. Based on Weisskopf estimates, and comparing to the observed branching ratios, if the 390-keV line were to be an $E2$ and the 23 keV line an $E1$, then the former would be around $3{\cdot}10^{-5}$ times less retarded than the $E1$ transition at low energy. This means that the $E2$ transition is a factor of 30 000 times faster than the $E1$. This is another fact, consistent with the overall experimental data in this mass region [End79], as from Fig.1 in the latter work, it is clear that the $E2$ transitions are a factor of 10 enhanced compared to the Weisskopf estimates, while the $E1$ – about a factor of 1 000 times retarded, in agreement with this experimental case.

Such a multipolarity assignment for the two transitions sets the spin and parity for the 390-keV state to either $(5/2^-)$ or $(7/2^-)$, shown in the right hand-side of Fig 7.10 in light blue, depending on the isomeric, and thus on the ground state's spin and parity. This time the 367- and the 390-keV states differ in spins and parities.

It is interesting to analyze what spin and parities are allowed for the excited states that feed both the 367- and the 390-keV states, in the situation where the latter have different parities. Those levels are shown in Fig 7.10 with de-exciting transitions towards the two low-lying states drawn in blue. If the spin and parity configuration of the levels with energies 948, 1359, 1806 and 3054 keV is assumed to be either $1/2^-$, $3/2^{-/+}$, $5/2^{-/+}$ or $7/2^-$, based on single-particle estimates, including the corrections for retardation/enhancement in the respective mass region [End79], and comparing the experimentally deduced branching ratios of the gammas de-exciting those states only the situation with $1/2^-$, $3/2^+$ and $5/2^-$ for the spin and parity of the ground state, the 367 keV and the 390 keV levels, respectively, gives branchings results compatible with the experimentally observed ones.

For example, given the branching ratios for the transitions de-exciting the state at 1806 keV, regardless of the assumed spin and parity of that state, the calculated Weisskopf estimates imply, that the fastest transition should be the ground-state one, provided that $3/2^-$ were to be the spin and parity of the ground state of iron. This transition, though, was not observed in this data set and only an upper limit was deduced for its relative intensity. Thus, in the case of configurations of $(1/2^-)$, $(3/2^+)$ and $(5/2^-)$ for the ground-state, the 367-keV and the 390-keV level, the allowed spin and parities for the excited states, listed above, are: $(3/2^+)$, $(5/2^+)$, $(5/2^+)$, and $(3/2^-, 3/2^+)$, respectively. This is an indication, that the spin in parity of the isomeric state is $(7/2^+)$.

According to calculations in [Del10], which can be visualized in [Hil13], for a deformation parameter of $\beta \sim 0.2$, the calculated single-particle states for neutrons have the spins and parities of $1/2^-$, $3/2^+$ and $5/2^-$ for the first three states. These could be the ground, the 367-keV and the 390-keV states, which also supports the $(7/2^+)$ assignment for the isomeric state at 388.5 keV.

This short discussion proposes several options for the spin and parity assignments of the prompt 389.8-keV state, consistent with the experimental observations, thus a firm assignment can only be made when its half-life is precisely known. The knowledge of the value for the lifetime, along with the systematics of the $E1$ and $M1$ transition in this mass region can point to the right multipolarity

of the ground state transition.

It was mentioned earlier (Section 7.3), that there is yet another possibility for the placement of the μs-isomeric state in ^{67}Fe. Let's then elaborate on the idea, that another isomeric, low-energy, gamma transition stems from a yet unresolved $(9/2^+)$, excited state and feeds a $(5/2^+)$ spin and parity level at 388.5 keV. Much like what is experimentally observed for ^{65}Fe, but this time the $(9/2^+)$ state is above the $(5/2^+)$. The question that arises is, would that be consistent with the experimental observations here?

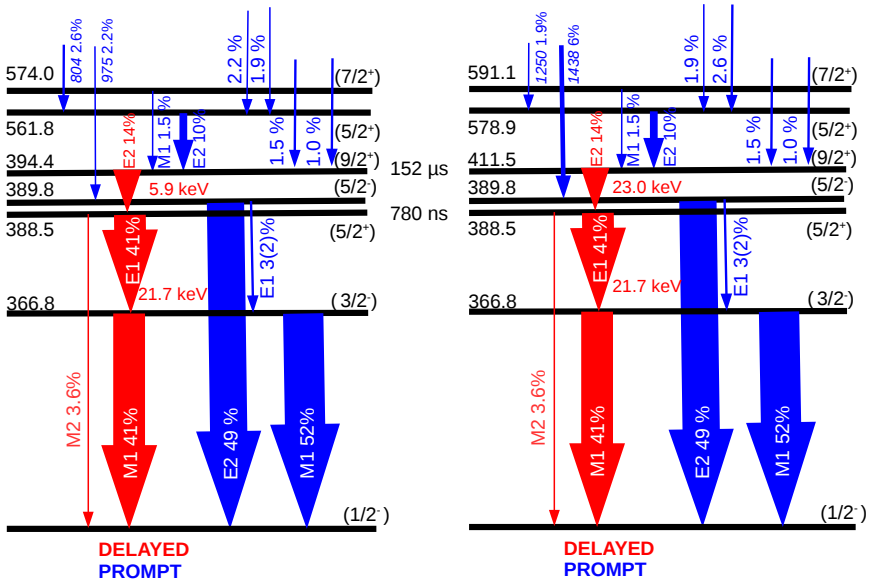

Figure 7.11: Partial level scheme of ^{67}Fe with two isomeric states (see text for details).

The $(5/2^+)$ level at 388.5 keV would then de-excite towards the 367-keV state via a 21.7-keV, $(E1)$ transition and towards the ground state by an $M2$. This also implies that the 388.5-keV should be a second isomeric level in ^{67}Fe, with a half-life shorter than the one observed here (152 μs).

One thing to note is that the $M2$ transition de-exciting the latter level is much more retarded, compared to the $M2$ transition in ^{63}Fe, if we use the way of

comparing in the beginning of this Section.
If the 21.7-keV, ($E1$) transition, is scaled in energy and compared to the 34-keV one in ^{65}Fe with conversion coefficient taken into account ($\alpha = 40$), one deduces an estimated partial half-life of the order of 780 ns. The excitation energy of the $(9/2^+)$ level could then be fixed by either the 804-keV, de-exciting the 1365-keV level along with the 975-keV one, or the 1250-keV line de-exciting the 1829-keV level together with the 1439-keV. Both the 804- and the 1250-keV lines are in prompt coincidence with the 167-keV transition.
Then, in the first case the energy separation between the two, lowest-lying, positive-parity states, based on the determined gamma-ray energies, is 5.9 keV, while in the second case the difference is 23.0 keV. Notice that both energies of the gamma transitions are below the gamma detection limit of the set-up and could then be consistent with the observed experimental data.

In both these cases, only one observed gamma transition, in prompt coincidence with the 167-keV line, would be de-exciting an excited level already defined by prompt coincidences with the 367- and the 390-keV transitions. This also means that such a view on the results obtained here requires the creation of several new excited states, defined by the other prompt coincidences with the 167-keV line. The long-living isomeric state at either 394.4 keV (if the $E2$ is 5.9 keV), or at 411.5 keV, will be then decaying by a single transition, observed to dominate the delayed beta-gated gamma spectrum.

Interesting to note is that the energy of 394.4 keV in the first case is very close to the energy of the $(9/2^+)$ state at 393.3 keV in the $N = 39$ iron isotope.
In both these cases though, one would expect to see the shorter component of the isomeric decay, namely the 780-ns one, as Fig 7.11 suggests that a non-zero direct beta-decay feeding of the $(5/2^+)$ state of about 8% is present. Such a component was not observed in the beta-gated delayed gamma-spectrum at a time scale enhancing such a half-life, but in view of the expected feeding with regards to the statistics in the case of ^{67}Mn decay, such an option cannot be completely excluded.

It is clear that the statistics and the sensitivity of the experimental set-up was not sufficient to completely disregard any of the proposed spin and parity configurations for the low-lying excited and the ground state and more experiments should follow to determine the right one. Nevertheless, in Fig 7.7 and Table 7.4 the version with only one isomeric state is presented and discussed later on.

Regardless of the structure at low energy, the excited level at 942 keV can be tentatively assigned as $(3/2^-)$ on the basis of the determined logft value of

around 5.
If we take a look at the exhaustive experimental data for ^{59}Fe [NND13b], we find that the energy separation between two $3/2^-$ states at 726 and 1162 keV is of about 400 keV. The determined direct beta-feeding for the two states in question is around 30% and 10%, respectively [Oin01]. These arguments can then be used to assign a tentative $(3/2^-)$ for the level at 1359 keV in ^{67}Fe, for which Table 7.4 shows, that the calculated direct beta-decay intensity is of about 11% and the one for the level at 942 keV, already tentatively assigned as $(3/2^-)$, is 30%. The energy difference between the latter two is remarkably of about 400 keV.

Table 7.4: Excited levels and direct β-feeding in the decay of ^{67}Mn.

E (keV)	I_β %	logft	J^π	$T_{1/2}$
GS	< 5	> 6.1	$(1/2^-, 3/2^-)$	416(92) ms [Pau08a]
366.8(1)	2.3(11)	6.2(2)	$(3/2^+, 5/2^+)$	
388.5(2)	8.2(7)	5.6(1)	$(7/2^+, 9/2^+)$	152(11) μs
389.8(1)	4.9(11)	5.8(1)	$(5/2^-, 7/2^-)$	
			$(3/2^+, 5/2^+)$	
555.9(2)	1.1(4)	6.5(2)	$(5/2^+)$	
568.1(3)	0.45(8)	6.9(1)	$(7/2^+)$	
941.7(1)	30(1)	5.0(1)	$(3/2^-)$	
948.0(1)	1.3(5)	6.3(2)		
1025.2(2)	1.1(3)	6.4(2)		
1060.0(8)	0.42(15)	6.8(2)		
1089.0(4)	0.96(19)	6.4(1)		
1093.6(5)	0.46(15)	6.8(2)		
1359.4(1)	10.9(8)	5.3(1)	$(3/2^-)$	
1365.4(4)	0.64(20)	6.6(2)		
1570(1)	0.73(23)	6.5(2)	$(5/2^-)$	
1570.2(2)	14.4(9)	5.2(1)	$(3/2^-)$	
1805.8(2)	2.6(4)	5.9(1)		
1828.6(2)	1.7(3)	6.1(1)		
3054.0(3)	2.5(6)	5.6(2)		

The level at 1570(1) keV ($I_\beta = 0.73(23)\%$), part of a doublet here, has a transition de-exciting it to the isomeric level at 388.5 keV and is tentatively assigned as $(5/2^-)$, once again on the basis of a comparison to the nuclear structure in ^{59}Fe, where an excited state with an almost identical energy (1569.4 keV) and deduced beta-decay feeding ($I_\beta = 0.35(8)\%$ [Oin01]) is determined to

be with $5/2^-$ quantum numbers.

The level at 1570.2 keV is strongly fed in the beta-decay, and is tentatively assigned as $(3/2^-)$ on the basis of the the systematics of the lighter odd-A iron isotopes, where a second excited state with a low $\log ft$ value is expected, and also where the difference between the two is of around 650 keV (the first one being the 941-keV level).

7.4 Previous experimental information on ^{67}Co

The beta-decay of ^{67}Fe was studied in [Sor99, Sor00], where a strong transition of 189(1) keV was reported.

In a proton induced fission experiment on a ^{238}U target, with the help of laser ionization, the radioactive isotope of ^{67}Fe was produced and its subsequent beta-decay studied [Pau08a]. The same experimental set-up, as in the present work, was used to study that decay. Using a novel correlation technique [Pau08b], it was shown, that a transition of 492 keV is de-exciting an isomeric state with the same energy with a half-life of $T_{1/2} = 493(33)$ ms in cobalt.

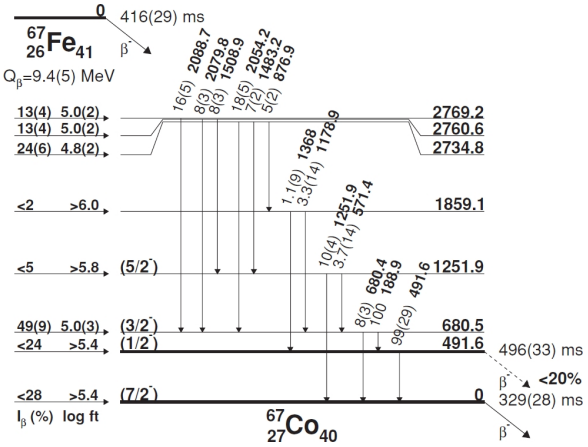

Figure 7.12: Decay scheme of ^{67}Fe constructed by Pauwels et al. [Pau08a].

The deduced decay scheme from the former reference is shown in Fig 7.12. The half-life of the ground state of ^{67}Co was deduced as $T_{1/2} = 329(28)$ ms, while the assigned spins and parities in the figure are based on the tentative $(7/2^-)$ assignment of the ground state of cobalt. The newly established isomeric state has been interpreted as a prolate, proton-intruder state ($1/2^-$ [321]) coexisting with the spherical ground state.

The 681 and 1252 keV states were interpreted as the first two members of the deformed band, built on top of the $(1/2^-)$ isomeric level. The three excited states higher in energy were found to receive substantial feeding, but no transition connecting any of them to the deformed state or the ground state was found. Furthermore, the highest-lying state is observed to only decay to the $(3/2^-)$

one at 681 keV. Based on the logft values, determined in the experiment, the latter considerations and Weisskopf estimates, those states were assigned with tentative spin and parities of $(3/2^-)$, $(3/2^-)$ and $(1/2^-)$, respectively [Pau09b].

The isomeric state at 491.6 keV was recently confirmed in a Penning Trap mass measurement experiment, in the work of Ferrer et al. [Fer10]. The deduced excitation energy of that level was deduced to be 493(14) keV, in perfect agreement with the β-decay study.

In a multi-nucleon transfer experiment using the PRISMA-CLARA set-up, Recchia et al. [Rec12] observed four strong transitions, at energies of 190, 1186, 1613 and 2273 keV. Except the 190 keV, the observed lines are thought to be yrast or near yrast. In that study an asymmetry (R_{ASYM}) ratio was extracted for the strongest observed line (the 1613 keV), which suggested a stretched quadrupole character, thus defining an excited state with $(11/2^-)$ quantum numbers. From energy level systematics of the lighter odd-A cobalt isotopes and based on the observed intensities of the other two high-energy transitions, the candidate for the $(9/2^-) \rightarrow (7/2^-)$ is the 2273 keV line, supported by the presence of a weak transition of 660 keV, matching the energy difference between the two states. The proposed level scheme is shown in Fig 7.13. As in the case

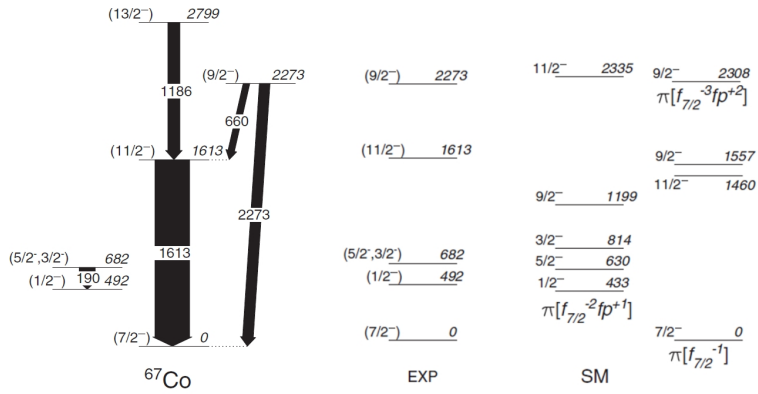

Figure 7.13: Yrast and near level scheme of ^{67}Co, compared to large-scale shell model calculation, using the LNPS interaction, taken from [Rec12].

of ^{65}Co, large-scale shell model calculations indicate an inversion of the $(9/2^-)$ and $(11/2^-)$ excited states, suggesting that the former is no longer an yrast level.

7.5 Results for ^{67}Fe decay

Figure 7.14 shows a clean ^{67}Fe + ^{67}Co decay spectrum, with all contribution from manganese decay subtracted (Section 5.2). It is spanned in the range from 1800 until 2350 keV, where observed transitions are labeled by their energy. Interesting to note are the three weak transitions above 2200 keV, which match

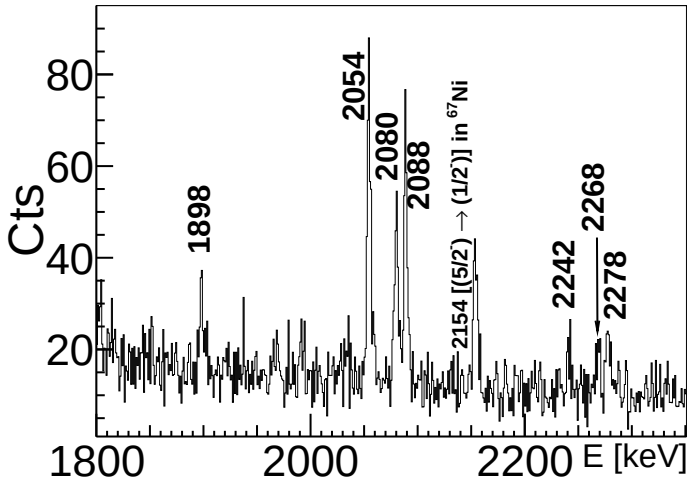

Figure 7.14: Selected part of the clean ^{67}Fe + ^{67}Co decay spectrum, constructed from the $\beta\gamma$-tree. Indicated are transitions in ^{67}Co, as well as in ^{67}Ni.

the energy difference of the previously identified excited states of 2735, 2760 and 2769 keV and the deformed, $\pi p^{+1}_{1/2}$-interpreted level at 492 keV. These three cross-over lines were not observed in the previous decay study, due to the lack in statistics.

A prompt gamma-gamma-coincidence spectrum, gated on the 190-keV line, is shown in Fig 7.15. As expected from the decay scheme in Fig 7.12, three transitions around 2 MeV are found in coincidence with the latter, indicated in the lower panel. The line of 1898 keV, in coincidence with the low-energy transition, is placed on top of the 680-keV level and is also observed in the clean spectrum. This prompt coincidence defines an excited state at the energy of 2578 keV. All of the observed coincidence relationships are given in Table 7.5.

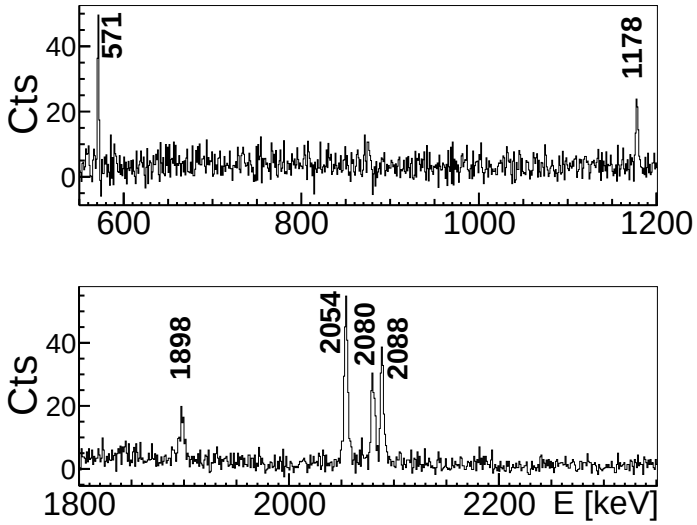

Figure 7.15: Prompt gamma-gamma-coincidence gate, set on the 190-keV transition. Coincident transitions are labelled in keV.

As in the case of manganese decay, described in a previous section, the number of iron decays, deduced from the observed ground-state transitions is compared to the calculated number of cobalt decays, using the 694 keV and line its deduced absolute branching and a difference of 4(3)% is calculated using Method.1.

Using Method.2 in Section 7.3, we are able to deduce the missing or unobserved intensity on the basis only of the half-life of ^{67}Fe. The number of calculated beta particles is compared to the gamma-decay intensity of the 190-keV line in the decay data giving a difference of 24(18)%.

Analyzing the clean ^{67}Fe decay gamma spectrum in Method.3 and comparing it to the number of deduced betas, related only to the decay of ^{67}Fe determines an apparent difference of 25(21)%.
Here it should be noted, that in the latter gamma spectrum a transition of 471 keV, following the decay of ^{66}Fe was observed, thus the correlated with that decay number of betas was deduced on the basis of the absolute branching of that transition [Pau13].

The aforementioned results indicate, that the direct ground-state feeding in

Table 7.5: Gamma transitions and relative intensities, identified as following ^{67}Fe decay. For absolute intensities per 100 decays, multiply by 0.793(53). Transitions below the horizontal line are found in the clean ^{67}(Fe + Co) decay spectrum, but not placed in the decay scheme.

E_γ (keV)	Rel. I_γ %	Rel. I_γ % [Pau08a]	Observed coincidence transitions (keV):
188.8(1)	86(4)	100	571, 876, 1178, 1898, 2054, 2080, 2089
255.6(2)	0.7(3)	—	1229
491.5(1)	100	99(29)	—
570.8(3)	2.9(3)	3.7(14)	189
680.2(1)	5.7(8)	8(3)	571, 2080, 2089
875.8(3)	3(1)	5(2)	189, 1178
1178.2(2)	4.2(6)	3.3(14)	189, 876
1228.8(3)	1.7(4)	—	255
1251.3(2)	19(1)	10(4)	1229
1368.2(2)	1.8(8)	1.1(9)	876
1483.3(1)	9.1(9)	7(2)	571
1508.6(1)	6.6(7)	8(3)	571, 1251
1897.8(2)	4.4(8)	—	189
2054.4(1)	16(1)	18(5)	189
2080.2(2)	10(1)	8(3)	189
2088.8(1)	12(1)	16(5)	189
2242.4(6)	5(2)	—	—
2267.6(5)	2.2(10)	—	—
2277.5(3)	1.9(6)	—	—
2734.6(5)	1.2(5)	—	—
882.1(5)	4(1)	—	—
969.2(5)	5(1)	—	—
1721.6(5)	2(1)	—	—

the decay of ^{67}Fe is consistent with zero, and the differences between betas and gammas can be assigned to unobserved ground-state transitions. This also supports the assignment of $(1/2^-, 3/2^-)$ spin and parity for the ground state of the mother.

The identified excited states in the decay of ^{67}Fe and their calculated beta-feeding and strength can be seen in Table 7.6, where the value adopted for the direct feeding of the ground state of ^{67}Co is the weighted average of the three methods described above, and should be understood as an upper limit due to

unobserved ground-state-feeding transitions.

Table 7.6: Excited levels and direct β-feeding in the decay of ^{67}Fe. States indicated by a "*" are new in this study.

E (keV)	I_β %	logft	J^π [Pau09a]	$T_{1/2}$
GS	5(2)	6.2(4)	$(7/2^-)$	329(28) [Pau09a]
491.5(1)	<4.4	>6.1	$(1/2^-)$	496(33) [Pau09a]
680.2(1)	31(4)	5.2(1)	$(3/2^-)$	
1251.3(1)	3.4(14)	6.0(2)	$(5/2^-)$	
1859.0(1)	2.5(11)	6.0(2)		
2480.1(2)*	0.81(37)	6.3(2)		
2578.0(2)*	3.3(6)	5.7(1)		
2734.6(1)	27(2)	4.7(1)		
2760.1(1)	14(1)	5.0(1)		
2769.0(1)	11(1)	5.1(2)		

The ^{67}Fe decay scheme.

An extended decay scheme of ^{67}Fe is deduced in this study, containing nine excited states, of which two, at 2480 and 2578 keV, are new. Three cross-over transitions, connecting previously observed higher-lying excited levels with the $(1/2^-)$ state at 492 keV are observed. An upper limit of direct feeding in the beta-decay of the $(1/2^-, 3/2^-)$ ground state of ^{67}Fe towards the latter level is determined.

The ground state of ^{67}Co is tentatively assigned as $(7/2^-)$ spin and parity, on the basis of the odd-A cobalt systematics and expectations from shell-model. The spin and parity assignments of the excited levels are from [Pau08a]. The complete decay scheme of ^{67}Fe can be see in Fig 7.16.

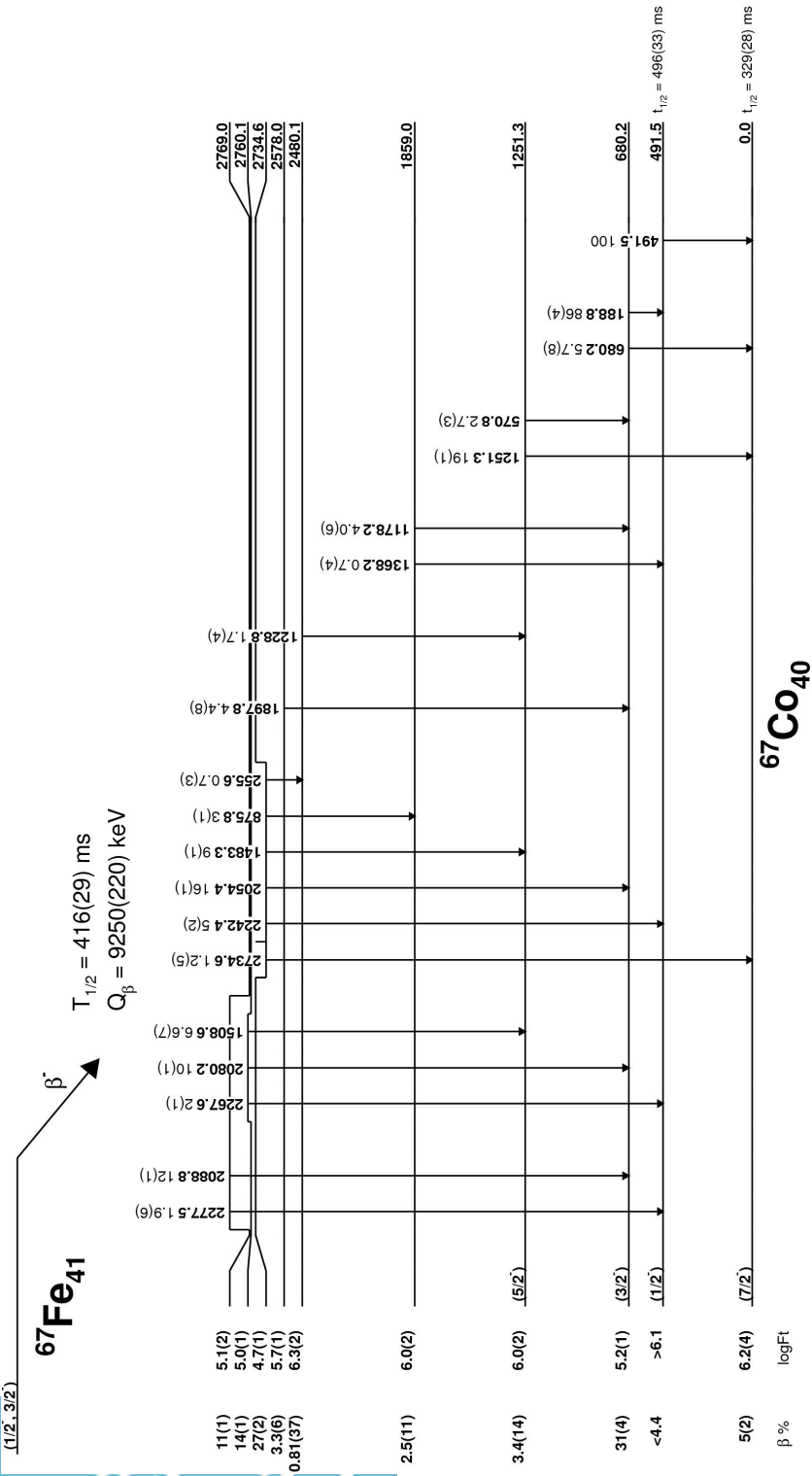

Figure 7.16: Decay scheme of ^{67}Fe, constructed in this study.

7.6 Previous experimental information on ^{67}Ni

Only limited information is available on the low-lying energy structure of ^{67}Ni. The decay of ^{67}Co was investigated in a dedicated study by Weissman et al. [Wei99], the results of which are presented in Fig 7.17. Three excited states were

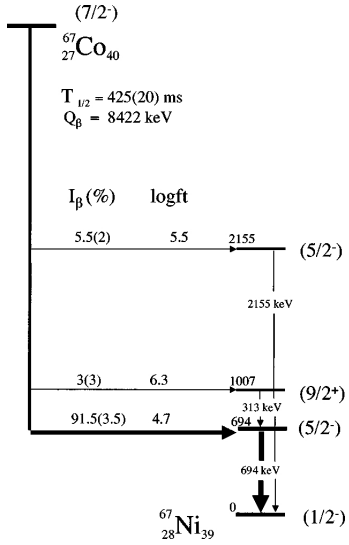

Figure 7.17: Decay scheme of ^{67}Co, constructed by Weissman et al. [Wei99].

found to be fed in the beta-decay, where more than 90% of the beta-strength was assigned towards an excited state at 694 keV, with a logft of 4.7. A small branch towards the previously identified $(9/2^+)$ isomeric level [Paw94, Grz98] was also observed. In the latter study by Grzywacz et al., the half-life of the metastable state was determined to be 13.3(2) μs. The cited works associate the spin and parity of the long-living state with the occupation of a neutron of the single particle $g_{9/2}$ orbital.

The existence of the observed decay patterns, especially the branch to the $(9/2^+)$ state, indicates a significant admixture of $\pi f_{7/2}\nu g^2_{9/2}p^{-2}_{1/2}$ configuration in the ground state of ^{67}Co, found to be in agreement with the calculated occupancy of the $\nu g_{9/2}$ orbital [Wei99].

In his thesis work, Pauwels [Pau09b] observes also the 694, 313 and 2155 keV in the decay of ^{67}Co. A transition with an energy of 1460 keV, that matches the energy difference between the 2155 and 694 keV states, was tentatively

attributed to the decay of ^{67}Co, due to observed 2(2) counts in coincidence with the 694 keV, when 6(2) counts were expected from estimations.

The magnetic dipole moment of the ground state was measured to be $+0.601(5)\mu_N$, close to the the $p_{1/2}$ single-particle value and this fixes the spin and parity to $1/2^-$ [Rik00]. For the isomeric state, a g-factor value of $|g| = 0.125(6)$ was reported by Georgiev et al., in [Geo03] and was interpreted as a 2% admixture of a $\pi(f_{7/2}^{-1}f_{5/2})_{1^+} \oplus \nu g_{9/2}$ configuration, involving a proton excitation across the $Z = 28$ gap into the supposedly pure $\nu g_{9/2}$ state, hinting for the importance of proton excitations across Z = 28.

A recent transfer reaction experiment, in inverse kinematics – ^{66}Ni$(d,p)^{67}$Ni – performed with the REX-ISOLDE set-up at CERN, populated numerous negative-parity states at low excitation energy and up to 5.8 MeV [Dir13a]. The results from the analysis show the identification of the known $\nu g_{9/2}$ and new $\nu d_{5/2}$ positive-parity states, while the extracted relative spectroscopic factors indicate, that a large part of the neutron $d_{5/2}$ single-particle strength is split over two excited states at relatively low energies of 2207 and 3277 keV, pointing to the influence of this orbital in the mass region. The estimated size of the $N = 50$ gap, coming from this measurement is of about 2.6 MeV, showing no deviation from the lighter nickel isotopes [Dir13a]. A detailed level scheme was also deduced.

In a deep-inelastic reaction of a ^{64}Ni beam on a thick ^{238}U target, yrast and near yrast excited states in ^{67}Ni were populated [Zhu12]. The experimental yield of the nickel isotope, allowed for angular correlation measurements of the gamma-cascades, when statics would allow. It was concluded, that the pattern of the 313-694 keV cascade, resembled a sequence of two stretched quadrupole transitions (see Fig 6a) in [Zhu12]), further confirming the spin-sequence: $9/2^+ \rightarrow 5/2^- \rightarrow 1/2^-$.

7.7 Results for ^{67}Co decay

The decay scheme of ^{67}Co was built on the basis of coincidence relationships, between the observed transitions and the available information from the previous decay studies [Pau09b, Wei99]. The quality of the coincidence statistics in this decay can be inspected in Fig 7.18.

Panel *a*) shows a selected part of the γ-γ-prompt ($\pm$ 700 ns) coincidence gate, set on the 694 keV transition, the strongest in the decay of cobalt. The prompt gate, set on the 313 keV line returns the coincident 694 keV, as can be seen in panel *b*). In Section 7.6, it was mentioned that a transition of 1460 keV is tentatively placed in the decay scheme of ^{67}Co [Pau09b], based on the energy difference between the two observed negative-parity excited levels. Such a transition was observed in the present singles data, usually attributed to the background gamma-radiation with origins in the decay of ^{40}K towards the 2^+ state of ^{40}Ar.

A weak transition with the same energy was also observed in the clean ^{67}Fe decay spectrum, constructed from the $\beta\gamma$-tree, which means, that a correlation, between a beta-decay followed by emitting a gamma-ray with an energy of 1460 keV, exists. Thus, at least part of the intensity of that transition, observed in singles (total of 2050 cts), could come after the decay of ^{67}Co.

Panel *c*) shows the prompt gamma-gamma coincidence gate, set on the 1460 keV, where we observe a transition of 694 keV in coincidence. Using Fig 7.18c), 75 counts in the area of the former line were attributed to the transition of 1460 keV, following the decay of cobalt, making its relative intensity 0.79(33)%. Finally, the last panel in the figure, shows the delayed γ-γ-coincidence gate set on the 313-keV line.

A weak line of 1328(1) keV is observed in that spectrum. A transition with a similar energy (1330.6(7) keV) in delayed coincidence with the 313-keV was also observed in [Dir13b]. The difference in the energy of the transition in both works can be due to the very little statistics observed in the beta-decay. Nevertheless, the positive number of counts observed in Fig 7.18d) confirm the placement of the latter, feeding the $9/2^+$ level.

Taking into account all this information, as well as the observed intensity of the 2154-keV transition in the singles data, the decay scheme seen in Fig 7.19 was established. The observe coincidence relationships can be seen in Table 7.7, while the calculated β-feeding is presented in Table 7.8.

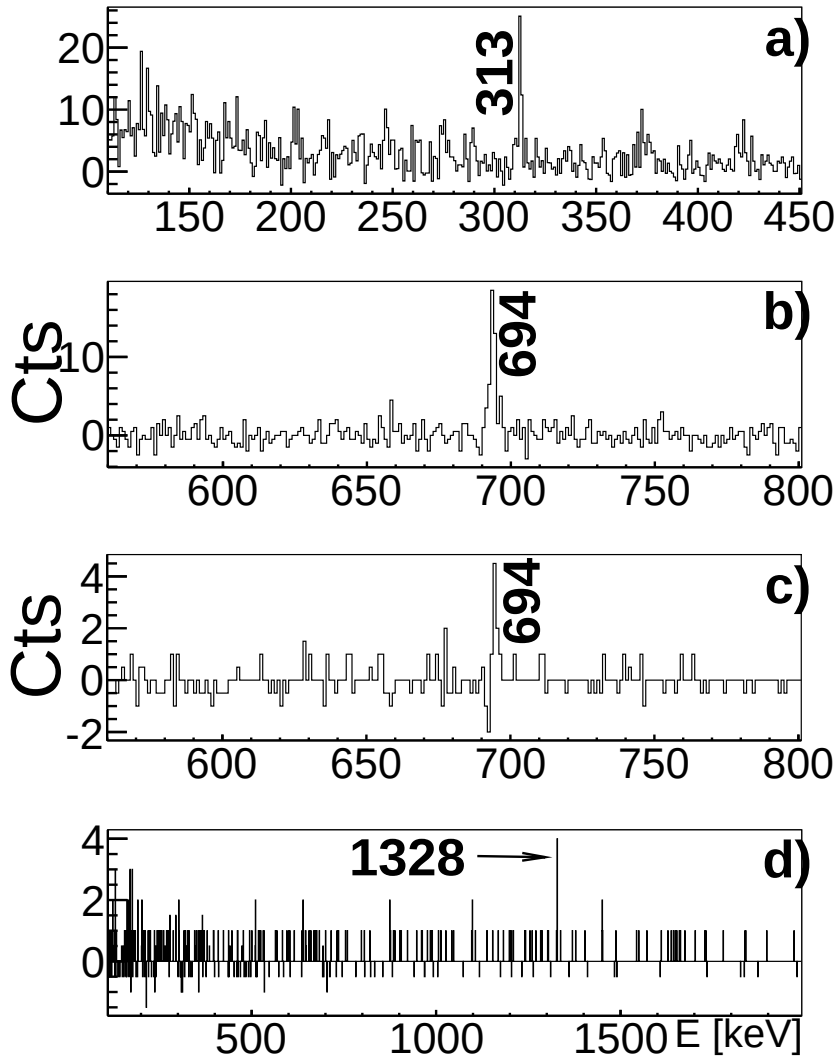

Figure 7.18: Selected part of the prompt (± 700 ns) coincidence gates, set on the *a*) 694 keV, *b*) the 313 keV, and *c*) the 1460 keV. Panel *d*) shows the delayed (1 – 46 μs) gate on the 313 keV line, where a transition of 1328(1) keV is indicated with an arrow.

Table 7.7: Gamma transitions and relative intensities, identified as following ^{67}Co decay. Italic font denotes delayed (1 – 46 μs) coincidence relationship. Transitions below the horizontal line are found in the clean ^{67}(Fe + Co) decay spectrum, but not placed in the decay scheme. For absolute intensities per 100 decays, multiply by 0.945(20).

E_γ (keV)	Rel. I_γ %	Observed coincidence transitions (keV):
313.0(3)	2.2(3)	694, *1328(1)*
694.1(2)	100	313, 1460
1328(1)	0.51(21)	—
1459.7(5)	0.79(33)	694
2153.8(2)	5.8(7)	—
882.1(5)	4(1)	—
969.2(5)	5(1)	—
1721.6(5)	2(1)	—

The ^{67}Co decay scheme.

Four excited levels, one of which is new, were identified in the β-decay of ^{67}Co. The calculated beta-decay decay branching is in excellent agreement with the study in [Wei99]. The spins and parities in the decay scheme are adopted from

Table 7.8: Excited levels and direct β-feeding in the decay of ^{67}Co.

E (keV)	I_β %	logft	J^π [NND13b]	$T_{1/2}$
GS	—	—	$1/2^-$	21(1) s [Jun05]
694.1(2)	92(1)	4.4(1)	$5/2^-$	
1007.1(5)	1.6(4)	6.1(1)	$9/2^+$	13.3(2)μs [Grz98]
2153.8(5)	6.3(8)	5.2(1)	$(5/2^-)$	
2335(1)	0.48(20)	6.2(2)		

the previous β-decay works, [Wei99, Pau08a], as they are consistent with the observed β-feeding here.

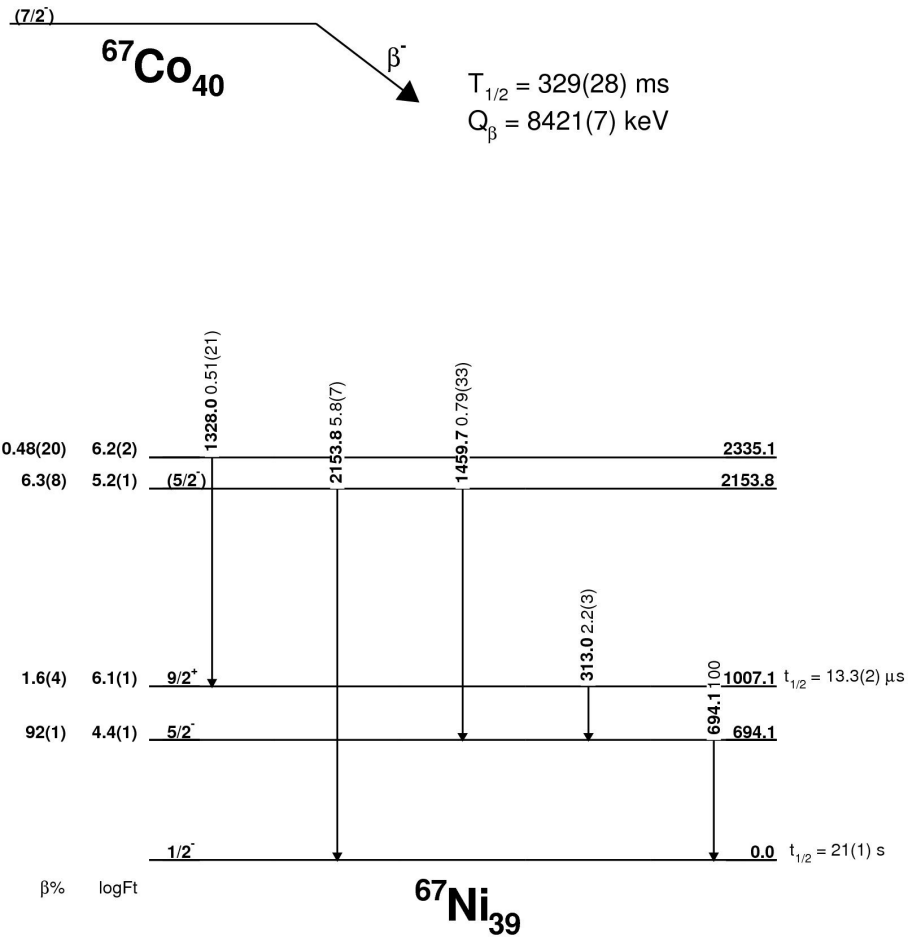

Figure 7.19: Decay scheme of ^{67}Co, constructed using the current data set.

Chapter 8

Discussion on the nuclear structure of the neutron-rich iron isotopes

8.1 The negative parity states

The experimental results concerning the excited states of four odd-even iron isotopes have been presented in the previous chapters. These new data largely enhance the available information on the odd-A manganese decay chains with excited states, gamma transitions and beta-decay feeding patterns. They allow us to judge on the completeness of the constructed decays schemes and set restrictions on possible spins and parities of the beta-decaying state of the manganese mother and the excited states in the corresponding iron isotopes. All of this information has been extracted the basis of gamma-gamma coincidence, implantation-decay time behaviour of the intensity of the observed γ-transitions and comparison between the β- and γ-rays, assuming pure manganese implantation sources were produced at the ISOLDE facility.

An important feature of the ^{61}Mn decay study is the large amount of data collected and the likelihood that most, if not all, levels below 2 MeV with spins below 9/2 have been observed. In Fig 8.1 a comparison between the experimental levels of ^{61}Fe to those of ^{59}Fe is made. The level structure in ^{61}Fe is found to be similar to that in ^{59}Fe, based on the finding of the same amount of negative-parity levels up to $\sim$ 2 MeV in both nuclei. This is also supported by the exhaustive data sets available for ^{59}Fe [McL72, Tay80, Ven80, Oin01, Dea07]. In other words, the careful study of the levels in ^{61}Fe has revealed neither a much

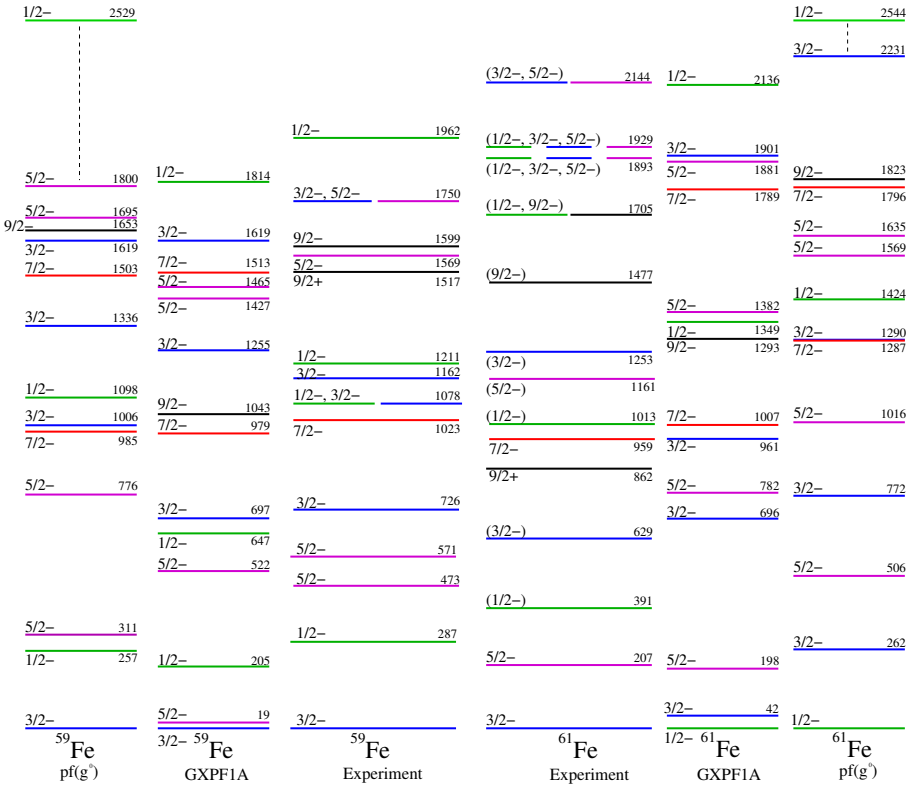

Figure 8.1: Comparison of the experimental data on the odd-A ^{59,61}Fe isotopes with shell-model calculations performed with two different interactions. Only negative-parity states are shown in the two experimental data sets with the exception of the $9/2^+$ excited state in both nuclei.

larger nor a much smaller level density below that energy cut-off, compared to ^{59}Fe. Hence the question can be raised as to why the addition of two neutrons has so little impact on the observed structure. The little impact on the number of levels and their ordering in ^{61}Fe with respect to ^{59}Fe might be due to the closure of the sub-shell gap above which the $\nu g_{9/2}$ orbital lies. With a smaller energy gap to overcome, the strong pairing force provides for enhanced probability for neutron-pair occupancy of the latter orbital. The pairing force will keep the extra coupled neutrons in ^{61}Fe in the $\nu g_{9/2}$ orbital and prevent them from breaking in a way, that can mix new configurations into the other low-spin negative-parity levels. Hence, leaving the energies of the negative-parity levels

and their ordering largely unperturbed.

Two sets of shell-model calculations have been performed for the negative-parity levels in ^{59,61}Fe. The comparison of the latter to the experimental spectra of states for the two iron isotopes can also be seen in Fig 8.1. One set of levels was calculated with the code ANTOINE [Cau99] using the GXPF1A [Hon05] effective interaction with a ^{40}Ca core. The model space included protons and neutrons in the pf shell, although the $f_{7/2}$ neutron sub-shell was frozen with a full complement of eight neutrons, resulting in an effective ^{48}Ca core. The other calculations were performed with the Oslo shell-model code [Hjo95], with the pfg interaction and a ^{48}Ca core as described in [Hot10]. The model space includes protons in the pf shell and neutrons in the $p_{3/2}$, $f_{5/2}$, $p_{1/2}$, and $g_{9/2}$ orbitals; here, however, excitations into the $g_{9/2}$ neutron orbital were blocked. Thus, both calculations were performed in the same model space but with different two-body matrix elements and single-particle energies for the active pf orbitals and only for the negative-parity states.

Comparing the experimental spectra to the model calculations, two features stand out: the inability of either model to place two $5/2^-$ levels close together at low energy in ^{59}Fe and a $1/2^-$ ground-state spin and parity assignment by both of the models for ^{61}Fe. Furthermore, the calculated levels for ^{59}Fe provide at least as good fit to the observed levels of ^{61}Fe as do the levels calculated with the addition of another pair of neutrons. This is especially pertinent, given that both calculations for ^{61}Fe show a $1/2^-$ spin and parity for the ground state.

The similarity of the level structure in ^{59,61}Fe is also consistent with the nearly constant $B(E2 : 2^+ \rightarrow 0^+)$ values in the even-even isotopes up to ^{62}Fe. A large increase for the latter value is observed for ^{64}Fe and ^{66}Fe [Rot11]. The added occupancy of the $\nu g_{9/2}$ and/or the $\nu d_{5/2}$ orbital in the the latter isotopes can polarize the nucleus to a much stronger degree [Cau02, Len10].

A limited summary of the systematic of negative-parity states in the odd-A $^{59-67}$Fe, below 1600 keV, is presented in Fig 8.2. An additional information in that figure is the approximate location of the first 2^+ excited state in the adjacent even-even iron isotopes, marked by an ellipse.

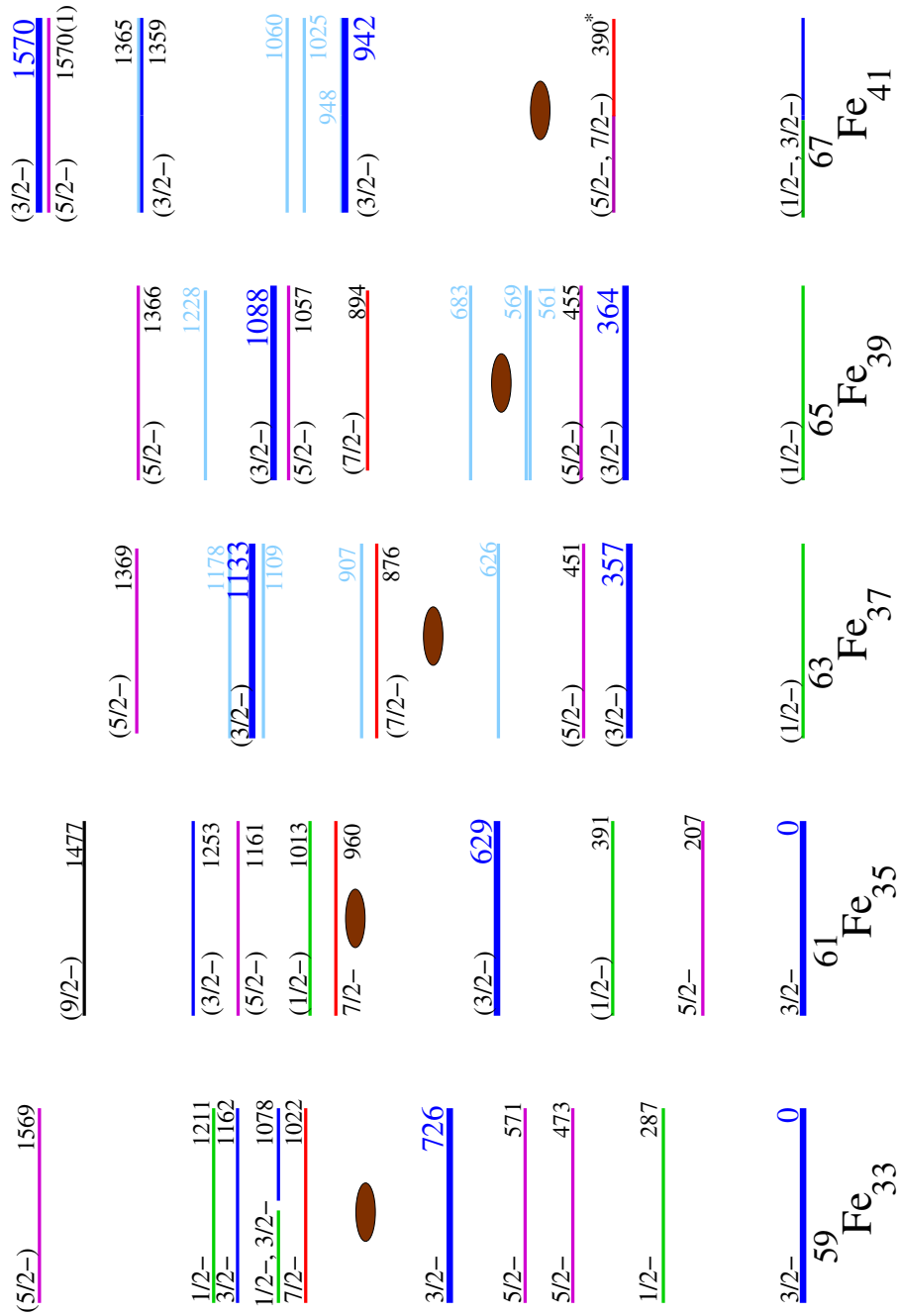

Figure 8.2: Limited systematic of the negative-parity states in the odd-A $^{59-67}Fe_{33-41}$ isotopes. The brown ellipse denotes the location of the 2^+ state in the adjacent even-even iron isotopes. The data for $N = 33$ is from [NND13b]. The **bolder/thicker** levels indicate a pair of excited states in each isotope, found to possess similar characteristics (see text for details). *The prompt 389.8-keV level is consistent with a negative parity assignment (see Section 7.3 for a discussion).

The neutron Fermi level in ^{59}Fe and ^{61}Fe (with 33 and 35 neutrons, respectively) is located at the $\nu f_{5/2}$ orbital, which is half full in the case of the latter. The ground-state spin and parity in both cases is found to be $3/2^-$. This assignment may correspond to a hole in the $\nu 2p_{3/2}$ orbital with a coupled pair(s) in the orbital above ($\nu 1f_{5/2}$). The $3/2^-$ ground state could also be interpreted as arising from the Nilsson 3/2[301] orbital with an $f_{5/2}$ parentage (see Fig 1.4).

At heavier mass, previous experimental results for the ^{63,65}Fe indicate, that with the addition of two more neutrons with respect to ^{61}Fe, the ground state of iron changes its spin to 1/2. This information is supported by the results obtained in this study. A similarity between the energy levels in these two isotopes is also observed. This is indeed consistent with the measured half-lives of the first two, negative-parity, excited states in the two isotopes [Ola13], tentatively assigned as $(3/2^-)$ and $(5/2^-)$, respectively. Furthermore, the levels with $\log ft$ values around 5 are at very similar energies in the two cases – 357 and 1133 keV for the isotope with $N = 37$ and 364 and 1089 keV for the one with $N = 39$. The ground-states' spin and parity of $(1/2^-)$ can be related to the occupation of the neutron $p_{1/2}$ orbital, rising below the $\nu f_{5/2}$ one. This may be the case if the nuclei possess a large enough deformation ($\beta > 0.2$, see Fig 1.4). Indeed, the ^{66,68}Fe iron isotopes have already been proposed to possess such [Cra13]. For the odd-mass isotopes, this would mean that the tentative spin and parities of the first two excited states have a $\nu f_{5/2}$ parentage. Another interpretation for the spin and parities of the first three states can be presented using the calculations in Fig.11 of [Dau11]. The latter calculation shows that the spin and parity of $(1/2^-)$ for the ground state and the two negative parity excited states, might be due exclusively to the $\nu f_{5/2}$ orbit. This is because the $\nu f_{5/2}$ orbital is being pushed-up by the proton-neutron interaction and rises above the $p_{1/2}$ orbital. Important to note here is that the performed beyond-mean-field calculations in [Dau11] for the even-even ^{66,68}Fe isotopes, suggest a triaxial deformation for the two ground states with mean deformation parameters of $<\beta>_{0^+} = 0.261$ and $<\beta>_{0^+} = 0.254$, respectively, and $<\gamma>_{0^+} \approx 20°$.

In the heaviest investigated iron isotope – ^{67}Fe – none of the possibilities for the spins and parities of the low-lying states, discussed in Section 7.2, can be overruled at this point. The level of statistics is such, that one cannot firmly disregard any of the possible spin and parity configurations. Nonetheless, the possibility including one isomeric state – at 388.5 keV with a half-life of 152 μs – is depicted Fig 8.2. In the framework of the systematic it is noteworthy to be reminded of the inferred similarity of three of the excited states in ^{67}Fe to excited states in the 8-neutron-lighter ^{59}Fe, already proposed in Section 7.3. The tentative $(3/2^-)$ levels at 942 keV and 1359 keV and the $(5/2^-)$ level at 1570(1) keV in ^{67}Fe look similar to the 726-keV, 1162-keV and 1569-keV states

in ^{59}Fe, determined to be $3/2^-$, $3/2^-$ and $5/2^-$, in terms of energy and energy differences.

In the framework of the particle plus core coupling model [Oro00], some of the low-lying excited states in $^{59-63}$Fe isotopes can be interpreted as a neutron coupling to the first excited state in the adjacent even-even core [Wal13]. With the exception of the three single-particle states ($1/2^-_1$, $3/2^-_1$, $5/2^-_1$), one should observe up to 11 levels in each isotope, arising from the coupling of the neutron to the 2^+ level in the adjacent even-even neighbour. Their spins and parities should range from $1/2^-$ ($3/2^- \oplus 2^+$) to $9/2^-$ ($5/2^- \oplus 2^+$). Such excited states can be tentatively identified in the above-mentioned nuclei, near the energy of the excited 2^+_1 core levels. In ^{65,67}Fe due to the lowering of the 2^+ and 4^+ levels in the adjacent ^{66,68}Fe isotopes, more states are expected to be observed in the $\sim$ 1500 keV region. While in the case of ^{65}Fe this seems to be case, in the heavier ^{67}Fe not many levels have been observed around 521 keV (2^+ level in ^{68}Fe [Pau13]).

A feature of the experimental results in this study is the similarity of a pair of states in each investigated iron isotope with an energy separation of about 650 keV, indicated in Fig 8.2 in bold. Furthermore, the two levels in each of the pairs, share together more than half of the beta-decay intensity in each of the manganese decays. The energies, the deduced logft values and the calculated direct beta-decay feeding for each state in the pair are summarized in Table 8.1. Recently, the structure of the low-energy, odd-A $^{59-63}$Mn has

A	E (keV)	logft	I_β %	J^π
59	0	5.3(2)	23(8)	$3/2^-$
59	726	4.9(1)	32(5)	$3/2^-$
61	0	5.0(1)	33(1)	$(3/2^-)$
61	629	4.8(1)	39(1)	$(3/2^-)$
63	357	5.0(1)	30(1)	$(3/2^-)$
63	1133	4.8(1)	29(1)	$(3/2^-)$
65	364	4.8(1)	35(1)	$(3/2^-)$
65	1089	4.9(1)	17(1)	$(3/2^-)$
67	942	5.0(1)	30(1)	$(3/2^-)$
67	1570	5.2(1)	14(1)	$(3/2^-)$

Table 8.1: Logft values and the intensity of the calculated direct beta-decay feeding in the 5 similar pairs of states in the $^{59-67}$Fe isotopes. The data for A = 59 is from [Oin01].

been investigated [Val08] and the set of data shows, that ^{59}Mn and ^{61}Mn have

an almost identical structure. Finding a pair of excited states with similar characteristics in each of the odd-A iron isotopes, supports the notion that ground states in the odd-A manganese isotopic chain have the same spin and parity along it. It is experimentally observed here, that the discussed pair of states moves higher in excitation energy with the addition of neutrons – from the ground state and the excited 629-keV state in ^{61}Fe to the two excited 941.7-keV and 1570.2-keV states in ^{67}Fe (see Fig 8.2).

8.2 The positive parity states

The experimentally observed isomerism in this region is due to the presence of the opposite-parity $\nu g_{9/2}$ orbital close to the pf shell. This is manifested by the isomeric states observed in the $^{61-67}$Fe odd-A iron isotopes. In this study, the previously unobserved isomeric state in ^{63}Fe has been identified. Its half-life was found to be 30(5) ms and its excitation energy – 475 keV (Section 5.2); the energy of the 1.1(2) s, beta-decaying isomer in ^{65}Fe has been precisely determined at 393.3(1) keV (Section 6.2); a half-life value for the isomeric state in ^{67}Fe of $T_{1/2} = 152(11)$ μs has been obtained, found to be twice as large as the value reported in [Saw03]; a precise excitation energy of 388.5(2) keV for the latter isomeric state has been determined (see Section 7.3). The findings in this study complete the systematics of the positive-parity isomers in the odd-A irons (see Fig 8.3, where also the systematics of the $9/2^+$ in the nickel isotopes is presented).

In the cases of ^{61,63}Fe the spin isomerism is manifested through the parity-changing magnetic quadrupole ($M2$) transition, $(9/2^+) \rightarrow (5/2^-)$ which is systematically retarded in this mass region. In ^{65}Fe, it is a retarded 34-keV transition of $E1$ type de-exciting the low-lying $(5/2^+)$ state, that makes up for a half-life of 428(11) ns. No conclusive evidence for an $M2$ $((5/2^+)\rightarrow(1/2^-))$ cross-over transition with an energy of 397 keV is found in the current study. Since the 393-keV, $(9/2^+)$ state in ^{65}Fe is found to be below the $(5/2^-)$ level, the former excited level decays via the means of a β-emission and a half-life of 1.1 s [Pau09a].

In ^{67}Fe the isomeric character of the excited state is due to a retarded $E2$-type transition. Such retarded transitions, are found in other isotopes in this mass region. Their experimental half-lives are found to be consistent with the half-life of the proposed low-energy transition in ^{67}Fe and therefore with the $E2$ multipolarity assigned for the latter.

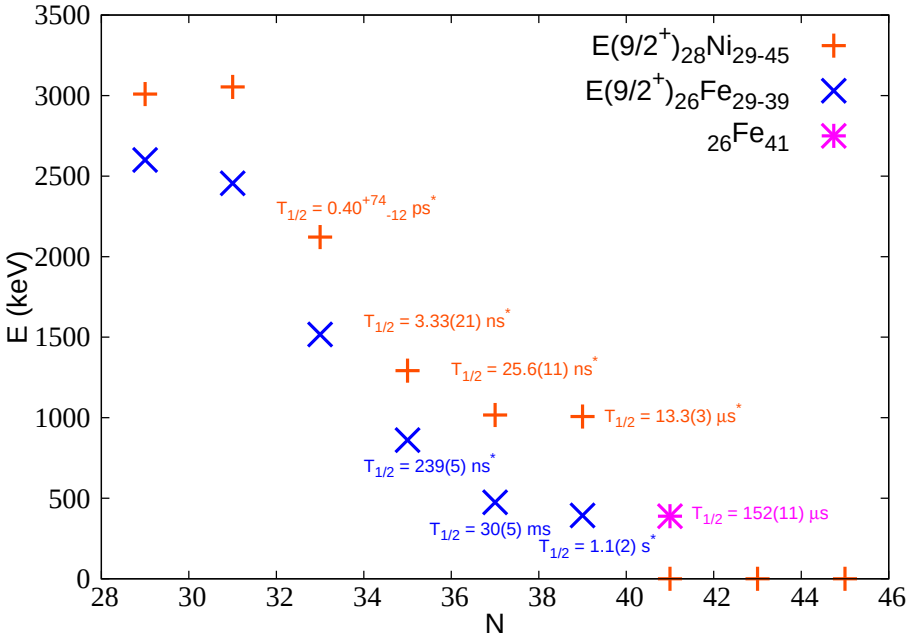

Figure 8.3: Systematics of the energy of the positive-parity isomeric levels in the nickel and iron isotopes, including the findings from this study. The **orange** + and **blue x** both indicate $I = 9/2$ states, while the spin of the **magenta** * in ^{67}Fe is not yet certain (see Section 7.3).
* – the half-life values are taken from [NND13b].

A $1/2^-$ excited state at 86.7 keV is found to decay to the ground state of $^{69}Ge_{37}$ via an $E2$ transition with a half-life of 5.1 μs [NND13b]. An estimation of the expected half-life of the latter transition can be made on the basis of the transition's energy and using Table 1.2. Such a calculation results in a partial half-life of 2.9 μs for the low-energy transition in germanium, found to be consistent with the one deduced experimentally (less than two times retarded, see Table 8.2).

In $^{71}Ge_{39}$ an $E2$ transition ($5/2^- \rightarrow 1/2^-$) with an energy of 174.9 keV has a measured half-life of 79 ns [NND13b]. This is about two times shorter, than the expected Weisskopf single-particle estimate.

Two neutrons farther, the deduced half-life of the 13.3 keV $E2$ transition ($5/2^+$

Isotope	E_γ (keV)	ML	$T^{exp}_{1/2}$	$T^{s.p.}_{1/2}$	$T^{exp}/T^{s.p.}$	$J^\pi_i \rightarrow J^\pi_f$
$^{69}Ge_{37}$	87	$E2$	5.1(2) μs*	2.93 μs	1.74	$1/2^- \rightarrow 5/2^-$
$^{71}Ge_{39}$	175	$E2$	79(2) ns*	178 ns	0.44	$5/2^- \rightarrow 1/2^-$
$^{73}Ge_{41}$	13	$E2$	2.92(3) μs*	71.8 μs	0.04	$5/2^+ \rightarrow 9/2^+$
$^{67}Fe_{41}$	22	$E2$	165 μs	47 μs	3.49	$x/2^+ \rightarrow y/2^+$

Table 8.2: Experimental transitions' energies, multipolarities and experimental half-lives (* – from [NND13b]), compared to the estimated Weisskopf values for the corresponding transition and multipolarity using Table 1.2 and adjusting for the electron conversion coefficients ($x = 7$ or 9; $y = 3$ or 5 – see Chapter 7.3).

$\rightarrow 9/2^+$) in $^{73}Ge_{41}$ is 2.92(3) μs [NND13b]. This half-life is found to be 25 times shorter, than the theoretical one in Table 8.2.

The low-energy transition in ^{67}Fe is found to be 3.5 times more retarded compared to the Weisskopf estimate for an $E2$ transition of the same energy.

To further compare the experimental results for the odd-A iron isotopes, a systematic plot showing excited states with tentative and firm spin and parity is presented in Fig 8.4. Note that the excited levels are drawn with respect to the energy of the lowest-lying positive-parity excited state. The measured half-lives of the isomeric states are also given.

On the basis of a comparison to the excited states in ^{59}Fe, the state at 1262 keV in the neighbouring ^{61}Fe, could be inferred to have a tentative $(5/2^+)$ spin and parity. From then on up to ^{65}Fe this excited state is observed to decrease in energy relative to the $I = 9/2$ state. It is such, that in ^{65}Fe the energy difference between the two levels is only 4 keV (Fig 8.4).

Another similarity between the depicted $^{59-65}$Fe odd mass isotopes is the relative location of the band built on top of the $9/2^+$ state, interpreted as a decoupled one [Lun07]. The band's relative positions stays rather constant within the isotopic chain. Although the statistics in [Lun07] was not enough to observe high-spin transition in ^{67}Fe, based on the systematics of the lighter isotopes, one may suggest that the analogous high-spin states in ^{67}Fe are located around 1.2 and 2.3 MeV, respectively. Such high-spin levels will not be directly fed in the beta-decay of a $(5/2^-)$ ^{67}Mn ground state, thus are not observed in the present study.

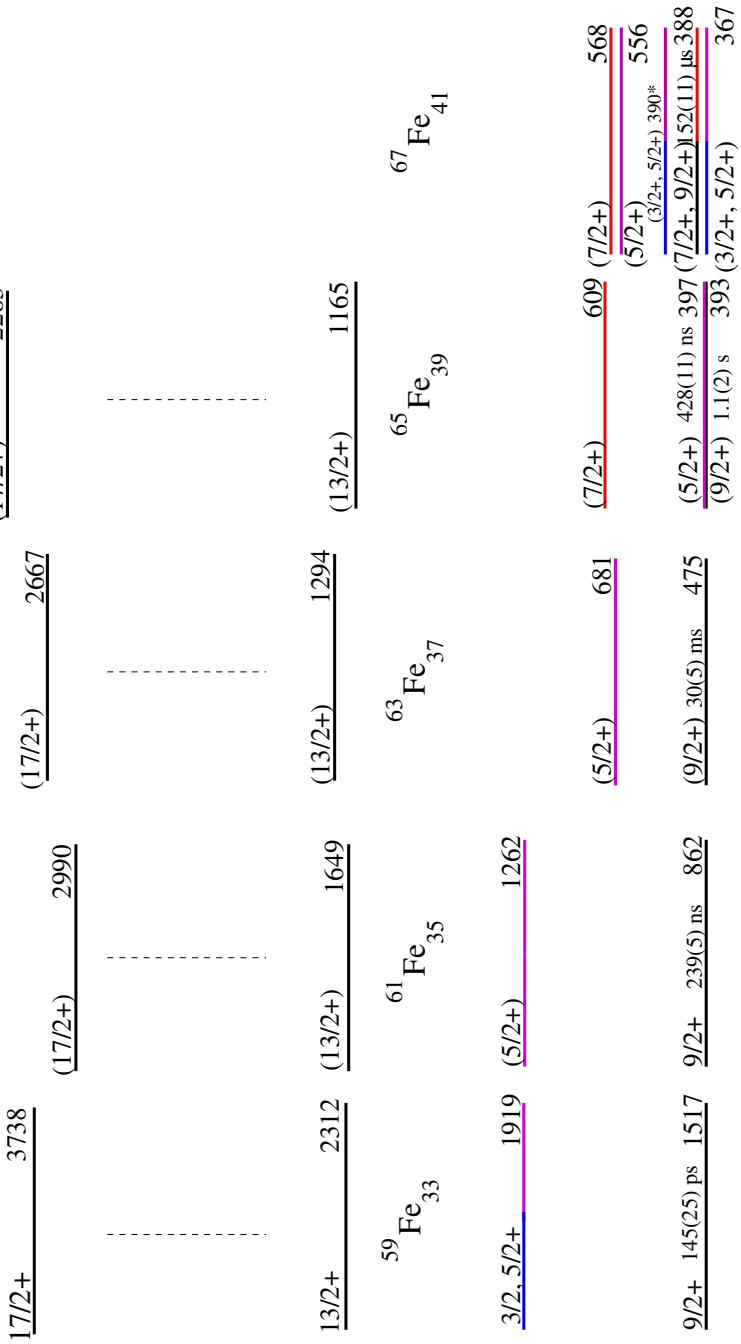

Figure 8.4: Systematics of the positive parity excited levels in the odd-A $^{59-67}$Fe$_{33-41}$ isotopes. States are drawn with respect to the lowest-lying (tentative) positive-parity state and the J^π is multiplied by 2. The data for $I > 9/2$; $N = 33$ and $T_{1/2}$(862, 393 keV) is taken from [Dea07, Lun07] and [NND13b], respectively. *The prompt 389.8-keV level is consistent with a positive parity assignment and its spin depend on its half-life – see Section 7.3 in the previous chapter for more details.

At $N = 41$, from a simple shell-model perspective, the expected configuration for the ground state of ^{67}Fe is $9/2^+$. It is so, since the two holes in the $f_{7/2}$ proton orbital couple to spin zero and the 41^{st} neutron particle would then reside in the $\nu g_{9/2}$ orbital. In the odd-A ^{69}Ni, the spin and parity of the ground state is the expected $9/2^+$ [NND13b] (see Fig 8.3). Note here, that in the latter isotope the first excited state is only 321 keV above the ground state and has a tentative $(1/2^-)$ assignment [NND13b]. The different parity of this excited state can again be interpreted as due to the energy gain in pairing when the occupation of the $\nu g_{9/2}$ orbital increases. Thus, it is energetically more favorable to excite a pair of neutrons in that orbital.

For ^{67}Fe, the experimental information on the decay pattern of that isotopes, towards the tentative, low-spin excited states in ^{67}Co allows us to conclude, that the parity of its ground state is most likely negative, associated with a neutron hole in the pf shell. The negative-parity assignment is also based on the determined low $\log ft$ values for direct beta-decay towards low-spin excited states in the daughter nucleus – ^{67}Co.

As stated before, recently it has been suggested that the ground states of ^{66,68}Fe isotopes, in the vicinity of $N = 40$, have a triaxial shape [Dau11] with a considerable quadrupole deformation. In that sense, it is interesting to compare the tentatively assigned positive-parity states in ^{67}Fe (in between ^{66}Fe and ^{68}Fe), to a theoretical model proposed in [MTV75]. It was developed to describe odd-mass transitional nuclei in the $A = 135$ and $A = 190$ mass region. It is based on an odd nucleon coupled to a triaxial rotating core.

The calculated single-particle energies can be applied to unique-parity spectra, based on particle or hole states in a $j = 11/2$ orbital, but should also hold for $j = 9/2$ [MTV75], as is the case of iron.

Of particular interest is Fig 8.5, depicting the energy spectrum based on an odd nucleon in the $j = 11/2$ orbit. If one imagines a vertical line at the triaxiality parameter (γ) of around 20° and substitutes j with j - 1, one can observe a remarkable similarity of the calculated level structure to the one observed for the positive-parity levels in ^{67}Fe. If the lowest-lying positive-parity state is the $9/2^+$, the model predicts a $5/2^+$ and a $7/2^+$ states very close in energy at γ of around 20°. The latter two states could then be the identified as the 556 and the 568 keV excited levels (Fig 8.4), while the former would be the 388.5-keV state.

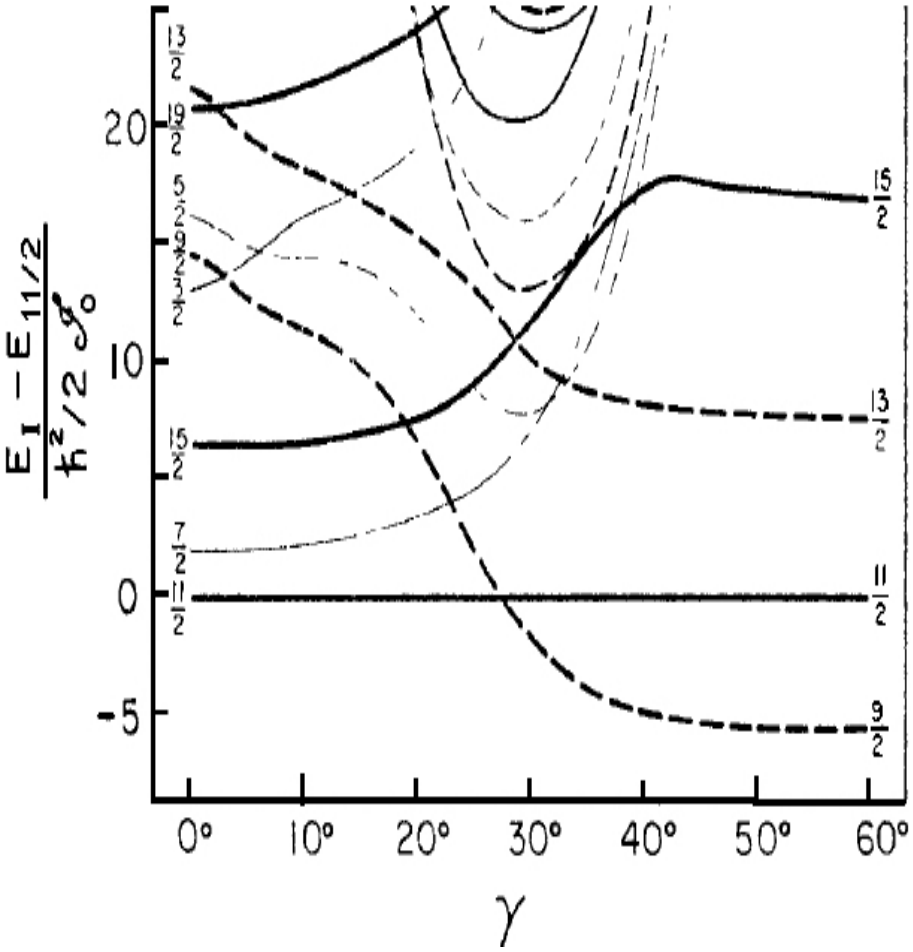

Figure 8.5: Odd-A energy spectrum as a function of triaxiality parameter (γ) for $\beta A^{2/3} = 7$, and $j = 11/2$. Thick/thin full lines indicate j +/- 2 and j +/- 4 states, while thick/thin dashed lines – j +/- 1 and j +/- 3 levels. The figure is adapted from [MTV75].
Note, that j, j +/- 2, j +/- 4, etc. band sequence, indicating a strongly decoupled structure is found at the prolate ($\gamma < 30°$) side of the energy spectrum, while a coupled band sequence of j, j +/- 1, j +/- 2, etc. is found on the oblate side ($\gamma > 30°$).

Chapter 9

Conclusion and outlook

The subject of this thesis is the study of the β-decay of the neutron-rich odd-A manganese isotopes (A = 61, 63, 65 and 67), in the region around $N = 40$. The experimental study took place at ISOLDE (CERN), where pure beams of the corresponding manganese isotopes were produced using resonance laser ionization. From previous experiments and recent theoretical developments it has been suggested that while the properties of ^{68}Ni ($Z = 28$, $N = 40$) are consistent with a spherical nucleus, a swift onset of collectivity is observed for the even-even iron ($Z = 26$) and chromium ($Z = 24$) isotopes around $N = 40$.

A description of the experimental technique and the methods of analysis has been presented. Due to the production of almost 100% pure manganese source it has been possible to follow the intensities of γ- and β-rays in the decay chains of the investigated isotopes in order to judge the completeness of the constructed decay schemes, with respect to missed γ intensity or direct β-decay feeding towards the respective ground states.

This decay study has revealed extensive and detailed new experimental information for the odd-A iron isotopic chain. The previously known experimental information is presented in the beginning of each of the results chapters, in order to reference the extensive contribution and easily acknowledge the new values and findings. The data presented here can serve as a benchmark for testing theoretical models and develop proper nucleon-nucleon interactions in this mass region of the nuclear chart. It can also be used to improve on the model interactions that are currently widely used.

Following the feeding patterns and taking into account the calculated logft values, made it possible to assign tentative and firm spins and parities in

numerous cases and to narrow down ranges of spins existing in the literature. For the first time, in ^{63}Fe, an isomeric state has been observed and its half-life determined, completing the systematics of the experimental energies of the $(9/2^+)$ excited states in the neutron-rich $^{61-67}$Fe isotopes. Noteworthy to mention is also the precise determination of the excitation energy of the $(9/2^+)$, 1.1(2) s, isomeric state in ^{65}Fe, as well as the precise excitation energy of the isomeric state in ^{67}Fe.

The experimental information on the low-spin excited states in the odd-A iron and cobalt decay chains has also been also greatly improved, with the addition of new excited states, γ-transitions and detailed feeding and de-excitation patterns. In many cases tentative spin and parities could be assigned or ranges of existing in the literature spins be narrowed down. In the case of the decay of the two isomers in ^{65}Fe a linking transition, connecting the two decay schemes constructed before, has been found.

It will be most interesting to compare our findings to large-scale shell-model calculations using different interactions. So far such calculations are not available for the isotopes of interest with $Z = 26$ and $A \geq 61$.

Due to the nature of experimental set-up, some important low-energy transitions in the decay of manganese remained unobserved or hampered by the limitations in the experimental energy thresholds. With the future development of improved radioactive beams in terms of purity and intensity, an experimental campaign using a dedicated electron- or low-energy gamma-detection set-up coupled to fast-timing measurements set-up would be very beneficial. First steps along this direction are currently implemented with the ISOLDE Decay Station project (IDS [Col13]). The complementary set-up is necessary in order to detect and confirm the 24-keV transition in ^{63}Fe ($T_{1/2} = 30(5)$ ms), the 34-keV line in ^{65}Fe ($T_{1/2} = 428(11)$ ns) with a better gamma-efficiency and the low-energy transition(s), de-exciting the isomeric state in ^{67}Fe ($T_{1/2} = 152(11)$ μs). The coupled fast-timing part of the set-up could be used to resolve the half-lives of the low-lying excited states in the latter isotope in order to try to firmly assign their spins and parities.

Appendix A

Appendix

Following are spectra, which were used in the analyses of the data for the different decay chains.

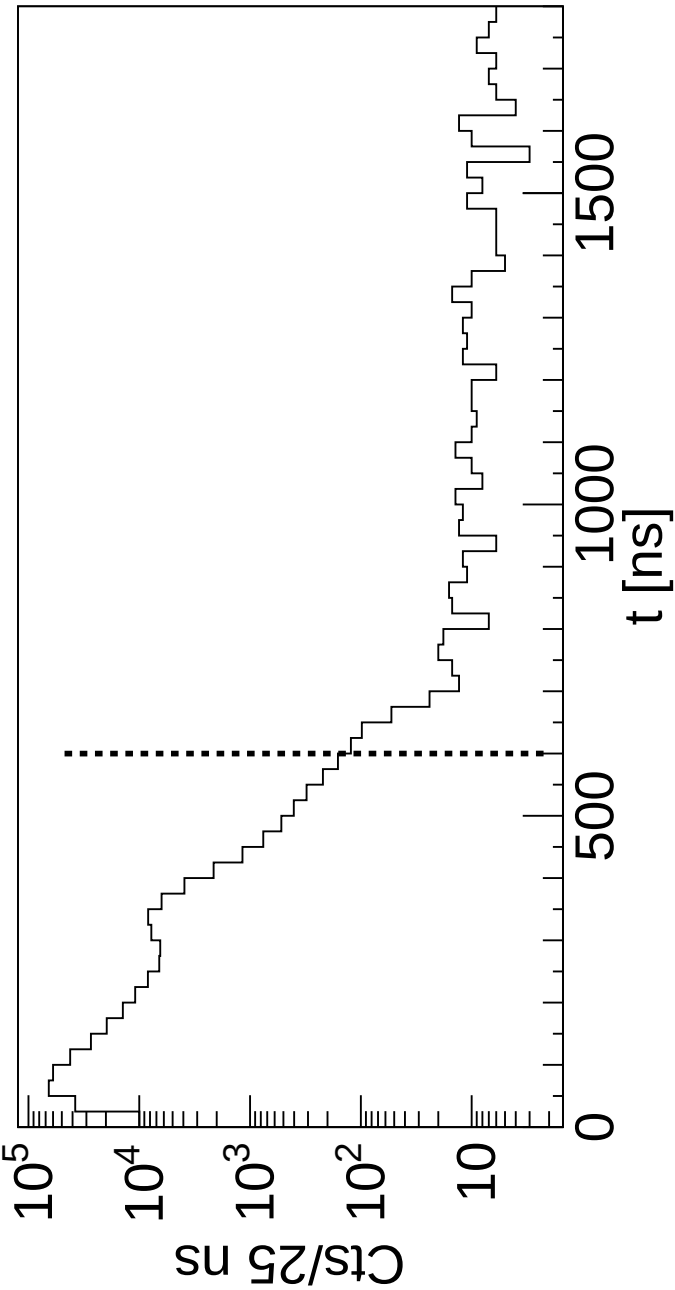

Figure A.1: Time difference between a beta and a gamma event. The used, in the analysis, prompt time window is from 0 – 600 ns, indicated with a dashed vertical line.

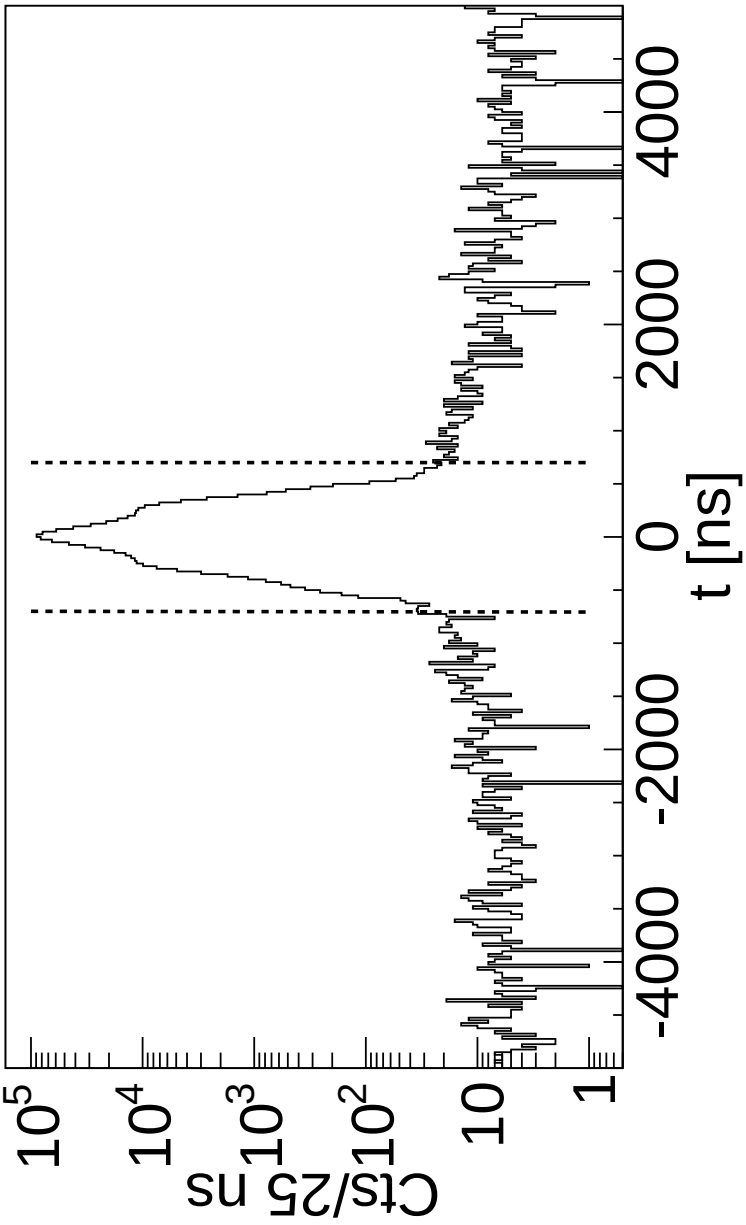

Figure A.2: Time difference between two gamma events. The used, in the analysis, prompt time window is ± 700 ns, indicated with dashed vertical lines.

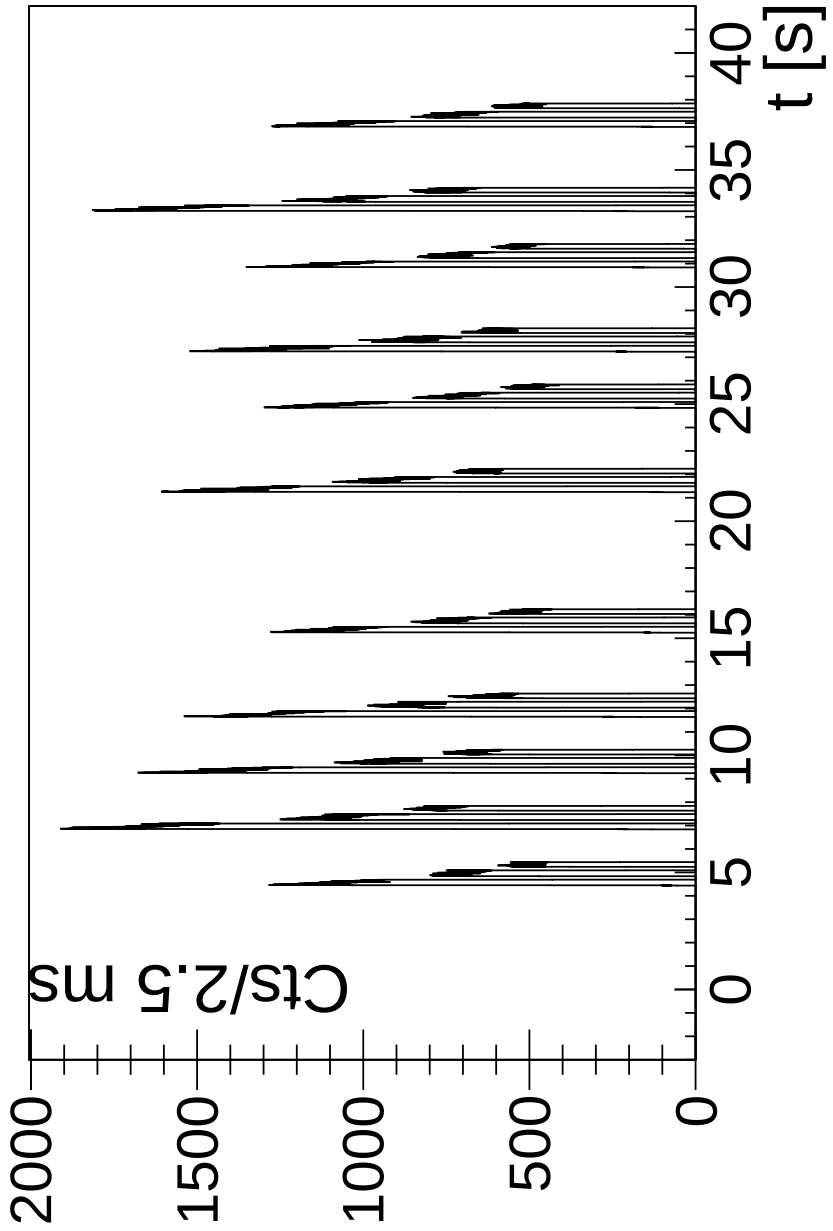

Figure A.3: Time difference between a beta event and the PP signal in $A = \mathbf{61}$ **decay chain**.

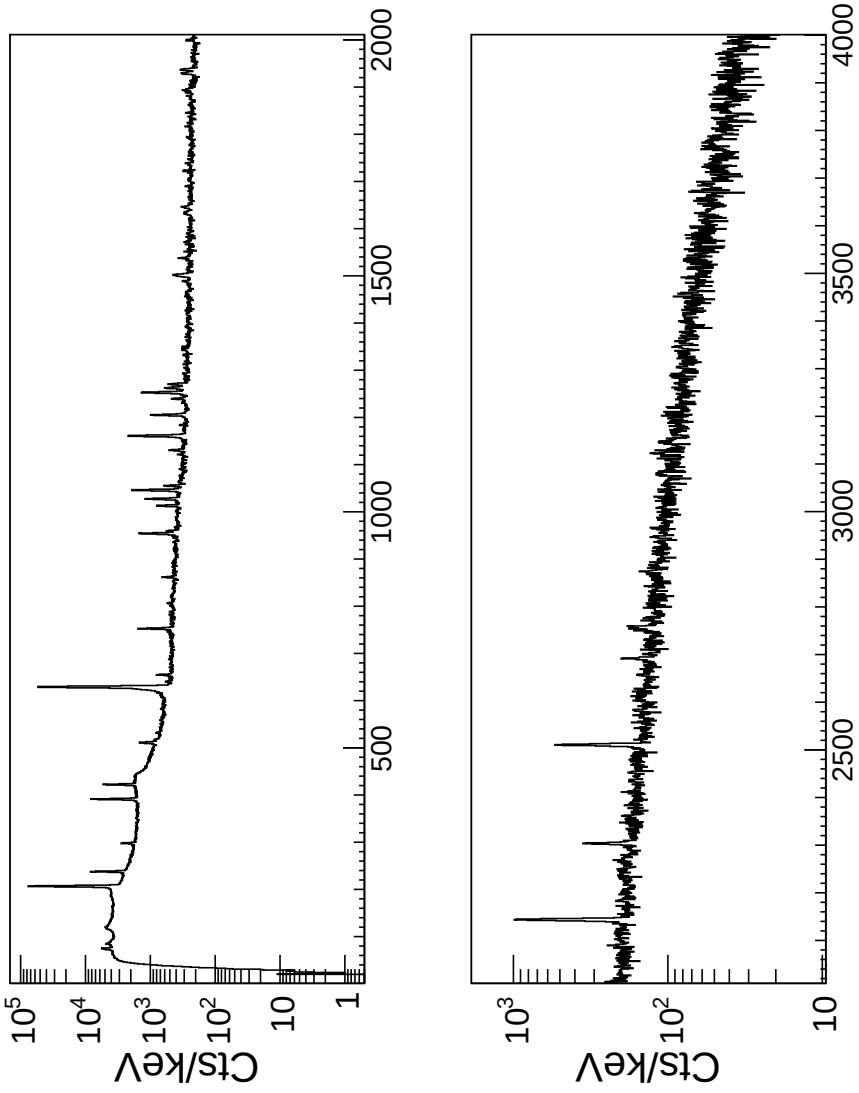

Figure A.4: Singles' spectrum in the $A = \mathbf{61}$ **decay chain**.

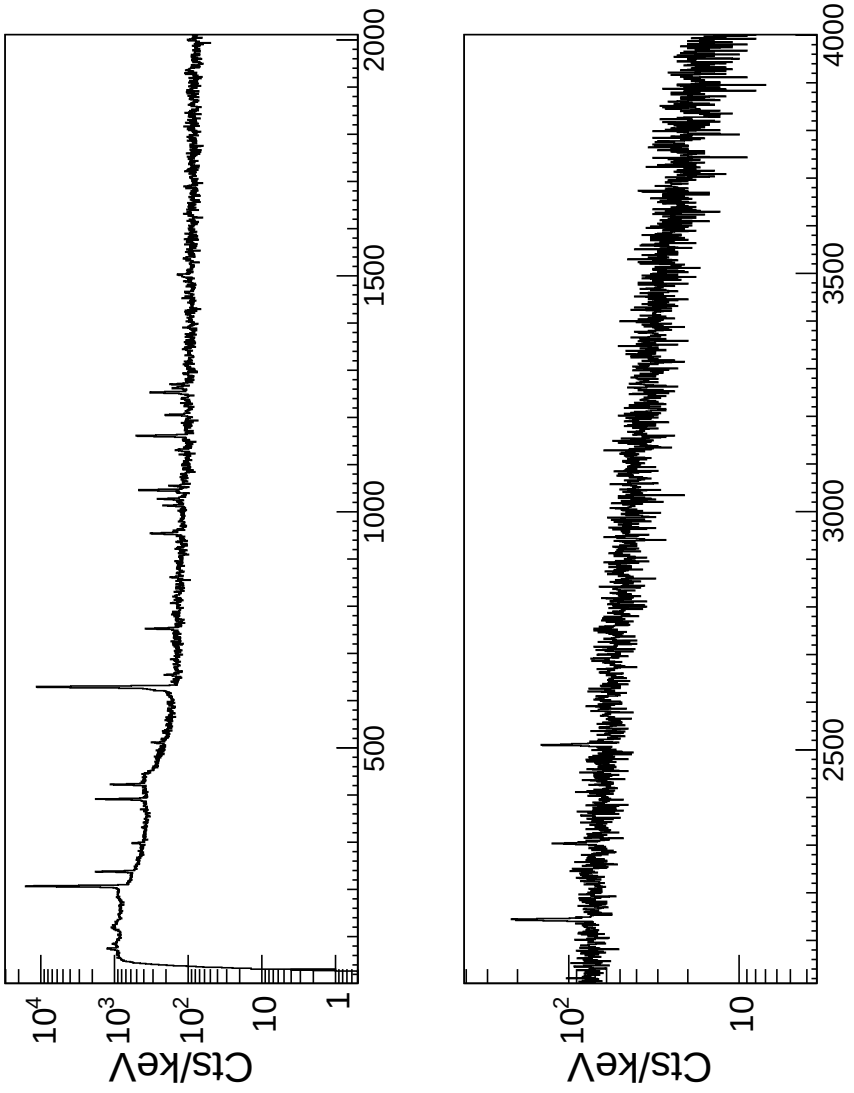

Figure A.5: Beta-gated prompt spectrum in the $A = \mathbf{61}$ **decay chain**.

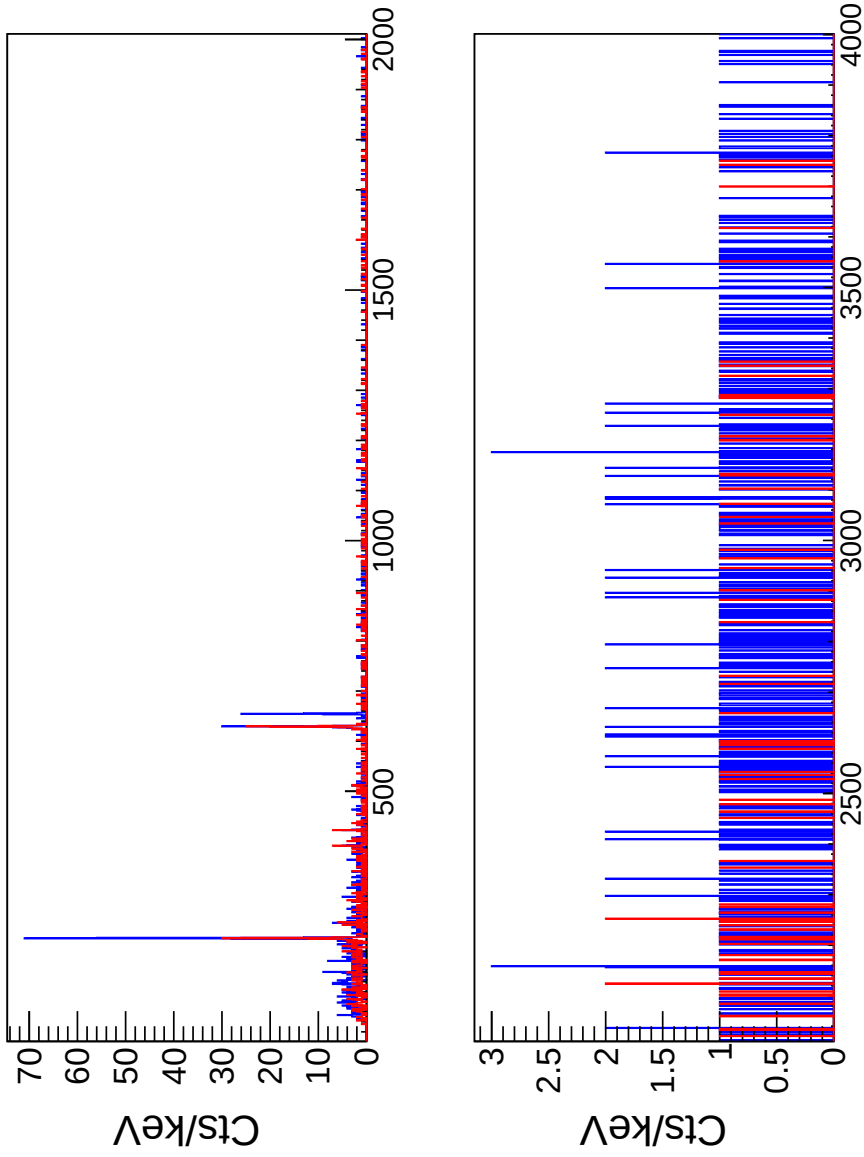

Figure A.6: Beta-gated delayed (600 – 1320 ns) gamma spectrum, compared to the a spectrum in the randoms (10.00 – 11.32 μs) time interval in the $A = \mathbf{61}$ **data set**.

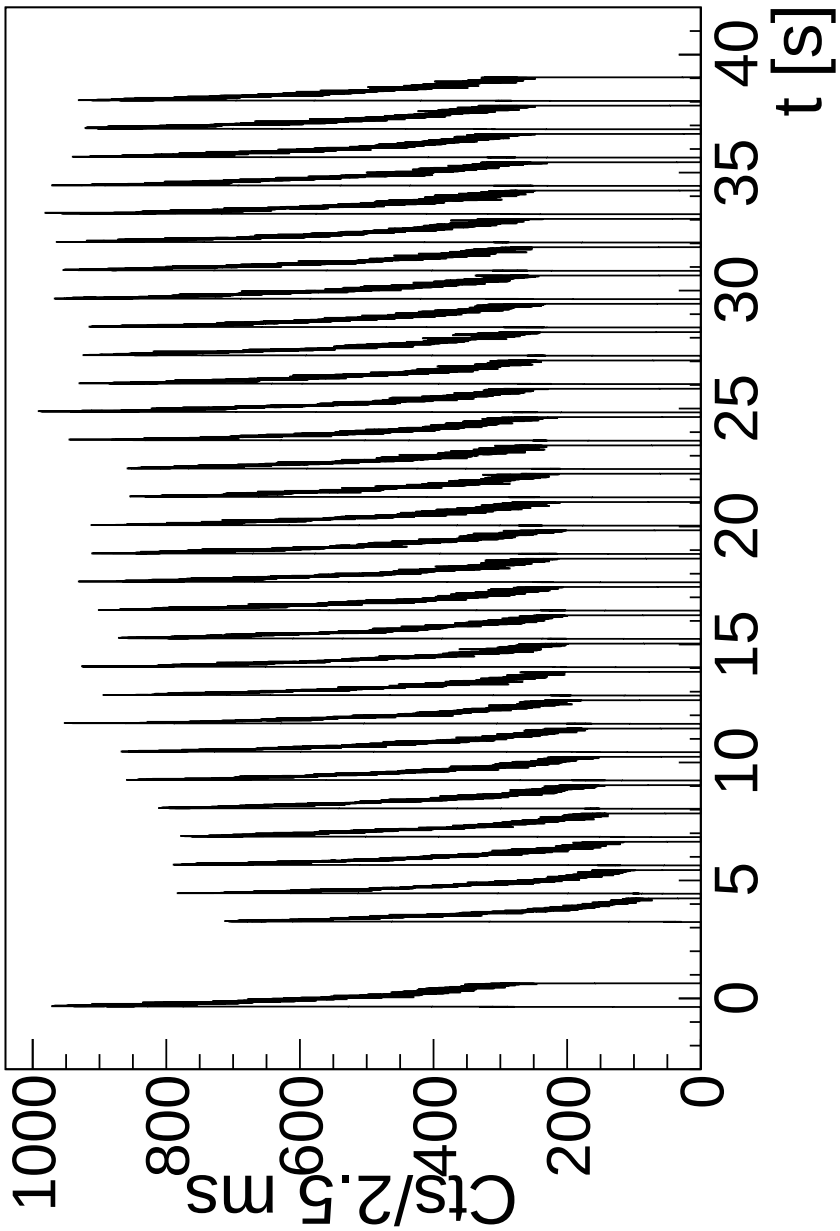

Figure A.7: Time difference between a beta event and the PP signal in $A = 63$ **decay chain**.

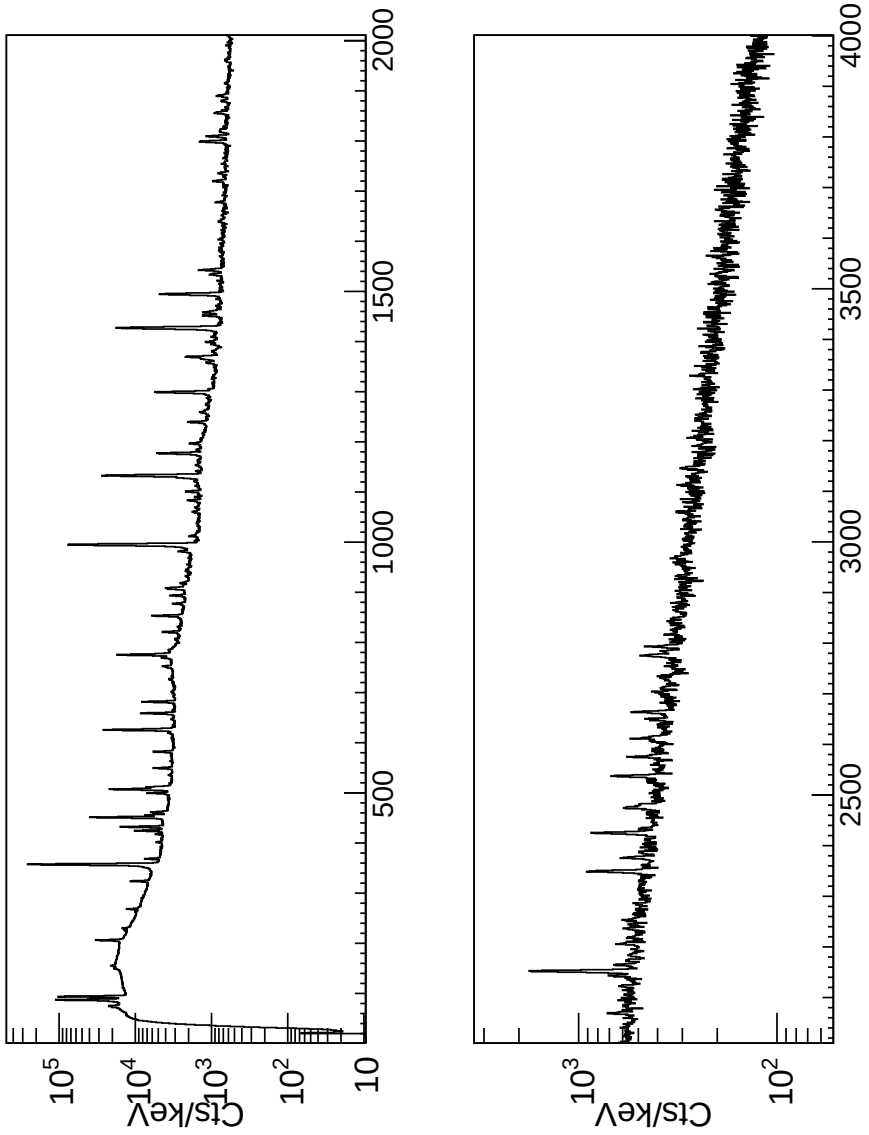

Figure A.8: Singles' spectrum in the $A = \mathbf{63}$ **decay chain**.

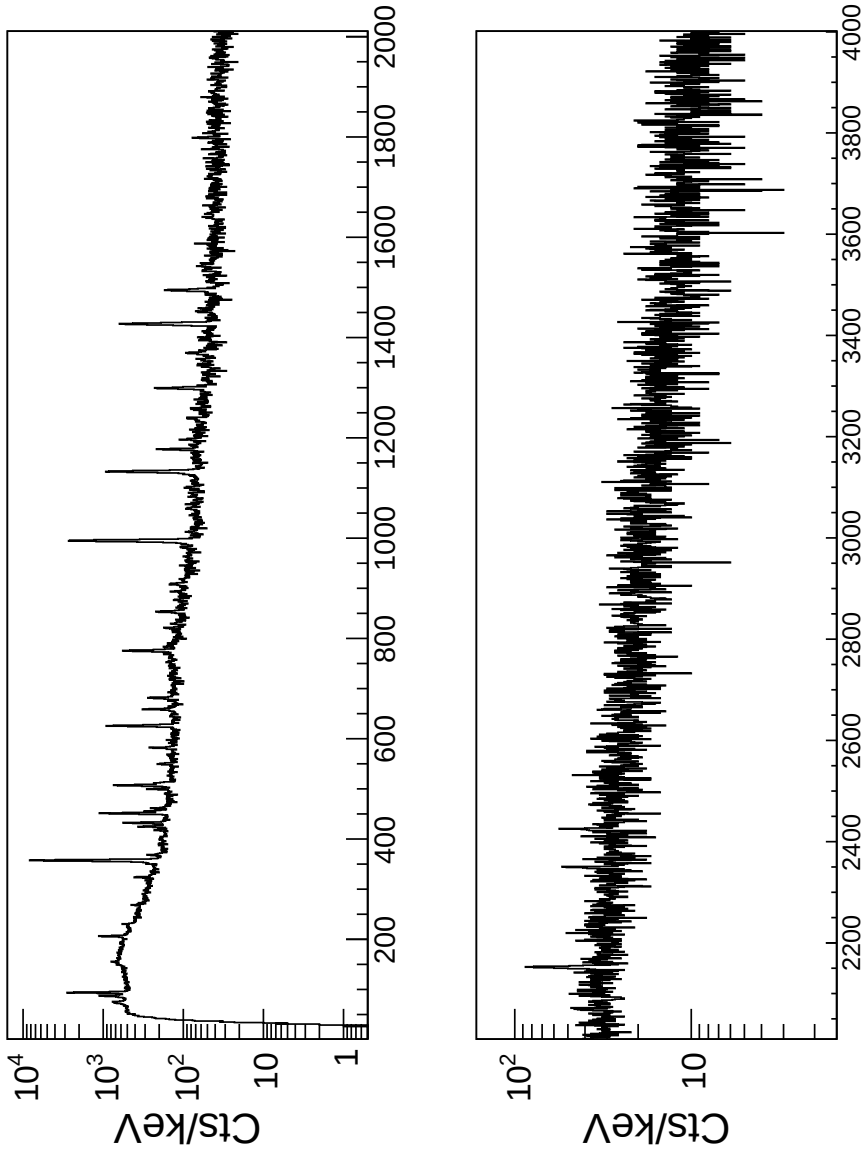

Figure A.9: Beta-gated prompt spectrum in the $A = \mathbf{63}$ **decay chain**.

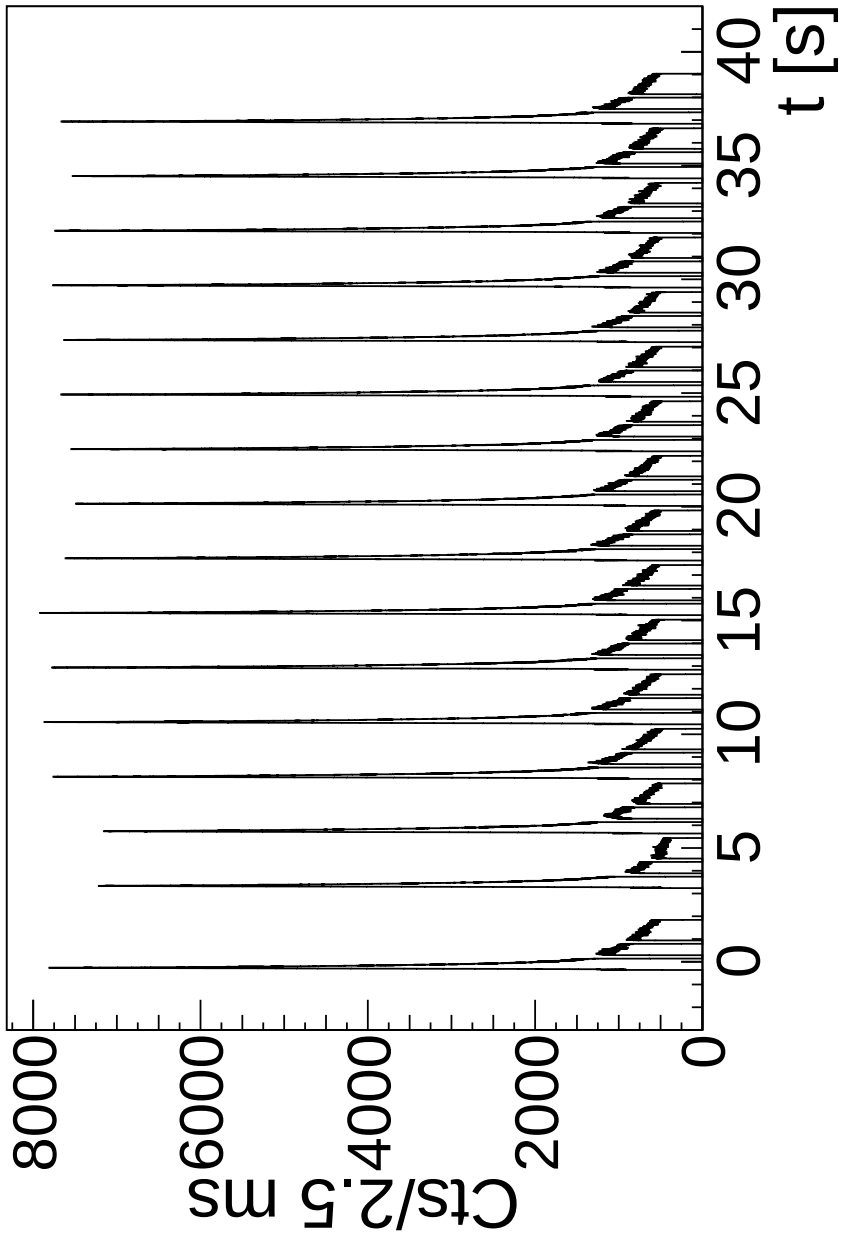

Figure A.10: Time difference between a beta event and the PP signal in $A =$ **65 decay chain**.

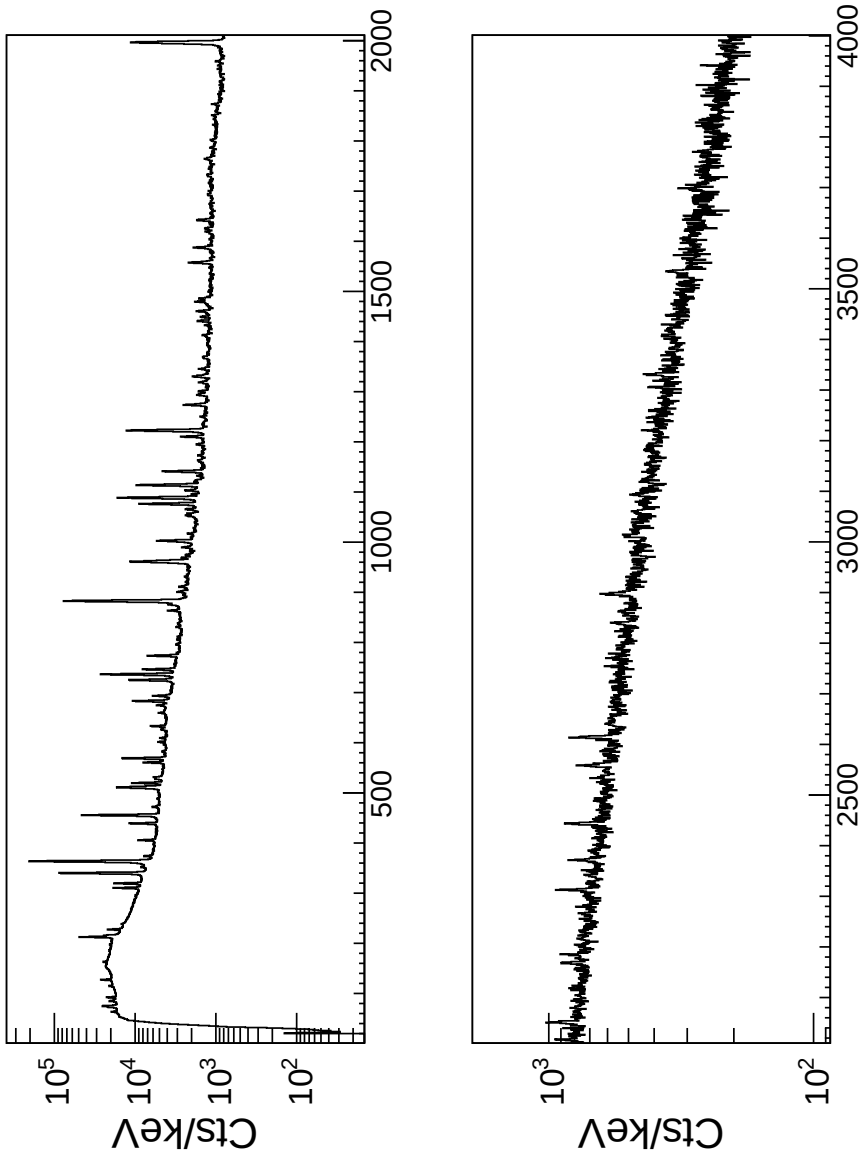

Figure A.11: Singles' spectrum in the $A = \mathbf{65}$ **decay chain**.

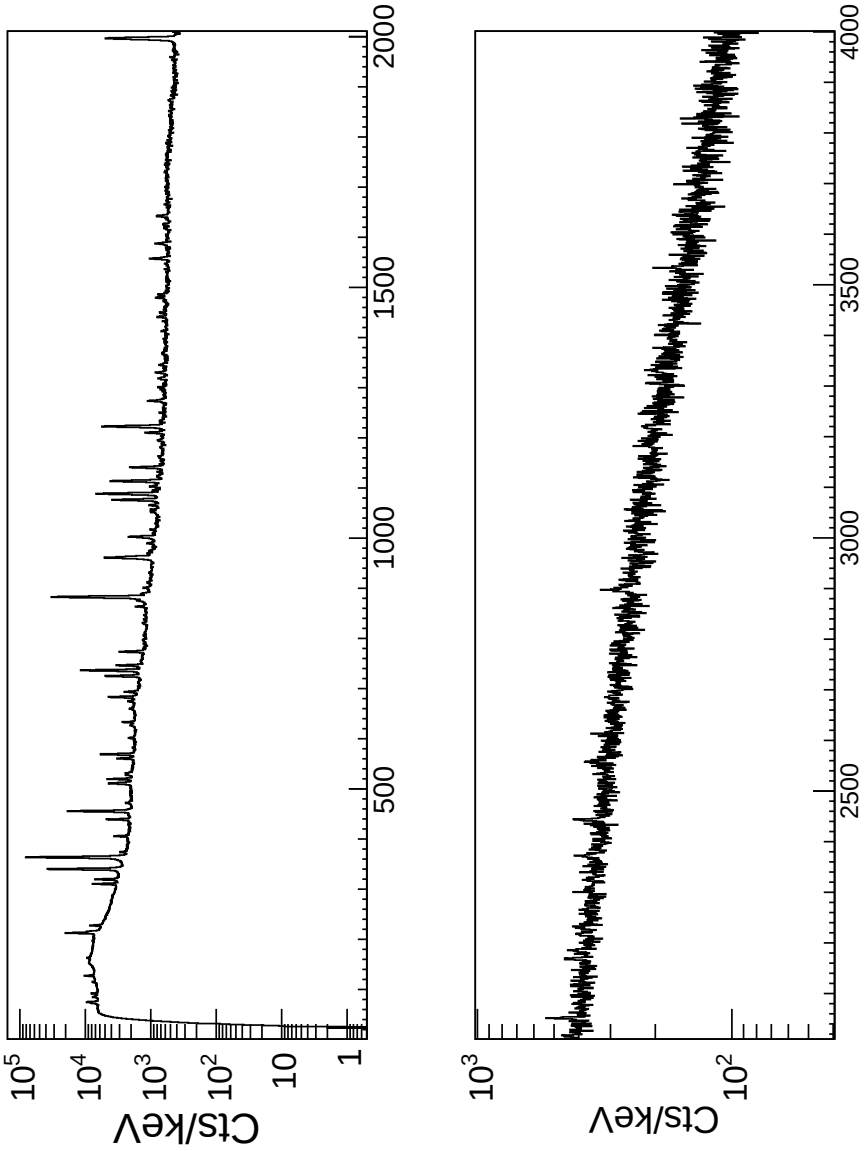

Figure A.12: Beta-gated prompt spectrum in the $A = \mathbf{65}$ **decay chain**.

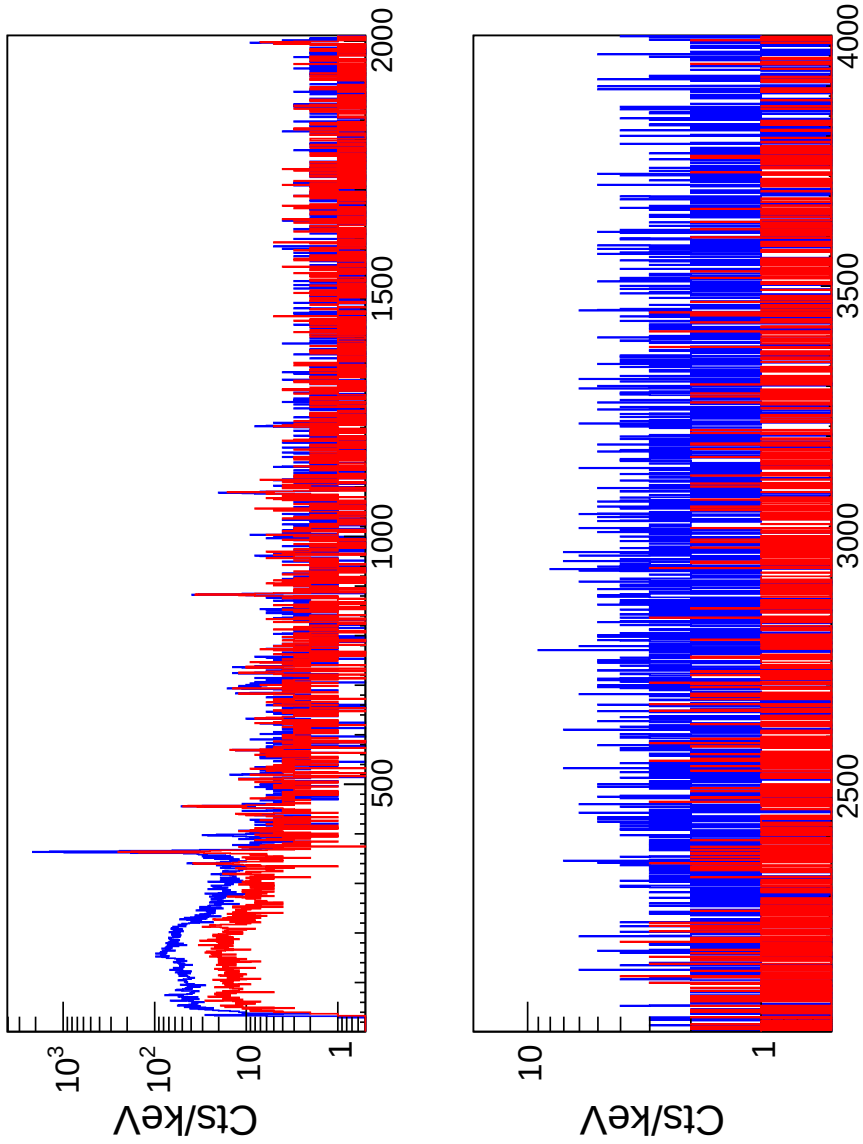

Figure A.13: Beta-gated delayed (600 – 1875 ns) gamma spectrum, compared to the a spectrum in the randoms (3000 – 4275 ns) time interval in the $A = \mathbf{65}$ **data set**.

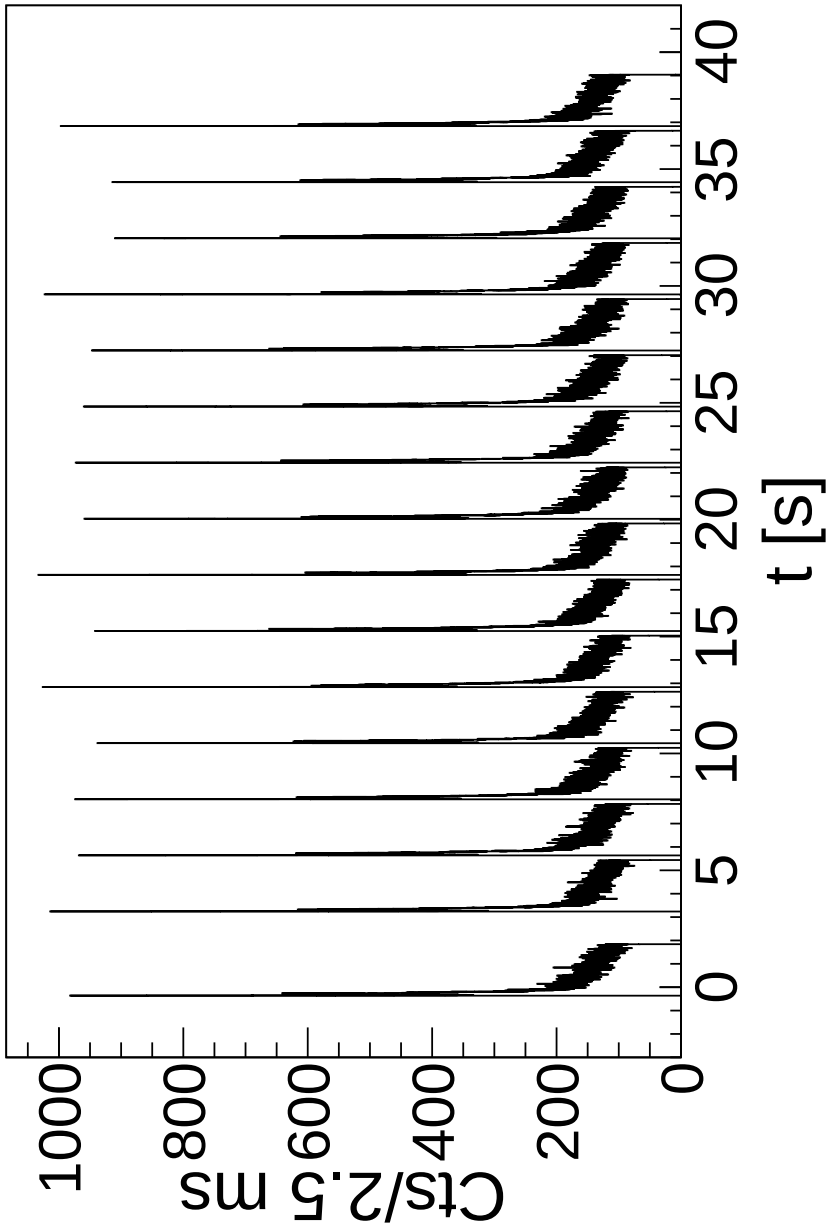

Figure A.14: Time difference between a beta event and the PP signal in $A =$ **67 decay chain**.

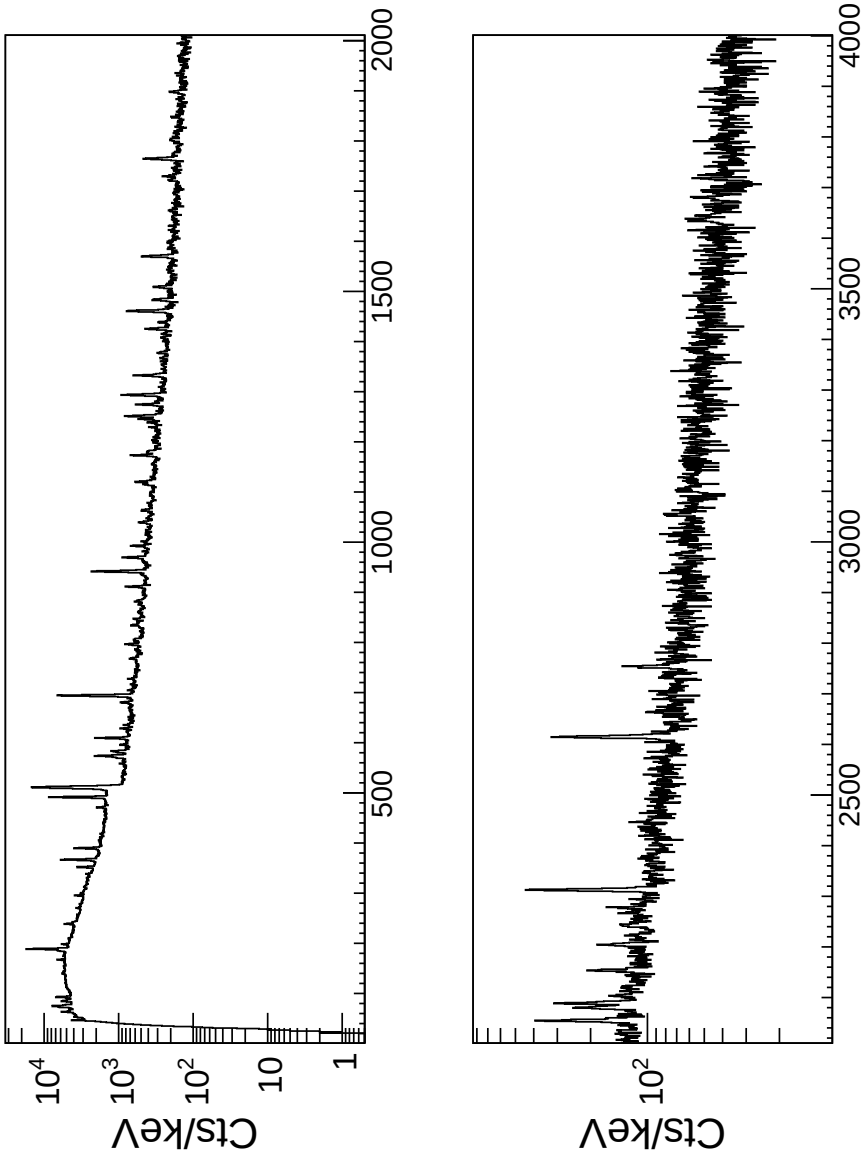

Figure A.15: Singles' spectrum in the $A = \mathbf{67}$ **decay chain**.

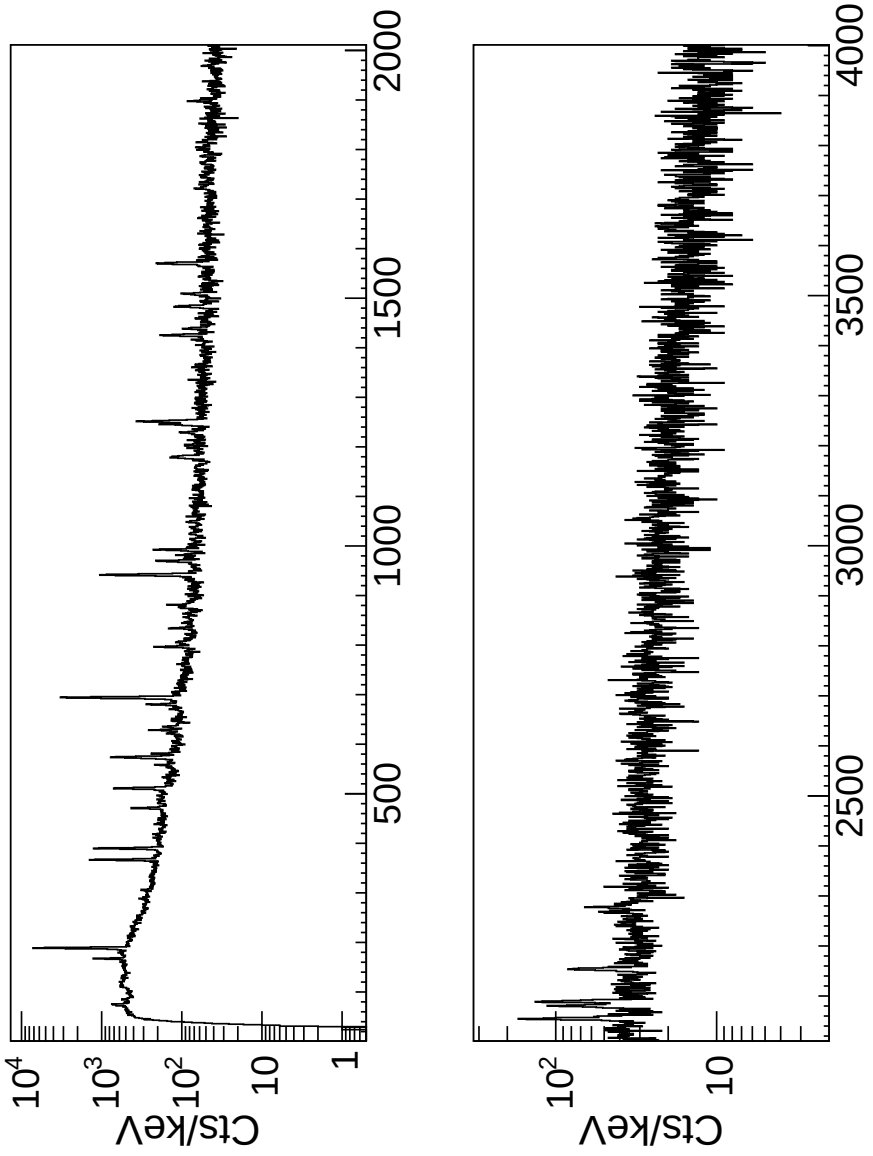

Figure A.16: Beta-gated prompt spectrum in the $A = \mathbf{67}$ **decay chain**.

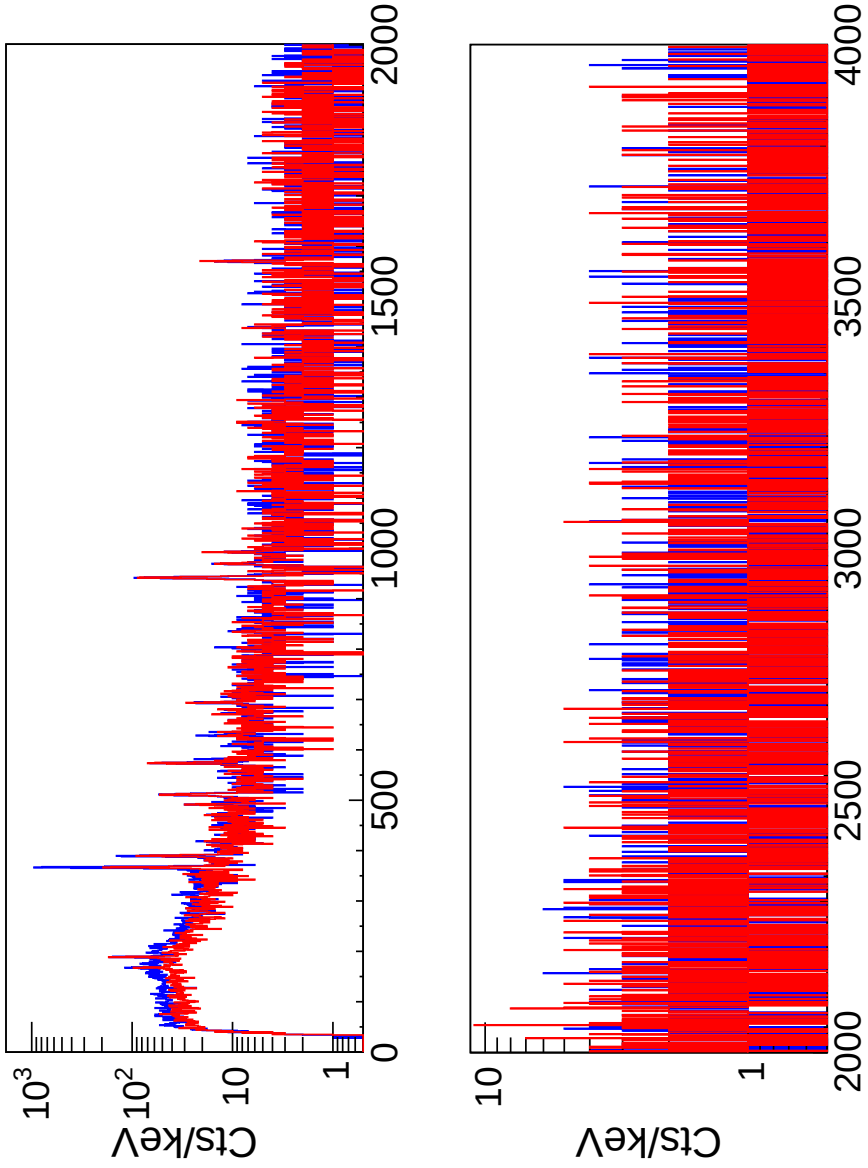

Figure A.17: Beta-gated delayed (1 – 451 μs) gamma spectrum, compared to the a spectrum in the randoms (1000 – 1450 μs) time interval in the $A = \mathbf{67}$ **data set**, within $9\times^{67}Mn T_{1/2}$.

Bibliography

[Anf70] T. R. Anfinsen, K. Bjorndal, A. Graue, J. R. Lien, G. E. Sandvik, L. O. Tveita, K. Ytterstad, and E. R. Cosman. Nuclear reaction studies in the nickel isotopes: The ^{62}Ni(d, p)^{63}Ni and ^{64}Ni(d, p)^{65}Ni reactions. *Nuclear Physics A*, 157 (1970) 561 – 576.

[Arn71] S. E. Arnell, R. Hardell, A. Hasselgren, C. G. Mattsson, and O. Skeppstedt. Thermal Neutron Capture in ^{50}Ti and ^{64}Ni. *Phys.Scr.*, 4 (1971) 89.

[Ber82] M. Bernas, Ph. Dessagne, M. Langevin, J. Payet, F. Pougheon, and P. Roussel. Magic features of ^{68}Ni. *Physics Letters B*, 113 (1982) 279 – 282.

[Bha99] M. R. Bhat. Nuclear Data Sheets for $A = 61$. *Nuclear Data Sheets*, 88 (1999) 417 – 532.

[Bla66] A. G. Blair and D. D. Armstrong. (t,^{4}He) Reaction on the Even Ni Isotopes. *Phys. Rev.*, 151 (1966) 930–939.

[Blo08] M. Block, C. Bachelet, G. Bollen, M. Facina, C. M. Folden, C. Guénaut, A. A. Kwiatkowski, D. J. Morrissey, G. K. Pang, A. Prinke, R. Ringle, J. Savory, P. Schury, and S. Schwarz. Discovery of a Nuclear Isomer in ^{65}Fe with PenningTrap Mass Spectrometry. *Phys. Rev. Lett.*, 100 (2008) 132501.

[Bos85] U. Bosch, W. D. Schmidt-Ott, P. Tidemand-Petersson, E. Runte, W. Hillebrandt, M. Lechle, F. K. Thielemann, R. Kirchner, O. Klepper, E. Roeckl, K. Rykaczewski, D. Schardt, N. Kaffrell, M. Bernas, Ph. Dessagne, and W. Kurcewicz. Beta-decay half-lives of new neutron-rich chromium-to-nickel isotopes and their consequences for the astrophysical r-process. *Physics Letters B*, 164 (1985) 22 – 26.

[Bos88] U. Bosch, W. D. Schmidt-Ott, E. Runte, P. Tidemand-Petersson, P. Koschel, F. Meissner, R. Kirchner, O. Klepper, E. Roeckl, K. Rykaczewski, and D. Schardt. Beta- and gamma-decay studies of neutron-rich chromium, manganese, cobalt and nickel isotopes including the new isotopes ^{60}Cr and ^{60g}Mn. *Nuclear Physics A*, 477 (1988) 89 – 104.

[BrI13] BrIcc. *Conversion coefficient calculator*, 2013.

[Bro75] J. Bron, H. W. Jongsma, and H. Verheul. Decay of ^{61}Fe to levels in ^{61}Co. *Phys. Rev. C*, 11 (1975) 966–973.

[Bro95] R. Broda, B. Fornal, W. Królas, T. Pawlat, D. Bazzacco, S. Lunardi, C. Rossi-Alvarez, R. Menegazzo, G. de Angelis, P. Bednarczyk, J. Rico, D. De Acuña, P. J. Daly, R. H. Mayer, M. Sferrazza, H. Grawe, K. H. Maier, and R. Schubart. $N = 40$ Neutron Subshell Closure in the ^{68}Ni Nucleus. *Phys. Rev. Lett.*, 74 (1995) 868–871.

[Bro98] R. Broda et al. Proceedings of the International Conference on Fission and Properties of Neutron-Rich Nuclei, Sanibel Island, 1997. *Proceedings of the International Conference on Fission and Properties of Neutron-Rich Nuclei, Sanibel Island, 1997*, 1998.

[Bro10] E. Browne and J.K. Tuli. Nuclear Data Sheets for $A = 65$. *Nuclear Data Sheets*, 111 (2010) 2425 – 2553.

[Bru97] Rene Brun and Fons Rademakers. ROOT - An Object Oriented Data Analysis Framework. *Nucl. Inst. and Meth. in Phys. Res. A*, 389 (1997) 81–86.

[Car13] M. P. Carpenter, R. V. F. Janssens, and S. Zhu. Shape coexistence in neutron-rich nuclei near $N = 40$. *Phys. Rev. C*, 87 (2013) 041305.

[Cas90] R. F. Casten. *Nuclear Structure from a Simple Perspective*. Oxford University Press, 1990.

[Cau99] Etienne Caurier and Frederic Nowacki. Present Status of Shell Model Techniques. *Acta Physica Plonica B*, 30 (1999) 705.

[Cau02] E. Caurier, F. Nowacki, and A. Poves. Large-scale shell model calculations for exotic nuclei. *The European Physical Journal A - Hadrons and Nuclei*, 15 (2002) 145–150.

[Cha10] F. C. Charlwood. *Ground state properties of Mn and Mo using laser spectroscopic methods*. PhD thesis, University of Manchester, 2010.

[Chi12] C. J. Chiara, R. Broda, W. B. Walters, R. V. F. Janssens, M. Albers, M. Alcorta, P. F. Bertone, M. P. Carpenter, C. R. Hoffman, T. Lauritsen, A. M. Rogers, D. Seweryniak, S. Zhu, F. G. Kondev, B. Fornal, W. Królas, J. Wrzesiński, N. Larson, S. N. Liddick, C. Prokop, S. Suchyta, H. M. David, and D. T. Doherty. Low-spin states and the non-observation of a proposed 2202-keV, 0^+ isomer in ^{68}Ni. *Phys. Rev. C*, 86 (2012) 041304.

[Col13] ISOLDE Decay Station Collaboration. *IDS*, 2013.

[Com71] J. R. Comfort, P. Wasielewski, F. B. Malik, and W. Scholz. Properties of ^{55}Mn, ^{56}Mn and ^{57}Fe in the unified rotational model. *Nuclear Physics A*, 160 (1971) 385 – 408.

[Cos77] J. D. Cossairt, R. E. Tribble, and R. A. Kenefick. Masses of ^{61}Fe and ^{62}Fe. *Phys. Rev. C*, 15 (1977) 1685–1689.

[Cra13] H. L. Crawford, R. M. Clark, P. Fallon, A. O. Macchiavelli, T. Baugher, D. Bazin, C. W. Beausang, J. S. Berryman, D. L. Bleuel, C. M. Campbell, M. Cromaz, G. de Angelis, A. Gade, R. O. Hughes, I. Y. Lee, S. M. Lenzi, F. Nowacki, S. Paschalis, M. Petri, A. Poves, A. Ratkiewicz, T. J. Ross, E. Sahin, D. Weisshaar, K. Wimmer, and R. Winkler. Quadrupole Collectivity in Neutron-Rich Fe and Cr Isotopes. *Phys. Rev. Lett.*, 110 (2013) 242701.

[Cza94] S. Czajkowski, M. Bernas, P. Armbruster, H. Geissel, C. Kozhuharov, G. Münzenberg, D. Vieira, Ph. Dessagne, Ch. Miehe, E. Hanelt, G. Audi, and J. K. P. Lee. Separation and implantation of relativistic ^{86}Kr-fragments at the FrS; half-life measurement by ion-β time-correlations. *Zeitschrift für Physik A Hadrons and Nuclei*, 348 (1994) 267–272.

[Dae68] W. W. Daehnick and Y. S. Park. Spectroscopy of Odd-Odd Nuclei with Direct (d,α) Reactions. *Phys. Rev. Lett.*, 20 (1968) 110–113.

[Dau06] J. M. Daugas, M. Sawicka, M. Pfützner, I. Matea, H. Grawe, R. Grzywacz, N. L. Achouri, J. C. Angélique, D. Baiborodin, F. Becker, et al. Isomeric island in the vicinity of ^{66}Fe. *AIP Conference Proceedings*, 831 (2006) 427 – 429.

[Dau11] J. M. Daugas, I. Matea, J.-P. Delaroche, M. Pfützner, M. Sawicka, F. Becker, G. Bélier, C. R. Bingham, R. Borcea, E. Bouchez, A. Buta, E. Dragulescu, G. Georgiev, J. Giovinazzo, M. Girod, H. Grawe, R. Grzywacz, F. Hammache, F. Ibrahim, M. Lewitowicz, J. Libert, P. Mayet, V. Méot, F. Negoita, F. de Oliveira Santos, O. Perru,

O. Roig, K. Rykaczewski, M. G. Saint-Laurent, J. E. Sauvestre, O. Sorlin, M. Stanoiu, I. Stefan, Ch. Stodel, Ch. Theisen, D. Verney, and J. Żylicz. β-decay measurements for $N > 40$ Mn nuclei and inference of collectivity for neutron-rich Fe isotopes. *Phys. Rev. C*, 83 (2011) 054312.

[Dea07] A. N. Deacon, S. J. Freeman, R. V. F. Janssens, M. Honma, M. P. Carpenter, P. Chowdhury, T. Lauritsen, C. J. Lister, D. Seweryniak, J. F. Smith, S. L. Tabor, B. J. Varley, F. R. Xu, and S. Zhu. Yrast structures in the neutron-rich isotopes ^{59,60}Fe and the role of the $g_{9/2}$ orbital. *Phys. Rev. C*, 76 (2007) 054303.

[Del10] J. P. Delaroche, M. Girod, J. Libert, H. Goutte, S. Hilaire, S. Péru, N. Pillet, and G. F. Bertsch. Structure of even-even nuclei using a mapped collective Hamiltonian and the D1S Gogny interaction. *Phys. Rev. C*, 81 (2010) 014303.

[Dij11] A. Dijon, E. Clément, G. de France, P. Van Isacker, J. Ljungvall, A. Görgen, A. Obertelli, W. Korten, A. Dewald, A. Gadea, L. Gaudefroy, M. Hackstein, D. Mengoni, Th. Pissulla, F. Recchia, M. Rejmund, W. Rother, E. Sahin, C. Schmitt, A. Shrivastava, J. J. Valiente-Dobón, K. O. Zell, and M. Zielińska. Lifetime measurements in ^{63}Co and ^{65}Co. *Phys. Rev. C*, 83 (2011) 064321.

[Dij12a] A. Dijon, E. Clément, G. de France, G. de Angelis, G. Duchêne, J. Dudouet, S. Franchoo, A. Gadea, A. Gottardo, T. Hüyük, B. Jacquot, A. Kusoglu, D. Lebhertz, G. Lehaut, M. Martini, D. R. Napoli, F. Nowacki, S. Péru, A. Poves, F. Recchia, N. Redon, E. Sahin, C. Schmitt, M. Sferrazza, K. Sieja, O. Stezowski, J. J. Valiente-Dobón, A. Vancraeyenest, and Y. Zheng. Discovery of a new isomeric state in ^{68}Ni: Evidence for a highly deformed proton intruder state. *Phys. Rev. C*, 85 (2012) 031301.

[Dij12b] Aurore Dijon. *Evolution de Ia collectivite autour du ^{68}Ni: role des etats intrus.* PhD thesis, l'Universite de CAEN, 2012.

[Dir13a] J. Diriken, N. Patronis, A. Andreyev, S. Antalic, V. Bildstein, A. Blazhev, I. G. Darby, H. De Witte, J. Eberth, J. Elseviers, V. N. Fedosseev, F. Flavigny, Ch. Fransen, G. Georgiev, R. Gernhauser, H. Hess, M. Huyse, J. Jolie, Th. Kroll, R. Krucken, R. Lutter, B. A. Marsh, T. Mertzimekis, D. Muecher, R. Orlandi, A. Pakou, R. Raabe, G. Randisi, P. Reiter, T. Roger, M. Seidlitz, M. Seliverstov, C. Sotty, H. Tornqvist, J. Van De Walle, P. Van Duppen, D. Voulot, N. Warr, F. Wenander, and K. Wimmer. Study of the 66Ni(d,p)67Ni one-neutron transfer reaction. *Physical Review C*, 2013. to be published.

[Dir13b] Jan Diriken. *Probing positive-parity states in $^{67}_{28}Ni_{39}$ through one-neutron transfer reactions.* . PhD thesis, KU Leuven, 2013.

[Ebe01] J. Eberth, G. Pascovici, H. G. Thomas, N. Warr, D. Weisshaar, D. Habs, P. Reiter, P. Thirolf, D. Schwalm, C. Gund, H. Scheit, M. Lauer, P. Van Duppen, S. Franchoo, M. Huyse, R. M. Lieder, W. Gast, J. Gerl, and K. P. Lieb. MINIBALL A Ge detector array for radioactive ion beam facilities. *Progress in Particle and Nuclear Physics*, 46 (2001) 389 – 398.

[Ehr67] D. Ehrlich. Der Radioaktive Zerfall des ^{61}Fe. *Zeitschrift für Physik*, 207 (1967) 268.

[End79] P. M. Endt. Strengths of gamma-ray transitions in $A = 45$–90 nuclei. *Atomic Data and Nuclear Data Tables*, 23 (1979) 547 – 585.

[Erj01] Bai Erjun and Huo Junde. Nuclear Data Sheets for $A = 63$. *Nuclear Data Sheets*, 92 (2001) 147 – 251.

[Erl12] Jochen Erler, Noah Birge, Markus Kortelainen, Witold Nazarewicz, Erik Olsen, Alexander M. Perhac, and Mario Stoitsov. The limits of the nuclear landscape. *Nature*, 486 (2012) 509.

[Fed12] V. N. Fedosseev, L. E. Berg, D. V. Fedorov, D. Fink, O. J. Launila, R. Losito, B. A. Marsh, R. E. Rossel, S. Rothe, M. D. Seliverstov, A. M. Sjödin, and K. D. A. Wendt. Upgrade of the resonance ionization laser ion source at ISOLDE on-line isotope separation facility: New lasers and new ion beams. *Review of Scientific Instruments*, 83 (2012) 02A903 –02A903–3.

[Fer10] R. Ferrer, M. Block, C. Bachelet, B. R. Barquest, G. Bollen, C. M. Campbell, M. Facina, C. M. Folden, C. Guénaut, A. A. Kwiatkowski, D. L. Lincoln, D. J. Morrissey, G. K. Pang, A. M. Prinke, R. Ringle, J. Savory, P. Schury, and S. Schwarz. Penning trap mass spectrometry of neutron-rich Fe and Co isotopes around $N = 40$ with the LEBIT mass spectrometer. *Phys. Rev. C*, 81 (2010) 044318.

[Fir96] R. B. Firestone. *Table of Isotopes: Volume II.* John Wiley & Sons, 1996.

[Fla09] K. T. Flanagan, P. Vingerhoets, M. Avgoulea, J. Billowes, M. L. Bissell, K. Blaum, B. Cheal, M. De Rydt, V. N. Fedosseev, D. H. Forest, Ch. Geppert, U. Köster, M. Kowalska, J. Krämer, K. L. Kratz, A. Krieger, E. Mané, B. A. Marsh, T. Materna, L. Mathieu, P. L. Molkanov, R. Neugart, G. Neyens, W. Nörtershäuser, M. D. Seliverstov, O. Serot, M. Schug, M. A. Sjoedin, J. R. Stone, N. J.

Stone, H. H. Stroke, G. Tungate, D. T. Yordanov, and Yu. M. Volkov. Nuclear Spins and Magnetic Moments of ^{71,73,75}Cu: Inversion of $\pi 2p_{3/2}$ and $\pi 1f_{5/2}$ Levels in ^{75}Cu. *Phys. Rev. Lett.*, 103 (2009) 142501.

[Fla13] F. Flaviny et al. to be published, 2013.

[Fly79] E. R. Flynn, Ronald E. Brown, F. D. Correll, D. L. Hanson, and R. A. Hardekopf. Total Angular Momentum Determinations from the $(\vec{t}, d)$ Reaction on ^{58,64}Ni. *Phys. Rev. Lett.*, 42 (1979) 626–629.

[For94] B. Fornal. IFJ Cracow Annual Report. Technical report, IFJ, 1994.

[Fra98] S. Franchoo, M. Huyse, K. Kruglov, Y. Kudryavtsev, W. F. Mueller, R. Raabe, I. Reusen, P. Van Duppen, J. Van Roosbroeck, L. Vermeeren, A. Wöhr, K.-L. Kratz, B. Pfeiffer, and W. B. Walters. Beta Decay of $^{68\check{}74}$Ni and Level Structure of Neutron-Rich Cu Isotopes. *Phys. Rev. Lett.*, 81 (1998) 3100–3103.

[Fri81] G. Friedlander, J. W. Kennedy, E. S. Macias, and J. M. Miller. *Nuclear and Radiochemistry.* John Wiley & Sons, 3 edition, 1981.

[Ful65] R. H. Fulmer and W. W. Daehnick. Nuclear-Structure Studies in the Nickel Isotopes with $(d,\ t)$ Reactions. *Phys. Rev.*, 139 (1965) B579–B592.

[Gad10] A. Gade, R. V. F. Janssens, T. Baugher, D. Bazin, B. A. Brown, M. P. Carpenter, C. J. Chiara, A. N. Deacon, S. J. Freeman, G. F. Grinyer, C. R. Hoffman, B. P. Kay, F. G. Kondev, T. Lauritsen, S. McDaniel, K. Meierbachtol, A. Ratkiewicz, S. R. Stroberg, K. A. Walsh, D. Weisshaar, R. Winkler, and S. Zhu. Collectivity at $N = 40$ in neutron-rich ^{64}Cr. *Phys. Rev. C*, 81 (2010) 051304.

[Gau05] Laurent Gaudefroy. *Etude de la fermeture de couche $N = 28$ autour noyau $^{46}Ar_{28}$ par reaction de transfert d'un neutron: application a l'astrophysique et Spectroscopie $\beta\gamma$ de noyaux riches en neutrons autour de $N = 32/34$ et $N = 40$.* PhD thesis, Universite de Paris XI, U.F.R. Scientifique d'Orsay, 2005.

[Geo03] G. Georgiev, G. Neyens, M. Hass, D. L. Balabanski, C. Bingham, C. Borcea, N. Coulier, R. Coussement, J. M. Daugas, G. France, M. Górska, H. Grawe, R. Grzywacz, M. Lewitowicz, H. Mach, I. Matea, F. Oliveira Santos, R.D. Page, M. Pfützner, Yu. E. Penionzhkevich, Z. Podolyák, P. H. Regan, K. Rykaczewski, M. Sawicka, N. A. Smirnova, Yu Sobolev, M. Stanoiu, S. Teughels, and K. Vyvey. g-factors of isomeric states in the neutron-rich nuclei.

The European Physical Journal A - Hadrons and Nuclei, 20 (2003) 93–94.

[Gre96] W. Greiner and J. A. Maruhn. *Nuclear Models*. Springer, 1996.

[Grz98] R. Grzywacz, R. Béraud, C. Borcea, A. Emsallem, M. Glogowski, H. Grawe, D. Guillemaud-Mueller, M. Hjorth-Jensen, M. Houry, M. Lewitowicz, A. C. Mueller, A. Nowak, A. Plochocki, M. Pfützner, K. Rykaczewski, M. G. Saint-Laurent, J. E. Sauvestre, M. Schaefer, O. Sorlin, J. Szerypo, W. Trinder, S. Viteritti, and J. Winfield. New Island of μs Isomers in Neutron-Rich Nuclei around the $Z = 28$ and $N = 40$ Shell Closures. *Phys. Rev. Lett.*, 81 (1998) 766–769.

[Han79] Ole Hansen, M. N. Harakeh, J. V. Maher, L. W. Put, and J. C. Vermeulen. Proton hole states in ^{63}Co and ^{63}Cu. *Nuclear Physics A*, 313 (1979) 95 – 108.

[Han99] M. Hannawald, T. Kautzsch, A. Wöhr, W. B. Walters, K. L. Kratz, V. N. Fedoseyev, V. I. Mishin, W. Böhmer, B. Pfeiffer, V. Sebastian, Y. Jading, U. Köster, J. Lettry, H. L. Ravn, and the ISOLDE Collaboration. Decay of Neutron-Rich Mn Nuclides and Deformation of Heavy Fe Isotopes. *Phys. Rev. Lett.*, 82 (1999) 1391–1394.

[Han00] M. Hannawald. *Kernspektroskopie an $N \simeq 40$ und $N \simeq 82$ Nukliden*. PhD thesis, University of Mainz, 2000.

[Hax49] Otto Haxel, J. Hans D. Jensen, and Hans E. Suess. On the Magic Numbers in Nuclear Structure. *Phys. Rev.*, 75 (1949) 1766–1766.

[Hel83] O. Helene. Upper limit of peak area . *Nuclear Instruments and Methods in Physics Research*, 212 (1983) 319 – 322.

[Hey99] K. Heyde. *Basic Ideas and Concepts in Nuclear Physics*. Institute of Physics Publishing, 2 edition, 1999.

[Hil13] S. Hilaire and M. Girod. *Hartree – Fock – Bogoliubov Results Based On The Gogny Force*, 2013.

[Hjo95] Morten Hjorth-Jensen, Thomas T.S. Kuo, and Eivind Osnes. Realistic effective interactions for nuclear systems. *Physics Reports*, 261 (1995) 125 – 270.

[Hon05] M. Honma, T. Otsuka, B.A. Brown, and T. Mizusaki. Shell-model description of neutron-rich pf-shell nuclei with a new effective interaction GXPF1. *The European Physical Journal A - Hadrons and Nuclei*, 25 (2005) 499–502.

[Hot06] N. Hoteling, W. B. Walters, R. V. F. Janssens, R. Broda, M. P. Carpenter, B. Fornal, A. A. Hecht, M. Hjorth-Jensen, W. Królas, T. Lauritsen, T. Pawlat, D. Seweryniak, X. Wang, A. Wöhr, J. Wrzesiński, and S. Zhu. Yrast structure of ^{64}Fe. *Phys. Rev. C*, 74 (2006) 064313.

[Hot08] N. Hoteling, W. B. Walters, R. V. F. Janssens, R. Broda, M. P. Carpenter, B. Fornal, A. A. Hecht, M. Hjorth-Jensen, W. Królas, T. Lauritsen, T. Pawlat, D. Seweryniak, J. R. Stone, X. Wang, A. Wöhr, J. Wrzesiński, and S. Zhu. Rotation-aligned coupling in ^{61}Fe. *Phys. Rev. C*, 77 (2008) 044314.

[Hot10] N. Hoteling, C. J. Chiara, R. Broda, W. B. Walters, R. V. F. Janssens, M. Hjorth-Jensen, M. P. Carpenter, B. Fornal, A. A. Hecht, W. Królas, T. Lauritsen, T. Pawlat, D. Seweryniak, X. Wang, A. Wöhr, J. Wrzesiński, and S. Zhu. Structure of ^{60,62}Fe and the onset of $\nu g_{9/2}$ occupancy. *Phys. Rev. C*, 82 (2010) 044305.

[Iva07] Oleg Ivanov. *Decay of ^{66}Fe, studied with a new β–γ detection set-up at LISOL*. PhD thesis, KU Leuven, 2007.

[Jun05] Huo Junde, Huang Xiaolong, and J. K. Tuli. Nuclear Data Sheets for $A = 67$. *Nuclear Data Sheets*, 106 (2005) 159 – 250.

[Kra87] Kenneth S. Krane. *Introductory Nuclear Physics*. John Wiley & Sons, 1987.

[Len10] S. M. Lenzi, F. Nowacki, A. Poves, and K. Sieja. Island of inversion around ^{64}Cr. *Phys. Rev. C*, 82 (2010) 054301.

[Lit72] V. F. Litvin, Yu. A. Nemilov, L. V. Krasnov, K. A. Gridnev, K. I. Zherebtzova, Yu. A. Lakomkin, T. V. Orlova, V. P. Bochin, and V. S. Romanov. Coulomb stripping in ^{58,62,64}Ni$(d,p)^{59,63,65}$Ni. *Nuclear Physics A*, 184 (1972) 105 – 112.

[Lju10] J. Ljungvall, A. Görgen, A. Obertelli, W. Korten, E. Clément, G. de France, A. Bürger, J. P. Delaroche, A. Dewald, A. Gadea, L. Gaudefroy, M. Girod, M. Hackstein, J. Libert, D. Mengoni, F. Nowacki, T. Pissulla, A. Poves, F. Recchia, M. Rejmund, W. Rother, E. Sahin, C. Schmitt, A. Shrivastava, K. Sieja, J. J. Valiente-Dobón, K. O. Zell, and M. Zielińska. Onset of collectivity in neutron-rich Fe isotopes: Toward a new island of inversion? *Phys. Rev. C*, 81 (2010) 061301.

[Lom83] R.J. Lombard and D. Mas. Shell effects at Z or $N = 40$: The example of ^{68}Ni. *Physics Letters B*, 120 (1983) 23 – 26.

[Lun07] S. Lunardi, S. M. Lenzi, F. Della Vedova, E. Farnea, A. Gadea, N. Mărginean, D. Bazzacco, S. Beghini, P. G. Bizzeti, A. M. Bizzeti-Sona, D. Bucurescu, L. Corradi, A. N. Deacon, G. de Angelis, E. Fioretto, S. J. Freeman, M. Ionescu-Bujor, A. Iordachescu, P. Mason, D. Mengoni, G. Montagnoli, D. R. Napoli, F. Nowacki, R. Orlandi, G. Pollarolo, F. Recchia, F. Scarlassara, J. F. Smith, A. M. Stefanini, S. Szilner, C. A. Ur, J. J. Valiente-Dobón, and B. J. Varley. Spectroscopy of neutron-rich Fe isotopes populated in the ^{64}Ni + ^{238}U reaction. *Phys. Rev. C*, 76 (2007) 034303.

[Mac09] H. Mach, A. M. Baluyut, E. Ruchowska, U. Köster, L. M. Fraile, R. Boutami, H. Bradley, N. Braun, C. Fransen, J. Jolie, et al. Structure of Heavy Fe Nuclei at the Point of Transition at N $\sim$ 37. *Acta Physica Polonica B*, 40 (2009) 477.

[Mar82] M. J. Martin. Reduced Gamma-Ray Matrix Elements, Transition Probabilities, and Single Particle Estimates, September 1982. NS MEMO 1B/1 (82).

[Mat04] I. Matea, G. Georgiev, J. M. Daugas, M. Hass, G. Neyens, R. Astabatyan, L. T. Baby, D. L. Balabanski, G. Bélier, D. Borremans, G. Goldring, H. Goutte, P. Himpe, M. Lewitowicz, S. Lukyanov, V. Méot, F. de Oliveira Santos, Yu. E. Penionzhkevich, O. Roig, and M. Sawicka. Magnetic Moment of the Fragmentation-Aligned ^{61}Fe, $(9/2^+)$ Isomer. *Phys. Rev. Lett.*, 93 (2004) 142503.

[May49] Maria Goeppert Mayer. On Closed Shells in Nuclei. II. *Phys. Rev.*, 75 (1949) 1969–1970.

[McL72] K. C. McLean, S. M. Dalgliesh, S. S. Ipson, and G. Brown. The ^{57}Fe$(t,p)^{59}$Fe and ^{58}Fe$(d,p)^{59}$Fe reactions. *Nuclear Physics A*, 191 (1972) 417 – 437.

[Mou12] Mohammad Moukaddam. *Evolution of the shell structure in mediom-mass nuclei: Search for the $2d_{5/2}$ neutron orbital in ^{69}Ni.* PhD thesis, University of Strasbourg, 2012.

[MTV75] J. Meyer-Ter-Vehn. Collective model description of transitional odd-A nuclei: (I). The triaxial-rotor-plus-particle model. *Nuclear Physics A*, 249 (1975) 111 – 140.

[Nat78] A. M. Nathan, J. W. Olness, E. K. Warburton, and J. B. McGrory. Yrast decay schemes from heavy-ion + ^{48}Ca fusion-evaporation reactions. III. ^{57,58}Fe, ^{54,55}Cr, and ^{57,58}Mn. *Phys. Rev. C*, 17 (1978) 1008–1025.

[Nil55] S. S. G. Nilsson. *K. Danske Vidensk. Selsk. mat.-fys. Medd.*, 29 (1955) .

[NND13a] NNDC. *eXperimental Unvaluated Nuclear Data List*, 2013.

[NND13b] NNDC. *Evaluated and Compiled Nuclear Structure Data Files*, 2013.

[Oin01] M. Oinonen, U. Köster, J. Äystö, V. Fedoseyev, V. Mishin, J. Huikari, A. Jokinen, A. Nieminen, K. Peräjärvi, A. Knipper, and G. Walter. Ground-state spin of ^{59}Mn. *The European Physical Journal A - Hadrons and Nuclei*, 10 (2001) 123–127.

[Ola11] B. Olaizola. Fast-timing study of n-rich Fe nuclei populated in the beta-decay of Mn. *Advances in Radioactive Isotope Science*, 2011.

[Ola13] B. Olaizola, L. M. Fraile, H. Mach, A. Aprahamian, J. A. Briz, J. Cal-González, D. Ghiţa, U. Köster, W. Kurcewicz, S. R. Lesher, D. Pauwels, E. Picado, A. Poves, D. Radulov, G. S. Simpson, and J. M. Udías. β^- decay of ^{65}Mn to ^{65}Fe. *Phys. Rev. C*, 88 (2013) 044306.

[Oro00] A. M. Oros-Peusquens and P. F. Mantica. Particle-core coupling around ^{68}Ni: a study of the subshell closure at $N = 40$. *Nuclear Physics A*, 669 (2000) 81 – 100.

[Ots01] Takaharu Otsuka, Rintaro Fujimoto, Yutaka Utsuno, B. Alex Brown, Michio Honma, and Takahiro Mizusaki. Magic Numbers in Exotic Nuclei and Spin-Isospin Properties of the *NN* Interaction. *Phys. Rev. Lett.*, 87 (2001) 082502.

[Ots05] Takaharu Otsuka, Toshio Suzuki, Rintaro Fujimoto, Hubert Grawe, and Yoshinori Akaishi. Evolution of Nuclear Shells due to the Tensor Force. *Phys. Rev. Lett.*, 95 (2005) 232502.

[Paa73] V. Paar. Coupling of a three-particle (hole) valence-shell cluster to quadrupole vibrations (Alaga model): The $Z = 50$ region: odd Ag and I isotopes; and the $Z = 28$ region: odd Mn and Ga isotopes. *Nuclear Physics A*, 211 (1973) 29 – 76.

[Pau08a] D. Pauwels, O. Ivanov, N. Bree, J. Büscher, T. E. Cocolios, J. Gentens, M. Huyse, A. Korgul, Yu. Kudryavtsev, R. Raabe, M. Sawicka, I. Stefanescu, J. Van de Walle, P. Van den Bergh, P. Van Duppen, and W. B. Walters. Shape isomerism at $N = 40$: Discovery of a proton intruder state in ^{67}Co. *Phys. Rev. C*, 78 (2008) 041307.

[Pau08b] D. Pauwels, O. Ivanov, J. Büscher, T.E. Cocolios, J. Gentens, M. Huyse, A. Korgul, Yu. Kudryavtsev, R. Raabe, M. Sawicka, I. Stefanescu, J. Van de Walle, P. Van den Bergh, and P. Van Duppen. Decay correlations in the seconds range with laser-ionized, mass-separated beams. *Nuclear Instruments and Methods in Physics Research Section B: Beam Interactions with Materials and Atoms*, 266 (2008) 4600 – 4605.

[Pau09a] D. Pauwels, O. Ivanov, N. Bree, J. Büscher, T. E. Cocolios, M. Huyse, Yu. Kudryavtsev, R. Raabe, M. Sawicka, J. Van de Walle, P. Van Duppen, A. Korgul, I. Stefanescu, A. A. Hecht, N. Hoteling, A. Wöhr, W. B. Walters, R. Broda, B. Fornal, W. Krolas, T. Pawlat, J. Wrzesinski, M. P. Carpenter, R. V. F. Janssens, T. Lauritsen, D. Seweryniak, S. Zhu, J. R. Stone, and X. Wang. Structure of ^{65,67}Co studied through the β-decay of ^{65,67}Fe and a deep-inelastic reaction. *Phys. Rev. C*, 79 (2009) 044309.

[Pau09b] Dieter Pauwels. *Nuclear Structure around $Z = 28$ and $N = 40$ investigated by the beta-decay of Fe, Co and Ni isotopes.* PhD thesis, KU Leuven, 2009.

[Pau10] D. Pauwels, J. L. Wood, K. Heyde, M. Huyse, R. Julin, and P. Van Duppen. Pairing-excitation versus intruder states in ^{68}Ni and ^{90}Zr. *Phys. Rev. C*, 82 (2010) 027304.

[Pau13] D. Pauwels. Private Communications, 2013.

[Paw94] T. Pawlat, R. Broda, W. Królas, A. Maj, M. Zieblinski, H. Grawe, R. Schubart, K.H. Maier, J. Heese, H. Kluge, and M. Schramm. Spectroscopy of neutron-rich Ni isotopes produced in ^{208}Pb + ^{64}Ni collisions. *Nuclear Physics A*, 574 (1994) 623 – 641.

[Rec12] F. Recchia, S. M. Lenzi, S. Lunardi, E. Farnea, A. Gadea, N. Mărginean, D. R. Napoli, F. Nowacki, A. Poves, J. J. Valiente-Dobón, M. Axiotis, S. Aydin, D. Bazzacco, G. Benzoni, P. G. Bizzeti, A. M. Bizzeti-Sona, A. Bracco, D. Bucurescu, E. Caurier, L. Corradi, G. de Angelis, F. Della Vedova, E. Fioretto, A. Gottardo, M. Ionescu-Bujor, A. Iordachescu, S. Leoni, R. Mărginean, P. Mason, R. Menegazzo, D. Mengoni, B. Million, G. Montagnoli, R. Orlandi, G. Pollarolo, E. Sahin, F. Scarlassara, R. P. Singh, A. M. Stefanini, S. Szilner, C. A. Ur, and O. Wieland. Spectroscopy of odd-mass cobalt isotopes toward the $N = 40$ subshell closure and shell-model description of spherical and deformed states. *Phys. Rev. C*, 85 (2012) 064305.

[Rec13] F. Recchia, C. J. Chiara, R. V. F. Janssens, D. Weisshaar, A. Gade, W. B. Walters, M. Albers, M. Alcorta, V. M. Bader, T. Baugher, D. Bazin, J. S. Berryman, P. F. Bertone, B. A. Brown, C. M. Campbell, M. P. Carpenter, J. Chen, H. L. Crawford, H. M. David, D. T. Doherty, C. R. Hoffman, F. G. Kondev, A. Korichi, C. Langer, N. Larson, T. Lauritsen, S. N. Liddick, E. Lunderberg, A. O. Macchiavelli, S. Noji, C. Prokop, A. M. Rogers, D. Seweryniak, S. R. Stroberg, S. Suchyta, S. Williams, K. Wimmer, and S. Zhu. Configuration mixing and relative transition rates between low-spin states in ^{68}Ni. *Phys. Rev. C*, 88 (2013) 041302.

[Reg96] P. H. Regan, J. W. Arrison, U. J. Hüttmeier, and D. P. Balamuth. Yrast γ-ray spectroscopy of the neutron rich isotopes ^{61,63}Co. *Phys. Rev. C*, 54 (1996) 1084–1097.

[Rii10] Karsten Riisager, B. Jonson. The ISOLDE facility. *Scholarpedia*, 5 (2010) 9742.

[Rik00] J. Rikovska, T. Giles, N. J. Stone, K. van Esbroeck, G. White, A. Wöhr, M. Veskovic, I. S. Towner, P. F. Mantica, J. I. Prisciandaro, D. J. Morrissey, V. N. Fedoseyev, V. I. Mishin, U. Köster, W. B. Walters, the NICOLE, and ISOLDE Collaboration. First On-Line Beta-NMR on Oriented Nuclei: Magnetic Dipole Moments of the $\nu p_{1/2}^{-1}$ $1/2^-$ Ground State in ^{67}Ni and $\pi p_{3/2}^{+1}$ $3/2^-$ Ground State in ^{69}Cu. *Phys. Rev. Lett.*, 85 (2000) 1392–1395.

[RIL13a] RILIS. *Ionization scheme of Mn*, 2013.

[RIL13b] RILIS. *Production of Mn*, 2013.

[Rot11] W. Rother, A. Dewald, H. Iwasaki, S. M. Lenzi, K. Starosta, D. Bazin, T. Baugher, B. A. Brown, H. L. Crawford, C. Fransen, A. Gade, T. N. Ginter, T. Glasmacher, G. F. Grinyer, M. Hackstein, G. Ilie, J. Jolie, S. McDaniel, D. Miller, P. Petkov, Th. Pissulla, A. Ratkiewicz, C. A. Ur, P. Voss, K. A. Walsh, D. Weisshaar, and K. O. Zell. Enhanced Quadrupole Collectivity at $N = 40$: The Case of Neutron-Rich Fe Isotopes. *Phys. Rev. Lett.*, 106 (2011) 022502.

[Rou70] P. Roussel, G. Bruge, A. Bussiere, H. Faraggi, and J. E. Testoni. Etude des reactions de transfert (α, t), (α, ^{3}He) dans la couche fp: Mecanisme et utilisation spectroscopique. *Nuclear Physics A*, 155 (1970) 306 – 336.

[Run68] D. E. Rundquist, M. K. Brussel, and A. I. Yavin. (He^3, α) Reactions from Nickel and Zirconium Isotopes. *Phys. Rev.*, 168 (1968) 1296–1311.

[Run83] E. Runte, W. D. Schmidt-Ott, P. Tidemand-Petersson, R. Kirchner, O. Klepper, W. Kurcewicz, E. Roeckl, N. Kaffrell, P. Peuser, K. Rykaczewski, M. Bernas, P. Dessagne, and M. Langevin. Decay studies of neutron-rich products from ^{76}Ge induced multinucleon transfer reactions including the new isotopes ^{62}Mn, ^{63}Fe and ^{71,72,73}Cu. *Nuclear Physics A*, 399 (1983) 163 – 180.

[Run85] E. Runte, K. L. Gippert, W. D. Schmidt-Ott, P. Tidemand-Petersson, L. Ziegeler, R. Kirchner, O. Klepper, P. O. Larsson, E. Roeckl, D. Schardt, N. Kaffrell, P. Peuser, M. Bernas, P. Dessagne, M. Langevin, and K. Rykaczewski. Decay studies of neutron-rich isotopes of manganese, iron, cobalt, nickel, copper and zinc. *Nuclear Physics A*, 441 (1985) 237 – 260.

[Saw03] M. Sawicka, J. M. Daugas, H. Grawe, S. Cwiok, D. L. Balabanski, R. Béraud, C. Bingham, C. Borcea, M. La Commara, G. de France, G. Georgiev, M. Górska, R. Grzywacz, M. Hass, M. Hellström, Z. Janas, M. Lewitowicz, H. Mach, I. Matea, G. Neyens, C. O' Leary, F. de Oliveira Santos, R. D. Page, M. Pfützner, Zs. Podolyák, K. Rykaczewski, M. Stanoiu, and J. Żylicz. Isomeric decay of ^{67}Fe –Evidence for deformation. *The European Physical Journal A - Hadrons and Nuclei*, 16 (2003) 51–54.

[See91] M. Seeger, Th. Kihm, K. T. Knöpfle, U. Schmidt-Rohr, J. Hebenstreit, D. Paul, and P. Von Rossen. Study of proton-hole states in ^{63}Cu and ^{63}Co (I). Spectroscopy of $(d,^3He)$ reactions at $E_d = 52$ MeV. *Nuclear Physics A*, 533 (1991) 1 – 24.

[See92] M. Seeger, Th. Kihm, K. T. Knöpfle, G. Mairle, and U. Schmidt-Rohr. Study of proton hole states in ^{63}Cu and ^{63}Co (II). The γ-decay of proton hole states. *Nuclear Physics A*, 539 (1992) 223 – 248.

[Shi12] Noritaka Shimizu, Takashi Abe, Yusuke Tsunoda, Yutaka Utsuno, Tooru Yoshida, Takahiro Mizusaki, Michio Honma, and Takaharu Otsuka. New-generation monte carlo shell model for the k computer era. *Progress of Theoretical and Experimental Physics*, 2012 (2012) .

[Sor99] O. Sorlin, C. Donzaud, L. Axelsson, M. Belleguic, R. Béraud, C. Borcea, G. Canchel, E. Chabanat, J. M. Daugas, A. Emsallem, D. Guillemaud-Mueller, K. L. Kratz, S. Leenhardt, M. Lewitowicz, C. Longour, M. J. Lopez, F. de Oliveira Santos, L. Petizon, B. Pfeiffer, F. Pougheon, M. G. Saint-Laurent, and J. E. Sauvestre. Beta decay half-lives of neutron rich Ti–Co isotopes around $N = 40$. *Nuclear Physics A*, 660 (1999) 3 – 19.

[Sor00] O. Sorlin, C. Donzaud, L. Axelsson, M. Belleguic, R. Béraud, C. Borcea, G. Canchel, E. Chabanat, J.M. Daugas, A. Emsallem, M. Girod, D. Guillemaud-Mueller, K. L. Kratz, S. Leenhardt, M. Lewitowicz, C. Longour, M. J. Lopez, F. de Oliveira Santos, L. Petizon, B. Pfeiffer, F. Pougheon, M. G. Saint-Laurent, and J. E. Sauvestre. Erratum to Beta decay half-lives of neutron rich Ti–Co isotopes around $N = 40$ [Nucl. Phys. A 660 (1999) 3–19]. *Nuclear Physics A*, 669 (2000) 351 – 367.

[Sor02] O. Sorlin, S. Leenhardt, C. Donzaud, J. Duprat, F. Azaiez, F. Nowacki, H. Grawe, Zs. Dombrádi, F. Amorini, A. Astier, D. Baiborodin, M. Belleguic, C. Borcea, C. Bourgeois, D. M. Cullen, Z. Dlouhy, E. Dragulescu, M. Górska, S. Grévy, D. Guillemaud-Mueller, G. Hagemann, B. Herskind, J. Kiener, R. Lemmon, M. Lewitowicz, S. M. Lukyanov, P. Mayet, F. de Oliveira Santos, D. Pantalica, Yu.-E. Penionzhkevich, F. Pougheon, A. Poves, N. Redon, M. G. Saint-Laurent, J. A. Scarpaci, G. Sletten, M. Stanoiu, O. Tarasov, and Ch. Theisen. $^{68}_{28}Ni_{40}$: Magicity versus Superfluidity. *Phys. Rev. Lett.*, 88 (2002) 092501.

[Sor03a] O. Sorlin, C. Donzaud, F. Azaiez, C. Bourgeois, L. Gaudefroy, F. Ibrahim, D. Guillemaud-Mueller, F. Pougheon, M. Lewitowicz, F. de Oliveira Santos, M. G. Saint-Laurent, M. Stanoiu, S.M. Lukyanov, Yu. E. Penionzhkevich, J.C. Angélique, S. Grévy, K.-L. Kratz, B. Pfeiffer, F. Nowacki, Z. Dlouhy, and J. Mrasek. Beta decay studies of neutron-rich ^{21}Sc–^{27}Co nuclei at GANIL. *Nuclear Physics A*, 719 (2003) C193 – C200.

[Sor03b] O. Sorlin, C. Donzaud, F. Nowacki, J.C. Angélique, F. Azaiez, C. Bourgeois, V. Chiste, Z. Dlouhy, S. Grévy, D. Guillemaud-Mueller, F. Ibrahim, K. L Kratz, M. Lewitowicz, S. M. Lukyanov, J. Mrasek, Yu. E. Penionzhkevich, F. de Oliveira Santos, B. Pfeiffer, F. Pougheon, A. Poves, M. G. Saint-Laurent, and M. Stanoiu. New region of deformation in the neutron-rich $^{60}Cr_{36}$ and $^{62}Cr_{38}$. *The European Physical Journal A - Hadrons and Nuclei*, 16 (2003) 55–61.

[Sor08] O. Sorlin and M. G. Porquet. Nuclear magic numbers: New features far from stability. *Progress in Particle and Nuclear Physics*, 61 (2008) 602 – 673.

[Ste08] I. Stefanescu, G. Georgiev, D. L. Balabanski, N. Blasi, A. Blazhev, N. Bree, J. Cederkäll, T. E. Cocolios, T. Davinson, J. Diriken, J. Eberth, A. Ekström, D. Fedorov, V. N. Fedosseev, L. M. Fraile, S. Franchoo, K. Gladnishki, M. Huyse, O. Ivanov, V. Ivanov,

J. Iwanicki, J. Jolie, T. Konstantinopoulos, Th. Kröll, R. Krücken, U. Köster, A. Lagoyannis, G. Lo Bianco, P. Maierbeck, B. A. Marsh, P. Napiorkowski, N. Patronis, D. Pauwels, G. Rainovski, P. Reiter, K. Riisager, M. Seliverstov, G. Sletten, J. Van de Walle, P. Van Duppen, D. Voulot, N. Warr, F. Wenander, and K. Wrzosek. Interplay between Single-Particle and Collective Effects in the Odd-A Cu Isotopes beyond $N = 40$. *Phys. Rev. Lett.*, 100 (2008) 112502.

[Tay80] T. Taylor and J. A. Cameron. ^{54}Cr, ^{54,58}Fe, ^{58}Ni$(d,p)^{55}$Cr, ^{55,59}Fe, ^{59}Ni Vector analyzing power measurements. *Nuclear Physics A*, 337 (1980) 389 – 400.

[Tsu13] Yusuke Tsunoda, Takaharu Otsuka, Noritaka Shimizu, Michio Honma, and Yutaka Utsuno. Novel shape evolution in exotic Ni isotopes and Type II shell evolution. *arXiv*, 13.09 (2013) 1309.5851.

[Val08] J. J. Valiente-Dobón, S. M. Lenzi, S. J. Freeman, S. Lunardi, J. F. Smith, A. Gottardo, F. Della Vedova, E. Farnea, A. Gadea, D. R. Napoli, M. Axiotis, S. Aydin, D. Bazzacco, P. G. Bizzeti, A. M. Bizzeti-Sona, G. Benzoni, D. Bucurescu, L. Corradi, A. N. Deacon, G. De Angelis, E. Fioretto, B. Guiot, M. Ionescu-Bujor, A. Iordachescu, S. Leoni, N. Mărginean, R. Mărginean, P. Mason, R. Menegazzo, D. Mengoni, B. Million, G. Montagnoli, R. Orlandi, F. Recchia, E. Sahin, F. Scarlassara, R. P. Singh, A. M. Stefanini, D. Steppenbeck, S. Szilner, C. A. Ur, B. J. Varley, and O. Wieland. Spectroscopy of neutron-rich $^{59-63}$Mn isotopes. *Phys. Rev. C*, 78 (2008) 024302.

[Ven78] R. Vennink, W. Ratynski, and J. Kopecky. Circular polarization of neutron capture γ-rays from Ca, Ti, Fe and Ni. *Nuclear Physics A*, 299 (1978) 429 – 441.

[Ven80] R. Vennink, J. Kopecky, P. M. Endt, and P. W. M. Glaudemans. Investigation of the ^{56}Fe$(n,\gamma)^{57}$Fe and ^{58}Fe$(n,\gamma)^{59}$Fe reactions. *Nuclear Physics A*, 344 (1980) 421 – 445.

[Ven10] M. Venhart. GEANT4 Monte Carlo simulations of the efficiency of HPGe detectors., 2010.

[Ver07] N. Vermeulen, S. K. Chamoli, J. M. Daugas, M. Hass, D. L. Balabanski, J. P. Delaroche, F. de Oliveira-Santos, G. Georgiev, M. Girod, G. Goldring, H. Goutte, S. Grévy, I. Matea, P. Morel, B. S. Nara Singh, Yu. E. Penionzkevich, L. Perrot, O. Perru, S. Péru, O. Roig, F. Sarazin, G. S. Simpson, Yu. Sobolev, I. Stefan, C. Stodel, D. T. Yordanov, and G. Neyens. First isomeric quadrupole moment

measured in fragmentation reactions: The case of $^{61}Fe^{m}(9/2^{+})$. *Phys. Rev. C*, 75 (2007) 051302.

[Wai] M. Waite et al. to be published.

[Wal99] Philip Walker and George Dracoulis. Energy traps in atomic nuclei. *Nature*, 399 (1999) 35.

[Wal09] J. Van de Walle, V. Bildstein, N. Bree, J. Cederkäll, P. Delahaye, J. Diriken, A. Ekström, V. N. Fedosseev, R. Gernhäuser, A. Gustafsson, A. Herlert, M. Huyse, O. Ivanov, T. Kröll, R. Krücken, B. Marsh, N. Partronis, P. Van Duppen, D. Voulot, N. Warr, F. Wenander, K. Wimmer, and S. M. Lenzi. In-trap decay of ^{61}Mn and Coulomb excitation of ^{61}Mn/^{61}Fe. *The European Physical Journal A*, 42 (2009) 401–406.

[Wal13] W. B. Walters. Private Communications, 2013.

[Wan12] M. Wang, G. Audi, A. H. Wapstra, F. G. Kondev, M. MacCormick, X. Xu, and B. Pfeiffer. The AME2012 atomic mass evaluation (II). Tables, graphs and references. *Chinese Physics C*, 36 (2012) 1603–2014.

[War77] E. K. Warburton, J. W. Olness, A. M. Nathan, J. J. Kolata, and J. B. McGrory. Yrast decay schemes from heavy-ion + ^{48}Ca fusion-evaporation reactions. II. $^{59-60}$Fe and $^{59-60}$Co. *Phys. Rev. C*, 16 (1977) 1027–1039.

[War78] E. K. Warburton, J. W. Olness, A. M. Nathan, and A. R. Poletti. Yrast decay schemes from heavy-ion + ^{48}Ca fusion-evaporation reactions: IV: ^{53}Cr, ^{54}V, ^{62}Co, and $^{61-63}$Ni. *Phys. Rev. C*, 18 (1978) 1637–1650.

[War13] N. Warr, J. Walle, M. Albers, F. Ames, B. Bastin, C. Bauer, V. Bildstein, A. Blazhev, S. Bönig, N. Bree, B. Bruyneel, P.A. Butler, J. Cederkäll, E. Clément, T.E. Cocolios, T. Davinson, H. Witte, P. Delahaye, D.D. DiJulio, J. Diriken, J. Eberth, A. Ekström, J. Elseviers, S. Emhofer, D.V. Fedorov, V.N. Fedosseev, S. Franchoo, C. Fransen, L.P. Gaffney, J. Gerl, G. Georgiev, R. Gernhäuser, T. Grahn, D. Habs, H. Hess, A.M. Hurst, M. Huyse, O. Ivanov, J. Iwanicki, D.G. Jenkins, J. Jolie, N. Kesteloot, O. Kester, U. Köster, M. Krauth, T. Kröll, R. Krücken, M. Lauer, J. Leske, K.P. Lieb, R. Lutter, L. Maier, B.A. Marsh, D. Mücher, M. Münch, O. Niedermaier, J. Pakarinen, M. Pantea, G. Pascovici, N. Patronis, D. Pauwels, A. Petts, N. Pietralla, R. Raabe, E. Rapisarda,

P. Reiter, A. Richter, O. Schaile, M. Scheck, H. Scheit, G. Schrieder, D. Schwalm, M. Seidlitz, M. Seliverstov, T. Sieber, H. Simon, K.-H. Speidel, C. Stahl, I. Stefanescu, P.G. Thirolf, H.-G. Thomas, M. Thürauf, P. Duppen, D. Voulot, R. Wadsworth, G. Walter, D. Weisshaar, F. Wenander, A. Wiens, K. Wimmer, B.H. Wolf, P.J. Woods, K. Wrzosek-Lipska, and K.O. Zell. The Miniball spectrometer. *The European Physical Journal A*, 49 (2013) .

[Wei99] L. Weissman, A. Andreyev, B. Bruyneel, S. Franchoo, M. Huyse, K. Kruglov, Y. Kudryavtsev, W. F. Mueller, R. Raabe, I. Reusen, P. Van Duppen, J. Van Roosbroeck, L. Vermeeren, U. Köster, K. L. Kratz, B. Pfeiffer, P. Thirolf, and W. B. Walters. β decay of ^{67}Co. *Phys. Rev. C*, 59 (1999) 2004–2008.

[Zhu12] S. Zhu, R. V. F. Janssens, M. P. Carpenter, C. J. Chiara, R. Broda, B. Fornal, N. Hoteling, W. Królas, T. Lauritsen, T. Pawlat, D. Seweryniak, I. Stefanescu, J. R. Stone, W. B. Walters, X. Wang, and J. Wrzesiński. Nature of yrast excitations near $N = 40$: Level structure of ^{67}Ni. *Phys. Rev. C*, 85 (2012) 034336.